ABSTRACT

Title of Dissertation: **HISTATIN 5 MODIFICATIONS IMPACT PROTEOLYTIC STABILITY IN THE PRESENCE OF FUNGAL AND SALIVARY PROTEASES**

Wright K. Makambi, Doctor of Philosophy, 2024

Dissertation directed by: Professor Amy J. Karlsson, Department of Chemical and Biomolecular Engineering

Candida albicans, found in the oral cavities of 30-50% of the global population, can lead to oral candidiasis, particularly in immunocompromised individuals like those with HIV or diabetes. The current treatments, small-molecule antifungals, often fall short due to drug resistance and toxicity. To address these challenges, histatin 5 (Hst5), a 24-amino-acid peptide naturally present in human saliva, has been studied as a potential antifungal therapy.

Hst5, however, is susceptible to degradation by secreted aspartyl proteases (Saps) produced by *C. albicans* and salivary enzymes, limiting its potential efficacy as a therapeutic. We have engineered Hst5 variants utilizing rational design in order to understand the interactions with Saps and Saliva. We have also made advancements in developing a novel screening method utilizing the directed evolution technique yeast surface display.

Our study employed rational design to modify Hst5, at its lysine residues (K5, K11, K13, and K17), substituting them with leucine or arginine to examine their influence on interactions with

Saps (Sap1, Sap2, Sap3, Sap5, Sap6, Sap9, and Sap10). Sap5, Sap6, and Sap10 did not degrade Hst5 at the tested conditions, while Sap1, Sap2, Sap3, and Sap9 did. Some modifications, such as K13L, are particularly susceptible to proteolysis by Sap1, Sap2, Sap3, and Sap9. In contrast, K17L substantially increases the stability and antifungal activity of Hst5 in the presence of Saps. Additionally, although the K11RK17L variant was degraded more than the K17L variant, their antifungal activities were largely similar. The proteolysis products of were also identified by mass spectrometry identifying the [4-24], [1-17], and [14-24] Sap proteolysis products. We also evaluated the proteolytic stability of these variants in saliva. Both K17L and K5R showed improved stability; however, the enhancements were modest, suggesting that further engineering is required to achieve significant improvements. Further experiments evaluated how additional amino acid substitutions at K13 and K17 affect the peptide's proteolytic stability in the presence of Saps (with and without zinc). Our findings suggest that the positive charge at K13 is important for the proteolytic stability of Hst5, as all other variants tested except K13R reduce overall proteolytic stability. Furthermore, many substitutions at K17, including tryptophan, significantly enhance proteolytic resistance and antifungal activity following incubation with Saps. The K17W variant showed improved stability and antifungal efficacy, maintaining its function even in the presence of zinc and exhibiting stronger antibiofilm activity than the parent Hst5.

In addition to the rational design work, we have advanced the development of a directed evolution yeast surface display platform for screening peptides for proteolytic stability. This would allow for the expression of large peptide libraries on the surface of *Saccharomyces cerevisiae*. Through optimization of expression and display conditions, we determined an induction media at 30°C with a pH of 3.5 and devoid of glucose improved the expression and display of Hst5 peptides on the surface of *S. cerevisiae.* We also optimized the degradation

conditions for Sap2 37°C, a pH not exceeding 7.4, and a Sap2 concentration of 0.78 μg/mL led to the best discrepancy between proteolytically stable variants. Additionally, we found that a 40 amino acid linker between the peptide and the yeast surface provided the best observing proteolytic degradation. Using the optimized system, we showed that yeast surface display can be used to discriminate between peptide variants with different levels of proteolytic stability. This lays the foundation for future work to screen large libraries of peptides for proteolytic stability.

From these results, we have gained a deeper understanding of the interactions between Hst5 and Saps, showing that modification at different lysine residues greatly impacts the proteolytic stability of Hst5. Furthermore, we have shown that the yeast surface display platform can be used to screen the proteolytic stability of peptides. Looking forward, this peptide should be engineered for proteolytic stability in saliva. Furthermore, mock screens should be made before screening a library of peptides using the yeast surface display platform.

HISTATIN 5 MODIFICATIONS IMPACT PROTEOLYTIC STABILITY IN THE PRESENCE OF FUNGAL AND SALIVARY PROTEASES

by

Wright K. Makambi

Dissertation submitted to the Faculty of the Graduate School of the
University of Maryland, College Park, in partial fulfillment
of the requirements for the degree of
Doctor of Philosophy
2024

Advisory Committee:
Professor Amy J. Karlsson, Chair
Jeffery B. Klauda
Srinivasa R. Raghavan
Hannah Zierden
Gregg Duncan

Dedication

I dedicate my PhD dissertation to my Mom (Pamela Makambi), my Dad (Kepher Makambi), and my Brother (Durell Makambi) for supporting me and guiding me through my PhD studies.

Acknowledgments

I would like to thank my advisor Dr. Amy Karlsson, for guiding me from the time that I was an undergraduate student. Even before I was her student, she mentored me and educated me, and now as her student she has provided me friendship and guidance. My growth as an individual and a professional starts at you and I cannot express my gratitude enough.

I would like to thank my mentees, Victoria Chiu, for her assistance on the metal binding experiments and Natalya Brown, for helping me optimize the yeast surface display construct. They made my mentorship experience unforgettable and enjoyable, and I would like to congratulate them on getting into Medical school and a PhD program.

I would also like to thank my fellow graduate students who made valuable contributions to my research: Dr. Dinara Konakbayeva, Futoon Al-Jirafi, Marzy-Kheradmand-Hajibashi, Dr. Shakiba Nikfarjam, Talia Solomon, Ren-Jhe Chung, and Dr. Robert Allsopp, for offering their help and collaboration, building knowledge together and sharing the graduate experience with me. I would specifically like to thank Dinara for her guidance in cloning the yeast surface display construct, as well as our Dr. Svetlana Ikonomova for her guidance and advice in this dissertation.

I would also like to thank my mentors and supervisors during my internship at Codexis: Paul Jordan, Ariana Celis Luna, and Judy Viduya for their friendship, enhancing my knowledge of the industrial world, and making me a better protein engineer.

Dr. Asa Awuku and Dr. Jeffery Klauda, for acting as my secondary advisors and supporting me through the PhD program, whether by email or in-person. My letter of recommendation providers for graduate school Dr. Ganesh Sriram, Dr. Deborah Goldberg for supporting my research endeavors and making materials in lectures accessible to all students.

The chemical engineering staff at the University of Maryland for their professionalism, organization, and kindness, especially Kathy and Jenna.

We acknowledge Kenneth Class of the MPRI Flow cytometry facility for the use of the BD FACSCanto II, and his guidance in analyzing the flow cytometry data.; We acknowledge Dr. Yue Li and the Mass Spec Facility in the department of Chemistry and Biochemistry at the University of Maryland–College Park for use of the Bruker Maxis-II QTOF + Waters Acquity LC for assistance determining the degradation products formed after degradation of histatin 5 by saliva and Saps.; I also acknowledge bruker agent Yeni P. Yung, for her patience and time in understanding the Q-ToF and utilizing the BioTool and Sequence editor softwares.

We acknowledge the Future Faculty Program, the Clark Fellowship Program, and The Graduate Assistance in Areas of National Need Program, for their funding and making this project possible.

We acknowledge the National Institute of Health (NIH) for funding grant DE029270-02; Dr. Bernhard Hube (Friedrich Schiller University, Germany) for the Sap enzymes; Dr. Benjamin Hackel (University of Minnesota) for the yeast surface display constructs.

To my D5 family (Derick, Alex, Turi, Archi, Xiomi, Loic, Jairo, Keri, Nisha, Bethany, Chandler, Harrison, Josh, Sarah), that showed me love, care and patience, and being my light outside of school.

To my extended (Kenyan and church) family, that helped raise me and bring me to this point in my life.

Lastly, my parents and brother, who have been my guides and caretakers from birth, have shaped who I am through the kindness they show in everyday life.

Table of Contents

Dedication ..... **ii**
Acknowledgments ..... **iii**
List of Tables ..... **ix**
List of Figures ..... **xi**
List of Abbreviations ..... **xxii**
1. Chapter 1: Introduction **1**
1.1. Candida albicans 1
1.2. Antifungal drug resistance 2
1.3. Antimicrobial peptides 4
1.4. Secreted aspartyl proteases 5
1.5. Interactions of Hst5 with Saps 8
1.6. Saliva 9
1.7. Engineering strategies 11
1.7.1. Rational design 12
1.7.2. Directed evolution 12
1.7.2.1 Surface display 13
1.8. Overview of the thesis. 14
2. Chapter 2: Review of engineering and enhancing the antifungal properties of histatin 5 ..... **16**
2.1. Histatin 5 overview 16
2.2. Hst5 structure and mechanism of action 16
2.3. Engineering for antifungal activity 18
2.4. Proteolytic stability 22
2.5. Metal binding 23
2.6. Conclusion 26
3. Chapter 3: Impact of Hst5 modification on proteolytic stability **28**
3.1. Introduction 28
3.2. Methods and materials 30
3.2.1. Peptides and enzymes 30
3.2.2. Proteolytic degradation of the peptides by Saps 31
3.2.3. Proteolytic degradation of the peptides by saliva 32
3.2.4. Gel electrophoresis data analysis 32
3.2.5. Candidacidal assay of intact peptides 33
3.2.6. Candidacidal assay of degraded peptides 34
3.2.7. Quantification of peptide fragments 35
3.3. Results and Discussion 36
3.3.1. Histatin 5 modifications impact proteolytic stability to secreted aspartyl proteases 38
3.3.2. Mass spectrometry reveals that proteolysis may result in other stable fragments43
3.3.3. Modification can impact antifungal activity after being treated with protease 52
3.3.4. Saliva degrades Hst5 variants 57

3.3.5. Saliva proteolysis results in stable fragments 59
3.4. Conclusion 62
4. Chapter 4: Investigating the impact of amino acid substitutions at K13 and K17 on the proteolytic stability and antifungal activity of Hst5..... 63
4.1. Introduction..... 63
4.2. Material and methods..... 66
4.2.1. Peptides and reagents..... 67
4.2.2. Proteolytic degradation of the peptides by Saps..... 67
4.2.3. Proteolytic degradation of the peptides by saliva 68
4.2.4. Gel electrophoresis data analysis..... 69
4.2.5. Quantifying overall proteolytic stability of variants..... 69
4.2.6. Candidacidal assay using full-length peptide 70
4.2.7. Candidacidal assay of degraded peptide..... 71
4.2.8. Zincon competition assay 72
4.2.9. Candidacidal assay using full-length peptides in the presence of zinc. 72
4.2.10. Proteolysis of peptide variants in the presence of Zinc 73
4.2.11. Antifungal assay of Hst5 variants after degradation by Saps in the presence of zinc..... 73
4.2.12. Biofilm prevention assay using full-length peptide. 74
4.3. Results..... 76
4.3.1. K17 variants generally show an improvement in proteolytic stability 77
4.3.2. K13 variants generally show a reduction in proteolytic stability 79
4.3.3. K17W shows the greatest improvement in proteolytic stability in the presence of Saps..... 79
4.3.4. Substitutions to negatively charged residues reduce the antifungal activity of Hst5..... 81
4.3.5. K17 variants retain antifungal activity following incubation with Saps 82
4.3.6. Positive charge residues at K13 have the greatest antifungal activity 83
4.3.7. K17 variants show minimal improvement in the presence of saliva .. 85
4.3.8. Hst5 and variants bind to zinc..... 86
4.3.9. Zinc reduces the antifungal activity of Hst5 at large zinc-to-peptide ratios 88
4.3.10. K17W retains proteolytic stability in the presence of zinc 89
4.3.11. K17W retains antifungal activity after incubation with zinc and Sap2 90
4.3.12. K17W prevents biofilm formation better than parent Hst5 91
4.4. Discussion..... 94
4.5. Conclusion 98
5. Chapter 5: Development of a screen for proteolytic stability of peptides . 100
5.1. Introduction..... 100
5.2. Methods..... 104
5.2.1. Strains, proteases, and plasmids..... 104
5.2.2. Plasmid construction..... 104
5.2.3. Culture conditions..... 107

5.2.4. Western blotting 108
5.2.5. Proteolysis of yeast surface display construct 110
5.2.6. Flow cytometry 110
5.2.7. Mass spectrometry 111
5.3. Results 112
5.3.1. Peptide variants can be expressed on the YSD construct 113
5.3.2. Degradation can be observed on the surface of S. cerevisiae 122
5.3.3. Differences in proteolytic stability can be observed 128
5.4. Discussion 130
5.5. Conclusion 132
6. Chapter 6: Summary and recommendation for future work 134
6.1. Screening a library of peptides using the yeast surface display system and potential further improvements 135
6.2. Yeast extracellular reticulum sequestration screening 137
6.3. Production and purification of Saps 138
6.4. Designing variants with improved proteolytic stability in the presence of Hst5 and proteases in saliva 139
6.5. Assessing the activity of Hst5 variants in the presence of metals 140
6.6. Creating coatings with antifungal peptides 141
A. Appendix A 143
B. Appendix B 150
C. Appendix C 156
Bibliography 168

List of Tables

1. Chapter 1: Introduction

Table 1.1. Summary of the fragments found from the degradation of Hst5 by Sap1-10 as found in the literature. 9
Table 1.2. Fragments found from the degradation of Hst5 by saliva. 10
Table 2.1. The sequence of Hst3 and proteolytic biproduct in the presence of saliva Hst5. 16
Table 2.2. Truncations of Hst5 designed to assess antifungal activity against *C. albicans*. 19
Table 2.3. Mutants of Hst5 designed to assess antifungal activity and their antifungal activity against *C. albicans.* The activity reported is with respect to the parent peptide for each section Hst5, dh-5, and P-113. 20
Table 2.4. Mutants of Hst5 designed to assess proteolytic stability. The stability reported is with respect to the parent peptide Hst5. 23
Table 2.5. Mutants of Hst5 designed to assess Zn^{2+} affinity. The binding reported is with respect to the parent peptide Hst5. 26
Table 3.1. Final concentration of Saps in degradation assay. 31
Table 3.2. Sequence of peptides in this study. 37
Table 4.1. Concentration of Saps after mixing with peptides. 68
Table 4.2. Table of designed peptide variants. 76
Table 4.3. Normalized intact peptide values for K17 and K13 variants. 80
Table 4.4. Designed peptide variants used to assess metal binding. 87
Table 5.1. Sequence of oligonucleotides used to construct pCT40 and pCT641 plasmids. 106
Table 5.2. Components for growth media and protein induction media. 108
Table 5.5. Optimized conditions for protein expression and construct degradation. 131
Table 6.1. Recommendation for Hst5 variants with improved properties. 140
Appendix Table A.1. P-values for proteolysis of Hst5 and variants by Saps and saliva. Two-way ANOVA tests with α = .05 and Dunnett's multiple comparison tests (degraded Hst5 as the control) were performed for statistical analysis. 143
Appendix Table A.2. P-values for proteolysis of Hst5 and variants by Saps and saliva. Two-way ANOVA tests with α = .05 and Dunnett's multiple comparison tests (degraded Hst5 as the control for Samples treated with Saps and undegraded Hst5 as the control for untreated sample) were performed for statistical analysis. 143
Appendix Table B.1. P-values for proteolysis of Hst5 and variants by Saps and saliva. Two-way ANOVA tests with α = .05 and Dunnett's multiple comparison tests (degraded Hst5 as the control) were performed for statistical analysis. 150
Appendix Table B.B.2. P-values for proteolysis of Hst5 and variants by Saps and saliva. Two-way ANOVA tests with α =.05 and Dunnett's multiple comparison tests (degraded Hst5 as the control for Samples treated with Saps and undegraded Hst5 as the control for untreated sample) were performed for statistical analysis. 152

Appendix Table B.3. *P*-values for zinc competition of Hst5 and variants against Zincon. Two-way ANOVA tests with α = .05 and Dunnett's multiple comparison tests (Hst5 as the control) were performed for statistical analysis..... 154
Appendix Table B.4. *P*-values for Hst5 and variants antifungal activity against *C. albicans* in the presence of different titrations of zinc. Two-way ANOVA tests with α = .05 and Dunnett's multiple comparison tests (Hst5 as the control) were performed for statistical analysis..... 154
Appendix Table B.5. *P*-values for Hst5 biofilm formation in the presence and absence of zinc and Sap2. Two-way ANOVA tests with α = .05 and Dunnett's multiple comparison tests (Hst5 as the control) were performed for statistical analysis. 155
Appendix Table B.6. *P*-values for Hst5 biofilm formation prevention activity against *C. albicans*. Two-way ANOVA tests with α = .05 and Dunnett's multiple comparison tests (Hst5 as the control) were performed for statistical analysis..... 155

List of Figures

1. Chapter 1: Introduction

Figure 1.1. Microscope image of the yeast and hyphae morphologies of *C. albicans*. 1
Figure 1.2. Mechanism of action and example of antifungal agents against *C. albicans.* **A)** Polyene such as AmB interact with ergosterol to disrupt the cell membrane, **B)** azoles such as fluconazole inhibit the formation of ergosterol and instead form toxic sterols that cause membrane stress, and **C)** echinocandins such as caspofungin prevent the formation (1,3) β-D glucan synthase. Figure reprinted with permission from [23]. Copyright © 2020, American Chemical Society. 3
Figure 1.3. Mechanism of resistance to antifungal agents by *C. albicans*. **A)** For polyenes, alternative sterols are used to maintain the membrane structure. **B)** Resistance to azoles can occur through multiple mechanisms, overexpression of ergosterol, and expression of efflux pumps to remove azoles from the cell. **C)** For echinocandins, mutations in Fks1p prevent binding. Figure reprinted with permission from [23]. Copyright © 2020, American Chemical Society. 4
Figure 1.4. Schematic of the mechanism of secretion for Saps. mRNA is translated in the rough endoplasmic reticulum (ER) and forms the enzymes in their preproenzyme form. The signaling peptide is removed via by a signal peptidase forming the proenzyme. This enzyme is further processed by Kex-2 proteinase, which activates them to their mature form. These enzymes are transported by vacuoles either to their GPI anchor or the extracellular space. Figure reprinted with permission from [41]. Copyright © 2022, Future Medicine. 6
Figure 1.5. Structure of Sap2 (1eag PDB), predicted by Robetta. Figure reprinted with permission from Copyright © 2019, Springer Natural Limited. 7
Figure 1.6. Schematic of the mechanism of action for aspartyl proteases mediated by the Asp32 and Asp215 residues. **1)** Asp32 is deprotonated by the carboxyl oxygen of the protein, Asp215 deprotonates water, and the oxygen in water acts as a nucleophile and bonds to the carboxyl carbon of the protein. **2)** The protein rotates at the amino acid amine group. **3)** Asp32 deprotonates hydroxyl oxygen, which forms a carboxyl double bond in the protein, Asp215 donates hydrogen to the protein amine group, and the amine acts as a leaving group, completing the hydrolysis. **4)** The final structure with Asp32 and Asp215 returned to their original state and the protein cleaved. Figure reprinted with permission from Copyright © 2008, American Chemical Society. 7
Figure 1.7. Schematic of the engineering strategies to make improved antifungal peptides. Figure reprinted and adapted with permission from [51] Copyright © 2023, Elsevier Ltd. 11
Figure 2.1. Schematic of the mechanism of action of Hst5 against *C. albicans*. The Hst5 peptide 1) interacts with the Ssa2 heat shock protein receptor, 2) transports through the Dur3/31 transporters, and 3) interacts with the mitochondria leading to release of reactive oxygen species. Figure made in BioRender.com 17
Figure 2.2. The amino acid sequence of Hst5. The Zn2+ binding motifs are highlighted in blue. 24
Figure 2.3. Schematic of the role of Zn^{2+} in the antifungal activity of Hst5. At high Zn^{2+} concentrations, Hst5 binds $Zn^{2+,}$ preventing internalization into *C. albicans*, when exposure to Zn^{2+} is reduced by chelators like EDTA, Hst5 can internalize and

reduce the activity of Hst5. Figure reprinted with permission from [81]. Copyright © 2022, American Chemical Society. 24
Figure 2.4. Hst5 interacting with Zinc. Zinc (Pink circle) is interacting with the H19 and H15 residues of Hst5 [82]. 26
Figure 3.1. Degradation of Hst5 by purified Sap1, Sap2, Sap3, and Sap9. After incubation for 2 h at 37 °C, the intact peptide and degradation fragments were separated by gel electrophoresis and quantified by densitometry. Error bars represent the standard error of the mean (N = 9 for the Hst5 controls with and without Sap and N = 3 for the Hst5 variants). 40
Figure 3.2. Fragments produced by incubation of Hst5 and variants with Sap1. The peptides were each incubated with Sap1 for 2 h at 37 ℃, and mass spectrometry was used to identify the fragments formed. Values shown are the average (N=2) normalized relative abundance of the fragment with respect to the standard MRFA. Black represents the fully intact peptide, while all other fragments are colored red. An asterisk (*) represent fragments that have the same mass and could, therefore, not be distinguished by mass spectrometry. 46
Figure 3.3. Fragments produced by incubation of Hst5 and variants with Sap2. The peptides were each incubated with Sap2 for 2 h at 37 ℃, and mass spectrometry was used to identify the fragments formed. Values shown are the average (N=2) normalized relative abundance of the fragment with respect to the standard MRFA. Black represents the fully intact peptide, while all other fragments are colored red. An asterisk (*) represent fragments that have the same mass and could, therefore, not be distinguished by mass spectrometry. 47
Figure 3.4. Fragments produced by incubation of Hst5 and variants with Sap3. The peptides were each incubated with Sap3 for 2 h at 37 ℃, and mass spectrometry was used to identify the fragments formed. Values shown are the average (N=2) normalized relative abundance of the fragment with respect to the standard MRFA. Black represents the fully intact peptide, while all other fragments are colored red. An asterisk (*) represent fragments that have the same mass and could, therefore, not be distinguished by mass spectrometry. 48
Figure 3.5. Fragments produced by incubation of Hst5 and variants with Sap9. The peptides were each incubated with Sap9 for 2 h at 37 ℃, and mass spectrometry was used to identify the fragments formed. Values shown are the average (N=2) normalized relative abundance of the fragment with respect to the standard MRFA. Black represents the fully intact peptide, while all other fragments are colored red. An asterisk (*) represent fragments that have the same mass and could, therefore, not be distinguished by mass spectrometry. 49
Figure 3.6. Antifungal activity of intact Hst5 variants. Hst5 variants were serially diluted, mixed with *C. albicans* cells, and incubated for 30 min at 30 °C in 1 mM NaPB. Error bars represent the standard error of the mean (N = 18 for Hst5 with and without Sap, while N = 6 for all Hst5 variants). 53
Figure 3.7. Antifungal activity of Hst5 variants after incubation with Sap1, Sap2, Sap3, or Sap9. After incubation for 2 h at 37 °C, Samples were serially diluted in a 96-well plate from 75 μg/mL to 0.14 μg/mL. Samples were then mixed with *C. albicans* cells at 5.0×10^5 cells/mL and incubated for 30 min at 30 °C in 1 mM NaPB, after which cells were inoculated and cultured. Error bars represent the

standard error of the mean (N = 18 Hst5 No Sap and Hst5 + Sap, while N = 6 for all other variants). 55
Figure 3.8. Degradation of Hst5 by saliva. After incubation for 2 h at 37 °C. We then used gel electrophoresis to separate fragments from fully intact peptides and quantified the gel images using densitometric analysis. Error bars represent the standard error of the mean (N = 9 Hst5 No Sap and Hst5, while N = 3 for all other variants)..... 58
Figure 3.9. Fragments produced by incubation of Hst5 and variants with saliva. The peptides were each incubated with saliva for 2 h at 37 ℃, and mass spectrometry was used to identify the fragments formed. Values shown are the average (N=2) normalized relative abundance of the fragment with respect to the standard MRFA. Black represents the fully intact peptide, while all other fragments are colored red. An asterisk (*) represent fragments that have the same mass and could, therefore, not be distinguished by mass spectrometry.. 60
Figure 4.1. Degradation of Hst5 by purified Sap1, Sap2, Sap3, and Sap9. After incubation for 2 h at 37 °C, the intact peptide and degradation fragments were separated by gel electrophoresis and quantified densitometry. Error bars represent the standard error of the mean (N = 6 for the Hst5 controls with and without Sap and N = 3 for the Hst5 variants). Gel images in **Appendix Figure B.1**..... 78
Figure 4.2. Antifungal activity of intact Hst5 variants. Hst5 variants were serially diluted, mixed with *C. albicans* cells, and incubated for 30 min at 30 °C in 1 mM NaPB. Error bars represent the standard error of the mean (N = 12 for Hst5 with and without Sap, while N = 6 for all Hst5 variants)..... 82
Figure 4.3. Antifungal activity of Hst5 variants after incubation with Sap1, Sap2, Sap3, or Sap9. After incubation for 2 h at 37 °C, Samples were serially diluted in a 96-well plate from 75 μg/mL to 0.14 μg/mL. Samples were then mixed with *C. albicans* cells at 5.0×10^5 cells/mL and incubated for 30 min at 30 °C in 1 mM NaPB, after which cells were inoculated and cultured. Error bars represent the standard error of the mean (N = 12 Hst5 No Saβand Hst5 + Sap, while N = 6 for all other variants). 85
Figure 4.4. Degradation of Hst5 by saliva. After incubation for 2 h at 37 °C. We then used gel electrophoresis to separate fragments from fully intact peptides and quantified the gel images using densitometric analysis. Error bars represent the standard error of the mean (N = 6 Hst5 No Sap and Hst5, while N = 3 for all other variants)..... 86
Figure 4.5. Zinc competition between peptide and Zincon. After titrating zinc into an equimolar mixture of Zincon and peptide, the absorbance was measured via absorbance at 621nm. Error bars represent the standard error of the mean (N = 3)... 87
Figure 4.6. Antifungal activity of Hst5 variants in the presence of Zinc. Zinc was serial diluted (1200 μM to 1.2 μM) and equal volume of 60 μM peptide was added to each well. Samples were then mixed with *C. albicans* cells at 5.0×10^5 cells/mL and incubated for 30 min at 30 °C in 1 mM NaPB, after which cells were inoculated and cultured. Error bars represent the standard error of the mean (*N = 4)*. 89
Figure 4.7. Proteolysis of Hst5 variants after incubation with sap2 and with or without zinc. After incubation for 2 h at 37 °C, we then used gel electrophoresis to

separate fragments from fully intact peptides and quantified the gel images using densitometric analysis ($N = 2$). 90
Figure 4.8. Antifungal activity of Hst5, K17W, and K13H after incubation with zinc at a 2:1 zinc-to-peptide ratio and Sap2. After incubation for 2 hrs at 37 °C, Samples were serially diluted in a 96-well plate from 75 µg/mL to .14 µg/mL. Samples were then mixed with *C. albicans* cells at 5.0×10^5 cells/mL and incubated for 30 min at 30 °C in 1 mM NaPB, after which cells were inoculated and cultured. Error bars represent the standard error of the mean ($N = 3$). 91
Figure 4.9. Prevention of Biofilm formation by of Hst5 variants. Peptide were is serial diluted 2:1 in water until from 1500 µM to 1.5 µM. Samples were then mixed with *C. albicans* cells at 1.0×10^6 cells/mL and incubated for 24 h at 37 °C in RPMI1640. A) 0.5 g/L of XTT with 1µM menadione was then added to wells and absorbance was measured at 621 nm. Error bars represent the standard error of the mean ($N = 4$). B) Images were taken of wells treated with 187.5 µg/mL of peptide using n inverted fluorescence microscope (20 × magnification). 93
Figure 4.10. Helical wheel structure of Hst5 generated at https://clemlab.github.io/helicalwheel/ 98
Figure 5.1. Schematic of the yeast surface display platform. The YSD construct is anchored on the cell wall of *S. cerevisiae* by disulfide bonds between Aga1p and Aga2p. Aga2p is linked to the HA epitope tag with is connected via a short liker to the peptide of interest. The C-terminus of the peptide of interest is the c-myc tag which identifies the full construct on the surface of *S. cerevisiae*. Figure made in BioRender.com 101
Figure 5.2. Schematic of engineered a library of the *Staphylococcus aureus* serin-protease-like protease SplB to cleave a bait-peptide on alpha-2-macroglobulins. A) The protease cleaves the bait peptide and the buried Cys-Gln thioester covalently traps the protease in A2M. B) The protease of interest is displayed on the yeast surface display construct with a fluorescein isothiocyanate (FITC)-conjugated anti-myc tag antibody, and A2M is linked to biotin, which binds to a Phycoerythrin-conjugated streptavidin (SA), which s can be recognized by a Phycoerythrin conjugated anti-streptavidin antibody containing Phycoerythrin. Figure reprinted from open access journal *[61]* licensed under a Creative Commons Attribution 4.0 International License. 102
Figure 5.3. Plasmid map for the pCT40-Hst5 plasmid. This contains the Gal1/10 promoter, the yeast surface display construct containing an HA tag, 40 amino acid linker containing, Hst5, and the c-myc tag. 105
Figure 5.4. Schematic for inserting Hst5 oligonucleotides into the pCT40 plasmid. A) Hst5 two pairs of Hst5 oligonucleotides are annealed separately. B) The backbone for the pCT40 plasmid is prepared by cleaving the previous insert out using the NhedI and BamHI restriction enzymes. The pCT40 backbone is then purified. C) The two annealed oligo pairs and the backbone are ligated together. 107
Figure 5.5. Schematic of the degradation of the Hst5 on the surface of *S. cerevisiae*. Before the protease cleaves the peptide of interest, both HA and c-myc tags are present, and a majority of the events in the bivariate plot are in Q2. After the protease cleaves the peptide of interest, a majority of cell should contain only the HA tag and remain in Q3. Figure made in BioRender.com 113

Figure 5.6. Western blot of Aga2-Hst5 in the pCTcon2, pCT40, and pCT641 plasmids. Protein expression was induced at 20 °C for 1 day for all linkers and 3 days for pCT40-Hst5 to determine if experience improves. Detection of the c-myc epitope tag. S and P represent samples collected from the supernatant and the pellet of the cells, respectively. 114
Figure 5.7. Western blot of Aga2-K13L, Aga2-K11RK17R, and Aga2-Hst5 the pCT40 plasmids. Detection of the c-myc epitope tag is shown with the Bio-Rad all-blue molecular weight ladder. Protein expression is enhanced at higher temperature and lower pH. 115
Figure 5.8. Expression time optimization for pCTCon2-Hst5 at 20 °C. The percentage of cells with both the HA and c-myc epitope tag, as well as only the HA tag is plotted from 1 day and 3 days. A bivariate plot of the intensity for both HA (Alexa-Flour 488 antibody) and c-myc (Alexa-Flour 647 antibody) used to generate this bar graph is in **Appendix Figure C.1**. 116
Figure 5.9. Expression temperature and time optimization for pCTCon2-Hst5. The percentage of cells with both the HA and c-myc epitope tag, as well as only the HA tag is plotted from 1 day and 3 days. A bivariate plot of the intensity for both HA (Alexa-Flour 488 antibody) and c-myc (Alexa-Flour 647 antibody) used to generate this bar graph is in **Appendix Figure C.2**. 117
Figure 5.10. Western Blot of Aga2-Hst5 in the pCT40 plasmids. Protein expression was induced at 20 °C, 30 °C, and 37 °C. Detection of c-myc epitope tag is shown with the Bio-Rad all blue molecular weight ladder. 118
Figure 5.11. Linker length optimization profiles for pCTcon2-Hst5, pCT40-Hst5, pCT641-Hst5. Protein expression was induced at 30 °C for 24 hours. The percentage of cells with both the HA and c-myc epitope tag, as well as only the HA tag is plotted. A bivariate plot of the intensity for both HA (Alexa-Flour 488 antibody) and c-myc (Alexa-Flour 647 antibody) used to generate this bar graph is in **Appendix Figure C.3**. 119
Figure 5.12. Differentiation between harvested cell and cells that were not harvested for pCTcon2-Hst5 and pCT40-Hst5. Protein expression was induced at 30 °C for 24 hours, following which cells were pelleted, decanted, and stored at -20 °C. Cells that were not stored were prepared, and the results were compared. The percentage of cells with both the HA and c-myc epitope tag, as well as only the HA tag is plotted. A bivariate plot of the intensity for both HA (Alexa-Flour 488 antibody) and c-myc (Alexa-Flour 647 antibody) used to generate this bar graph is in **Appendix Figure C.4**. 120
Figure 5.13. Western Blot of Aga2-Hst5 in the pCT40 plasmids. Protein expression was induced in SG-CAA media previously described at pH 3.5, pH 4.5, pH 5.5, and pH 6.0 and at 30 °C. Detection of the c-myc epitope tag is shown with the Bio-Rad all-blue molecular weight ladder. 121
Figure 5.14. Western Blot of Aga2-Hst5 in the pCT40 plasmids. Protein expression was induced in SG-CAA media with varying dextrose levels: No glucose, 1× glucose, and 2× glucose at pH 3.5 and 30 °C. We also tested the rich media Yeast extract peptone galactose at 30 °C. Detection of the c-myc epitope tag is shown with the Bio-Rad all-blue molecular weight ladder. Optimization of degradation conditions. 122

Figure 5.15. Initial degradation profile for pCT40-Hst5 at varying concentrations. Protein expression was induced at 30 °C for 24 hours. Cells were then pelleted, washed, and suspended in Sap9 at varying concentrations in 2 mM NaPB. Samples were incubated at 30 °C for 24 hours. The percentage of cells with both the HA and c-myc epitope tag, as well as only the HA tag is plotted from 1 day and 3 days. A bivariate plot of the intensity for both HA (Alexa-Flour 488 antibody) and c-myc (Alexa-Flour 647 antibody) used to generate this bar graph is in **Appendix Figure C.5**..... 123
Figure 5.16. Degradation profile for pCT40-Hst5 with Sap9 at varying pH. Protein expression was induced at 30 °C for 24 hours. Cells were then pelleted, washed, and suspended in 100 µL of 100 µg/mL Sap9 in 2 mM NaPB at various pH. Samples were incubated at 37 °C for 24 hours. The percentage of cells with both the HA and c-myc epitope tag, as well as only the HA tag is plotted. A bivariate plot of the intensity for both HA (Alexa-Flour 488 antibody) and c-myc (Alexa-Flour 647 antibody) used to generate this bar graph is in **Appendix Figure C.6**. 124
Figure 5.17. Degradation profile for pCT40-Hst5 with No Sap, Sap1, Sap2, Sap3, and Sap9. Protein expression was induced at 30 °C for 24 hours. Cells were then pelleted, washed, and suspended in 100 µL of 100 µg/mL Sap9 in 2 mM NaPB at pH 7.4. Samples were incubated at 37 °C for 24 hours. The percentage of cells with both the HA and c-myc epitope tag, as well as only the HA tag is plotted. A bivariate plot of the intensity for both HA (Alexa-Flour 488 antibody) and c-myc (Alexa-Flour 647 antibody) used to generate this bar graph is in **Appendix Figure C.7**..... 125
Figure 5.18. Degradation of pCT40-Hst5 after incubation with Sap2 at varying times. Protein expression was induced at 30 °C for 24 hours. Cells were then pelleted, washed, and suspended in 100 µL of 100 µg/mL Sap2 in 2 mM NaPB at pH 7.4. Samples were incubated at 37 °C for 24 hours. The percentage of cells with both the HA and c-myc epitope tag, as well as only the HA tag is plotted. A bivariate plot of the intensity for both HA (Alexa-Flour 488 antibody) and c-myc (Alexa-Flour 647 antibody) used to generate this bar graph is in **Appendix Figure C.8**..... 126
Figure 5.19. Degradation profile for pCT40-Hst5 after incubation with Sap2 at varying concentrations. Protein expression was induced at 30 °C for 24 hours. Cells were then pelleted, washed, and suspended in 100 µL of Sap2 (at concentrations listed in the figure) in 2 mM NaPB at pH 7.4. Samples were incubated at 37 °C for 30 min. The percentage of cells with both the HA and c-myc epitope tag, as well as only the HA tag is plotted. A bivariate plot of the intensity for both HA (Alexa-Flour 488 antibody) and c-myc (Alexa-Flour 647 antibody) used to generate this paragraph is in **Appendix Figure C.9**..... 127
Figure 5.20. Fragments identified from degradation of YSD construct by Sap2 at varying concentrations. Protein expression was induced at 30 °C for 24 hours. Cells were then pelleted, washed, and suspended in 100 µL of Sap2 (at concentrations listed in the figure) in 2 mM NaPB at pH 7.4. Samples were incubated at 37 °C for 30 min, after which cells were pelleted and the supernatant was collected, and fragments were identified using mass spectrometry. Undegraded pCT40 was also analyzed to identify fragments formed before adding proteases, these fragments are 4-35, 51-83, and 40-72. Figure made in BioRender.com. 128

Figure 5.21. Degradation profile for pCTCon2-st5, pCT40-Hst5, and pCT641-Hst5 after incubation with Sap2. Protein expression was induced at 30 °C for 24 hours. Cells were then pelleted, washed, and suspended in 100 µL of 0.39 µg/mL Sap2 in 2 mM NaPB at pH 7.4. Samples were incubated at 37 °C for 30 min. The percentage of cells with both the HA and c-myc epitope tag, as well as only the HA tag is plotted. A bivariate plot of the intensity for both HA (Alexa-Flour 488 antibody) and c-myc (Alexa-Flour 647 antibody) used to generate this bar graph is in **Appendix Figure C.10**..... 129
Figure 5.22. Degradation profile for pCT40-Hst5, pCT40-K11RK17R, and pCT40-K13L after incubation with Sap2. Protein expression was induced at 30 °C for 24 hours. Cells were then pelleted, washed, and suspended in 100 µL of 0.39 µg/mL Sap2 in 2 mM NaPB at pH 7.4. Samples were incubated at 37 °C for 30 min. The percentage of cells with both the HA and c-myc epitope tag, as well as only the HA tag is plotted. A bivariate plot of the intensity for both HA (Alexa-Flour 488 antibody) and c-myc (Alexa-Flour 647 antibody) used to generate this bar graph is in **Appendix Figure C.11**..... 130
Figure 6.1. Schematic library design and screening portions. First, lyse the bacteria strain with the plasmid of interest. Next, use ep-PCR to build a diverse library. Finally, transform *S. cerevisiae* with the plasmid to finish the library design portion. Next, screen using FACS, collecting c-myc and HA positive samples and repeat the analysis on the collection for enrichment. Samples are plated and inoculated, after which steps 1-6 are repeated. After the final inoculation, plasmids from the isolated cells can be sequenced to identify the stable mutants. Figure made in BioRender.com. 136
Figure 6.2. Schematic of the yeast endoplasmic reticulum sequestration screening. The peptide construct and protease are signaled for the endoplasmic reticulum, where proteolysis occurs. The peptide construct is then displayed on the surface of the yeast to be screened by flow cytometry. The figure is taken from [117]..... 138
Appendix Figure A.1. Gel images for proteolysis of Hst5 variants by Sap1, Sap2, Sap3, and Sap9..... 144
Appendix Figure A.2. Degradation of Hst5 by purified Sap5, Sap6, or Sap10. After incubation for 2 h at 37 °C, we used gel electrophoresis to separate fragments from fully intact peptides and quantified the gel images using densitometric analysis. Error bars represent the standard error of the mean (N = 9 Hst5 No Sap and Hst5 + Sap, while N = 3 for all other variants). The number of asterisks indicates the level of statistical significance against parent Hst-5 incubated with cells: NS for P > 0.05, * for $P \leq 0.05$, ** for $P \leq 0.01$, and **** for $P \leq 0.0001$..... 145
Appendix Figure A.3. Gel images for proteolysis of Hst5 variants by Sap1, Sap2, Sap3, and Sap9..... 146
Appendix Figure A.4. Mass spectra for the degradation of Hst5, by Sap5, Sap6, and Sap10..... 147
Appendix Figure A.5. Antifungal activity of Hst5 variants after incubation with Sap5, Sap6, or Sap10. After incubation for 2 hrs at 37 °C, Samples were serially diluted in a 96-well plate from 75 µg/mL to .14 µg/mL. Samples were then mixed with *C. albicans* cells at 5.0 × 105 cells/mL and incubated for 30 min at 30 °C in 1 mM NaPB, after which cells were inoculated and cultured. Error bars represent the

standard error of the mean (*N* = 18 Hst5 No Sap and Hst5 + Sap, while *N* = 6 for all other variants). Two-way ANOVA tests with α = .05 and Dunnett's multiple comparison tests (degraded Hst5 as the control) were performed for statistical analysis. P < .05 was deemed as significant. 148
Appendix Figure A.6. Gel images for proteolysis of Hst5 variants by saliva. 149
Appendix Figure B.1. Gel images for proteolysis of Hst5 variants by Sap1, Sap2, Sap3, and Sap9. 150
Appendix Figure B.2. Antifungal activity of Hst5 variants after incubation with Sap5, Sap6, or Sap10. After incubation for 2 hrs at 37 °C, Samples were serially diluted in a 96-well plate from 75 μg/mL to .14 μg/mL. Samples were then mixed with *C. albicans* cells at 5.0 × 105 cells/mL and incubated for 30 min at 30 °C in 1 mM NaPB, after which cells were inoculated and cultured. Error bars represent the standard error of the mean (*N*= 18 Hst5 No Sap and Hst5 + Sap, while *N* = 6 for all other variants). Two-way ANOVA tests with α = .05 and Dunnett's multiple comparison tests (degraded Hst5 as the control) were performed for statistical analysis. P < .05 was deemed as significant. 151
Appendix Figure B.3. Gel images for proteolysis of Hst5 variants by Sap1, Sap2, Sap3, and Sap9. 153
Appendix Figure B.4. Gel images for proteolysis of Hst5 variants by saliva. 154
Appendix Figure C.1. Expression time optimization profiles for pCTCon2-Hst5 at 20 °C. Bivariate plots of the intensity for both HA (Alexa-Flour 488 antibody) and c-myc (Alexa-Flour 647 antibody) were plotted with quadrants based the *Saccharomyces cerevisiae* EBY100 strain without plasmids. Each dot corresponds to a single cell and heatmaps indicate the number of cells in an area. Percentages represent the percent of total events (cell count) in each quadrant. Q1 represents cells with the c-myc tag but without the HA tag (not expected as the construct starts with the HA tag, possible degradation products), Q2 represents cells with both the c-myc and HA tag (fully expressed construct), Q3 represents cells without both c-myc and HA tag (none of the construct expressed), and Q4 represent represents cells without the c-myc tag but with the HA tag (partially expressed construct). 156
Appendix Figure C.2. Expression temperature and time optimization profiles for pCTCon2-Hst5. Bivariate plots of the intensity for both HA (Alexa-Flour 488 antibody) and c-myc (Alexa-Flour 647 antibody) were plotted with quadrants based the Saccharomyces cerevisiae EBY100 strain without plasmids. Each dot corresponds to a single cell and heatmaps indicate the number of cells in an area. Percentages represent the percent of total events (cell count) in each quadrant. Q1 represents cells with the c-myc tag but without the HA tag (not expected as the construct starts with the HA tag, possible degradation products), Q2 represents cells with both the c-myc and HA tag (fully expressed construct), Q3 represents cells without both c-myc and HA tag (none of the construct expressed), and Q4 represent represents cells without the c-myc tag but with the HA tag (partially expressed construct). 157
Appendix Figure C.3. Linker length optimization profiles for pCTcon2-Hst5, pCT40-Hst5, pCT641-Hst5. Protein expression was induced at 30 °C for 24 hours. Bivariate plots of the intensity for both HA (Alexa-Flour 488 antibody) and c-myc (Alexa-Flour 647 antibody) were plotted with quadrants based the *Saccharomyces cerevisiae* EBY100 strain without plasmids. Each dot corresponds to a single cell and

heatmaps indicate the number of cells in an area. Percentages represent the percent of total events (cell count) in each quadrant. Q1 represents cells with the c-myc tag but without the HA tag (not expected as the construct starts with the HA tag, possible degradation products), Q2 represents cells with both the c-myc and HA tag (fully expressed construct), Q3 represents cells without both c-myc and HA tag (none of the construct expressed), and Q4 represent represents cells without the c-myc tag but with the HA tag (partially expressed construct)..... 158
Appendix Figure C.4. Differentiation between harvested cell and cells that were not harvested for pCTcon2-Hst5 and pCT40-Hst5. Protein expression was induced at 30 °C for 24 hours, harvested cells were pelleted, decanted, and stored at 20 °C, unharvested cells were prepared and the results were compared. Bivariate plots of the intensity for both HA (Alexa-Flour 488 antibody) and c-myc (Alexa-Flour 647 antibody) were plotted with quadrants based the Saccharomyces cerevisiae EBY100 strain without plasmids. Each dot corresponds to a single cell and heatmaps indicate the number of cells in an area. Percentages represent the percent of total events (cell count) in each quadrant. Q1 represents cells with the c-myc tag but without the HA tag (not expected as the construct starts with the HA tag, possible degradation products), Q2 represents cells with both the c-myc and HA tag (fully expressed construct), Q3 represents cells without both c-myc and HA tag (none of the construct expressed), and Q4 represent represents cells without the c-myc tag but with the HA tag (partially expressed construct). 159
Appendix Figure C.5. Initial degradation profile for pCT40-Hst5 at varying concentrations. Protein expression was induced at 30 °C for 24 hours. Cells were then pelleted, washed, and suspended in Sap9 at varying concentrations in 2 mM NaPB. Samples were incubated at 30 °C for 24 hours. Bivariate plots of the intensity for both HA (Alexa-Flour 488 antibody) and c-myc (Alexa-Flour 647 antibody) were plotted with quadrants based the Saccharomyces cerevisiae EBY100 strain without plasmids. Each dot corresponds to a single cell and heatmaps indicate the number of cells in an area. Percentages represent the percent of total events (cell count) in each quadrant. Q1 represents cells with the c-myc tag but without the HA tag (not expected as the construct starts with the HA tag, possible degradation products), Q2 represents cells with both the c-myc and HA tag (fully expressed construct), Q3 represents cells without both c-myc and HA tag (none of the construct expressed), and Q4 represent represents cells without the c-myc tag but with the HA tag (partially expressed construct)..... 160
Appendix Figure C.6. Degradation profile for pCT40-Hst5 with Sap9 at varying pH. Protein expression was induced at 30 °C for 24 hours. Cells were then pelleted, washed, and suspended in 100 µL of 100 µg/mL Sap9 in 2 mM NaPB at various pH. Samples were incubated at 37 °C for 24 hours. Bivariate plots of the intensity for both HA (Alexa-Flour 488 antibody) and c-myc (Alexa-Flour 647 antibody) were plotted with quadrants based the Saccharomyces cerevisiae EBY100 strain without plasmids. Each dot corresponds to a single cell and heatmaps indicate the number of cells in an area. Percentages represent the percent of total events (cell count) in each quadrant. Q1 represents cells with the c-myc tag but without the HA tag (not expected as the construct starts with the HA tag, possible degradation products), Q2 represents cells with both the c-myc and HA tag (fully expressed construct), Q3 represents cells

without both c-myc and HA tag (none of the construct expressed), and Q4 represent represents cells without the c-myc tag but with the HA tag (partially expressed construct)..... 161
Appendix Figure C.7. Degradation profile for pCT40-Hst5 with No Sap, Sap1, Sap2, Sap3, and Sap9. Protein expression was induced at 30 °C for 24 hours. Cells were then pelleted, washed, and suspended in 100 µL of 100 µg/mL Sap9 in 2 mM NaPB at pH 7.4. Samples were incubated at 37 °C for 24 hours. Bivariate plots of the intensity for both HA (Alexa-Flour 488 antibody) and c-myc (Alexa-Flour 647 antibody) were plotted with quadrants based the *Saccharomyces cerevisiae* EBY100 strain without plasmids. Each dot corresponds to a single cell and heatmaps indicate the number of cells in an area. Percentages represent the percent of total events (cell count) in each quadrant. Q1 represents cells with the c-myc tag but without the HA tag (not expected as the construct starts with the HA tag, possible degradation products), Q2 represents cells with both the c-myc and HA tag (fully expressed construct), Q3 represents cells without both c-myc and HA tag (none of the construct expressed), and Q4 represent represents cells without the c-myc tag but with the HA tag (partially expressed construct). 162
Appendix Figure C.8. Degradation profile for pCT40-Hst5 after incubation with Sap2 at varying times. Protein expression was induced at 30 °C for 24 hours. Cells were then pelleted, washed, and suspended in 100 µL of 100 µg/mL Sap2 in 2 mM NaPB at pH 7.4. Samples were incubated at 37 °C for 24 hours. Bivariate plots of the intensity for both HA (Alexa-Flour 488 antibody) and c-myc (Alexa-Flour 647 antibody) were plotted with quadrants based the *Saccharomyces cerevisiae* EBY100 strain without plasmids. Each dot corresponds to a single cell and heatmaps indicate the number of cells in an area. Percentages represent the percent of total events (cell count) in each quadrant. Q1 represents cells with the c-myc tag but without the HA tag (not expected as the construct starts with the HA tag, possible degradation products), Q2 represents cells with both the c-myc and HA tag (fully expressed construct), Q3 represents cells without both c-myc and HA tag (none of the construct expressed), and Q4 represent represents cells without the c-myc tag but with the HA tag (partially expressed construct). 163
Appendix Figure C.9. Degradation profile for pCT40-Hst5 after incubation with Sap2 at varying concentrations. Protein expression was induced at 30 °C for 24 hours. Cells were then pelleted, washed, and suspended in 100 µL of Sap2 (at concentrations listed in the figure) in 2 mM NaPB at pH 7.4. Samples were incubated at 37 °C for 30 min. Bivariate plots of the intensity for both HA (Alexa-Flour 488 antibody) and c-myc (Alexa-Flour 647 antibody) were plotted with quadrants based the Saccharomyces cerevisiae EBY100 strain without plasmids. Each dot corresponds to a single cell and heatmaps indicate the number of cells in an area. Percentages represent the percent of total events (cell count) in each quadrant. Q1 represents cells with the c-myc tag but without the HA tag (not expected as the construct starts with the HA tag, possible degradation products), Q2 represents cells with both the c-myc and HA tag (fully expressed construct), Q3 represents cells without both c-myc and HA tag (none of the construct expressed), and Q4 represent represents cells without the c-myc tag but with the HA tag (partially expressed construct)..... 164

Appendix Figure C.10. Degradation profile for pCTCon2-st5, pCT40-Hst5, and pCT641-Hst5 after incubation with Sap2. Protein expression was induced at 30 °C for 24 hours. Cells were then pelleted, washed, and suspended in 100 µL of 0.39 µg/mL Sap2 in 2 mM NaPB at pH 7.4. Samples were incubated at 37 °C for 30 min. Bivariate plots of the intensity for both HA (Alexa-Flour 488 antibody) and c-myc (Alexa-Flour 647 antibody) were plotted with quadrants based the *Saccharomyces cerevisiae* EBY100 strain without plasmids. Each dot corresponds to a single cell and heatmaps indicate the number of cells in an area. Percentages represent the percent of total events (cell count) in each quadrant. Q1 represents cells with the c-myc tag but without the HA tag (not expected as the construct starts with the HA tag, possible degradation products), Q2 represents cells with both the c-myc and HA tag (fully expressed construct), Q3 represents cells without both c-myc and HA tag (none of the construct expressed), and Q4 represent represents cells without the c-myc tag but with the HA tag (partially expressed construct)..... 165
Appendix Figure C.11. Degradation profile for pCT40-Hst5, pCT40-K11RK17R, and pCT40-K13L after incubation with Sap2. Protein expression was induced at 30 °C for 24 hours. Cells were then pelleted, washed, and suspended in 100 µL of 0.39 µg/mL Sap2 in 2 mM NaPB at pH 7.4. Samples were incubated at 37 °C for 30 min. Bivariate plots of the intensity for both HA (Alexa-Flour 488 antibody) and c-myc (Alexa-Flour 647 antibody) were plotted with quadrants based the *Saccharomyces cerevisiae* EBY100 strain without plasmids. Each dot corresponds to a single cell and heatmaps indicate the number of cells in an area. Percentages represent the percent of total events (cell count) in each quadrant. Q1 represents cells with the c-myc tag but without the HA tag (not expected as the construct starts with the HA tag, possible degradation products), Q2 represents cells with both the c-myc and HA tag (fully expressed construct), Q3 represents cells without both c-myc and HA tag (none of the construct expressed), and Q4 represent represents cells without the c-myc tag but with the HA tag (partially expressed construct)..... 166

List of Abbreviations

HIV: Human immunodeficiency virus
C. albicans: Candida albicans
C. glabrata: Candida glabrata
AmB: Amphotericin B
AMP: Antimicrobial peptides
Hst: Histatin
Hst5: Histatin 5
Saps: Secreted aspartyl proteases
GPI: Glycosylphosphatidylinositol
NaPB: Sodium phosphate buffer
PBS: Phosphate buffered saline
YSD: Yeast surface display
YPD: Yeast extract-peptone-dextrose
OD_{600}: Optical density measured at 600 nm
XTT: 2,3-Bis-(2-Methoxy-4-Nitro-5-Sulfophenyl)-2H-Tetrazolium-5-Carboxanilide
SpIB: *Staphylococcus aureus* serin-protease-like protease
A2M: Alpha-2-macroglobulins
AmpR: Ampicillin resistance
S. cerevisiae: *Saccharomyces cerevisiae*
E. coli: Escherichia coli
GAL1/10: Galactose promotor
Aga1: a-agglutinin 1
Aga2: a-agglutinin 2
HA: Hemagglutinin
POI: Protein/peptide of interest
FITC: Fluorescein isothiocyanate
SA: Streptavidin
SD-CAA: Synthetic dextrose casamino acids
SG-CAA: Synthetic galactose casamino acids
YEP-gal Yeast extract peptone galactose
Q1-4: Quadrant 1-4
Ep-PCR: error prone PCR
ER: Endoplasmic reticulum
YESS: Yeast endoplasmic reticulum sequestration screening

1. Chapter 1: Introduction

1.1. *Candida albicans*

Candida albicans is a commensal fungal pathogen that inhabits the oral flora of 30% to 50% of people [1]. However, in patients who are immunocompromised with diseases such as diabetes and HIV, as well as genetic diseases such as Down syndrome [2-7], *C. albicans* can cause an array of infections, most notably oral candidiasis [4]. A key characteristic in the cell's virulence is the morphological switch, between yeast form or the hyphal form (**Figure 1.1**).

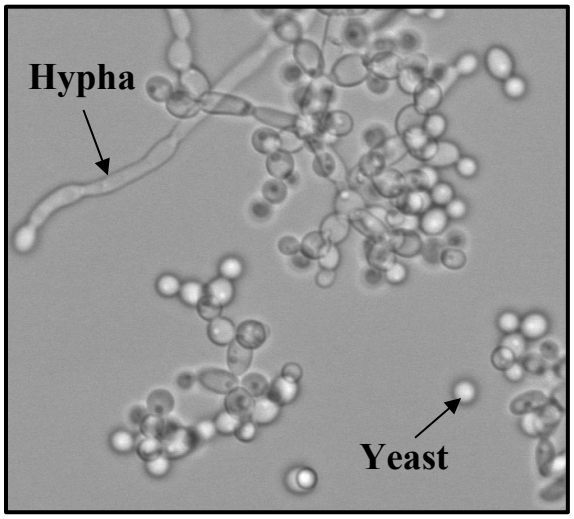

Figure 1.1. Microscope image of the yeast and hyphae morphologies of *C. albicans*.

While the structural compositions of the *C. albicans* cell membrane and cell wall change during the shift from yeast to hyphae, key components are retained. The cell

wall consists of β-(1,3)-glucans whose synthesis is governed by the genes FKS1, *FKS2*, and *FKS3* [8-10] and β-(1,6)-glucans, which links proteins to the cell wall [11]. The cell wall also consists of chitin, which helps maintain cell integrity [12], and mannoproteins, which make up the outer layer of the cell wall, while the cell membrane integrity is maintained by ergosterol and other lipids [13, 14]. These components form the protective barriers of the cell; however, they also provide targets for drug design.

1.2. Antifungal drug resistance

Small-molecule antifungal agents are effective in dealing with infections caused by *C. albicans* because of their selectivity for certain components in the cell structure. However, some of these agents can be toxic to human cells, and *C. albicans* can either be intrinsically or inherently resistant to these agents [8, 15-18]. The three most prominent classes of antifungal agents are polyenes, azoles, and echinocandins. Polyenes such as amphotericin B (AmB) interact with the ergosterol in the fungal cell membrane, eventually forming pores in the membrane [19-21] (**Figure 1.2**). Fungal cells can resist AmB by reducing the amount of ergosterol produced or using another sterol to maintain the cell wall [22] (**Figure 1.3**). Azoles, on the other hand, work as inhibitors of the 14-α-demethylase enzyme, which prevents ergosterol formation and increases toxic byproducts (**Figure 1.2**). These classes of drugs include itraconazole and fluconazole [23, 24]. Several mechanisms of resistance have been reported for resistance to azoles, such as mutations to 14-α-demethylase [16, 25], overexpression of the cdr1p and cdr2p efflux pumps [26], and overexpressing ergosterol [13] (**Figure**

1.3). Echinocandins such as caspofungin target (1,3) β-D glucan synthase, which is essential for the formation of the cell wall (**Figure 1.2**). Resistance to this class of drugs is through mutations in (1,3) β-D glucan synthase [9] (**Figure 1.3**). With toxicity and fungal resistance still contributing to the reduction in the efficacy of this agent, other potential therapeutic agents need to be considered.

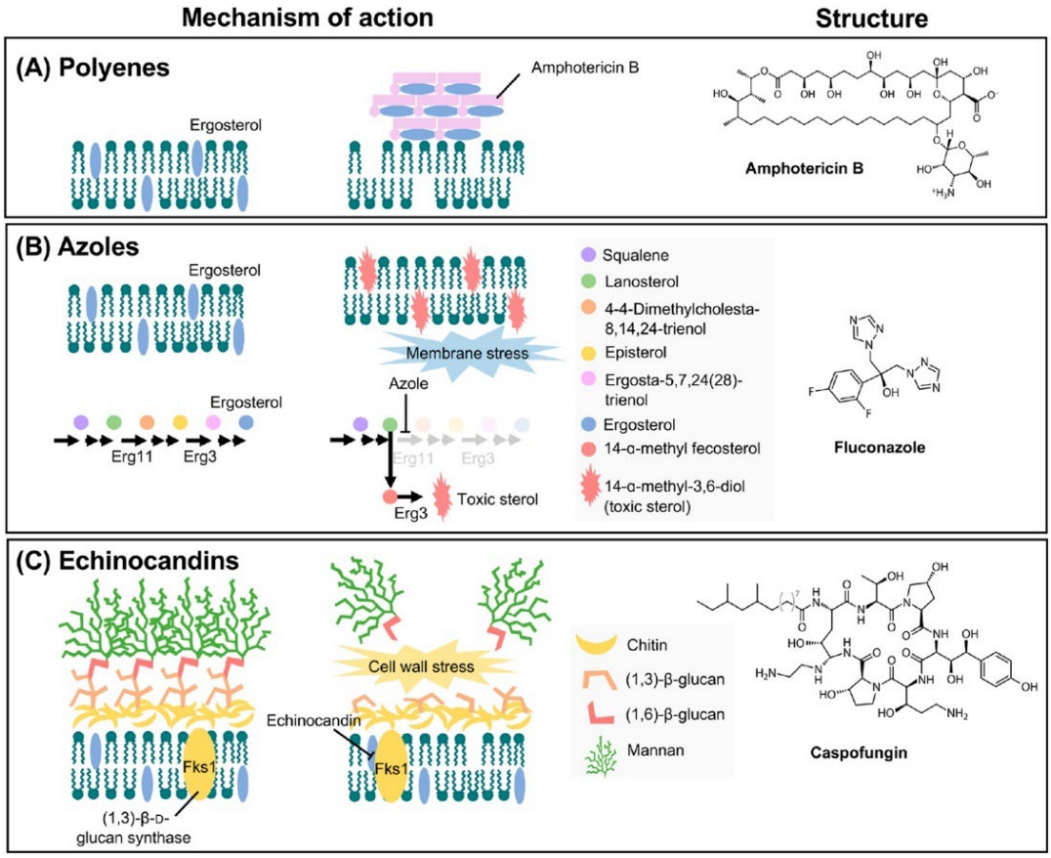

Figure 1.2. Mechanism of action and example of antifungal agents against *C. albicans.* **A)** Polyene such as AmB interact with ergosterol to disrupt the cell membrane, **B)** azoles such as fluconazole inhibit the formation of ergosterol and instead form toxic sterols that cause membrane stress, and **C)** echinocandins such as caspofungin prevent the formation (1,3) β-D glucan synthase. Figure reprinted with permission from [23]. Copyright © 2020, American Chemical Society.

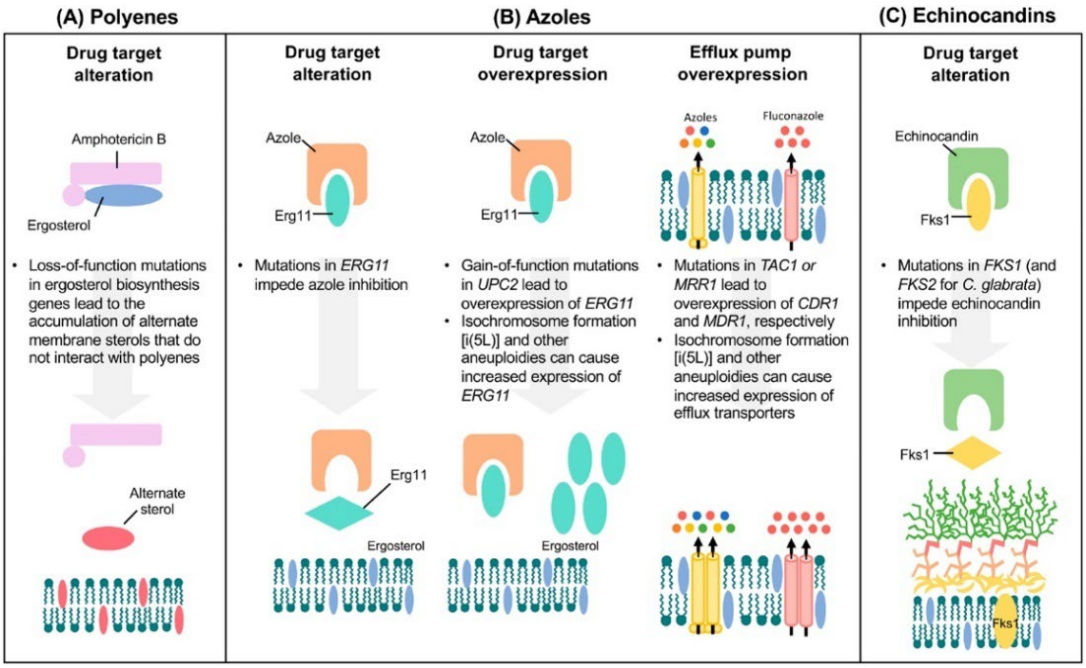

Figure 1.3. Mechanism of resistance to antifungal agents by *C. albicans*. **A)** For polyenes, alternative sterols are used to maintain the membrane structure. **B)** Resistance to azoles can occur through multiple mechanisms, overexpression of ergosterol, and expression of efflux pumps to remove azoles from the cell. **C)** For echinocandins, mutations in Fks1p prevent binding. Figure reprinted with permission from [23]. Copyright © 2020, American Chemical Society.

1.3. Antimicrobial peptides

AMPs are generally 10 to 60 amino acids in length and offer an attractive alternative to current small-molecule antimicrobial agents. Certain antimicrobial peptides (AMPs) can be found naturally in the human body, so they are often not toxic; additionally, the development of microbial resistance to AMPs is unlikely [27-29]. These peptides play an important role in the human immune system - for example, cathelicidin LL-37 and human beta-defensin 2 act as the body's first line of defense against pathogens like bacteria, fungi, and viruses [28].

The mechanisms of action of different AMPs vary, much like small-molecule antifungal drugs. As most AMPs interact with the cell membrane, interactions are separated into membrane targeting mechanisms, where pores are formed on the

surface of the cell, and non-membrane targeting mechanisms. The non-membrane targeting mechanisms involve inhibiting processes such as protein synthesis, enzymatic activity, and cell wall synthesis [28].

A small subset of these AMPs have antifungal activity. Histatins are a family of histidine-rich antimicrobial salivary peptides found in humans. From this family, the most active is Hst5, a 24 amino acid peptide with a sequence of DSHAKRHHGYKRKFHEKHHSHRGY and a proteolytic derivative of histatin 3 [30]. Hst5 has activity against most drug-resistant strains of *C. albicans* **[31],** making it an attractive option for further work. Reduced levels of Hst5 have been observed in HIV+ patients and children with Down syndrome, leading to oral legions. These patients are susceptible to more oral candidiasis, indicating that low levels of Hst5 could contribute to high levels of oral candidiasis [6, 32, 33]. Hst5 will be discussed in more detail in Chapter 2.

1.4. *Secreted aspartyl proteases*

One limitation of Hst5 is its proteolytic stability to proteases from *C. albicans* and other proteases in saliva [34-38]. Secreted aspartyl proteases (Saps) are a family of 10 proteases produced by *C. albicans* and are known to contribute to the virulence of the *C. albicans*. While the mechanism of production has only been shown for Sap2, it is hypothesized that these Saps are translated in the endoplasmic reticulum and undergo a series of post-translational modifications to produce the mature protease, which is fully secreted to either the extracellular space (Sap1-8) or glycosylphosphatidylinositol anchors (Sap9-10) [36, 39-42] (**Figure 1.4**).

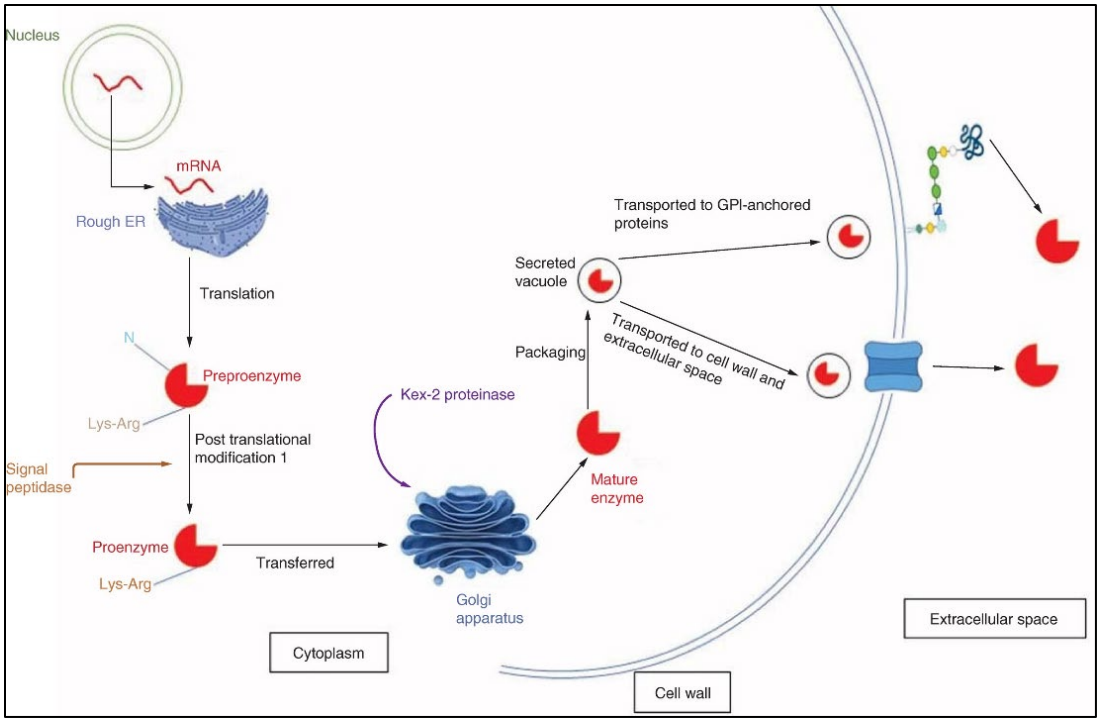

Figure 1.4. Schematic of the mechanism of secretion for Saps. mRNA is translated in the rough endoplasmic reticulum (ER) and forms the enzymes in their preproenzyme form. The signaling peptide is removed via by a signal peptidase forming the proenzyme. This enzyme is further processed by Kex-2 proteinase, which activates them to their mature form. These enzymes are transported by vacuoles either to their GPI anchor or the extracellular space. Figure reprinted with permission from [41]. Copyright © 2022, Future Medicine.

Similar to other aspartyl proteases, Saps contain the characteristic two catalytic aspartic acid residues in their active site (**Figure 1.5**). These proteases have been shown to degrade molecules that are essential to the immune resume such as C3b, C4, and C5 of the complement system as well as Hst5[36, 43]. Unlike most other proteases, their proposed mechanism of action does not involve an intermediate formed between the protease and protein. While hydrogen bonding maintains the interaction between the two molecules, a reactive water molecule acts as the nucleophile and hydrogen bond donor to perform the hydrolysis at the peptide bond of the protein [44] (**Figure 1.6**).

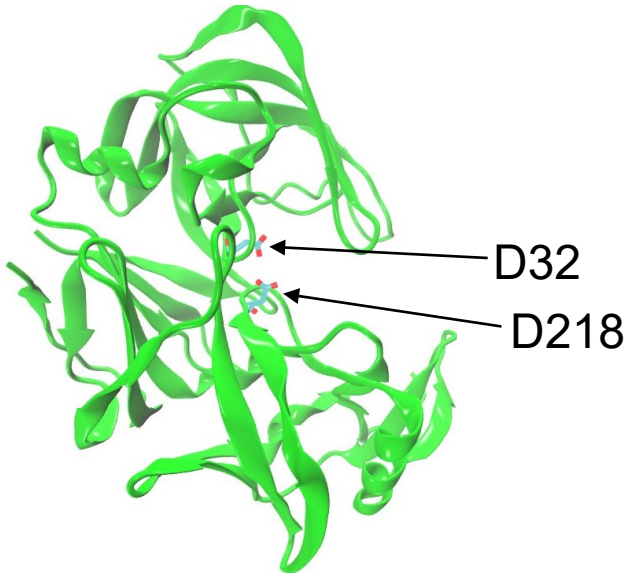

Figure 1.5. Structure of Sap2 (1eag PDB), predicted by Robetta. Figure reprinted with permission from Copyright © 2019, Springer Natural Limited.

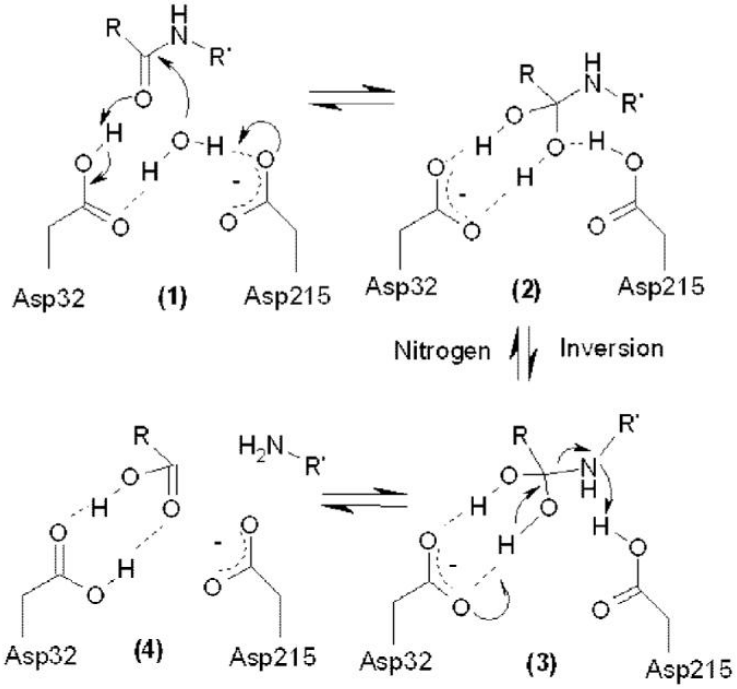

Figure 1.6. Schematic of the mechanism of action for aspartyl proteases mediated by the Asp32 and Asp215 residues. **1)** Asp32 is deprotonated by the carboxyl oxygen of the protein, Asp215

deprotonates water, and the oxygen in water acts as a nucleophile and bonds to the carboxyl carbon of the protein. **2)** The protein rotates at the amino acid amine group. **3)** Asp32 deprotonates hydroxyl oxygen, which forms a carboxyl double bond in the protein, Asp215 donates hydrogen to the protein amine group, and the amine acts as a leaving group, completing the hydrolysis. **4)** The final structure with Asp32 and Asp215 returned to their original state and the protein cleaved. Figure reprinted with permission from Copyright © 2008, American Chemical Society.

1.5. *Interactions of Hst5 with Saps*

While Hst5 is a promising antifungal option, its susceptibility to these proteases could hinder its use as an antifungal agent (**Table 1.1**). Puri et al. showed that Hst5 is cleaved by Sap6 when incubated for 1 h at 37 °C in 50 mM NaPB (pH 7.0)**,** and the activity of Hst5 is nearly eliminated after incubation at a 2:1 molar ratio of Hst5 to Sap6 [37]. In another study by Meiller et al., the authors found that Sap2 and Sap9, and, to a lesser extent, Sap10 cleave Hst5 [36]. Bochenska et al. tested these Saps at their optimal pHs – pH 4 (Sap2, Sap3**,** and Sap8), pH 5 (Sap1, Sap4-6 and Sap9) or pH 6 (Sap7 and Sap10) at 37°C. They found that, after incubation with Saps, the antifungal activity of Hst5 drops by more than ~20% for each Sap and that Sap1-6 and Sap8 prefer to cleave near positively charged (Arg and Lys) or large hydrophobic amino acids (Leu, Phe, and Tyr), while Sap7 and Sap9-10 prefer to cleave near Arg and His [38]. Ikonomva et al. designed variants of Hst5 in order to improve the proteolytic stability of the peptide against Sap2 and Sap9. This work shows that Hst5 is cleaved by both proteases when incubated for 2 h at 37 °C in 1 mM NaPB, However variants can be designed with improved proteolytic stability[34, 35]. Although groups looked at the cleavage of Hst5 littler work has been done to reduce the proteolysis by the Saps. **Table 1.1** summarizes the fragments that are formed after proteolysis of Hst5.

Table 1.1. Summary of the fragments found from the degradation of Hst5 by Sap1-10 as found in the literature.

Sequence																											
1	2	3	4	5	6	7	8	9	10	11	12	13	14	15	16	17	18	19	20	21	22	23	24			
D	S	H	A	K	R	H	H	G	Y	K	R	K	F	H	E	K	H	H	S	H	R	G	Y	Ref.	Activity[a]	Sap
D	S	H	A	K	R	H	H	G	Y	K	R	K	F											[35]	-	Sap9
D	S	H	A	K	R	H	H	G	Y	K	R	K												[34-36, 38]	No	Sap2,3, 9
D	S	H	A	K	R	H	H	G	Y	K	R													[34-36]	No	Sap2,9,10
																	H	H	S	H	R	G	Y	[34-36, 38]	No	Sap1,2,3,4,9
D	S	H	A	K	R	H	H	G	Y															[36, 38]	No	Sap2,3,4,8,9
			A	K	R	H	H	G	Y															[38]	-	Sap1
			A	K	R	H	H	G	Y	K	R	K	F	H	E	K									[38]	-	Sap1
D	S	H	A	K	R	H	H	G	Y	K	R	K	F	H	E	K									[34-36, 38]	Yes	Sap1,2,3,4,9
	S	H	A	K	R	H	H	G	Y	K	R	K	F	H	E	K									[35]	-	Sap2
D	S	H	A	K	R	H	H	G	Y	K	R	K	F	H	E	K	H								[34, 35]	Yes	Sap2,9
D	S	H	A	K	R	H	H	G	Y	K	R	K	F	H	E	K	H	H	S	H					[38]	-	Sap7
													F	H	E	K	H	H	S	H	R	G	Y	[34-36, 38]	-	Sap2,3,7,8,9,10
										K	R	K	F	H	E	K	H	H	S	H	R	G	Y	[38]	Yes	Sap4
											R	K	F	H	E	K	H	H	S	H	R	G	Y	[36]	Yes	Sap10
										K	R	K	F	H	E	K								[36, 38]	-	Sap1,2
					R	H	H	G	Y	K	R	K	F	H	E	K									[36]	-	Sap10
D	S	H	A	K	R	H	H	G	Y	K	R	K	F	H	E	K	H	H	S	H	R	G	Y	[34-36, 38]	Yes	Sap2,9,10

** Activity is determined as noted by Helmerhorst et al. [45].*

1.6. Saliva

While proteolysis by these Saps is a large concern, these *C. albicans* infections can happen in the oral microflora, which contains other organisms and their secreted proteases. Saliva is a complex mixture comprising various host proteases like cysteine cathepsins, the serine cathepsin A, the aspartic cathepsin D, and metalloproteases [46], along with microbial proteases secreted by organisms in the oral microbiome [47, 48]. Among these proteases are the Saps, namely Sap1-5, which are present in saliva [49, 50]. This complex mixture can cleave and reduce the activity of Hst5 (**Table 1.2**). Understanding the fragments formed by the proteolysis of Hst5 and saliva involves incubating saliva with Hst5, performing a separation using a reverse phase chromatography column to separate Hst5 and its fragments from each other, and assessing these fragments for further antifungal activity [45]. **Table 1.2**

summarizes the degradation products of Hst5 after incubation with saliva, found in literature. From the fragments two things can be noted: (1) Saps are not the only enzymes degrading on Hst5, (2) fragments made by the degradation of Hst5 can have no activity, potentially reducing the activity of the sample. In thinking about Hst5 as an oral therapeutic, designing these peptides must alse take into consideration salivary proteases.

Table 1.2. Fragments found from the degradation of Hst5 by saliva.

Sequence																										
1	2	3	4	5	6	7	8	9	10	11	12	13	14	15	16	17	18	19	20	21	22	23	24			
D	S	H	A	K	R	H	H	G	Y	K	R	K	F	H	E	K	H	H	S	H	R	G	Y	Ref.	Activity[a]	
				K	R	H	H	G	Y	K	R													[45]	No	
					R	H	H	G	Y	K	R	K												[45]	No	
D	S	H	A	K	R	H	H	G	Y	K														[45, 78]	No	
D	S	H	A	K	R	H	H	G	Y	K	R	K												[45, 78, 91]	No	
D	S	H	A	K	R	H	H	G	Y	K	R													[45, 78]	No	
																		H	S	H	R	G	Y	[45, 78]	No	
																	H	H	S	H	R	G	Y	[45, 78]	No	
D	S	H	A	K	R	H	H	G	Y															[45, 78]	No	
															E	K	H	H	S	H	R	G	Y	[45, 78]	No	
																K	H	H	S	H	R	G	Y	[45, 78]	No	
														H	E	K	H	H	S	H	R	G	Y	[78, 91]	-	
D	S	H	A	K	R	H	H	G	Y	K	R	K	F	H	E	K								[45, 78, 91]	Yes	
D	S	H	A	K	R	H	H	G	Y	K	R	K	F	H	E	K	H							[45, 78]	Yes	
D	S	H	A	K	R	H	H	G	Y	K	R	K	F	H										[45, 78]	Yes	
													F	H	E	K	H	H	S	H	R	G	Y	[45, 78]	-	
D	S	H	A	K	R	H	H	G	Y	K	R	K	F	H	E									[45, 78]	Yes	
										K	R	K	F	H	E	K	H	H	S	H	R	G	Y	[45, 78]	Yes	
											R	K	F	H	E	K	H	H	S	H	R	G	Y	[45, 78]	Yes	
												K	F	H	E	K	H	H	S	H	R	G	Y	[45, 78]	Yes	
													F	H	E	K	H	H	S	H	R			[91]	-	
					R	H	H	G	Y	K	R														[91]	-	
					R	H	H	G	Y	K	R	K	F	H	E	K									[91]	-	
					R	H	H	G	Y	K	R	K	F	H	E	K	H	H	S	H	R	G	Y	[91]	-	
D	S	H	A	K	R	H	H	G	Y	K	R	K	F	H	E	K	H	H	S	H	R	G	Y	[45, 78, 91]	Yes	

[a] *Activity is determined as note by Helmerhorst et al. [45].*

1.7. Engineering strategies

While AMPs are often engineered to improve activity against microbial organisms, their engineering strategies can be leveraged as a tool for understanding the interactions between host and pathogens. These engineering strategies involve either understanding the structure and function of proteins to make guided solutions or screening a library of peptides in a process mimicking natural selection, both aiming to understand how different mutations impact the desired properties of the protein (**Figure 1.7**).

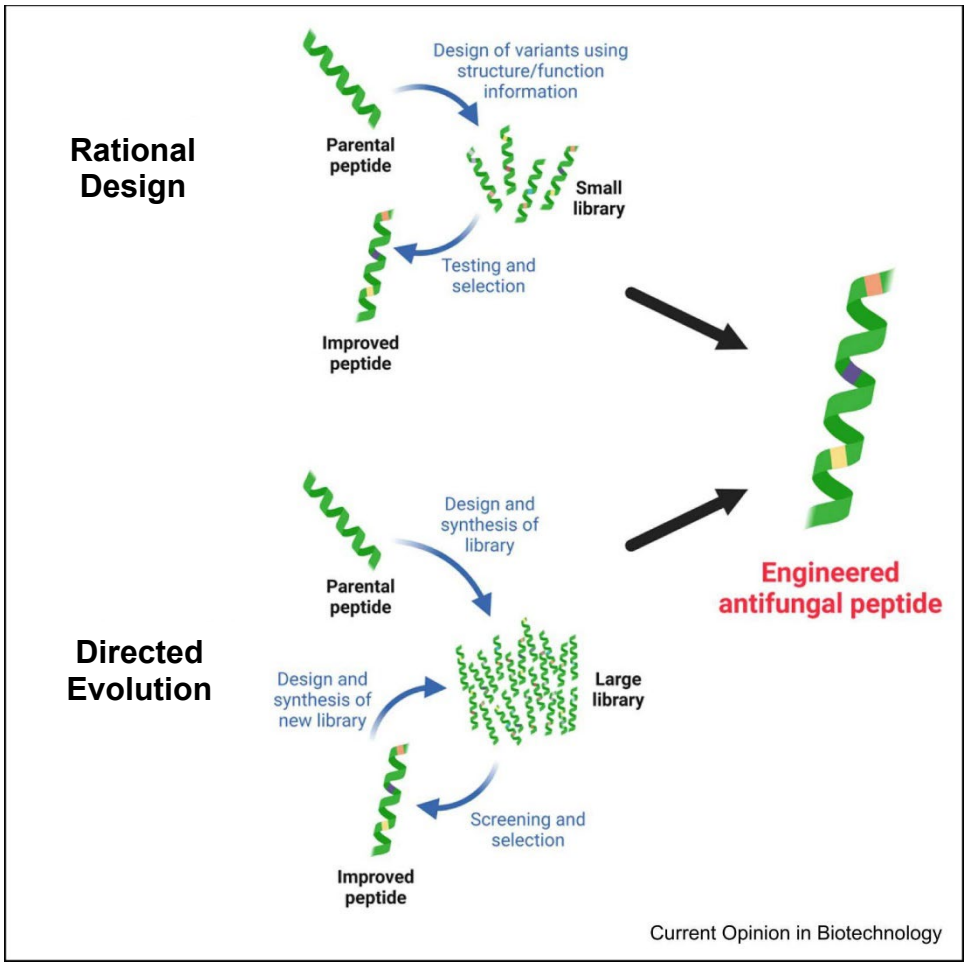

Figure 1.7. Schematic of the engineering strategies to make improved antifungal peptides. Figure reprinted and adapted with permission from [51] Copyright © 2023, Elsevier Ltd.

1.7.1. Rational design

Rational peptide design is a process that leverages knowledge of either the structure or the function of peptides to make rationally guided changes to the peptide sequence. This technique often yields small libraries of peptides that can be screened for desired properties. One example of this is Thennarasu et al. utilizing knowledge of antimicrobial peptide structure to make 3 substitutions (A4K, P7K, or S11K) to turn the 16-mer peptide (GFFALIPKIISSPLFK) that originally had no antimicrobial activity into an antimicrobial peptide, elucidating the roles of lysine in the structure of antimicrobial peptides [52]. Rational design has also been used in engineering protein and proteins for increased proteolytic stability. In order increase the proteolytic stability of ribonuclease A, Markert et al. designed the A20P variants of ribonuclease A, as protease often do not cleave near prolines residues. They were able to dramatically improve the proteolytic stability against both proteinase K and subtilisin Carlsberg [53]. In a study to improve the antibacterial activity of the antimicrobial peptide Pandinin 2, Carmona et al. replaced all of the amino acids in Pandinin 2 with their D isomers. This resulted in an increase in proteolytic stability in the presence of trypsin, elastase, and proteases from *Pseudomonas aeruginosa*. These examples show that rational design can be a powerful tool in enhancing the desired properties of proteins and peptides.

1.7.2. Directed evolution

Directed evolution is often compared to natural selection, where the fitness landscape of a peptide is explored to select the peptide with the desired properties. A key

component of this strategy is that the knowledge of the structure and function of proteins is not required, but it can aid in screening for desired properties [54]. However, an effective screening method is required for the success of this strategy, as variants that do not have an adaptive advantage must be differentiated from those with adaptive advantages [55]. The process of directed evolution is often iterative, where peptide libraries are designed, followed by screening for a desired property, peptides with desired properties are selected, then new peptide libraries are designed based on the new template. The process is repeated until one candidate is selected.

1.7.2.1 Surface display

Of the potential direct evolution platforms, surface display platforms provide a high throughput method of screening peptide libraries. Surface display platforms are used to express a library of proteins on the surface of a host. These proteins can then be screened for a desired property and sequenced to determine the variants of interest. As each cell contains one plasmid, each peptide mutation is linked to a singular cell. While high-yielding display systems such as phage displays and bacterial displays allow us to screen larger libraries of peptides, potentially leading to a more robust peptide discovery, sequences may potentially be toxic to the bacterial host and not be produced, so further optimization is necessary [56]. Furthermore, the small size of bacteriophages and the fact that phage display is primarily used to select for improved binders make it incompatible with fluorescence-activated cell sorting (FACS) or flow cytometry, often needing to be coupled with strategies such as yeast surface display [57].

Yeast surface display provides a powerful platform that utilizes the eukaryotic-like mechanics of yeast cells to produce proteins on their surface. Furthermore, unlike the phage display system, screen variants for desired properties can be performed using flow cytometry [58, 59]. This platform has been used for identifying the best binders [59, 60], and designing proteases to improve proteolytic activity in specific peptides [61]. However, this platform has not been used to screen a peptide library for improved proteolytic stability. The uses of yeast surface display will be covered in more detail in **Chapter 5**.

1.8. *Overview of the thesis.*

This dissertation presents the application of rational design and directed evolution engineering strategies to investigate the interaction between Hst5 and Saps and salivary proteases, aiming to enhance the proteolytic stability of the peptide. In **Chapter 2**, a comprehensive review of previous work to engineer Hst5 is provided, covering improved properties of the peptide, such as proteolytic stability, antifungal activity, and metal binding. **Chapter 3** covers the first experimental section, which introduces our first generation of Hst5 variants. Here, lysine residues are mutated to either leucine or arginine, and proteolytic stability is assessed against saliva and purified Saps, as well as antifungal activity against *C. albicans* SC5314. **Chapter 4** builds on this work by designing a second generation of Hst5 variants at the K13 and K17 residues. The impact of different properties on proteolytic stability and antifungal activity is evaluated. Four variants were selected based on the results: parent Hst5, K13H, K17W, and K11RK17R, and the effects of Zn^{2+} on the

proteolytic stability and antifungal activity of these four variants. **Chapter 5** explores the use of yeast surface display as a potential high throughput screening method for proteolytic stability. Finally, **Chapter 6** provides a summary of the conclusions of this work and recommendations for future studies.

2. Chapter 2: Review of engineering and enhancing the antifungal properties of histatin 5

2.1. *Histatin 5 overview*

Histatins (Hst) are histidine-rich peptides that are naturally found in saliva. While these histidine-rich proteins were first described in 1973 and further characterized in 1976 in the Longton lab [62, 63], their fungicidal ability against *C. albicans* was first described in the 1980s [30, 64]. Oppenheim et al. purified and identified the sequence of three of these Hsts (Hst1, Hst3, and Hst5) and determined that Hst5 is the most active against *C. albicans* [30]. Hst5 is a 24 amino acid, 3036 Da antimicrobial peptide this is produced when histatin 3 is proteolytically processed in saliva (**Table 2.1**) [30]. This peptide is known for having a broad array of activity against other *Candida* species and has a concentration of 2.1 – 16.9 μg/mL in saliva [31, 65].

Table 2.1. The sequence of Hst3 and proteolytic biproduct in the presence of saliva Hst5.

Peptide	Sequence																															
	1	2	3	4	5	6	7	8	9	10	11	12	13	14	15	16	17	18	19	20	21	22	23	24	25	26	27	28	29	30	31	32
Histatin 3	D	S	H	A	K	R	H	H	G	Y	K	R	K	F	H	E	K	H	H	S	H	R	G	Y	R	S	N	Y	L	Y	D	N
Histatin 5	D	S	H	A	K	R	H	H	G	Y	K	R	K	F	H	E	K	H	H	S	H	R	G	Y								

2.2. *Hst5 structure and mechanism of action*

The structure of antimicrobial peptides often plays an important role in their activity. Similar to other antimicrobial peptides, Hst5 is unstructured in water. However, in the presence of a hydrophobic solvent (trifluoroethanol) it adopts an α-helical structure [66]. While most antimicrobial peptides form α-helical structures to disrupt the

membrane and internalize into the cell, Hst5's exact mechanism for internalization is still unknown. It is believed that upon binding with the cell wall, Hst5 interacts with the heat shock protein Ssa1p/2p, which leads to the internalization of Hst5 into the cell through the Dur3p/31p transporters [67-70]. When Hst5 enters the cell, it targets the mitochondria, eventually causing an efflux of ATP and the formation of reactive oxygen species (**Figure 2.1**) [71]. Notably, while Hst5 has activity against a broad range of *Candida* spp, it lack activity against species like *C. glabrata* that lack Dur3p/Sur31p transporters [72].

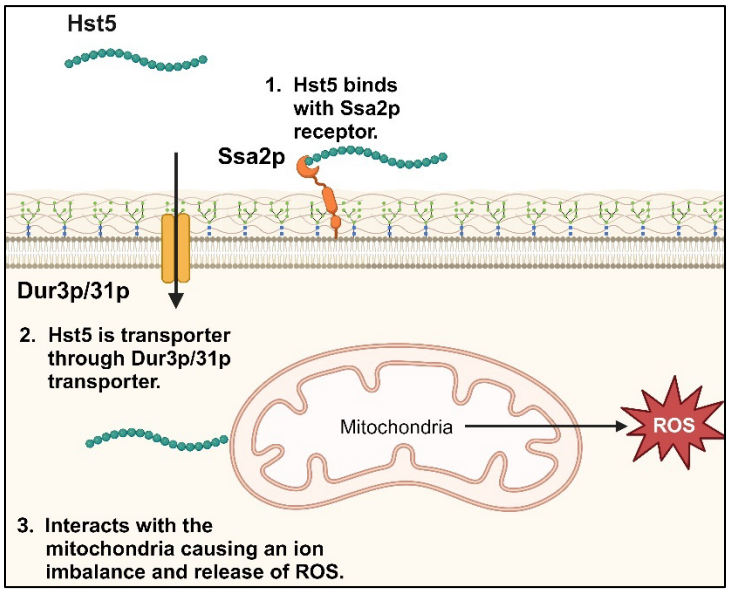

Figure 2.1. Schematic of the mechanism of action of Hst5 against *C. albicans*. The Hst5 peptide 1) interacts with the Ssa2 heat shock protein receptor, 2) transports through the Dur3/31 transporters, and 3) interacts with the mitochondria leading to release of reactive oxygen species. Figure made in BioRender.com

Rational design has been used to engineer various properties of Hst5 to deepen our understanding of how Hst5 interacts with *C. albicans*. In this section, we discuss the design and study of various Hst5 truncations and variants aimed at enhancing our grasp of these interactions. Through a detailed examination of these engineered

peptides, we seek to help develop more effective engineering strategies for future studies.

2.3. *Engineering for antifungal activity*

The most commonly engineer property for Hst5 is its antifungal activity. Hst5 has the greatest antifungal activity against *C. albicans*. However, the entire peptide is not necessary for its antimicrobial activity. Truncated versions of this peptide, such as P-113 and dh-5, have been shown to exhibit greater or similar antifungal activity compared to the parent Hst5 (**Table 2.2**) [72, 73], showing the fragments of Hst5 can retain their activity. Several truncations of the Hst5 peptide have been assessed in the identification of the P-113 (**Table 2.2**). Sequences such as P-112, P-114 – P-120, and P-123 which are different sequence truncations of Hst5, did not have antifungal activity at a concentration below 80 μg/mL. Only the P-113 had enhanced activity compared to Hst5 by a factor of ~2.0. A similar process was done to identify the dh-5, truncated variants of the Hst5 were designed beginning (N-terminus), end (C-terminus), or middle. These variants, named N16, C16, C14, C12, C10, and M10, were then tested for enhanced antifungal activity. Of these, only the dh-5, also known as C14, had similar activity to Hst5 (**Table 2.2**) [73]. The identification of the P-113 and dh-5 truncation shows further truncations of Hst5 may need to be considered and modification made to improve their antifungal activity.

Table 2.2. Truncations of Hst5 designed to assess antifungal activity against *C. albicans*.

	Sequence[a]																									
	1	2	3	4	5	6	7	8	9	10	11	12	13	14	15	16	17	18	19	20	21	22	23	24		
Name	D	S	H	A	K	R	H	H	G	Y	K	R	K	F	H	E	K	H	H	S	H	R	G	Y	Ref.	Activity
P-113				A	K	R	H	H	G	Y	K	R	K	F	H										[72]	Enhanced
dh-5/C14											K	R	K	F	H	E	K	H	H	S	H	R	G	Y	[73]	Similar
N16	D	S	H	A	K	R	H	H	G	Y	K	R	K	F	H	E									[73]	Reduced
C16									G	Y	K	R	K	F	H	E	K	H	H	S	H	R	G	Y	[73]	Similar
M10							H	H	G	Y	K	R	K	F	H	E									[73]	Reduced
C12/P-116													K	F	H	E	K	H	H	S	H	R	G	Y	[72,73]	Reduced
C10															H	E	K	H	H	S	H	R	G	Y	[73]	Reduced
P-123	D	S	H	A	K	R	H	H	G	Y	K	R	K	F											[72]	Reduced
P-103					K	R	H	H	G	Y	K	R	K	F	H	E	K	H	H	S	H	R			[72]	Reduced
P-112	D	S	H	A	K	R	H	H	G	Y	K	R													[72]	Reduced
P-114							H	H	G	Y	K	R	K	F	H	E	K	H							[72]	Reduced
P-115										Y	K	R	K	F	H	E	K	H	H	S	H				[72]	Reduced
P-117					K	R	H	H	G	Y	K	R	K	F	H										[72]	Reduced
P-118				A	K	R	H	H	G	Y	K	R	K	F											[72]	Reduced
P-119				A	K	R	H	H	G	Y	K	R	K												[72]	Reduced
P-120				A	K	R	H	H	G	Y	K	R													[72]	Reduced

[a] *The activity reported is with respect to the parent peptide Hst5.*

Rational design is not limited to identifying fragments that have a function of interest; mutations can be performed to identify the optimal amino acids to enhance function or possibly enhance them. Mutations in the amino acid sequence of a protein can help determine the effect of specific residues on the protein's properties and function. The ability of the Hst5 protein to internalize into *C. albicans* cells is a critical property. Certain substitutions to the P-113 peptide can prevent it from entering the cell, thereby hindering its antimicrobial activity. For example, the 113Q2.10 substitution allows the protein to accumulate on the surface of *C. albicans*, but it is not internalized (**Table 2.3**) [68]. In the study for antifungal activity studying variants of the truncated versions of peptides can further elucidate the role of specific residues on antifungal activity.

Table 2.3. Mutants of Hst5 designed to assess antifungal activity and their antifungal activity against *C. albicans.* The activity reported is with respect to the parent peptide for each section Hst5, dh-5, and P-113.

	Sequence [a,b,c]																										
	1	2	3	4	5	6	7	8	9	10	11	12	13	14	15	16	17	18	19	20	21	22	23	24			
Name	D	S	H	A	K	R	H	H	G	Y	K	R	K	F	H	E	K	H	H	S	H	R	G	Y		Ref.	Activity
F14A/H15A	-	-	-	-	-	-	-	-	-	-	-	-	-	A	A	-	-	-	-	-	-	-	-	-		[74]	Reduced
H18A/H19A	-	-	-	-	-	-	-	-	-	-	-	-	-	-	-	-	-	A	A	-	-	-	-	-		[74]	Reduced
reHsn-5	G	-	-	-	-	-	-	-	-	-	-	-	-	-	-	-	-	-	-	-	-	-	-	-		[74]	Similar
m1	-	-	-	-	-	-	-	-	-	-	-	I	-	-	-	-	-	-	-	-	-	-	-	-		[74]	Similar
m2	-	-	-	-	-	-	-	-	-	-	-	I	-	-	-	-	N	-	-	-	-	-	-	-		[74]	Similar
m12	-	-	-	-	-	-	-	-	-	-	-	I	-	-	-	-	-	-	-	-	L	-	-	-		[74]	Similar
m21	-	-	-	-	-	-	-	-	-	-	-	-	T	-	-	-	-	-	-	-	-	-	-	-		[74]	Reduced
m68	-	-	-	-	-	-	-	-	-	-	-	-	E	-	-	-	-	-	-	-	-	G	-	-		[74]	Reduced
m70	-	-	-	-	-	-	-	-	-	-	-	-	-	-	-	-	-	-	P	-	R		-	-		[74]	Similar
m71	-	-	-	-	-	-	-	-	-	-	-	-	E	-	-	-	-	-	-	-	-	-	-	-		[74]	Reduced
P-113				A	K	R	H	H	G	Y	K	R	K	F	H	NH_3											
P-113D				a	q	r	h	h	g	y	k	r	q	f	h	NH_3										[72]	Similar
113-F4.5.12				-	-	-	-	F	F	-	-	-	-	-	F	NH_3										[72]	Similar
113-Y4.5.12				-	-	-	-	Y	Y	-	-	-	-	-	Y	NH_3										[72]	Similar
113-L4.5.12				-	-	-	-	L	L	-	-	-	-	-	L	NH_3										[72]	Similar
113-Q2.10				-	-	Q		-	-	-	-	-	Q	-	-	NH_3										[72]	Reduced
113-Q3.9				-	-	-	Q	-	-	-	-	Q	-	-	-	NH_3										[72]	Reduced
113-Q2.3.9.10				-	-	Q	Q	-	-	-	-	Q	Q	-	-	NH_3										[72]	Reduced
113-K6				-	-	-	-	-	K	-	-	-	-	-	-	NH_3										[72]	Similar
113-H8				-	-	-	-	-	-	-	H	-	-	-	-	NH_3										[72]	Similar
113-K6H8				-	-	-	-	-	K	-	H	-	-	-	-	NH_3										[72]	Similar
dh-5/C14											K	R	K	F	H	E	K	H	H	S	H	R	G	Y			
dh15K											-	-	-	-	K	-	-	-	-	-	-	-	-	-		[76]	Similar
dh13L											K	R	K	L	F	H	E	K	H	H	S	H	R	G	Y	[76]	Similar
dh17L											-	-	-	-	-	-	L	-	-	-	-	-	-	-		[76]	Similar
dh18L											-	-	-	-	-	-	-	L	-	-	-	-	-	-		[76]	Similar
dh18K											-	-	-	-	-	-	-	K	-	-	-	-	-	-		[76]	Similar
dh19K											-	-	-	-	-	-	-	-	K	-	-	-	-	-		[76]	Similar
dh21F											-	-	-	-	-	-	-	-	-	-	F	-	-	-		[76]	Similar
dh23K											-	-	-	-	-	-	-	-	-	-	-	-	K	-		[76]	Similar
dhVar1											-	-	L	-	K	-	L	K	F	-	L	-	K	-		[76]	Enhanced
dhVar2											-	-	L	-	K	-	L	L	F	-	L	-	K	-		[76]	Enhanced
dhVar4											-	-	L	-	K	K	L	L	F	-	L	-	K	-		[77]	Enhanced
dhVar5											L	L	L	-	L	L	-	K	R	K	K	-	K	-		[77]	Enhanced

[a] *Red text represents insertion.*
[b] *The hyphens represent retained amino acids.*
[c] *NH_3 represents Hst5 variants with C terminal amidation.*

Understanding the mechanisms of action is important, but it can be time and resource-intensive. Screening for antifungal activity may just be sufficient. In this case, mutations could result in peptides with enhanced antifungal properties compared to the parent peptide. Tsai et al. used this strategy for substituting the D1, R12, K13,

K17, H19, H21, and R22 amino acids of Hst5 to identify important residues in the sequence (**Table 2.3**). Of these residues, K13 and Arg22 were important for the peptide [74]. Tsai et al. follow up this study with the variants F14A/H15A and H18A/H19A; both substitutions reduce the activity of Hst5, affirming the importance of the F14/H15 and H18/H19 residues [75]. In both cases, most mutations are coupled, and not all are individually assessed, so it may be difficult to differentiate important individual residues from combinations that may be important. When Rothstein et al. first described the peptide P-113, they studied how mutations to specific residues would impact the antifungal activity (**Table 2.3**). From these variants, we see that substituting all amino acids with their D-amino acid counterparts does not impact antifungal activity and that the lysine residues are essential for antifungal activity [72]. This shows following the direct path and engineering for the function, in this case antifungal activity, can also provide results.

The continuation of work by Tsai and Rothstein could involve substituting residues with amino acids of different properties to understand what interactions are important, followed by a separate investigation on how coupling different residues impacts activity. This will make for a time and resource-intensive investigation but would increase the likelihood of identifying important residues and coupled interactions. However, all residues may not need to be explored; knowledge of the peptide structure may reduce the sequence space that needs to be explored.

Knowledge of the structure of Hst5 also makes it possible to design more active variants. Hst5 forms a weakly amphipathic α-helix in hydrophobic solutions.

Utilizing this knowledge, Helmerhorst et al. designed variants of the dh-5 to assess the impact of amphipathicity on the peptide's antifungal activity (**Table 2.3**). While single point mutations did not impact the antifungal activity of the peptide (dh13L – dh23K), when they were combined into dhvar1 and dhvar2, the antifungal activity of the peptides was greatly improved [76]. To continue the study on the dhvar variants Ruissen et al. designed the dhvar4 (more amphipathic than Hst5) and dhvar5 (as amphipathic as Hst5). The role of amphathicity in the antifungal activity is clearly shown here, where all peptides were able to enter the cell; however, only dhvar4 was active despite incubating cells with NaN_3 which protects the mitochondria from Hst5, by reducing ATP output [77]. Increasing the peptide's amphiphilicity improved its antifungal activity, showing that engineering these peptides to enhance their secondary structure properties may potentially improve their antifungal activity.

2.4. *Proteolytic stability*

One limitation to Hst5, is that proteases secreted by *C. albicans* and proteases in saliva can cleave and reduce the activity of Hst5, highlighting the delicate balance and complexity of this system. These proteases degrade Hst5, producing a mix of peptide fragments that may not be as active as the parent Hst5 [34-36, 38, 45, 78]. In the primary work done with these variants, substitution at K17 were found to could protect the peptide from proteolysis (**Table 2.4**) [34]. This work was continued by further determining the effects of coupled substitution (K11RK17R) and replacing or adding acid residues (E16L, E16R, K13E). Except for E16L, variants such as K11RK17R maintained antifungal activity when proteolytic stability was improved

[35]. After incubation with Sap2, E16L proteolysis product exhibited greater antifungal activity than the degraded Hst5 despite being more degraded after exposure to Sap2 [35]. Here it is shown that we can engineer proteolytically stable variants of Hst5, and that proteolytic stability impacts the antifungal activity. In previous work, K17 variant was originally noted as not important to the peptides antifungal activity [74]. However, by exploring individual mutations followed by coupled mutation, we can see that we were able to identify more proteolytically stable variants of Hst5 which overall helped the peptide maintain its antifungal activity in the presence of proteases.

Table 2.4. Mutants of Hst5 designed to assess proteolytic stability. The stability reported is with respect to the parent peptide Hst5.

	Sequence [a]																											
	1	2	3	4	5	6	7	8	9	10	11	12	13	14	15	16	17	18	19	20	21	22	23	24		Sap2	Sap9
Name	D	S	H	A	K	R	H	H	G	Y	K	R	K	F	H	E	K	H	H	S	H	R	G	Y	Ref.	Stablity	Stablity
K5R	-	-	-	-	R	-	-	-	-	-	-	-	-	-	-	-	-	-	-	-	-	-	-	-	[35]	Enhanced	Similar
K5L	-	-	-	-	L	-	-	-	-	-	-	-	-	-	-	-	-	-	-	-	-	-	-	-	[35]	Enhanced	Reduced
K11R	-	-	-	-	-	-	-	-	-	-	R	-	-	-	-	-	-	-	-	-	-	-	-	-	[35]	Enhanced	Similar
K11L	-	-	-	-	-	-	-	-	-	-	L	-	-	-	-	-	-	-	-	-	-	-	-	-	[35]	Enhanced	Reduced
K13R	-	-	-	-	-	-	-	-	-	-	-	-	R	-	-	-	-	-	-	-	-	-	-	-	[35]	Reduced	Reduced
K13L	-	-	-	-	-	-	-	-	-	-	-	-	L	-	-	-	-	-	-	-	-	-	-	-	[35]	Enhanced	Reduced
K13H	-	-	-	-	-	-	-	-	-	-	-	-	H	-	-	-	-	-	-	-	-	-	-	-	[36]	Reduced	Reduced
K13E	-	-	-	-	-	-	-	-	-	-	-	-	E	-	-	-	-	-	-	-	-	-	-	-	[36]	Reduced	Reduced
E16R	-	-	-	-	-	-	-	-	-	-	-	-	-	-	-	R	-	-	-	-	-	-	-	-	[36]	Enhanced	Reduced
E16L	-	-	-	-	-	-	-	-	-	-	-	-	-	-	-	L	-	-	-	-	-	-	-	-	[36]	Reduced	Reduced
K17R	-	-	-	-	-	-	-	-	-	-	-	-	-	-	-	-	R	-	-	-	-	-	-	-	[35]	Enhanced	Enhanced
K17L	-	-	-	-	-	-	-	-	-	-	-	-	-	-	-	-	L	-	-	-	-	-	-	-	[35]	Enhanced	Enhanced
K11RK17R	-	-	-	-	-	-	-	-	-	-	R	-	-	-	-	-	R	-	-	-	-	-	-	-	[36]	Enhanced	Enhanced

[a] *The hyphens represent retained amino acids.*

2.5. *Metal binding*

Another property that is well studied is the metal binding properties of Hst, specifically to zinc and its potential role in antifungal activity. Hst5 is also known as metallopeptide, meaning that it can bind to metals. The zinc-binding domain of most metalloproteins contains a canonical HEXXH site that is present in residues 15 – 19

of Hst5 (**Figure 2.2)**. Additionally, residues 3 – 7 (HAKRHH) of Hst5 can also bind to zinc, but not as effectively [79]. The peptide's ability to interact with zinc may influence its activity, as zinc can be found in saliva at a concentration of 0.12 - 0.22 µg/mL [80].

		Zn^{2+}binding region						Sequence						Zn^{2+} binding region									
1	2	3	4	5	6	7	8	9	10	11	12	13	14	15	16	17	18	19	20	21	22	23	24
D	S	H	A	K	R	H	H	G	Y	K	R	K	F	H	E	K	H	H	S	H	R	G	Y

Figure 2.2. The amino acid sequence of Hst5. The Zn2+ binding motifs are highlighted in blue.

While the full mechanism of action remains to be established, hypotheses about the role of metal ions in the activity of Hst5 have been gaining more notice. According to Campbell et al., Hst5's antifungal activity may be regulated by zinc [81]. Higher concentrations may lead to binding to the cell wall without internalization, while restricted access to zinc can result in Hst5 internalization and killing of *C. albicans* [81] (**Figure 2.3**). This potential modulation of Hst5's activity by zinc, a common element, opens up exciting possibilities for future research.

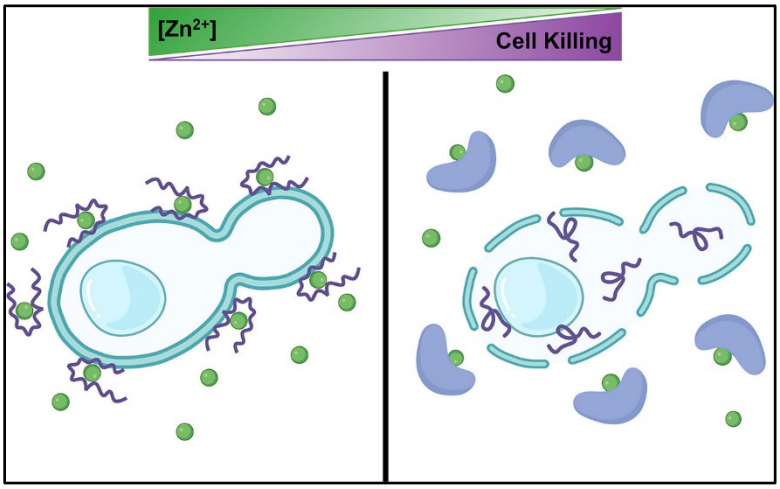

Figure 2.3. Schematic of the role of Zn^{2+} in the antifungal activity of Hst5. At high Zn^{2+} concentrations, Hst5 binds $Zn^{2+,}$ preventing internalization into *C. albicans*, when exposure to Zn^{2+} is

reduced by chelators like EDTA, Hst5 can internalize and reduce the activity of Hst5. Figure reprinted with permission from [81]. Copyright © 2022, American Chemical Society.

The role of Zn^{2+} in modulating the activity of Hst5 has gained interest, and rational design has been used to study and engineer this interaction. An important amino acid in this binding is histidine, which is known for binding to divalent metals. Specifically, H15 and H19 are believed to coordinate with Zn^{2+} to sustain the Hst5 α-helix (**Figure 2.4**) [82].

McCaslin et al. made mutations to the Hst5 sequence to try to understand the role of metals in the Hst5 and *C. albicans* interaction. Utilized previously designed variants (K13E/R22G and H18A/H19A) [74, 75], to determine how the structure of Hst5 is impacted by zinc. They found that mutating amino acids H15A/H19A, which are in the Zn^{2+} binding motif, reduced the peptide's stability. The same variants were found to have lower activity which may play a role in the reduction in antifungal activity [82]. In a more recent study by Norris et al. using variants Hst5 5ΔMB where residues in the HXXHH motif were substituted with glutamine, they determined that when this metal binding site is not present, not only is zinc binding significantly reduced, but the antifungal activity is also reduced (**Table 2.5**) [79]. These regions clearly play an important role in the metal binding capability, as when the substitutions are made metal binding is lost. Furthermore, these substitutions may impact the stability gained by metal binding, therefore reducing the antifungal activity.

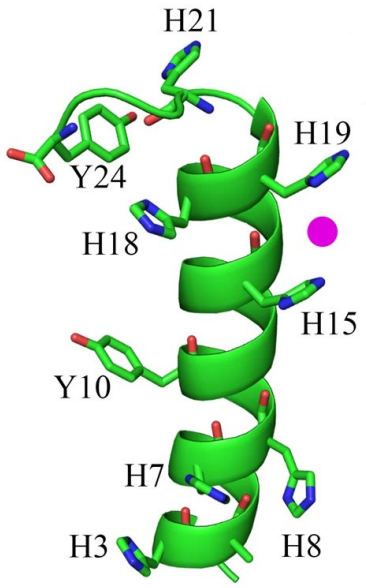

Figure 2.4. Hst5 interacting with Zinc. Zinc (Pink circle) is interacting with the H19 and H15 residues of Hst5 [82].

Table 2.5. Mutants of Hst5 designed to assess Zn^{2+} affinity. The binding reported is with respect to the parent peptide Hst5.

			Zn^{2+} binding region						Sequence [a]						Zn^{2+} binding region												
	1	2	3	4	5	6	7	8	9	10	11	12	13	14	15	16	17	18	19	20	21	22	23	24		
Name	D	S	H	A	K	R	H	H	G	Y	K	R	K	F	H	E	K	H	H	S	H	R	G	Y	Ref.	Binding
K13E/R22G	-	-	-	-	-	-	-	-	-	-	-	-	E	-	-	-	-	-	-	-	-	G	-	-	[74]	Reduced
H18A/H19A	-	-	-	-	-	-	-	-	-	-	-	-	-	-	-	-	-	A	A	-	-	-	-	-	[75]	Reduced
Hst5 5ΔMB	Q	Q	Q	-	-	-	-	-	-	-	-	-	-	-	Q	Q	Q	Q	Q	-	-	-	-	-	[79]	Reduced
P-113				A	K	R	H	H	G	Y	K	R	K	F	H										[79]	Reduced

[a] *The hyphens represent unchanged amino acid residues*

2.6. Conclusion

Hst5 is a promising antifungal agent that has shown significant activity against *C. albicans*. In this review, we have discussed the use of rational design to create variants of Hst5 with improved zinc binding, enhanced antifungal and greater proteolytic stability against *C. albicans*. Although these strategies have been helpful in understanding the interactions between Hst5 and *C. albicans*, there are still many aspects that require further exploration. For instance, the variants designed to enhance

proteolytic stability need to be assessed against a wider array of Saps. Additionally, the proteolytic stability of these variants should be evaluated in saliva as other proteases besides Saps are present there. Furthermore, these variants should be tested for their antifungal activities, as their proteolytic stability may be linked to their ability to reduce the viability of fungi. Lastly, as binding to zinc may play a role in these interactions, proteolysis and antifungal activity should be evaluated in the presence of zinc. In this dissertation we will implementing these efforts, gaining valuable insights from the study of Hst5 and apply them to develop future antifungal therapies more effectively.

3. Chapter 3: Impact of Hst5 modification on proteolytic stability

3.1. *Introduction*

Histatin 5 (Hst5) is an antimicrobial peptide from a family of histidine-rich peptides called histatins. Hst5 is a 24 amino-acid peptide that is secreted from the salivary gland and has activity against the human fungal pathogen *Candida albicans,* which can be found oral microbiome of 30% to 50% of people but can also cause oral candidiasis [30, 83]. Komatsu et al. found that patients with Down syndrome have reduced levels of Hst5 and are more prone to oral candidiasis [84], possibly linking Hst5 as a natural regulator of *C. albicans*.

One potential limitation of using Hst5 as a therapeutic is its susceptibility to proteolytic degradation by secreted aspartyl proteases (Saps) produced by *C. albicans. C. albicans* produces a family of ten Saps, each of which is known to contribute to the virulence of the cells [85-88]; Sap1-8 are secreted fully to the extracellular space, while Sap9 and Sap10 are anchored to the cell membrane via glycosylphosphatidylinositol (GPI) anchors or GPI proteins [36, 42]. As with other aspartyl proteases, Saps have two canonical aspartate residues in the active site and prefer to cleave sequences at lysine, arginine, and hydrophobic residues [42, 89]. Puri et al. showed that Hst5 is cleaved by Sap6 when incubated for 1 h at 37 °C in 50 mM sodium phosphate buffer (NaPB) (pH 7.0), and the antifungal activity of Hst5 is nearly eliminated after incubation at a 2:1 molar ratio of Hst5 to Sap6 [37]. In another study by Meiller et al., the authors found that Sap2 and Sap9, and, to a lesser extent,

Sap10 cleave Hst5 in phosphate buffered saline (PBS) at 37 °C for 2 h [36]. More recently, Bochenska et al. tested all Saps at 37 °C and their optimal conditions of 10 mM acetate buffer at pH 4 (Sap2, Sap3, and Sap8); 10 mM acetate buffer at pH 5 for Sap1, (Sap4–6, and Sap9), or 10 mM phosphate buffer at pH 6 (Sap7 and Sap10). After incubation with Saps, the antifungal activity of Hst5 drops by more than ~20% for each Sap, and Sap1-6 and Sap8 prefer to cleave near positively charged (Arg and Lys) or large hydrophobic amino acids (Leu, Phe, and Tyr), while Sap7 and Sap9-10 prefer to cleave near Arg and His [38]. In the Bochenska et al. experiments, Hst5 antifungal activity was reduced by Sap5 and Sap10 despite not being degraded by these Saps, which implies that the presence of Sap5 and Sap10 may inhibit Hst5's antifungal activity. In previous work in our lab, each lysine of Hst5 with substituted with either leucine or arginine and degraded with either Sap2 or Sap9, and the degradation products were analyzed. K13 variants (K13R and K13L) and leucine variants were more prone to proteolysis by Sap9; and both variants at K17 (K17R and K17L) were resistant to proteolysis by both Sap2 and Sap9 and had improved antifungal activity compared to Hst5 [34, 35]. However, it is worth noting that this study only examined the effects of two Saps, leaving the potential impact of other Saps and proteases found in saliva to be investigated in future research.

For Hst5 to be useful against oral candidiasis, its interaction with proteases found in the saliva is also important. Previous studies show that Saps, namely Sap1-5, are present in saliva [49, 50]. Along with the Saps, Lomate et al. notes the presence of serine protease, cathepsin, and aminopeptidase in saliva [46]. Previous studies also show that after mixing saliva with Hst5, Hst5 is degraded [78, 90, 91]. However, no

studies have been conducted to assess the proteolytic stability of Hst5 variants in the presence of saliva.

In this study, we aimed to improve our understanding of the effects of Hst5 modifications on its susceptibility to proteolytic degradation and antifungal activity. We built on previous research by analyzing the degradation of Hst5 variants with arginine and leucine substitutions at each of its lysine residues in the presence of Sap1, Sap2, Sap3, Sap5, Sap6, Sap9, and Sap10. Our analysis showed that Sap5, Sap6, and Sap10 do not significantly degrade Hst5 under the tested conditions. We found that the K17L variant is the most proteolytically stable when incubated with Sap1, Sap2, Sap9, and saliva and also has the highest antifungal activity. On the other hand, degradation by Sap3 causes variants with a leucine substitution to have reduced antifungal activity. We also identified fragments that are similar between each Hst5 variant after degradation by Saps and saliva, such as the [4-24] fragment for Sap1, the [1-17] fragment for Sap2 and Sap9, and the [13-24] fragment for degradation by saliva. Furthermore, we observed that proteolytic stability between variants remained largely unchanged from the parent Hst5 after incubation with saliva.

3.2. *Methods and materials*

3.2.1. *Peptides and enzymes*

The parent Hst5 peptide and all variants were commercially synthesized by Biomatik (Ontario, Canada) with a purity of ≥95% and trifluoroacetic acid removal to hydrochloride salt. Purified Sap1, Sap2, Sap3, Sap5, Sap6, Sap9, and Sap10 were gifted by B. Hube from Friedrich Schiller University, Germany. Sap1, Sap2, Sap3,

and Sap6 were purified by ion exchange chromatography and desalted into 0.1 M sodium citrate buffer. Sap5 was purified by ultrafiltration and desalted into 0.1M sodium citrate. Sap9 and Sap10 were produced without their GPI anchors and were purified by ion exchange chromatography and desalted into 0.1 M sodium citrate buffer [42].

3.2.2. Proteolytic degradation of the peptides by Saps

The extent of degradation of the peptides by the Saps was determined by incubating each purified Sap with each peptide. The concentration used for each Sap (**Table 3.1**) was selected as the concentration of the Sap required to degrade ~50% of the parent peptide Hst5 under the assay conditions.

Table 3.1. Final concentration of Saps in degradation assay.

Sap	Concentration (µg/mL)
Sap1	5.0
Sap2	0.1
Sap3	1.6
Sap5	5.0
Sap6	5.0
Sap9	3.1
Sap10	5.0

The Saps were each mixed to the specified concentration with Hst5 and the variants at a final concentration of 150 µg/mL of the peptide. Experiments were performed in 1 mM NaPB at pH 7.4. The mixtures were incubated at 37 °C for 2 h. Samples were then boiled for 5 min at 100 °C to inactivate the proteases and stored at 20 °C until later used.

3.2.3. Proteolytic degradation of the peptides by saliva

Saliva (gender-pooled, unfiltered, frozen) was purchased from BIOIVT (Westbury, NY). The saliva was centrifuged at 3,900 ×g for 5 minutes to remove any cells or debris. A 10 kDa molecular weight cutoff column was used to exchange the solution to 2 mM NaPB, and the saliva was stored at -20 °C until used. The solution was then diluted to a total protein concentration of 1.0 mg/mL with 2 mM NaPB to yield a concentration resulting in ~50% of the Hst5 peptide degraded under assay conditions.

The degradation of the peptides by saliva was evaluated using a procedure analogous to the one used for Saps. The assay was performed in NaPB, with a final peptide concentration of 150 μg/mL and a final total protein concentration of the saliva of 500 μg/mL. The mixtures were incubated at 37 °C for 2 h. Samples were then boiled for 5 min at 100 ℃ to inactivate the proteases in saliva and stored at 20 °C until later used. This assay was done in three replicates.

3.2.4. Gel electrophoresis data analysis

After proteolysis, samples were mixed with tricine sample buffer (200mM Tris-HCl, pH 6.8, 40% glycerol, 2% sodium dodecyl sulfate, without Coomassie Blue G250) containing 2% β-mercaptoethanol and boiled again for 5 min at 100 °C. The degraded and nondegraded peptides were separated by gel electrophoresis on 16.5% Tris-tricine gels (Bio-Rad; Hercules, CA), and the gels were fixed in a solution of 10% acetic acid, 40% methanol, and 50% water for 30 min. The fixed gels were stained in Bio-Safe Coomassie stain (Bio-Rad) for 1 h and then washed in autoclaved ultrapure water three times for 30 minutes and once overnight. The gels were imaged on a

ChemiDoc imager (Bio-Rad), and densitometric analysis was done using Image Lab software (Bio-Rad). In the analysis, the upper band of each lane was taken as the intact peptide, while all bands below were taken as degradation products.

Two-way ANOVA tests with $\alpha = 0.05$ and Dunnett's multiple comparison tests (degraded Hst5 as the control) were performed for statistical analysis. The number of asterisks indicates the level of statistical significance: * for $P < 0.05$, ** for $P < 0.01$, *** for $P < 0.001$, and **** for $P < 0.0001$. *P*-Values are provided in **Appendix Table A.1** and representative gel images are provided in **Appendix Figure A.1**.

3.2.5. *Candidacidal assay of intact peptides*

The antifungal activity of the intact peptides was assayed as previously reported [34, 35, 92]. A single colony of *C. albicans* strain SC5314 was inoculated into liquid yeast extract-peptone-dextrose (YPD) medium (10 g/L yeast extract, 20 g/L peptone, 20 g/L dextrose) and grown overnight at 30 °C while shaking. Cells were subcultured to an optical density measured at 600 nm (OD_{600}) of 0.1 and grown to an OD_{600} of 1-1.2 at 30 °C while shaking. Cultures were grown at 30 °C, as this produces cells primarily in the yeast (versus hyphal) morphology [93]. Cells were washed three times in 2 mM NaPB and diluted to a cell density of 5×10^7 cells/mL in 2 mM NaPB. Serial dilutions of peptide (20 µL) in water were prepared in 96-well plates and mixed with the cell suspension (20 µL) for a final cell concentration of 2.5×10^7 cells/mL and final peptide concentrations of 0.14 – 75 µg/mL in 1 mM NaPB. Control wells containing cells and no peptide were included. The plates were incubated at 30 °C for 30 min. After incubation 280 µL of 1 mM NaPB was loaded into each well to reduce

interaction between the peptide and cells [67]. Samples were further diluted to approximately 250 cells/well in the wells of a separate 96-well plate containing 100 µL of YPD and 100 µL of 1 mM NaPB in each well. Wells only containing YPD and NaPB served as sterility controls and provided the background OD_{600} signal. The OD_{600} was measured after overnight incubation on a microplate shaker at 30 °C. The reduction in viability was calculated as

$$\text{Reduction in viability (\%)} = \left[1 - \frac{\left(OD_{\text{with peptide}} - OD_{\text{background}}\right)}{\left(OD_{\text{no peptide}} - OD_{\text{background}}\right)}\right] \times 100 \qquad (3.1)$$

The assay was performed on three separate days with two replicates each day. Two-way ANOVA tests with $\alpha = 0.05$ and Dunnett's multiple comparison tests were performed for statistical analysis. Significance is determined by comparing each peptide to degraded Hst5 (Dashed black lines) at the first tested concentration that Hst5 exceeded 50% reduction in viability. $P \leq 0.05$ was deemed as significant *P*-Values in **Appendix Table A.2**.

3.2.6. Candidacidal assay of degraded peptides

To assay the antifungal activity of the peptides following degradation with Saps, the peptides were first degraded by Saps as described above. A *C. albicans* suspension was prepared as described for the assay with intact peptides, except the cell suspension was prepared in 1 mM NaPB. In 96-well plates, serial dilutions (20 µL) of the degraded peptide solutions (peptide concentration of 0.14 – 75 µg/mL prior to degradation) were prepared in 1 mM NaPB. Control wells containing no peptide were also included. The serial dilutions were mixed with an equal volume of the cell

suspension and incubated at 30 °C for 30 min. After incubation, the samples were processed in the same manner as described above for the assay with intact peptides to quantify the reduction in growth. The assay was performed on three separate days with two replicates on each day.

The assay was performed on three separate days with two replicates each day. Two-way ANOVA tests with $\alpha = 0.05$ and Dunnett's multiple comparison tests were performed for statistical analysis. Significance is determined by comparing each peptide to degraded Hst5 (Dashed black lines) at the first tested concentration that Hst5 exceeded 50% reduction in viability. $P \leq 0.05$ was deemed as significant *P*-Values in **Appendix Table A.2**.

3.2.7. Quantification of peptide fragments

Mass spectrometry was used to determine whether the Saps and saliva cleaved the peptides and compare the abundance of the fragments produced. After incubating the peptides with Saps or saliva as described for the proteolytic degradation assays, 30 µL of each sample was desalted using a C-18 TopTip microspin column (Glygen), following the manufacturer's protocol. The binding solution for each peptide was 0.1% formic acid, and the release solution was 0.1% formic acid and 80% acetonitrile. Each sample (19 µL) was spiked with 1 µL of the peptide MFRA (0.01 µg/mL in 0.1% formic acid and 80% acetonitrile) to facilitate comparison between samples. Samples were analyzed on a Bruker Maxis II mass spectrometer (in the University of Maryland Mass Spectrometry Facility) with an electron spray ionization source and quadrupole-time of flight analyzer. Samples were directly injected into the

Maxis II, and data were acquired between *m/z* 250 – 3200 with full sensitivity resolution of >50,000.

After acquiring the data, the mass spectra for each sample were analyzed using the Bruker Compass DataAnalysis software, using BioTools (Bruker; Billerica, MA) in tandem with Sequence Editor (Bruker; Billerica, MA) to identify each peak. In the Bruker Compass Software, each mass spectrum was individually deconvoluted to consolidate the *m/z* values for peptides with varying charges. The deconvoluted mass spectra were then transferred to BioTools and Sequence Editor where the molecular weights of the peptides and their fragments were calculated and compared to the mass spectra peaks with a tolerance of ± *m/z* = 0.2. After identifying fragment peaks, the data were filtered to focus on peaks with fragments greater than 7 amino acids. The intensities of the sample peaks were divided by the intensity of the MRFA standard peak. The data were then manually filtered to show the eight most abundant fragments with normalized intensities greater than 10% of the intensity of the fragment with the highest intensity. Data was collected in duplicate over two days.

3.3. Results and Discussion

To study the interactions of Hst5 with Saps and saliva, we evaluated the proteolysis of Hst5 and ten analogs with leucine or arginine substitutions at the lysine residues of Hst5 (**Table 3.2**). To determine the degree of degradation, we analyzed gel images using densitometric analysis and utilized mass spectrometry to identify the fragments that were formed by proteolysis of each analog. Prior work from our lab focused on degradation by Sap2 and Sap9 and how the substitution impacts proteolysis [34, 35].

We continued work from Ikonomova et al. with arginine and leucine variants designed at the Hst5 lysine residues5 [34] and the double variant K11RK17R which was the most proteolytically stable variant tested thus far [35]. We also introduced a novel variant, K11RK17L, to determine the effect of coupling substitutions with different properties on the proteolytic stability of Hst5. We also tested all variants against Sap1, Sap3, Sap5, and Sap6. Previous work has shown that Hst5 can be degraded by these Saps except for Sap5 [36-38]. However, after incubation with Sap5, antifungal activity substantially decreases [38]. Based on prior work from our lab [34, 35], we hypothesized that variants designed at K17 would be the most proteolytically stable against the Saps, while K13 variants will have reduced antifungal activity.

Table 3.2. Sequence of peptides in this study.

Peptide	Sequence [a]																							
	1	2	3	4	5	6	7	8	9	10	11	12	13	14	15	16	17	18	19	20	21	22	23	24
Hst5 5	D	S	H	A	K	R	H	H	G	Y	K	R	K	F	H	E	K	H	H	S	H	R	G	Y
K5R	-	-	-	-	R	-	-	-	-	-	-	-	-	-	-	-	-	-	-	-	-	-	-	-
K5L	-	-	-	-	L	-	-	-	-	-	-	-	-	-	-	-	-	-	-	-	-	-	-	-
K11R	-	-	-	-	-	-	-	-	-	-	R	-	-	-	-	-	-	-	-	-	-	-	-	-
K11L	-	-	-	-	-	-	-	-	-	-	L	-	-	-	-	-	-	-	-	-	-	-	-	-
K13R	-	-	-	-	-	-	-	-	-	-	-	-	R	-	-	-	-	-	-	-	-	-	-	-
K13L	-	-	-	-	-	-	-	-	-	-	-	-	L	-	-	-	-	-	-	-	-	-	-	-
K17R	-	-	-	-	-	-	-	-	-	-	-	-	-	-	-	-	R	-	-	-	-	-	-	-
K17L	-	-	-	-	-	-	-	-	-	-	-	-	-	-	-	-	L	-	-	-	-	-	-	-
K11RK17R	-	-	-	-	-	-	-	-	-	-	R	-	-	-	-	-	R	-	-	-	-	-	-	-
K11RK17L	-	-	-	-	-	-	-	-	-	-	R	-	-	-	-	-	L	-	-	-	-	-	-	-

[a] *The hyphens represent retained amino acids.*

3.3.1. Histatin 5 modifications impact proteolytic stability to secreted aspartyl proteases

When evaluating the degradation of Hst5 and its analogs by Saps, we selected Sap concentrations that ensured 30-50% of the parent Hst5 peptide remained fully intact after 2 h of exposure at 37 °C in 1 mM NaPB (pH 7.4). This approach facilitated the clear identification of variations in proteolytic stability among the peptides. Under the conditions tested, Sap1, Sap2, Sap3, and Sap9 cleaved Hst5 and the variants at levels that are dependent on the protease and the peptide modifications (**Figure 3.1**). After incubation with Sap1, 37.0% of Hst5 remained fully intact. The variants K11R, K11RK17R, K5L, K11L, K13L, and K11RK17L experienced greater fragmentation due to Sap1 than Hst5 with K11R, K5L, K11L, and K13L only showing between 2.2% and 9.3% of intact peptide. In contrast, K5R and K17L were more stable in the presence of Sap1 than Hst5, with 56.8% and 47.8%, respectively, of the peptides remaining intact. After incubation with Sap2, 50.4% of Hst5 remained fully intact. The variants K11R, K17R, K5L, K11L, K13L, and K11RK17L underwent more proteolysis than the parent peptide, while K17L was substantially more resistant to degradation with 72.9% intact peptide. When Sap3 was incubated with the peptide variants, 43.3% of Hst5 remained intact. All variants with arginine substitutions—except for K11RK17L —and K17L exhibited stability comparable to the parent peptide. In contrast, the remaining variants with leucine substitutions were more susceptible to degradation by Sap3 than the parent Hst5, with K5L, K11L, and K13L only showing between 2.2% and 9.3% of intact peptide. Incubation with Sap9 resulted in 41.5% of Hst5 remaining fully intact. However, K11L and K13L were

significantly less stable than Hst5 with 12.0% and 5.2% remaining fully intact. Interestingly, variants with a substitution at K17 were less affected by Sap9 degradation than Hst5, with K17R, K11RK17R, K17L, and K11RK17L retaining between 73.1% and 77.9% of intact peptide (**Figure 3.1**).

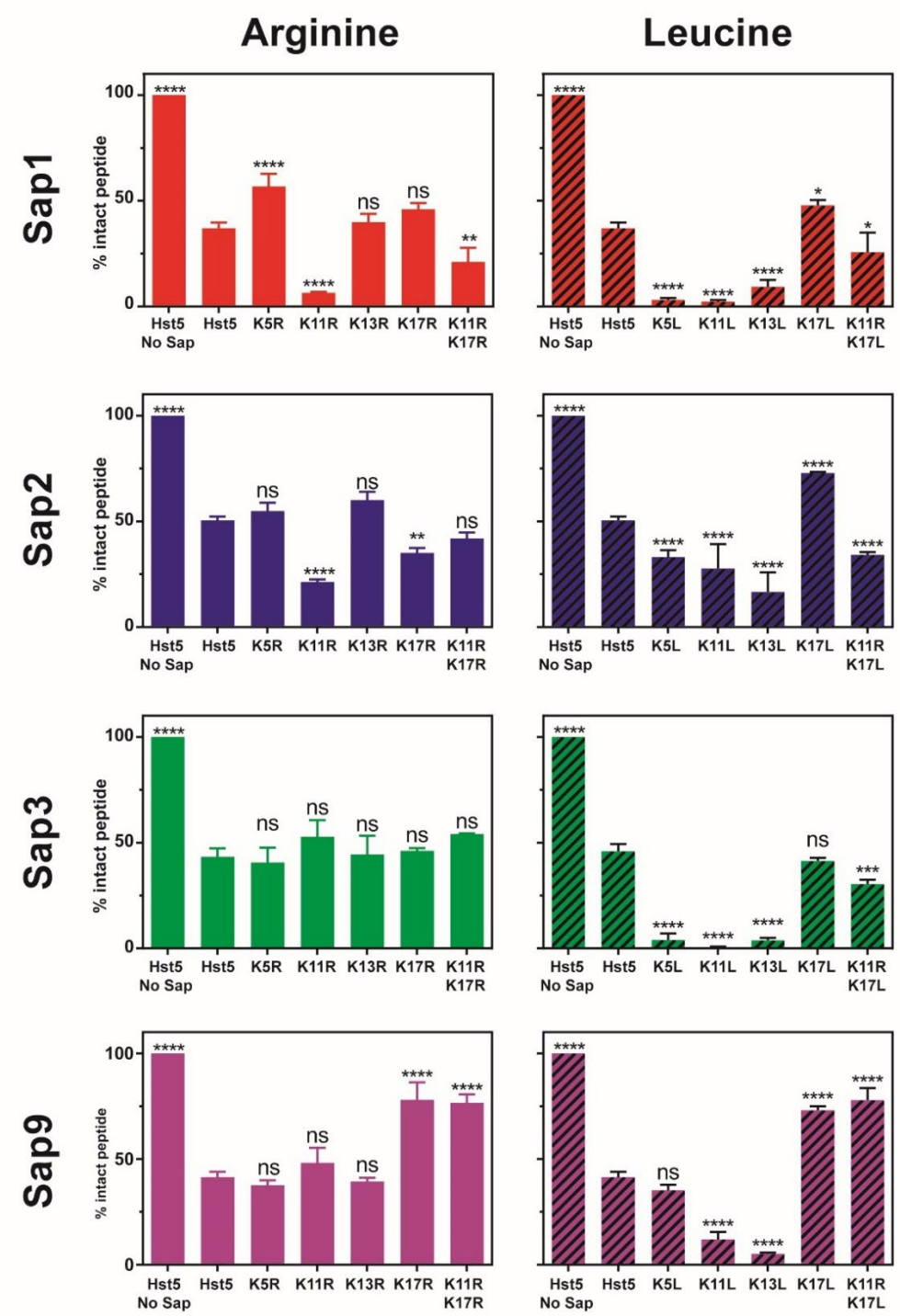

Figure 3.1. Degradation of Hst5 by purified Sap1, Sap2, Sap3, and Sap9. After incubation for 2 h at 37 °C, the intact peptide and degradation fragments were separated by gel electrophoresis and quantified by densitometry. Error bars represent the standard error of the mean ($N = 9$ for the Hst5 controls with and without Sap and $N = 3$ for the Hst5 variants).

Prior work has shown varying results that Sap5, Sap6, and Sap10 either do not degrade Hst5 or degrade it to a low extent [36-38]. In this work, we did not observe degradation by these Saps (**Appendix Figure 2 and 3**). At concentrations over an order of magnitude higher than those used for other Saps (up to 62.5 μg/mL), we still did not observe degradation (**data not shown**). The study conducted by Bochenska et al. found that Hst5 was not cleaved by Sap5, Sap6, and Sap10 when tested under optimal conditions. These conditions were determined by measuring the activity against BODIPY FL casein substrate (Invitrogen) using 10 mM acetate buffer at pH 5 for Sap5 and Sap6, and 10 mM phosphate buffer at pH 6 for Sap10 [38]. Meiller et al. performed the cleavage in phosphate-buffered saline (PBS) instead of 1 mM NaPB, and Sap10 cleaved Hst5 under these conditions [36]. As the Saps have different optimal pH, it is important to recognize that results using different buffering systems such as PBS, NaPB, and sodium acetate buffer should not be directly compared. When comparing results with the same buffer, it is essential to consider that the concentration and pH of the buffers may play a role in the proteolysis of the antifungal peptide.

Similarities in proteolytic activity of different Saps on Hst5 variants could be related to the structures of the Saps. Sap1 and Sap2 had very similar proteolytic activity on Hst5 variants, with K5L, K11R, K11L, K13L, and K11RK17L being more prone to proteolysis than Hst5 and K17L being more stable than Hst5. The Sap1 and Sap2 experienced similar degradation patterns is potentially because they are structurally homologous and could have similar substrates and interact with similar residues in Hst5 [94]. Sap3 is the next closest homolog to Sap1 and Sap2, and it experiences

mostly similar degradation patterns. These Saps have similar activity responses to all leucine variants, with the exception of K17L, as all the variants are more prone to proteolysis by Sap1, Sap2, and Sap3. Koelsch et al. and Bochenska et al. show that Sap1, Sap2, and Sap3, have a preferences for cleaving at hydrophobic residues [38, 89], so introducing leucine at K5, K11, and K13 leading to increase proteolysis is consistent with their findings. The difference in homology between Sap3 and the other two proteases can be seen in their ability to degrade the K11R and K17L variants. The K17L variant was generally the most stable among the leucine variants, with a higher percentage of intact peptide remaining than Hst5 following incubation with Sap1 and Sap2; however, after being degraded by Sap3, the amount of intact peptide remaining was similar to the parent Hst5. Koelsch et al. note that Sap3 has a greater preference for leucine over other residues [89], which could be the reason K17L is more stable after proteolysis by Sap1 and Sap2, but not Sap3. On the other hand, K11R is less stable than the parent Hst5 after being incubated by Sap1 and Sap2, but as stable as the Hst5 after being incubated with Sap3. This suggests a unique role for K11 and K17 in the stability of Hst5 in the interaction with Sap3 and that Sap3 unique substrates compared to the other two proteases.

Sap9 has the least homology among Sap1, Sap2, Sap3, and Sap9, which may contribute to the unique degradation patterns we observed. Sap9 degradation of the Hst5 variants with K11 and K13 substitutions was similar to the other Saps, where leucine substitutions were deleterious. However, unlike Sap1 and Sap2, both Sap3 and Sap9 retained proteolytic stability with arginine substitutions at K11 and K13. This suggests the positive charge at the K11 and K13 residues is crucial for

proteolytic stability in the presence of Sap3 and Sap9. In contrast, for Sap1 and Sap2, the K11R substitution was also less stable, indicating the lysine residue is important for maintaining proteolytic stability against these Saps. The differences between Sap9 and the other proteases are most apparent when analyzing the data for variants with K5 and K17 substitutions. Substitutions at K5 did not impact stability in the presence of Sap9, whereas K5L was always less stable than the parent peptide and K5R after proteolysis by Sap1, Sap2, and Sap3. Furthermore, all variants with substitutions at K17 improved overall stability in the presence of Sap9. Improved stability was only seen with K17L when incubated with Sap1 and Sap2. This suggests that K5 does not play a significant role in the interaction of Hst5 and Sap9, while the positive charge at K5 is important for stability in the presence of Sap1, Sap2, and Sap3. Moreover, K17 appears integral to the peptide-Sap9 interaction. The lysine residue itself likely plays an important role in this interaction, as substitutions at K17 significantly improve stability. Overall, these results show that homology may play a role in the degradation patterns observed by the degradation of Hst5 variants by Saps.

3.3.2. Mass spectrometry reveals that proteolysis may result in other stable fragments

While gel images can identify stable and unstable variants, mass spectrometry allows determination of the degradation products and identification of fragments that may be resistant to proteolysis by these Saps. After we incubated the peptides with the individual Saps, the reaction mixture was desalted and spiked with 1 μg/mL of the standard peptide MRFA for normalization. When analyzing the mass spectrometry data, we recorded the top 8 fragments with normalized intensities greater than 10%

the highest normalized intensity for each sample. Fragments such as fragment [7-14] and fragment [8-15] have the same "exact mass", as they are composed of the same distribution of amino acids (with histidine either at residue 7 or 15). Since we could not differentiate between fragments with the same mass, both fragments were listed as present at the total level of abundance of fragments of that size. After incubation with Sap1, Hst5 formed the fragments [14 - 24] and [4 - 24]. All variants except for K13R also formed the [14 - 24] fragment, and variants K5R, K13R, K11RK17R, K17R, K17L, and K11RK17L formed the [4 - 24] fragment. Notably, large fragments did not remain when K5L, K11R, K11L, and K13L were degraded by Sap1; only fragments less than 17 amino acids in size were identified (**Figure 3.2**). Hst5 proteolysis by Sap2 resulted in the full-length peptide [1-24] as the most abundant peak and formed the [1-17] fragment, which is similar to the variants with leucine substitutions following Sap2 incubation (**Figure 3.3**). When Hst5 was incubated with Sap3, the full-length peptide was again the most abundant peak, and the fragment [13-21], which was also formed by the K5R, K11R, K5L and K11L, was the next most abundant fragment. The [14-24] fragment was not a significant fragment following incubation of Hst5 with Sap3, but this fragment was one of the most abundant fragments for K13R, K17R, K5L, K11L, K13L, K17L, and K11RK17L. The fully intact peptide was the most abundant fragment produced by Sap3 degradation for variants with only arginine substitutions, with the exception of the K17R variant that had several smaller fragments in higher abundance. Additionally, the K5L, K11L, and K13L variants, formed the fragment [1-13] as one of the most abundant peaks after incubation with Sap3 (**Figure 3.4**). When incubated with Sap9,

Hst5 formed the fragments [1-17] and [14-24]. As expected from the gel proteolysis results, all variants with substitutions at K17 retained the full intact peptide as the most abundant fragment after proteolysis by Sap9. Additionally, the K17R and K17L variants formed the same [14-24] fragment as the parent peptide when incubated with Sap9. Likewise, the K5R, K11R, K5L, and K11L variants formed the [1-17] fragment produced by Hst5 and Sap9 (**Figure 3.5**).

Figure 3.2. Fragments produced by incubation of Hst5 and variants with Sap1. The peptides were each incubated with Sap1 for 2 h at 37 °C, and mass spectrometry was used to identify the fragments formed. Values shown are the average (N=2) normalized relative abundance of the fragment with respect to the standard MRFA. Black represents the fully intact peptide, while all other fragments are colored red. An asterisk (*) represent fragments that have the same mass and could, therefore, not be distinguished by mass spectrometry.

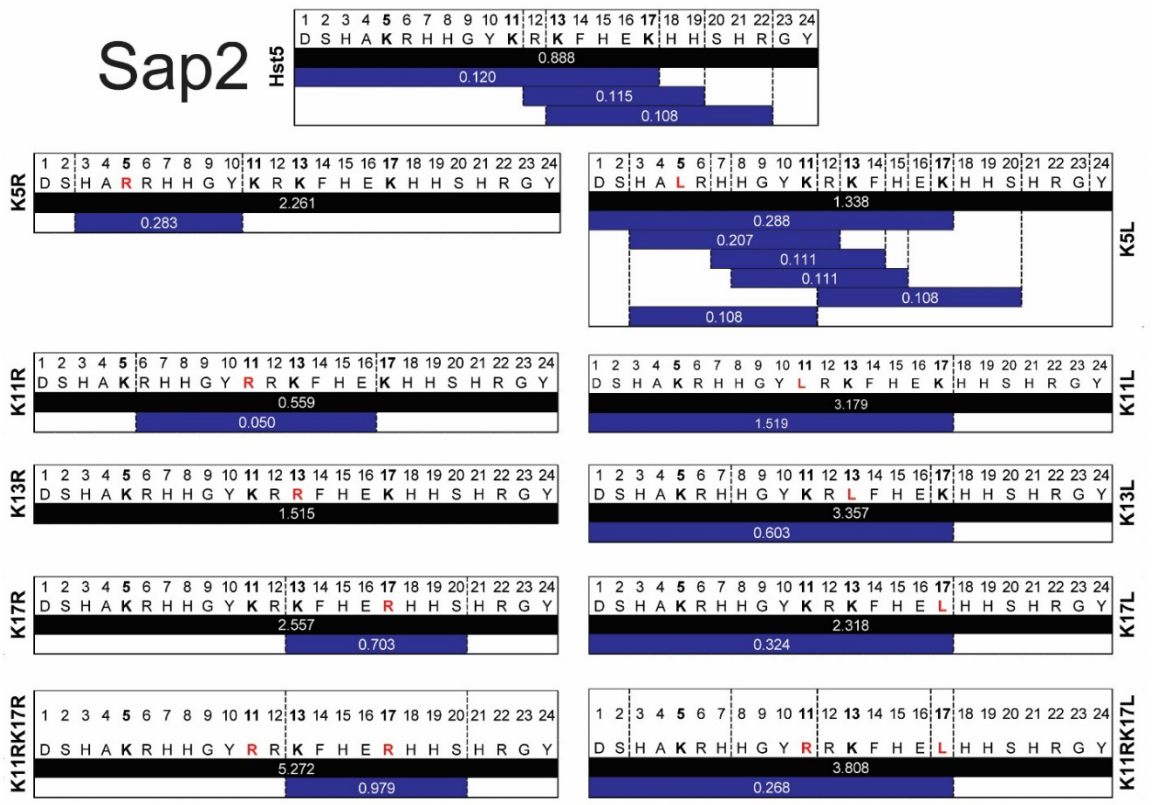

Figure 3.3. Fragments produced by incubation of Hst5 and variants with Sap2. The peptides were each incubated with Sap2 for 2 h at 37 ℃, and mass spectrometry was used to identify the fragments formed. Values shown are the average (*N*=2) normalized relative abundance of the fragment with respect to the standard MRFA. Black represents the fully intact peptide, while all other fragments are colored red. An asterisk (*) represent fragments that have the same mass and could, therefore, not be distinguished by mass spectrometry.

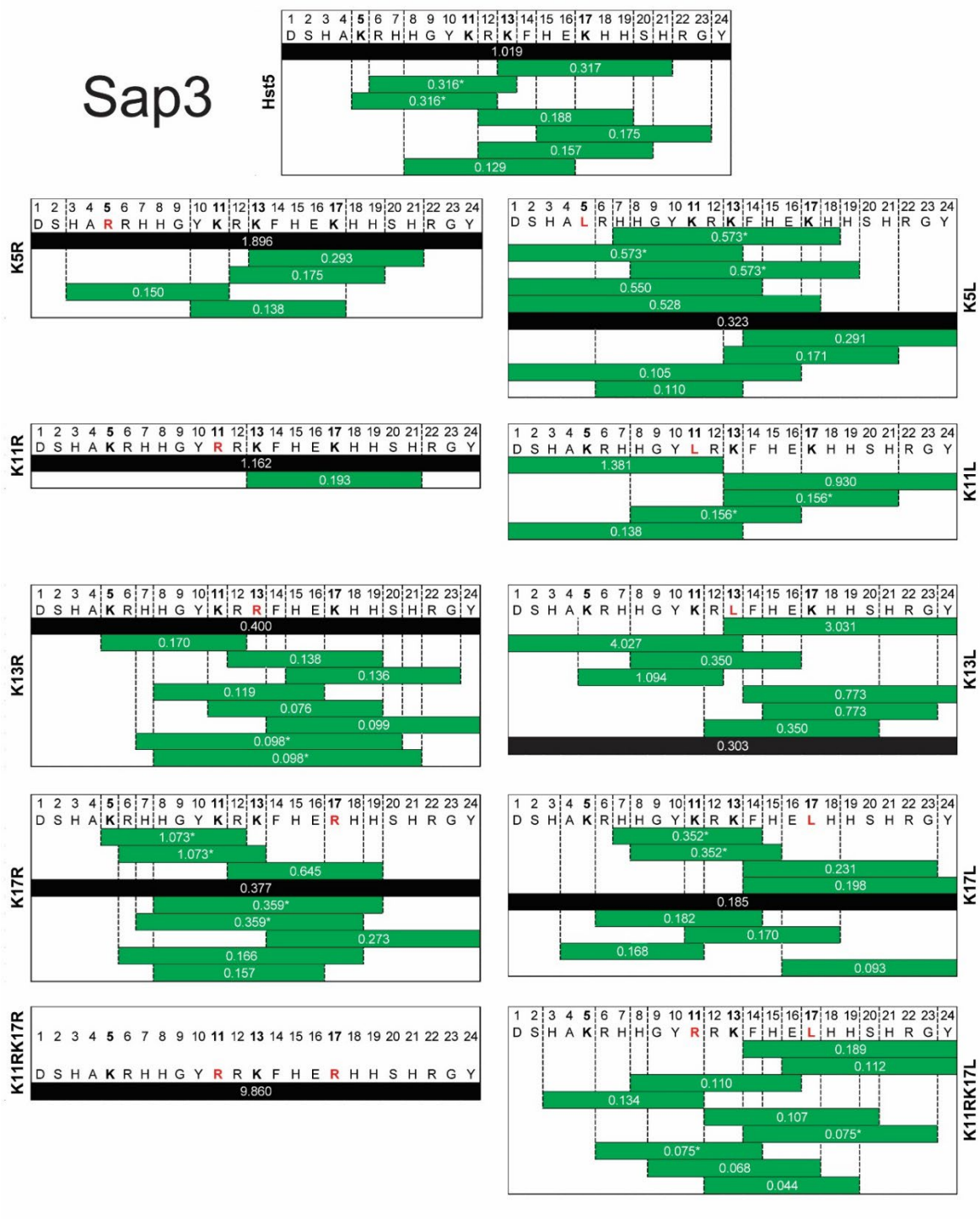

Figure 3.4. Fragments produced by incubation of Hst5 and variants with Sap3. The peptides were each incubated with Sap3 for 2 h at 37 ℃, and mass spectrometry was used to identify the fragments formed. Values shown are the average (*N*=2) normalized relative abundance of the fragment with respect to the standard MRFA. Black represents the fully intact peptide, while all other fragments are colored red. An asterisk (*) represent fragments that have the same mass and could, therefore, not be distinguished by mass spectrometry.

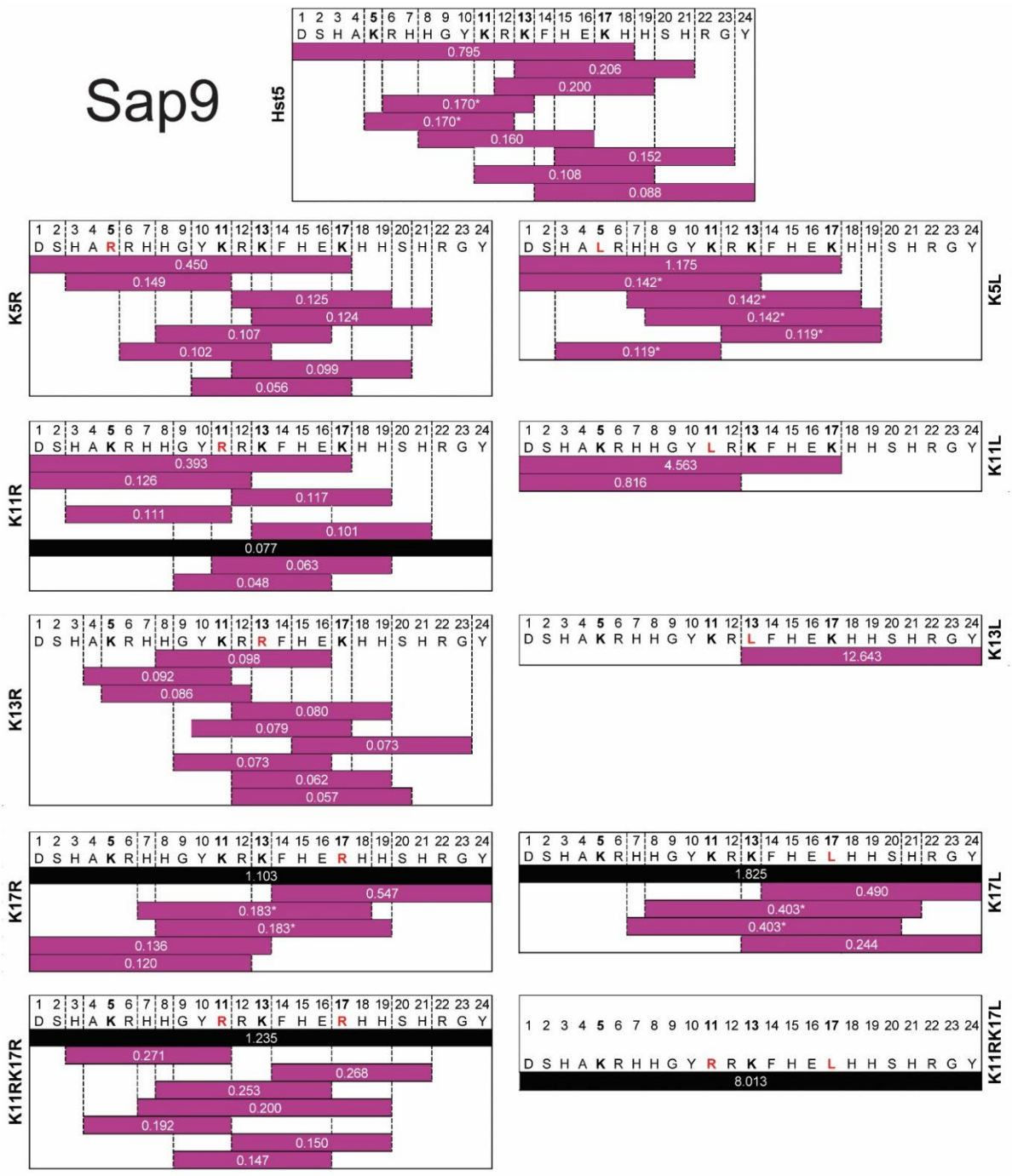

Figure 3.5. Fragments produced by incubation of Hst5 and variants with Sap9. The peptides were each incubated with Sap9 for 2 h at 37 °C, and mass spectrometry was used to identify the fragments formed. Values shown are the average (*N*=2) normalized relative abundance of the fragment with respect to the standard MRFA. Black represents the fully intact peptide, while all other fragments are colored red. An asterisk (*) represent fragments that have the same mass and could, therefore, not be distinguished by mass spectrometry.

The mass spectrometry data provided valuable information about the cleavage sites for the proteases and the most stable fragments resulting from proteolysis. In most cases, the results for mass spectrometry and the gel assay for proteolysis agreed. Sap5, Sap6, and Sap10 did not degrade Hst5 at the tested conditions, and nearly all of the peptide was present as the full-length peptide following incubation with these Saps (**Appendix Figure A.2, A.3, and A.4**). Both methods also identified variants that were more or less proteolytically stable than the parent Hst5. For example, after incubation with Sap9, variants with K17 substitution were all more stable than Hst5; also, after incubation with Sap3, variants with an arginine substitute were more stable than their leucine counterparts. The mass spectrometry results provide insight into Sap1 degradation that would be difficult to obtain with the gel-based assay. Mass spectrometry results indicate that proteolysis of K13R and K17R by Sap1 resulted in fragments [4-24] and [5-24], which would be difficult to distinguish from the full-length peptide on the gel. When the [4-24] fragment was present after proteolysis by Sap1, it was more abundant than the fully intact peptide, indicating it is a relatively stable fragment in the presence of Sap1. For peptides lacking the [4-24] fragment in the mass spectrometry data, the presence of smaller fragments potentially indicate further proteolysis of the [4-24] fragment following its formation. For example, the fragments [4-17], [4-12], and [4-13] formed after incubation of K5L, K11L, and K13L, respectively, with Sap1. Further degradation of [4-24] is not apparent for variants with only arginine substitutions, K17L, or K11RK17L, possibly indicating that these substitutions stabilize the [4-24] fragment . Proteolysis by Sap1 also resulted in all variants except for K13R, forming the fragment [14-24]. In some cases,

the [1-13] fragment, which would be expected to accompany [14-24] is not present at significant levels, indicating the [1-13] fragment may have undergone further proteolysis. Interestingly, the when leucine was substituted into K5, K11, or K13, the [1-13] fragment was present. These results suggest that regardless of which lysine substitution, proteolysis occurred forming [4-24] fragment, however, arginine or lysine at K5, K11, and K13 provided stability to the [4-24] fragment of peptide in the presence of Sap1, while K17 improves the stability of both the full-length peptide and [4-24] fragment. Furthermore, the presence of the [14-24] fragment without the [1-13] fragment shows that the [1-13] fragment substituting for a leucine within that sequence plays a role in stabilizing this fragments.

Using a mixture of different substrates, Koelsch et al. determined the preferred cleave sites for Sap1, Sap2, Sap3, and Sap6 and determined that cleavage does not occur [89]. However, the experiments were performed between pH 3 and 4, where histidine contains a positive charge. At similar conditions to those tested in this research, Ikonomova et al. observed cleavage near the histidine of Hst5 [34, 35]. While the charge of the histidine may play a role in producing the different results at the different pH values tested, Hst5 is a histidine-rich peptide, and the histidine residues are commonly near arginine, lysine, and phenylalanine, which are cleavage sites common for aspartyl acids. When determining cleavage sites pH plays a critical role, in the state of proteins such as histidine, and its interactions with residues surrounding it, so comparing results assessed at two different pH can be difficult.

Our data suggest that peptide fragments often underwent further proteolysis following their initial formation, producing fragments such as [13-21] or [7-17]. However, each variant has fragments formed near lysine, arginine, and histidine after proteolysis, similar to what previous work found [34-36, 38]. While some variants tested resulted in improved proteolytic, cleavage still occurred near those substituted residues; therefore, further engineering could identify substitutions that further improve proteolytic stability.

3.3.3. Modification can impact antifungal activity after being treated with protease

To determine the effect of the Hst5 modifications on antifungal activity, we first evaluated the antifungal activity of the intact peptides against *C. albicans*. Overall, the variants had similar activity to the parent Hst5 peptide (**Figure 3.6**), as previously reported for most of the peptides [34]. While some variants do show differences in antifungal activity (e.g., K17L and K5L had a statistically significant improvement and reduction, respectively, in antifungal activity at 4.69 μg/mL), the viability curves all approach ~100% reduction in cell viability at the same concentrations (9.38 μg/mL) and surpass ~50% reduction in cell viability between (2.34 and 4.69 μg/mL). Thus, the modifications do not have a major impact on the antifungal activity of Hst5 that has not been incubated with Saps.

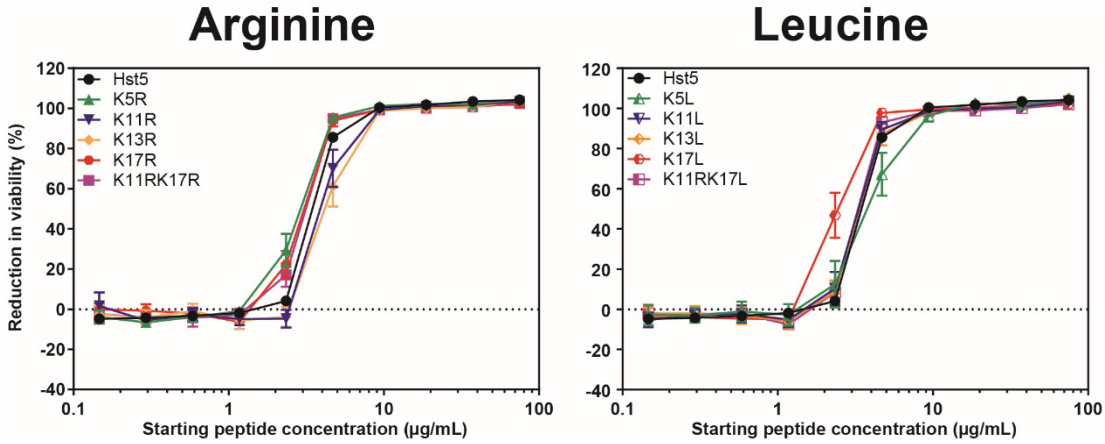

Figure 3.6. Antifungal activity of intact Hst5 variants. Hst5 variants were serially diluted, mixed with *C. albicans* cells, and incubated for 30 min at 30 °C in 1 mM NaPB. Error bars represent the standard error of the mean (N = 18 for Hst5 with and without Sap, while N = 6 for all Hst5 variants).

Building on previous work in our lab that showed incubation with Sap2 and Sap9 reduced the antifungal activity of Hst5 and many variants [34, 35], we evaluated how the interaction with additional Saps (Sap1, Sap3, Sap5, Sap6, and Sap10) impacted the antifungal activity of Hst5 and Hst5 variants. After incubating each variant with the Saps, we performed an antifungal activity assay using the degradation products to measure the activity retained after proteolysis by Saps. When determining statistically significant antifungal activity between different peptide variants, we analyzed the first measured concentration at which the protease-treated Hst5 showed a reduction in viability of over 50%. Incubation with Sap5, Sap6, and Sap10 did not affect Hst5 activity or the activity of Hst5 variants (**Appendix Figure A.5**), which was expected based on the lack of proteolysis of the peptides by these Saps. While modifications to the Hst5 peptide sequence caused little to no impact on the antifungal activity of the intact peptides, degrading these variants often caused significant differences in the activity dependent on the peptide modification and protease (**Figure 3.7**). After incubating Hst5 with Sap1, the antifungal activity of the resulting pool of degradation

fragments remained similar to the activity of the undegraded Hst5. Many of the Hst5 variants similarly maintained their activity after incubation with Sap1. However, degraded K11R, K13R, K5L, K11L, and K13L had a statistically significant reduction in antifungal activity compared to degraded Hst5, and degraded K17R and K11RK17L had greater antifungal activity than degraded Hst5. For Sap2, degradation of Hst5 resulted in a reduction in antifungal activity, as reported previously [34-36, 38]. The K11R, K5L, K11L, and K13L variants degraded by Sap2 had lower activity than Hst5 degraded by Sap2, similar to the reduction in activity resulting from Sap1 degradation; K17R, K11RK17R, K17L, and K11RK17L had greater activity than Hst5 following degradation by Sap2. Similar to Sap2, Hst5 degraded by Sap3 showed a reduction in antifungal activity in line with that observed by Bochenska et al [38]. Interestingly, all variants with leucine substitutions had a statistically significant reduction in antifungal activity after incubation with Sap3. K5L, K11L, and K13L had a particularly strong reduction in activity, with no residual antifungal activity detected under the conditions tested. The K17R and K11RK17R variants, however, had greater antifungal activity than Hst5 degraded by Sap3. Incubation with Sap9 led to a strong reduction in the activity of Hst5, as previously observed [34, 35, 38]. The degradation of the K13R, K5L, K11L, and K13L variants by Sap9 led to a lower antifungal activity compared to degraded Hst5, with K5R, K17R, K11RK17R, K17L, and K11RK17L having greater activity than Hst5 following degradation by Sap9. This shows that proteolysis by Saps can reduce the antifungal activity of Hst5 variants.

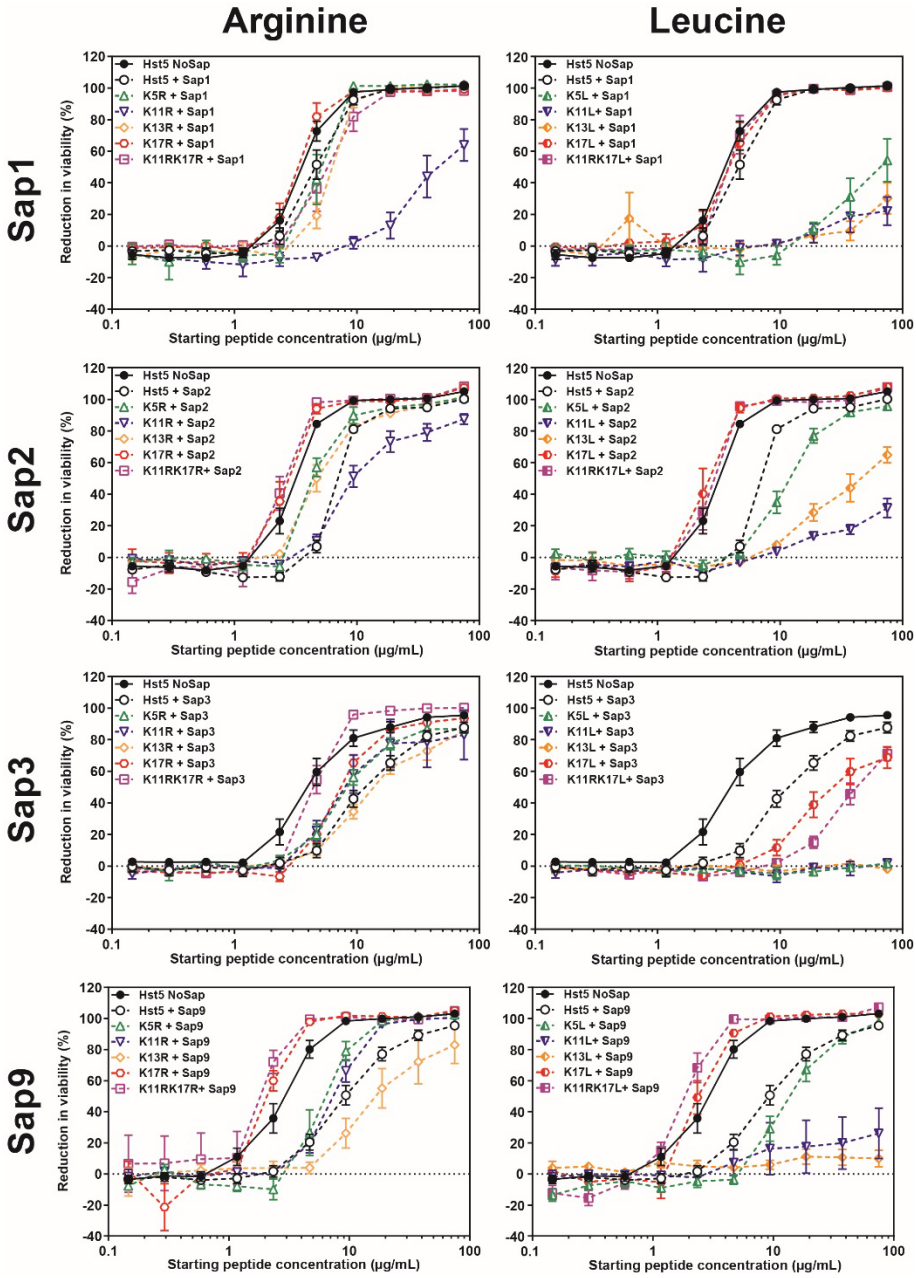

Figure 3.7. Antifungal activity of Hst5 variants after incubation with Sap1, Sap2, Sap3, or Sap9. After incubation for 2 h at 37 °C, Samples were serially diluted in a 96-well plate from 75 µg/mL to 0.14 µg/mL. Samples were then mixed with *C. albicans* cells at 5.0×10^5 cells/mL and incubated for 30 min at 30 °C in 1 mM NaPB, after which cells were inoculated and cultured. Error bars represent the standard error of the mean (N = 18 Hst5 No Sap and Hst5 + Sap, while N = 6 for all other variants).

Modifications of Hst5 can potentially impact the antifungal activity of the peptide after proteolysis by Saps. Incubation with Sap1, Sap2, Sap3, or Sap9, the K5L, K11L, and K13L variants consistently have lower antifungal activity than degraded Hst5,

indicating the peptide fragments formed by the degradation of these variants had less activity than the degradation products of Hst5. In contrast, K17R, K17L, K11RK17R, and K11RK17L had greater activity than degraded Hst5 following incubation with Sap2 and Sap9, with the activity being comparable to the undegraded Hst5. This was true for K17R and K11RK17R following degradation by Sap3. In contrast, incubation of K17L and K11RK17L with Sap3 led to lower activity than Hst5 degraded by Sap3, but these peptides still retained more activity than the other leucine-substituted peptides. After incubation with Sap1, many of the variants with substitutions at K17 were degraded at similar or increased levels compared to Hst5 (e.g., K17R, K11RK17R, and K11RK17L with Sap1); however, they also had similar or greater activity than degraded Hst5, indicating that the degradation products retained activity that was similar to that of the full-length peptides and Hst5.

In the case of incubation with Sap2 and Sap3, Hst5 and K5R exhibited more resistance to proteolysis than K5L, and antifungal activity followed a similar trend, with Hst5 and K5R retaining more antifungal activity following degradation than K5L. While these peptides were degraded by Sap1-3, the overall fragments formed by these variants maintained antifungal activity similar to or greater than the fully intact Hst5 peptide. When these K5 variants were incubated with Sap9, we observed that the proteolytic stability of K5R and K5L were similar to that of Hst5. However, degraded K5R retained more activity than degraded Hst5, while K5L retained less. While K5 may not play a role in the proteolytic stability of Hst5, the fragments formed from the K5L variant may have lower activity than the fragments formed from Hst5 and K5R. While proteolysis can reduce the antifungal activity of Hst5,

Rothstein et al. and Raj et al. show that truncations of Hst5, such as P-113 (AKRHHGYKRKFH) and C14/dh-5 (KRKFHEKHHSHRGY) respectively, can retain or improve antifungal activity [72, 73]. This is consistent with our results showing that although there are fragments formed by the proteolysis of the peptides, fragments of the parent peptide or variants may retain antifungal activity. Notably, not only was the proteolytic stability of all leucine variants except for K17L lower than that of Hst5 after incubation with Sap3, but their retained antifungal activity was also lower than the retained activity of Hst5. It is also worth noting that K17R and K17L are as proteolytically stable as Hst5 in the presence of Sap3. However, we did notice that the antifungal activity following Sap3 degradation is greater for K17R than Hst5, while that for K17L is lower. Similar to the case of the K5, the fragments formed by K17L variant may have lower activity than fragments formed by Hst5 and K17R.

3.3.4. *Saliva degrades Hst5 variants*

Hst5 normally resides in saliva, so interacts with various enzymes in saliva, making it important to assess the proteolytic stability of Hst5 variants in the presence of saliva. Of the *C. albicans* Saps, Sap1, Sap2, Sap3, Sap4, and Sap5 are found in saliva, with Sap1 and Sap3 having increased prevalence in patients with oral candidiasis[49] and Sap1 having increased prevalence in patients with severe early childhood tooth decay [50]. Saliva contains a complex mixture of enzymes, comprising various host proteases like cysteine cathepsins, the serine cathepsin A, the aspartic cathepsin D, and metalloproteases [95], along with microbial proteases secreted by organisms in the oral microbiome [47, 48].

To understand how proteases found in saliva degrade Hst5 and Hst variants, we incubated each Hst5 variant with saliva and quantified the degradation. We selected a saliva concentration resulting in about 40% of Hst5 remaining intact to facilitate visualization of both increased and decreased degradation. The degradation for most of the variants by saliva was not significantly different from the degradation of Hst5 (**Figure 3.8**); however, the K11R and K5L substitutions led to increased degradation, and the K17L substitution led to reduced degradation. Interestingly, while K5L was more prone to proteolysis, mimicking results seen from Sap1-3, K11L and K13L were as stable as the parent peptide in saliva, while they were more degraded by the Saps we tested. These results show that while modifications can be identified with varying proteolytic stability, the differences are moderate compared to those found in Saps, further engineering is necessary to identify variants that are more proteolytically stable in saliva, as saliva contains a complex mixture composed of more enzymes than Saps alone.

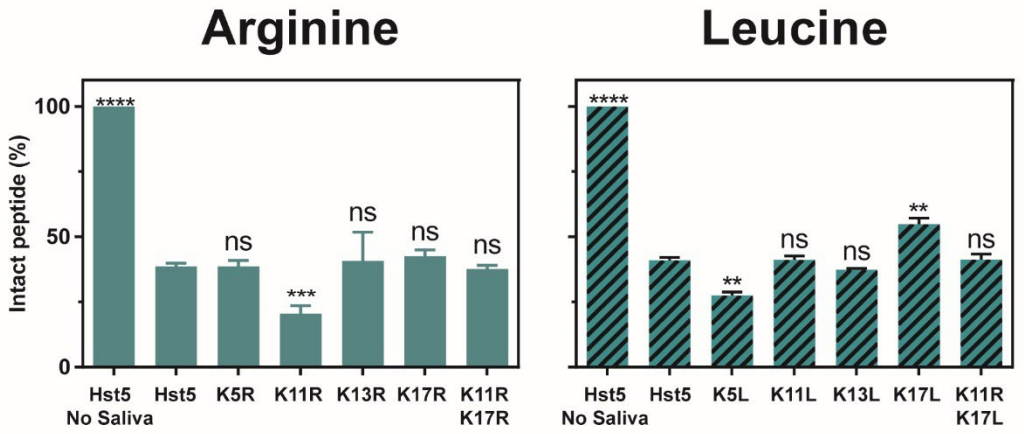

Figure 3.8. Degradation of Hst5 by saliva. After incubation for 2 h at 37 °C. We then used gel electrophoresis to separate fragments from fully intact peptides and quantified the gel images using densitometric analysis. Error bars represent the standard error of the mean (N = 9 Hst5 No Sap and Hst5, while N = 3 for all other variants).

3.3.5. Saliva proteolysis results in stable fragments

Similar to work done with the Saps, we utilized mass spectrometry for the determination of the degradation products and identification of fragments that may be resistant to proteolysis by saliva (**Figure 3.9**). After proteolysis by saliva, samples were prepared for analysis with mass spectrometry as described above. After proteolysis by saliva, Hst5 forms the fragments [1-12], [1-17], [1-18], [12-24], [13-24], [14-24], and [16-24]. Degradation of K5R by saliva yielded similar fragments to Hst5, though K5R did not form the [1-18] and [16-24] fragments. Instead, both the K5R and K5L variants formed the [6-24] fragment. Except for K11RK17L, variants with a substitution at K17 (K17R, K11RK17R, and K17L) formed the [1-18] fragment. All variants except K13R and K11RK17L formed the [13-24] fragment.

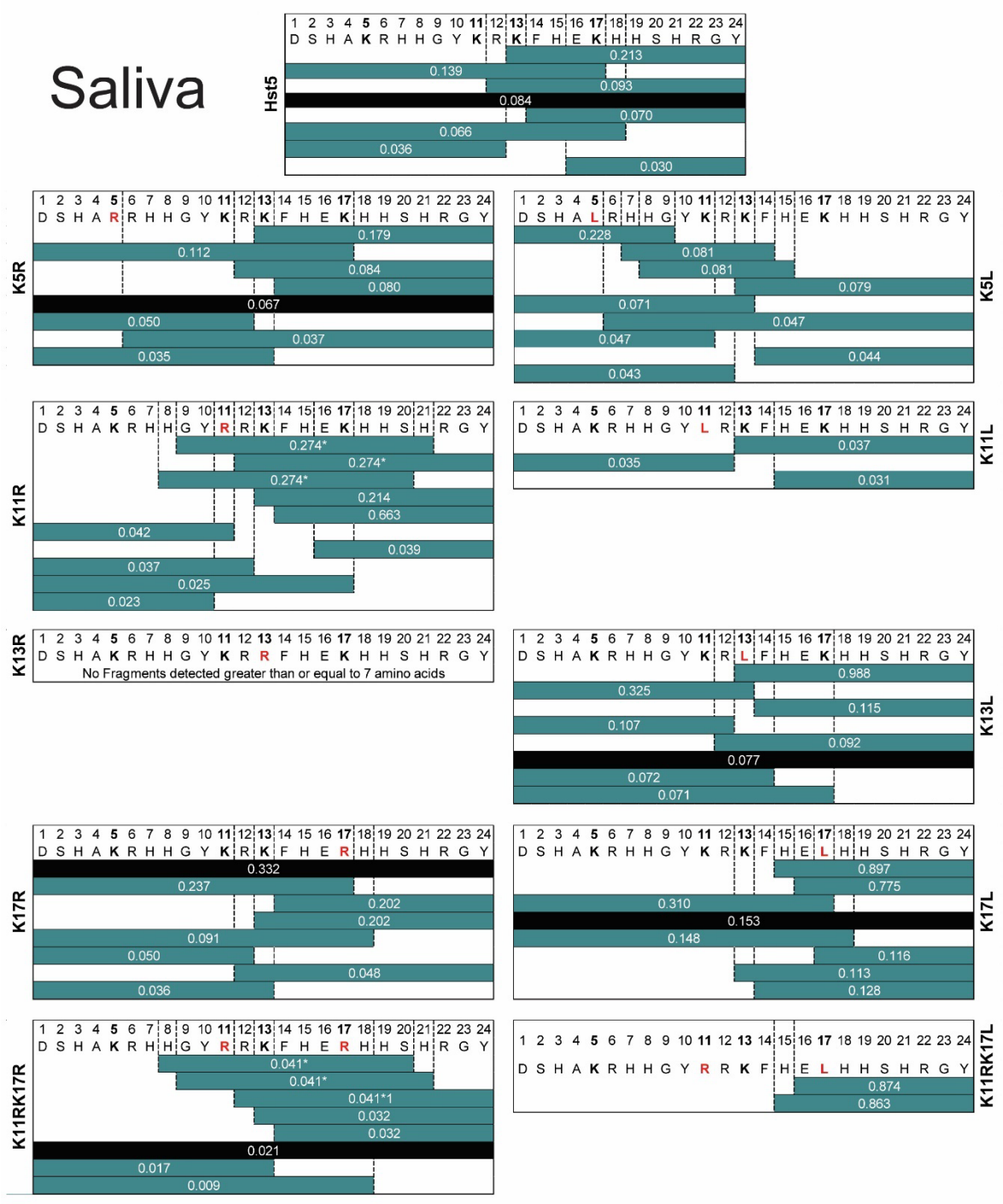

Figure 3.9. Fragments produced by incubation of Hst5 and variants with saliva. The peptides were each incubated with saliva for 2 h at 37 °C, and mass spectrometry was used to identify the fragments formed. Values shown are the average (*N*=2) normalized relative abundance of the fragment with respect to the standard MRFA. Black represents the fully intact peptide, while all other fragments are colored red. An asterisk (*) represent fragments that have the same mass and could, therefore, not be distinguished by mass spectrometry..

Similar to the proteolysis results, K5L and K11R were less stable than Hst5, as these variants did not have a detectable amount of the full-length peptide, while the K17L (relative intensity: 0.153) variant was more stable than Hst5 (relative intensity: 0.084 compared to). However, in the proteolysis data, all other peptides were meant to as stable as the parent Hst5 which is not the case in the mass spectrometry data. K11RK17R, K11L, and K11RK17L were all less stable than Hst5, as they had less full-length peptide after degradation by saliva than Hst5 and the K13R variant did not have any fragments greater than seven amino acids.

Degradation of Hst5 by saliva resulted in fragments that were generally consistent with the literature [37, 46, 90]. However, Puri et al. observed fragmentation of Hst5 near K5 and R6, which was not observed for Hst5 in our data. This could be because those fragments were further degraded or fragmentation did not occur at those residues. However, when substitutions were made at the K5 residue, fragmentation occurs at the C-terminal side of K5, making the fragment [6-24] one of the most abundant fragments. This could mean that the positive charge from lysine or arginine at K5 may help protect from proteolysis by saliva. Considering that Hst5 is a salivary peptide, the K5 may already be optimized to resist proteolysis in saliva. However, all variants maintained a similar trend where, despite the substitution, cleavage occurred between residues 11 and 18. Furthermore, K5R, K11R, K17R, K11RK17R, K13L, and K17L all have at least 5 fragments that are similar to the parent Hst5, showing that perhaps more than lysine residues need to be assessed to improve proteolytic stability against saliva. Overall, some modifications such as the K17L show a change in proteolytic stability in saliva and fragments that were more stable in saliva were

identified, however, further modifications need to be assessed to understand the interactions of Hst5 with protease found in saliva.

3.4. Conclusion

In this study, we have shown that substituting the lysine residues in Hst5 with arginine and leucine can impact its proteolytic stability after incubation with Saps and saliva. Furthermore, antifungal activity may be reduced after the variants are incubated with Saps. We determined that Sap5, Sap6, and Sap10, do not degrade or impact the antifungal activity of Hst5 and variants. We also identified the K17L variant as the most stable in the presence of saliva and other proteases, indicating its potential to resist proteolysis by more than just Saps. However, these variants were designed to resist proteolysis by Saps, which may not be enough, so other possible substitution sites should be considered beyond the lysines of Hst5. Understanding how Hst5 interacts with Saps and saliva could assist in developing future engineering strategies and further our understanding of the roles of Hst5 residues in the peptide's proteolytic stability.

4. Chapter 4: Investigating the impact of amino acid substitutions at K13 and K17 on the proteolytic stability and antifungal activity of Hst5

4.1. *Introduction*

Candida albicans is a commensal fungal pathogen that inhabits the oral microbiome [96]. However, in patients who are immunocompromised with diseases such as diabetes [2-4], HIV, and Down syndrome [5, 7, 84], *C. albicans* can cause an array of infections, such as oral thrush [83]. Currently, small-molecule antifungal agents are being used against *C. albicans* infections. However, due to toxicity and acquired resistance by *C. albicans* to these agents [8, 15-18], other methods have been explored to treat these infections.

Hst5 is a 24 amino acids antifungal peptide that is secreted from the salivary gland and has activity against *C. albicans* [30]. In patients with Down syndrome, reduced levels of Hst5 have been observe and are more prone to oral candidiasis [84], possibly linking Hst5 as a natural regulator of *C. albicans*. While other antifungal peptides form pores after interacting with targeted components on the surface of cells, Hst5 accumulates on the surface of *C. albicans*, interacts with the membrane proteins Ssa1p and Ssa2p [67], and then is translocated through the fungal cell membrane by the Dur3p or Dur31p transporter [68, 97]. Once in the cell, Hst5 is hypothesized to form reactive oxygen species inside of the mitochondria, reducing the viability of *C. albicans* [98].

While Hst5 can reduce the viability of *C. albicans*, it is susceptible to proteolytic degradation, hindering its potential in therapeutic applications. *C. albicans* produces a family of 10 secreted aspartyl proteases (Saps), Sap1-8 are secreted fully to the extracellular space, while Sap9 and Sap10 are anchored to the cell membrane via glycosylphosphatidylinositol (GPI) anchors or GPI proteins [36, 42]. As with other aspartyl proteases, Saps have 2 canonical aspartate residues in the active site and prefer to cleave near arginine and lysine, as well as hydrophobic residues [42, 89]. As the Hst5 sequence comprises 4 lysine, 3 arginine, and 3 large hydrophobic molecules, it is prone to proteolysis by these enzymes. Although these Saps each play a crucial role in the pathogenicity of *C. albicans,* there is little work on their ability to cleave Hst5. In previous work from our lab, variants were designed with substitutions at the lysine residues in Hst5 to either arginine or leucine. The results indicated that after treatment with Sap2 and Sap9 K13 variants (K13R and K13L) were more prone to proteolysis than the parents Hst5, while K17 variants (K17R and K17L) had enhanced proteolytic stability compared to the parent peptide [34]. Showing that the tested K17 mutations could work to protect the peptides from proteolysis, While K13 showed varying results in proteolytic stability, but always had reduced antifungal activity. The previous work showed the importance of the lysine residues in the interaction between Hst5 and Saps was explored; however, only leucine and arginine modifications were made, making different amino acid properties at K13 and K17 interesting prospects that will further be explored in this work.

As a salivary peptide, Hst5's natural environment is the saliva, which consists of a variety of different proteolytic enzymes such as cysteine cathepsins, the serine

cathepsin A, the aspartic cathepsin D, and metalloproteases [46, 95]. For Hst5 to be an effective antifungal agent it must retain proteolytic stability in the presence of saliva. Prior work has shown that after mixing saliva with Hst5, Hst5 is degraded [78, 90, 91]. In the previous chapter, we showed that Hst5 variant K17L has improved activity proteolytic stability after incubation with saliva. The marginal increase showed that assessing only arginine and leucine substitutions may not be enough, making further investigation necessary. Assessing further amino acid properties provides greater potential in determining the interactions between Hst5 and saliva.

Saliva does not only consist of proteolytic enzymes but there are also dietary metals such as zinc. Zinc has been linked to regulating the activity of Hst5 and promoting commensalism of *C. albicans* [81]. When in the presence of zinc, Hst5 can be found on the surface of *C. albicans* [81], and *C. albicans* sends signals to protect the cell wall integrity [99]. This means that zinc prevents Hst5 from entering into *C. albicans* to have its activity but still accumulates on the surface of the cell. However, Norris et al. noticed that when tested at a 1:2 zinc-to-peptide ratio in 10 mM NaPB, Hst5 reduced the viability of *C. albicans* [79, 99]. Campbell et al. found that increased zinc concentrations reduce the antifungal activity of Hst5 [81]. These findings indicate that zinc could work to regulate the activity of Hst5 against *C. albicans*. However, the impact of these metals on the proteolytic stability of Hst5 has not been assessed.

To improve the understanding of how Hst5 interacts with Saps, we have designed variants of Hst5 at the K13 and K17 residues. Substitutions were chosen to understand how the following residue properties impact interactions with Sap1, 2, 3,

5, 6, 9, and 10: arginine, a positively charged side group; leucine, a hydrophobic neutral side chain without hydrogen bond potential; tryptophan, a large hydrophobic side chain with hydrogen bond donating potential; histidine, both a hydrogen acceptor and electron donor; glutamine, a neutral charge side chain and a hydrogen bond donor and acceptor; alanine, a small neutral charged side chain with no hydrogen bond potential; and glutamate, a negative charge side group and a strong hydrogen bond acceptor. This work expands on previous work from our lab and in chapter 3 of testing proteolytic stability of Hst5 [34, 35]. Our study indicates that while the proteases Sap5, Sap6, and Sap10 do not degrade any Hst5 variants under our test conditions, the K17 variants show the highest proteolytic stability and enhanced antifungal activity. Contrarily, most K13 variants except K13R, reduce proteolytic stability, highlighting the importance of positive charge at this position. Additionally, the antifungal activity of K17L decreased after Sap3 proteolysis, whereas other K17 variants perform better than Hst5 treated with Sap3. The presence of zinc was found to lower the proteolytic stability of Hst5 when incubated with Sap2. Notably, the K17W variant not only demonstrated superior proteolytic stability but also increased antifungal efficacy, even in the presence of zinc, and significantly reduced *C. albicans* biofilms. This suggests that enhancing the proteolytic stability of Hst5 could improve its antifungal properties, though there is still room for improvement against saliva.

4.2. *Material and methods*

4.2.1. Peptides and reagents

Hst5 and Hst5 analogs were synthesized by Biomatik (Ontario, Canada) with a purity ≥95% and trifluoroacetic acid removal to hydrochloric acid salt. Zincon and zinc sulfate heptahydrate was purchased from Thermofisher and suspended in methanol and water respectively. B. Hube from Friedrich Schiller University in Germany kindly gifted the purified enzymes Sap1, Sap2, Sap3, Sap5, Sap6, Sap9, and Sap10. The purification of Sap1, Sap2, Sap3, and Sap6 involved ion exchange chromatography, followed by desalting into 0.1 M sodium citrate buffer. Sap5 was purified via ultrafiltration and subsequently desalted into 0.1M sodium citrate. Sap9 and Sap10, which were produced without their GPI anchors, underwent purification through ion exchange chromatography and were similarly desalted into 0.1 M sodium citrate buffer [42].

4.2.2. Proteolytic degradation of the peptides by Saps

The extent of degradation of the peptides by the Saps was evaluated at a pH 7.4. Hst5 and engineered analogs were each mixed with Saps, to a final concentration of 150 µg/mL of peptide and the protease concentration in the **Table 4.1**. Experiments were done in 1mM sodium phosphate buffer (NaPB). The mixtures were incubated at 37 ℃ for 2 h, and Hst5 in 1mM NaPB was used as a control. The concentration were chosen because this is when ~50% of the parent peptide Hst5 was observed after incubation of 2 h, making changes in proteolytic stability easier to observe. Samples were then boiled for 5 min at 100 ℃ to inactivate the protease. This assay was done with three replicates.

Table 4.1. Concentration of Saps after mixing with peptides.

Sap	Final concentration (μg/mL)
Sap1	5.0
Sap2	0.1
Sap3	1.6
Sap5	5.0
Sap6	5.0
Sap9	3.1
Sap10	5.0

4.2.3. Proteolytic degradation of the peptides by saliva

Saliva (gender-pooled, unfiltered, frozen) was purchased from BIOIVT (Westbury, NY). The saliva was centrifuged at 3,900 ×g for 5 minutes to remove any cells or debris. A 10 kDa molecular weight cutoff column was used to exchange the solution to 2 mM NaPB, and the saliva was stored in the at -20 °C freezer until later used. The solution was then diluted 1:1.15 with 2 mM NaPB to yield a concentration resulting in ~50% of the Hst5 peptide degraded under assay conditions.

The degradation of the peptides by saliva was evaluated using a procedure analogous to the one used for Saps. The assay was performed in NaPB, with a final peptide concentration of 150 μg/mL and a final dilution of the saliva of 1:2.3. The mixtures were incubated at 37 °C for 2 h. Samples were then boiled for 5 min at 100 ℃ to inactivate the proteases in saliva and stored at 20 °C until later used. This assay was done in three replicates.

4.2.4. Gel electrophoresis data analysis

After proteolysis, samples were mixed with tricine sample buffer (200mM Tris-HCl, pH 6.8, 40% glycerol, 2% sodium dodecyl sulfate, without Coomassie Blue G250) containing 2% β-mercaptoethanol and boiled again for 5 min at 100 °C. The degraded and nondegraded peptides were separated by gel electrophoresis on 16.5% Tris-tricine gels (Bio-Rad, Hercules, CA), and the gels were fixed in a solution of 10% acetic acid, 40% methanol, and 50% water for 30 min. The fixed gels were stained in Bio-Safe Coomassie stain (Bio-Rad) for 1 h and then washed in ultrapure water three times for 30 minutes and once overnight. The gels were imaged on a ChemiDoc imager (Bio-Rad), and densitometric analysis was done using Image Lab software (Bio-Rad). In the analysis, the upper band of each lane was taken as the intact peptide, while all bands below were taken as degradation products.

Two-way ANOVA tests with α = .05 and Dunnett's multiple comparison tests (degraded Hst5 as the control) were performed for statistical analysis. The number of asterisks indicates the level of statistical significance in figures: * for $P < 0.05$, ** for $P < 0.01$, *** for $P < 0.001$, and **** for $P < 0.0001$ Tables of the *P*-values obtained in the statistical analysis data are supplied in **Appendix Table B.1.**

4.2.5. Quantifying overall proteolytic stability of variants

To differentiate between peptides with an overall increase in proteolytically stability, we defined an increase or decrease in stability as a change in normalized intact peptide (NIP):

$$\frac{\sum_{Sapj} I_{Variant}}{\sum_{Sapj} I_{Hst5}} = NIP \tag{4.1}$$

where Sap j refers to the tested Sap (Sap1, Sap2, Sap3, or Sap9), the $I_{Variant}$ is the percent of intact peptide variant remaining after proteolysis by Sap j, the I_{Hst5} is the percent of intact Hst5 remaining after proteolysis by Sap j, and the $\sum_{Sapj} I_{variant}$ is the sum of P after degradation by Sapj. If this value is greater than 1 the value is defined as an increase in stability. If this value is less than 1 and we find the difference significant, the value is defined as a reduction in stability.

4.2.6. *Candidacidal assay using full-length peptide*

The antifungal activity of protease treated peptide was examined by an antifungal assay. A single colony of the SC5314 stain of *C. albicans* was inoculated into YPD. The culture was grown overnight, subcultured to an optical density measured at 600nm (OD_{600}) of 0.1, and grown to an OD_{600} range of 1-1.2. Cell cultures were grown at 30 °C as this promotes the growth of yeast cells, as opposed to hyphae (37 °C)[93] Cells were washed three times in 2 mM NaPB and diluted to a cell density of 5×10^5 cells/mL. Hst5 and engineered analogs were each mixed with 2 mM NaPB to a final concentration of 150 µg/mL of peptide. In 96 well plates, serial dilutions of the peptide (peptide concentration 75 – 0.14 µg/mL) were prepared in autoclave ultra-pure water. 20 µL of serial diluted peptide and cells were mixed and incubated at 30 °C for 30 min. After incubation, 280 µL of 1mM NaPB was loaded into each well to reduce interaction between the peptide and cells. Samples were further diluted to approximately 250 cells/well in a separate 96-well plate containing 200 µL of equal volume YPD and 1mM NaPB, where wells only containing YPD and

NaPB were sterility controls. The OD_{600} was measured on a microplate shaker at 30 °C after 17 h. The reduction in viability was calculated as

$$Reduction\ in\ viability\ (\%) = \left[1 - \frac{\left(OD_{\text{with peptide}} - OD_{\text{background}}\right)}{\left(OD_{\text{no peptide}} - OD_{\text{background}}\right)}\right] \times 100$$

The assay was performed on three separate days with two replicates each day. Two-way ANOVA tests with $\alpha = 0.05$ and Dunnett's multiple comparison tests (degraded Hst5 as the control) were performed for statistical analysis. $P < 0.05$ was deemed as significant (**Appendix Table B.2**).

4.2.7. Candidacidal assay of degraded peptide

To assay the antifungal activity of the peptides following degradation with Saps, the peptides were first degraded by Saps as described above. A *C. albicans* suspension was prepared as described for the assay with intact peptides, except the cell suspension was prepared in 1 mM NaPB. In 96-well plates, serial dilutions (20 µL) of the degraded peptide solutions (peptide concentration of 0.14 – 75 µg/mL prior to degradation) were prepared in 1 mM NaPB. Control wells containing no peptide were also included. The serial dilutions were mixed with an equal volume of the cell suspension and incubated at 30 °C for 30 min. After incubation, the samples were processed in the same manner as described above for the assay with intact peptides to quantify the reduction in growth. The assay was performed on three separate days with two replicates on each day.

Two-way ANOVA tests with $\alpha = .05$ and Dunnett's multiple comparison tests (degraded Hst5 as the control) were performed for statistical analysis. $P < .05$ was deemed as significant (**Appendix Table B.2**).

4.2.8. Zincon competition assay

To determine if Hst5 binds to zinc, a binding competition assay was carried out utilizing the colorimetric copper and zinc binding dye Zincon. In a 96 well plate, peptide variants were individually mixed 1:1 with Zincon to a final concentration of 30 μM in 10 mM NaPB. $ZnSO_4$ was then titrated with increasing equivalents to a final reaction volume of 100 μL, and absorbance at 621 nm was measured using a plate reader.

Data were collected in triplicate. Two-way ANOVA tests with $\alpha = .05$ and Dunnett's multiple comparison tests (Zincon as the control) were performed for statistical analysis. $p < .05$ was determined to be statistically different. Tables of the p-values obtained in the statistical analysis data are supplied in **Appendix Table B.3.**

4.2.9. Candidacidal assay using full-length peptides in the presence of zinc.

The antifungal activity of zinc treated peptide was examined by an antifungal assay. The cells were prepared as described above for the **Candidacidal assay using full-length peptides**. Zinc was mixed with water to a final concentration of 1200 μM. In a 96 well plates, 12.5 μL serial dilutions of the zinc (1200 – 1.2 μM) were prepared in autoclave DI water. Hst5 and engineered analogs were added equal volume to each well to a final concentration of 30 μM and a final sample volume of 25 μL. A volume of 25 μL of cells was added to the zinc and peptide mixture and incubated at 30 °C for 30 min. Sampled were prepared for analysis as described above for the **candidacidal assay using full-length peptides.**

Data for this assay were collected with two replicates over two days. Two-way ANOVA tests with $\alpha = .05$ and Dunnett's multiple comparison tests (Hst5 as the control) were performed for statistical analysis. $P < 0.05$ was deemed as significant (**Appendix Table B.4**).

4.2.10. *Proteolysis of peptide variants in the presence of Zinc*

To determine the impact of zinc on the proteolytic stability of each peptide variant, peptide variants were individually mixed with zinc (2:1 Zinc-to-peptide molar ratio) to a final concentration of 60 µM, this mixture was then mixed in equal volume with 0.2 µg/mL Sap2 in 2mM NaPB. The mixtures were incubated at 37 ℃ for 2 h, and Hst5 in 1mM NaPB was used as a control. An incubation of 2 h was chosen to observe 20-50% degradation of Hst5. Samples were then boiled for 5 min at 100 ℃ to inactivate the protease and visualized using gel electrophoresis.

4.2.11. *Antifungal assay of Hst5 variants after degradation by Saps in the presence of zinc*

The antifungal activity of zinc treated peptide was examined by an antifungal assay. The cells were prepared as described above for the **candidacidal assay using full-length peptides**. Peptide variants were individually mixed with zinc (2:1 Zinc-to-peptide molar ratio) to a final peptide concentration of 60 µM, this mixture was then mixed in equal volume with 0.2 µg/mL Sap2 in 2mM NaPB. The mixtures were incubated at 37 ℃ for 2 h. The samples were boiled at 100 °C to deactivate protease. In a 96 well plate 25 µL serial dilutions of the zinc and peptide mixture (30 – 0.03 µM) were prepared in autoclave DI water. A volume of 25 µL of cells was added to

the zinc and peptide mixture and incubated at 30 °C for 30 min. Sampled were prepared for analysis as described above for the **candidacidal assay using full-length peptides.**

This assay was performed with two replicates on two separate days. Two-way ANOVA tests with $\alpha = 0.05$ and Dunnett's multiple comparison tests (Hst5 as the control) were performed for statistical analysis. $P < 0.05$ was deemed as significant (**Appendix Table B.5**).

4.2.12. *Biofilm prevention assay using full-length peptide.*

The ability of the peptide to prevent biofilm formation was assessed. A single colony of *C. albicans* SC5314 was inoculated into YPD. The culture was grown overnight at 30 °C and then washed in 1× PBS and diluted into RPMI 1640 (with L-glutamine, and without sodium bicarbonate)(MP Biomedicals; Santa Ana, California), buffered in MOPS (3-[N-morpholino] propanesulfonic acid) (Glibco; Waltham, MA) to a pH of 7.0. The optical density was then adjusted to 1×10^6 cells/mL. In a 96-well plate, 50 µL serial dilutions of antifungal agents (32 µg/mL – 0.06 µg/mL) and peptides (1500 µg/mL – 1.5 µg/mL) were prepared in water. A volume of 50 µL of serially diluted peptide and an equal volume cells were mixed and incubated at 37 °C for 24 h. The plate were decanted and washed in 1×PB. After 100 µL of a solution containing 0.5 g/L XTT and 1 µM menadione was added to each well and incubated for 1.5 h in reduced light. Afterward, 75 µL of the solution was transferred to a corresponding well in a new 96-well plate, and the absorbance was measured at 490 nm using a plate reader. The reduction in growth is calculated as

$$Reduction\ in\ viability\ (\%) = \frac{\left(A_{490}^{No\ peptide} - A_{490}^{XTT}\right) - \left(A_{490} - A_{490}^{XTT}\right)}{\left(A_{490}^{No\ peptide} - A_{490}^{XTT}\right)} \quad (4.3)$$

where $A_{490}^{No\ peptide}$ is the average absorbance for wells with biofilms of a specified strain not formed in the presence of antifungal, A_{490}^{XTT} is the average absorbance for wells in rows of replicates for each drug/strain combination containing only XTT, and A_{490} is the absorbance for wells containing a specified concentration of peptide and a specified *C. albicans* strain.

This assay was performed with 2 replicates on 2 separate days. Two-way ANOVA tests with α = .05 and Dunnett's multiple comparison tests (Hst5 as the control) were performed for statistical analysis. $P < .05$ was deemed as significant (**Appendix Table B.6**).

4.3. *Results*

To study the interactions of Hst5 with *C. albicans* Saps and Saliva, we evaluated the proteolysis of Hst5 and 12 variants designed at either the K13 or K17 residues of Hst5 (**Table 4.2**). To determine the degree of degradation, we use gel electrophoresis. Prior work from our lab shows that K17 substitutions improve the proteolytic stability of Hst5 after incubation with Sap2, Sap9, and *C. albicans* **[34, 35]**. In Chapter 3, we expanded the number of Saps we assessed proteolytic stability against and also assess proteolytic stability against saliva. In this chapter, we continued prior work with 12 variants of Hst5, five introduced by Ikonomova et al. (K13R, K13L, K13H, K17R, and K17L) **[34, 35]**, one introduced by Tsai et al. (K13E) [74], and we introduced six novel variants with varying properties at K13 and K17 (K13Q, K13A, K17W, K17Q, K17A, and K17E) and assess their proteolytic stability against Saps and saliva.

Table 4.2. Table of designed peptide variants.

Peptide	Sequence[a]																							
	1	2	3	4	5	6	7	8	9	10	11	12	13	14	15	16	17	18	19	20	21	22	23	24
Hst5	D	S	H	A	K	R	H	H	G	Y	K	R	K	F	H	E	K	H	H	S	H	R	G	Y
K13R	-	-	-	-	-	-	-	-	-	-	-	-	R	-	-	-	-	-	-	-	-	-	-	-
K13L	-	-	-	-	-	-	-	-	-	-	-	-	L	-	-	-	-	-	-	-	-	-	-	-
K13H	-	-	-	-	-	-	-	-	-	-	-	-	H	-	-	-	-	-	-	-	-	-	-	-
K13Q	-	-	-	-	-	-	-	-	-	-	-	-	Q	-	-	-	-	-	-	-	-	-	-	-
K13A	-	-	-	-	-	-	-	-	-	-	-	-	A	-	-	-	-	-	-	-	-	-	-	-
K13E	-	-	-	-	-	-	-	-	-	-	-	-	E	-	-	-	-	-	-	-	-	-	-	-
K17R	-	-	-	-	-	-	-	-	-	-	-	-	-	-	-	-	R	-	-	-	-	-	-	-
K17L	-	-	-	-	-	-	-	-	-	-	-	-	-	-	-	-	L	-	-	-	-	-	-	-
K17W	-	-	-	-	-	-	-	-	-	-	-	-	-	-	-	-	W	-	-	-	-	-	-	-
K17Q	-	-	-	-	-	-	-	-	-	-	-	-	-	-	-	-	Q	-	-	-	-	-	-	-
K17A	-	-	-	-	-	-	-	-	-	-	-	-	-	-	-	-	A	-	-	-	-	-	-	-
K17E	-	-	-	-	-	-	-	-	-	-	-	-	-	-	-	-	E	-	-	-	-	-	-	-

[a] *The hyphens represent retained amino acid.*

4.3.1. K17 variants generally show an improvement in proteolytic stability

To assess the degradation of Hst5 and its analogs by Saps, we selected concentrations of Saps that preserved 25 - 50% of the fully intact Hst5 peptide after two hours at 37 °C in 1 mM NaPB (pH 7.4). This strategy allowed for the clear identification of differences in the proteolytic stability among the peptides. Similar to the results in Chapter 2, Sap5, Sap6, and Sap10 did not degrade Hst5 (**Appendix Figure B.2.**). The tests showed that Sap1, Sap2, Sap3, and Sap9 cleaved Hst5 and its variants at levels influenced by the specific protease and the peptide modifications (**Figure 4.1**). After incubation with Sap1, 36.6% of Hst5 remained fully intact. The variants K17Q and K17E had enhanced proteolytic stability compared to Hst5, with 51.4% and 49.6% of the peptide remaining fully intact, respectively. Incubation with Sap2 resulted in 49.2% of Hst5 remaining intact, and K17E was statistically similar to Hst5. The K17R variant was less proteolytically stable, with only 35.1% of the peptide remaining intact, while K17W, K17A, K17Q, and K17L had enhanced proteolytic stability with 81.1%, 77.2%, 74.0%, and 72.9% intact. When incubated with Sap3, 45.0% of Hst5 remained fully intact, while K17R and K17L were statistically similar. Other K17 variants showed an improvement in proteolytic stability in the presence of Sap3, with K17W, K17Q, K17E, and K17A having 66.9%, 60.6%, 59.6%, and 57.3% of fully intact peptides, respectively. Finally, after incubation with Sap9, 41.6% of Hst5 remained fully intact. All K17 variants had enhanced proteolytic stability with K17Q, K17W, K17R, K17E, K17L, and K17A having 79.0%, 78.0%, 77.9%, 77.8%, 73.1%, and 68.1% of peptide remaining intact respectively.

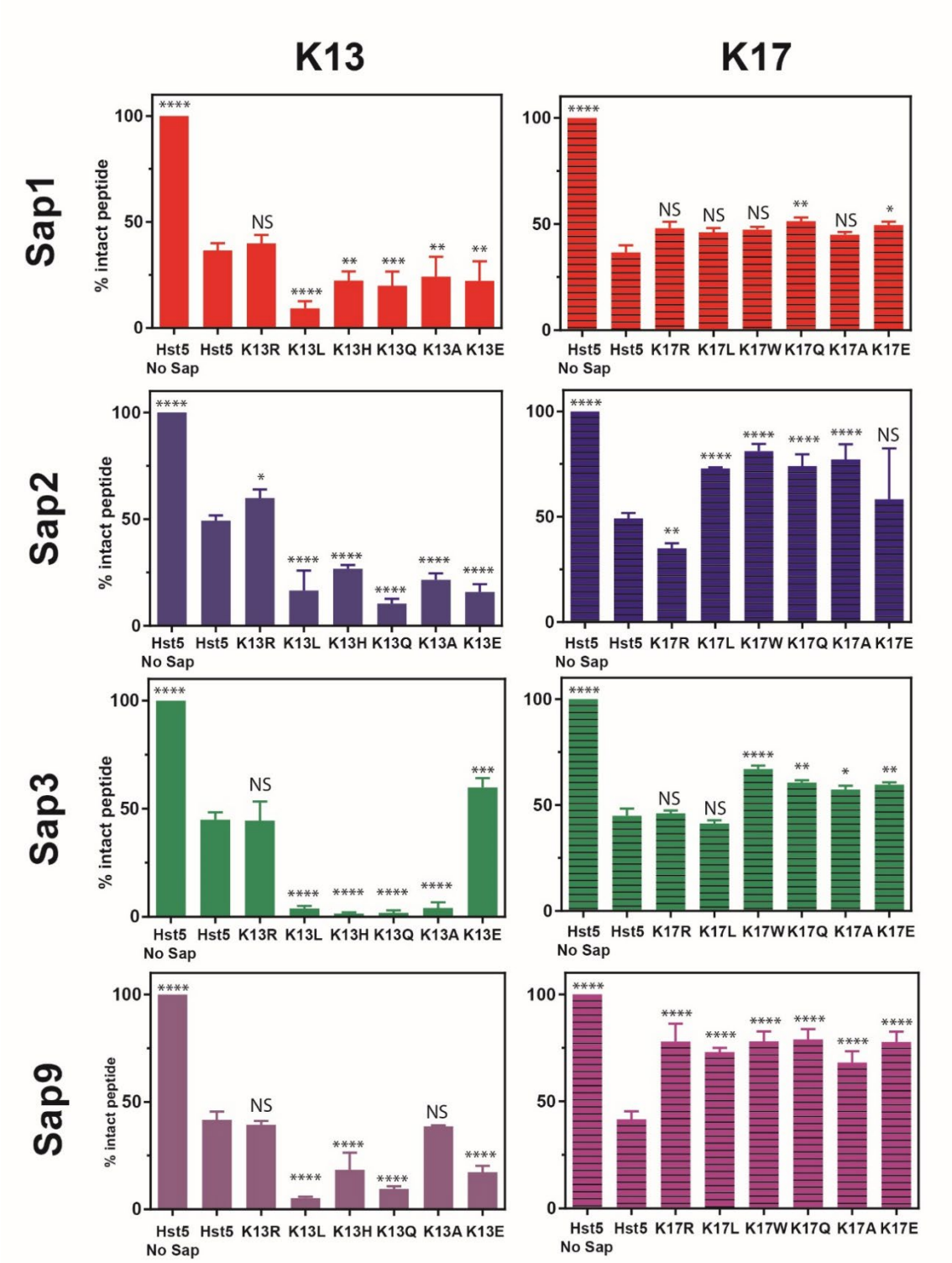

Figure 4.1. Degradation of Hst5 by purified Sap1, Sap2, Sap3, and Sap9. After incubation for 2 h at 37 °C, the intact peptide and degradation fragments were separated by gel electrophoresis and quantified densitometry. Error bars represent the standard error of the mean (N = 6 for the Hst5 controls with and without Sap and N = 3 for the Hst5 variants). Gel images in **Appendix Figure B.1**.

4.3.2. K13 variants generally show a reduction in proteolytic stability

Unlike K17 variants, K13 variants previously had similar or reduced proteolytic stability compared to the parent peptide after incubation with Saps. After incubation with Sap1, 36.6% of Hst5 remained fully intact. Only K13R was as stable as the parent peptide; all other variants were less stable, with K13A, K13H, K13E, K13Q, and K13L all within 9.3% – 24.2% intact. Incubation with Sap2 resulted in 49.2% of Hst5 remaining intact, and the only variant with enhanced stability was K13R, with 60.0% remaining fully intact peptide. All other variants, K13H, K13A, K13L, K13E, and K13Q had diminished stability, falling between 10.5% – 26.8%of the peptide remaining intact. Degradation by Sap3 left 45.0% of Hst5 fully intact, and K13R was as stable as the parent peptide. Only the K13E variants had enhanced proteolytic stability, with 59.8% remaining fully intact. Other variants were less stable, with K13H, K13Q, K13L, and K13A having less than 5% of the peptide remaining intact. Finally, after incubation with Sap9, 41.6% of Hst5 remains fully intact, with K13R and K13A being similar. The remaining variants all had reduced proteolytic stability. K13L, K13Q, K13E, and K13H were less proteolytically stable than Hst5 with 5.2%, 8.4%, 14.8%, and 15.0%, remaining intact, respectively.

4.3.3. K17W shows the greatest improvement in proteolytic stability in the presence of Saps

In order for the variants to be viable, they need to be proteolytically stable against a range of Saps. To identify the most improved variants, we compare the normalized

intact peptide (NIP) of all variants (**Equation 4.1**). The Nip values were determined by summing the average intact peptide for a variants after incubation with each Sap individually and normalizing them to the sum of the average intact Hst5 after incubation with each Sap individually. Values greater than 1 mean the variants are overall more proteolytically stable than the parent Hst5, while values less than 1 mean the variants are less proteolytically stable overall (**Table 4.3**). Of the variants designed at the K13 position, only K13R had overall improved proteolytic stability (NIP=1.09), while all other variants had NIP values between 0.21– 0.68. This suggests that the positively charged amino acid at K13 provides overall stability and protection from saps. The opposite is true in the case of K17, as the positive charge residue provided the least stability compared to the other variants tested (NIP=1.19). Other properties enhance the proteolytic stability (NIP between 1.3 –1.57), with the greatest enhancement in proteolytic stability coming from K17W (NIP=1.57). Suggesting the importance of positive charge residues in maintaining Hst5 interactions with Saps.

Table 4.3. Normalized intact peptide values for K17 and K13 variants.

Peptide	NIP[a,b,c]
Hst5	1.00
K13R	1.09
K13L	0.21
K13H	0.41
K13Q	0.25
K13A	0.52
K13E	0.68
K17R	1.19
K17L	1.34
K17W	1.57

K17Q	1.52
K17A	1.42
K17E	1.40

[a] NIP = Normalized average intact peptide
[b]Red represents the least overall stable variant.
[c]Green represents the most overall stable variants.

4.3.4. Substitutions to negatively charged residues reduce the antifungal activity of Hst5

While lysine substitutions often did not impact the antifungal activity of the full-length peptide similar to what was previously observed In **Chapter 2** and prior work from our lab [34]; When K13 was previously substituted for a glutamate, the antifungal activity of the full-length peptide decreased [35, 74]. To determine the impact of different amino acid properties at K13 and K17 on antifungal activity, we evaluate the antifungal activity of fully intact peptides against *C. albicans* (**Figure 4.2**). When assessing the antifungal activity, we determined if variants were statistically different by analyzing the first measured concentration at which the protease-treated Hst5 showed a reduction in viability of over 50%. While the variants K13R, K13H, K13Q, K13A, K17Q, and K17A had a statistically significant reduction in antifungal activity, and only K17L had statistically enhanced antifungal activity, the difference between these variants and the parent Hst5 is marginal as the curves all surpass 50% reduction in viability by 2.34 μg/mL. However, when glutamate, a negatively charged amino acid, is substituted at K13 or K17, a 95% reduction in viability is only surpassed at 75 μg/mL (the highest concentration tested), while other variants surpass this value at 18.75 μg/mL. The reduction in activity by K13E is

consistent with the literature, showing substituting a positive charge amino acid with a negatively charged amino acid reduces the antifungal activity of Hst5 [35, 74].

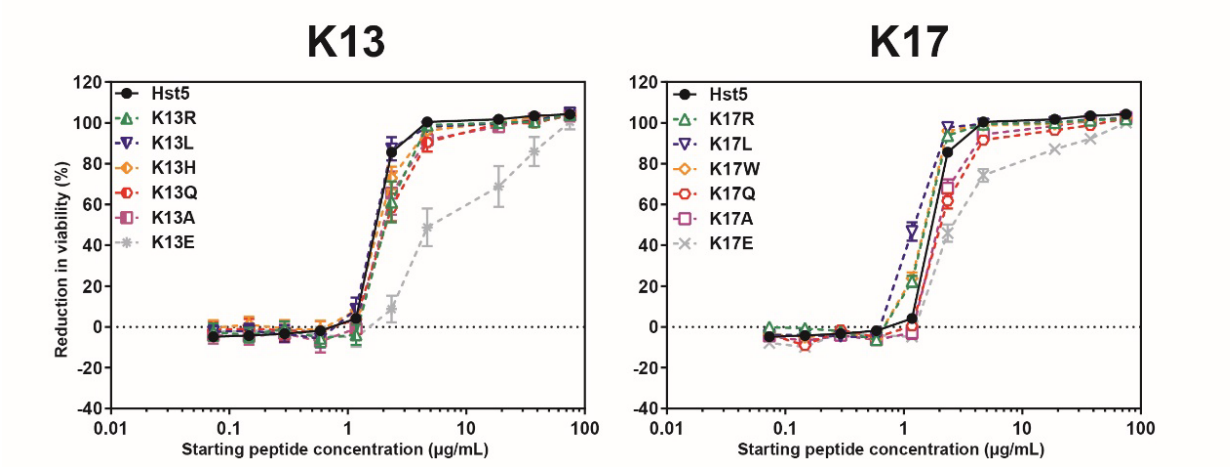

Figure 4.2. Antifungal activity of intact Hst5 variants. Hst5 variants were serially diluted, mixed with *C. albicans* cells, and incubated for 30 min at 30 °C in 1 mM NaPB. Error bars represent the standard error of the mean (N = 12 for Hst5 with and without Sap, while N = 6 for all Hst5 variants).

4.3.5. K17 variants retain antifungal activity following incubation with Saps

Hst5 is known to have decreased antifungal activity after degradation by Saps, making it essential to assess the antifungal activity of the peptides after incubation with Saps. In Chapter 3, we showed that K17L had improved antifungal activity in the presence of Sap1, Sap2, and Sap9 and that proteolysis by Sap3 reduced the proteolytic stability of leucine variants. Building on these results, in this chapter, we evaluated how proteolysis by Saps impacted the antifungal activity of variants with different amino acid properties (**Figure 4.3**). Proteolysis by Sap5, Sap6, and Sap10, does not affect the activity of Hst5 or Hst5 variants. Furthermore, all engineered variants were unaffected by Sap6 except for K13E, which had increased antifungal activity (**Appendix Figure B.2.**). After degradation by Sap1, the antifungal activity

of degraded K17 is similar to degraded Hst5, while all other K17 variants had statistically greater antifungal activity than Hst5; however, this increase was moderate as all variants surpass 50% reduction in viability at 2.34 µg/mL and surpass 90% at 4.69 µg/mL. Proteolysis by Sap2 reduces the antifungal activity of Hst5, while K17E has similar activity to degraded Hst5. However, other K17 variants all have improved antifungal activity compared to the degraded Hst5, having seemingly greater activity than undegraded Hst5. After incubation with Sap3, the activity of Hst5 is reduced. The K17L variant had lower than undegraded Hst5 antifungal activity, which is consistent with what was observed in the previous chapter, and K17W was the only variant with enhanced antifungal activity, surpassing 50% 2.34 µg/mL while the parent peptide only surpassed 50% at 9.38 µg/mL. Finally, after incubation with Sap9 all K17 variants had improved antifungal activity compared to degraded Hst5.

4.3.6. *Positive charge residues at K13 have the greatest antifungal activity*

Unlike the K17 variants, which mostly had similar or greater antifungal activity, K13 variants followed the opposite trend. After proteolysis by Sap1, degraded Hst5 had reduced activity compared to undegraded Hst5. However, as explained above, this difference was minimal. All K13 variants had lower activity antifungal activity than Hst5; however, Hst5 and K13R both surpass 90% reduction in viability at 4.68 µg/mL. After incubation with Sap2, K13R had similar activity to degraded Hst5. All other variants had reduced antifungal activity compared to Hst5. Proteolysis by Sap3 and Sap9 resulted in a reduction in antifungal activity for Hst5, with all of the K13 variants having reduced antifungal activity compared to degraded Hst5. Notably, the

K13R had the greatest activity compared to the other K13 variants implying the importance of the positive charge at K13 on antifungal activity.

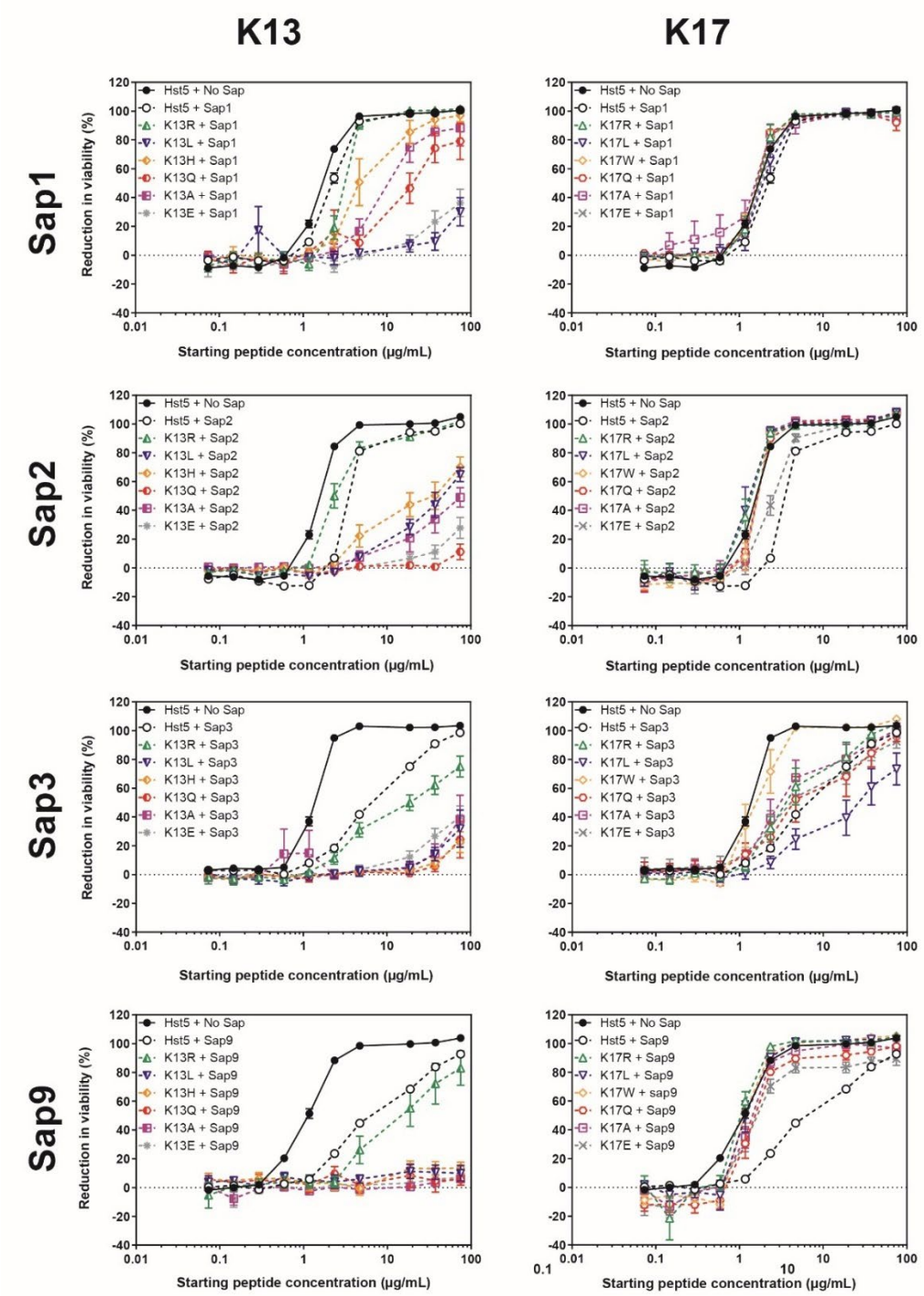

Figure 4.3. Antifungal activity of Hst5 variants after incubation with Sap1, Sap2, Sap3, or Sap9. After incubation for 2 h at 37 °C, Samples were serially diluted in a 96-well plate from 75 μg/mL to 0.14 μg/mL. Samples were then mixed with *C. albicans* cells at 5.0×10^5 cells/mL and incubated for 30 min at 30 °C in 1 mM NaPB, after which cells were inoculated and cultured. Error bars represent the standard error of the mean (N = 12 Hst5 No Saβand Hst5 + Sap, while N = 6 for all other variants).

4.3.7. K17 variants show minimal improvement in the presence of saliva

As a salivary peptide, Hst5 interacts with other enzymes in saliva, making it important to assess the proteolytic stability in the presence of saliva. To understand how proteases found in saliva degraded Hst5 and variants, we incubated each Hst5 variant with saliva and quantified the gel images using densitometric analysis (**Figure 4.4**). In **Chapter 2** we identified the K17L and K5R variants to have improved proteolytic stability, although the improvement was modest. We assessed additional K13 and K17 variants in the presence of saliva. After incubating Hst5 with saliva, 37.7% of Hst5 remains intact. Except for K13R, the K13 variants are as stable as the parent Hst5, while only the K17L and K17W showed improvement in proteolytic stability, with 52.9 and 52.8 of the peptides remaining intact. Other K17 were degraded similarly to the parent peptide. While both hydrophobic residues introduced at K17 may improve the proteolytic stability of the peptide. The improvement was modest, showing that engineering proteolytic stability against Saps does not substantially protect against other proteases in saliva. However, the variants designed will provide a good starting point for engineering more broadly proteolytically stable variants.

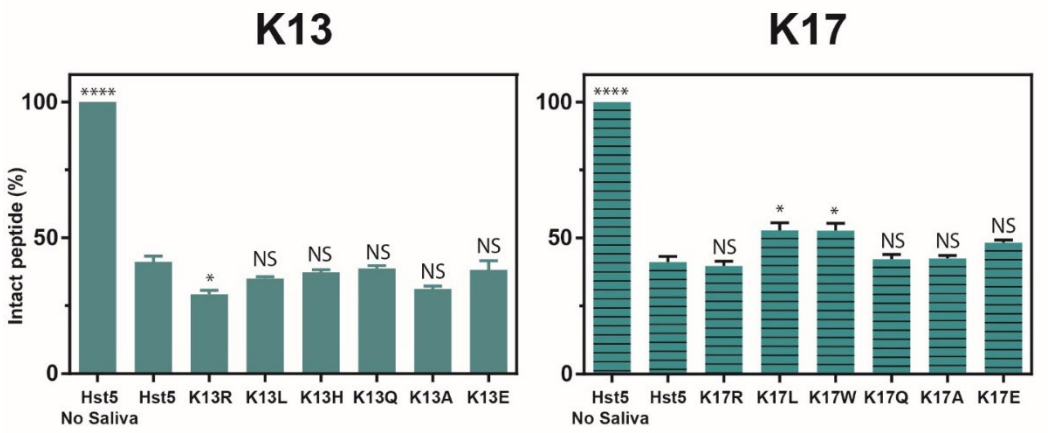

Figure 4.4. Degradation of Hst5 by saliva. After incubation for 2 h at 37 °C. We then used gel electrophoresis to separate fragments from fully intact peptides and quantified the gel images using densitometric analysis. Error bars represent the standard error of the mean (N = 6 Hst5 No Sap and Hst5, while N = 3 for all other variants).

4.3.8. Hst5 and variants bind to zinc

Metals such as zinc are essential in the catalytic activity of some enzymes and can assist in the folding of proteins [100] Along with other enzymes, saliva can also be composed of other dietary metals such as zinc. Zinc has been found to bind to either the HEKHH or HARKHH zinc-binding motifs of Hst5 [79, 81, 99]Previous work has shown that zinc binding to Hst5 can influence and reduce its activity; however, no work has been done to show the impact of zinc on Hst5's proteolytic stability. For these experiments, we used K17W (Table 4.4), as these were the variants with the greatest proteolytic stability, and K13H, as the introduction of a histidine residue should impact zinc binding.

Table 4.4. Designed peptide variants used to assess metal binding.

Peptide	Sequence [a]																							
	1	2	3	4	5	6	7	8	9	10	11	12	13	14	15	16	17	18	19	20	21	22	23	24
Hst5	D	S	H	A	K	R	H	H	G	Y	K	R	K	F	H	E	K	H	H	S	H	R	G	Y
K13H	-	-	-	-	-	-	-	-	-	-	-	-	H	-	-	-	-	-	-	-	-	-	-	-
K17W	-	-	-	-	-	-	-	-	-	-	-	-	-	-	-	-	W	-	-	-	-	-	-	-

[a] *The hyphens represent retained amino acids*

To determine if Hst5 and engineering analogs can bind to zinc, we measured Hst5's ability to compete for zinc using the indicator dye Zincon (**Figure 4.5**). Zincon has a high absorbance at 621 nm when zinc is bound and low absorbance when zinc is not bound. Consistent with the work of Norris et al., we saw that Hst5 binds zinc; additionally, K17W and K13H both bind zinc up to a 4:1 peptide-to-zinc ratio, with K13H binding the strongest to zinc.

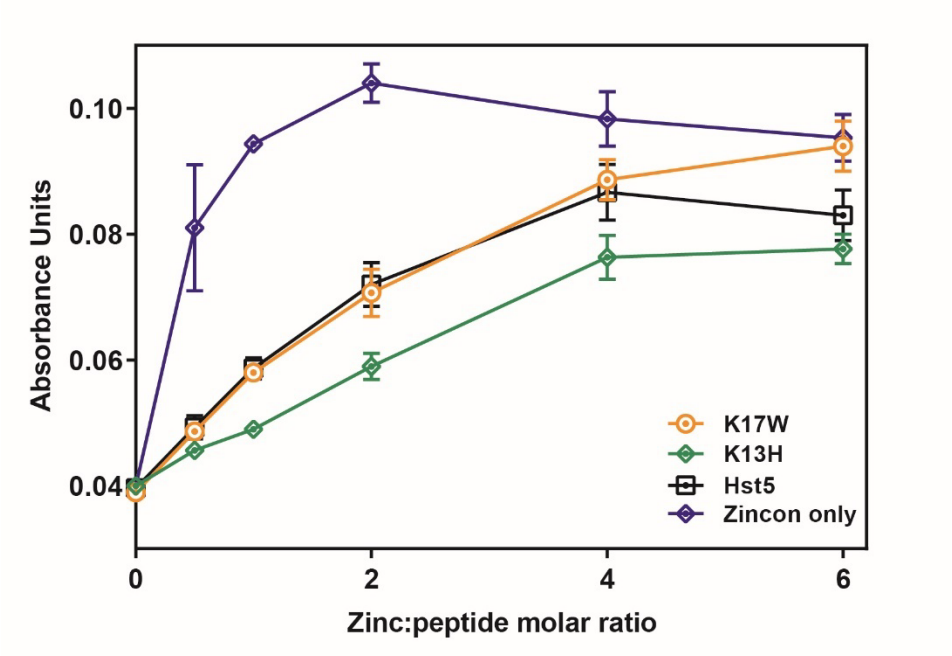

Figure 4.5. Zinc competition between peptide and Zincon. After titrating zinc into an equimolar mixture of Zincon and peptide, the absorbance was measured via absorbance at 621nm. Error bars represent the standard error of the mean (N = 3).

4.3.9. Zinc reduces the antifungal activity of Hst5 at large zinc-to-peptide ratios

Zinc binding to Hst5 has been linked with possibly modulating the antifungal activity of Hst5. Norris et al. showed that when Hst5 binds zinc at a 1:2 zinc-to-peptide molar ratio, the activity of Hst5 increases. Additionally, Campbell et al. have shown that a 20:1 zinc-to-Hst5 molar ratio is needed to see a reduction of 50% of Hst5 activity[81]. To understand the impact of zinc on the antifungal activity of the full-length Hst5, we performed a candidacidal assay using different molar ratios of zinc-to-Hst5 (**Figure 4.6**). At a 1.25:1 zinc-to-Hst5 ratio, peptide variants are able to reduce the viability of *C. albicans* completely; however, as the ratio-of-zinc increases, there was a reduction in activity until 20:1, where all variants antifungal activity was completely reduced. Notably, K13H was the least impacted at zinc-to-peptide ratios greater than 10:1 strong ability to bind to zinc. This shows that zinc at large zinc concentration the antifungal activity of Hst5 and variants can be reduced by zinc.

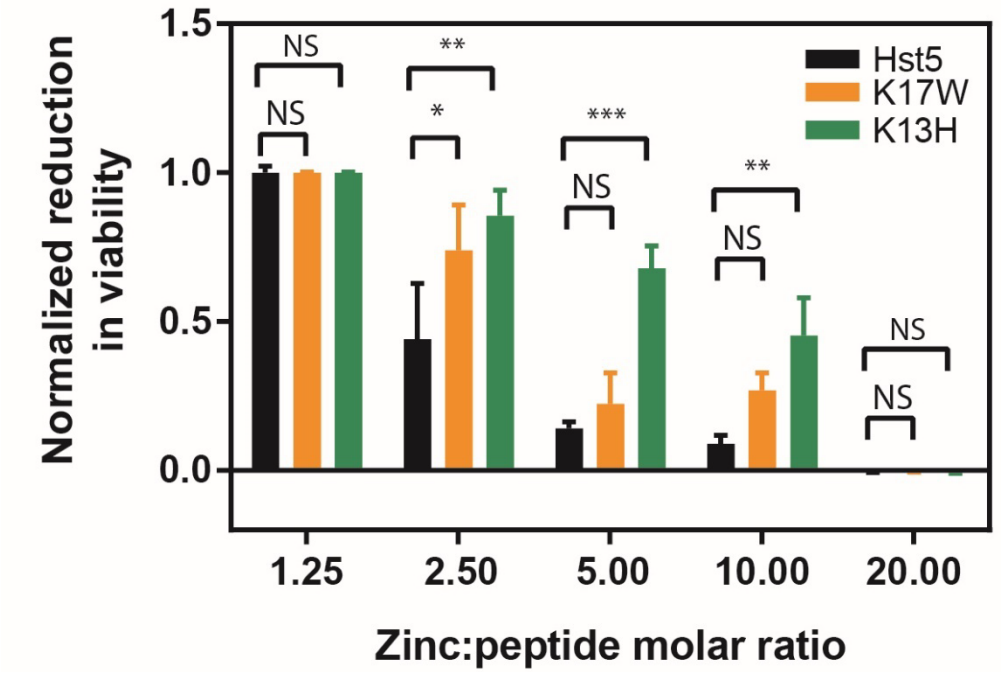

Figure 4.6. Antifungal activity of Hst5 variants in the presence of Zinc. Zinc was serial diluted (1200 µM to 1.2 µM) and equal volume of 60 µM peptide was added to each well. Samples were then mixed with *C. albicans* cells at 5.0×10^5 cells/mL and incubated for 30 min at 30 °C in 1 mM NaPB, after which cells were inoculated and cultured. Error bars represent the standard error of the mean (*N = 4)*.

4.3.10. *K17W retains proteolytic stability in the presence of zinc*

C. albicans secrete Saps into the oral microflora, meaning that these Saps may be in the presence of zinc. We have shown that Zinc can reduce the activity of Hst5 which is in agreement with work from Campbell et al.; however, there is no work on how the proteolytic stability of Hst5 can be impacted by zinc. To understand the impact of zinc binding on the proteolytic stability of Hst5, we first mixed peptide variants with zinc in a 2:1 molar ratio, as this showed the greatest discrepancy between K13H and other variants in the Zincon binding assay (**Figure 4.6**). While incubation with Sap6 did not impact the proteolytic stability (**data not shown**), suggesting that if the protease did not originally cleave the Hst5 at the tested conditions, zinc could not

change that. When these variants were degraded by Sap2 in the presence of zinc the proteolytic stability of Hst5 and K13H decreased, showing that zinc can reduce the proteolytic stability of Hst5. However, K17W retained its proteolytic stability as it does not get degraded by Sap2, even in the presence of zinc (**Figure 4.7**).

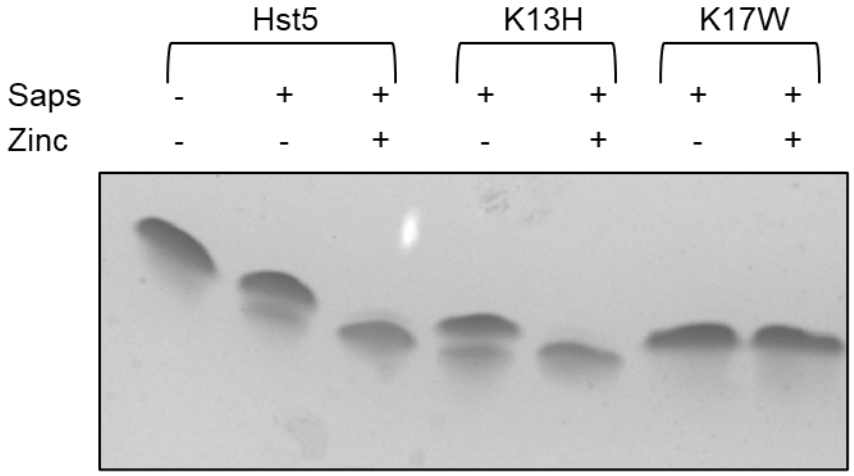

Figure 4.7. Proteolysis of Hst5 variants after incubation with sap2 and with or without zinc. After incubation for 2 h at 37 °C, we then used gel electrophoresis to separate fragments from fully intact peptides and quantified the gel images using densitometric analysis ($N = 2$).

4.3.11. K17W retains antifungal activity after incubation with zinc and Sap2

To determine the impact of proteolysis in the presence of zinc on antifungal activity, we mixed peptide, zinc, and protease under the previously mentioned conditions (**Figure 4.8**). As previously observed, full-length K13H and K17W have activity similar to Hst5, while, after incubation with Sap2, Hst5 and K13H have reduced activity and K17W retains activity. Peptides with zinc alone have reduced antifungal activity, although Hst5 and K17W treated with zinc approached 100% reduction in viability at the same time as Hst5 without zinc. Finally, when zinc and Saps are present, Hst5 and K13H have greatly reduced activity, while K17W activity is

reduced but still approaches 100% reduction in viability at the same time as untreated Hst5.

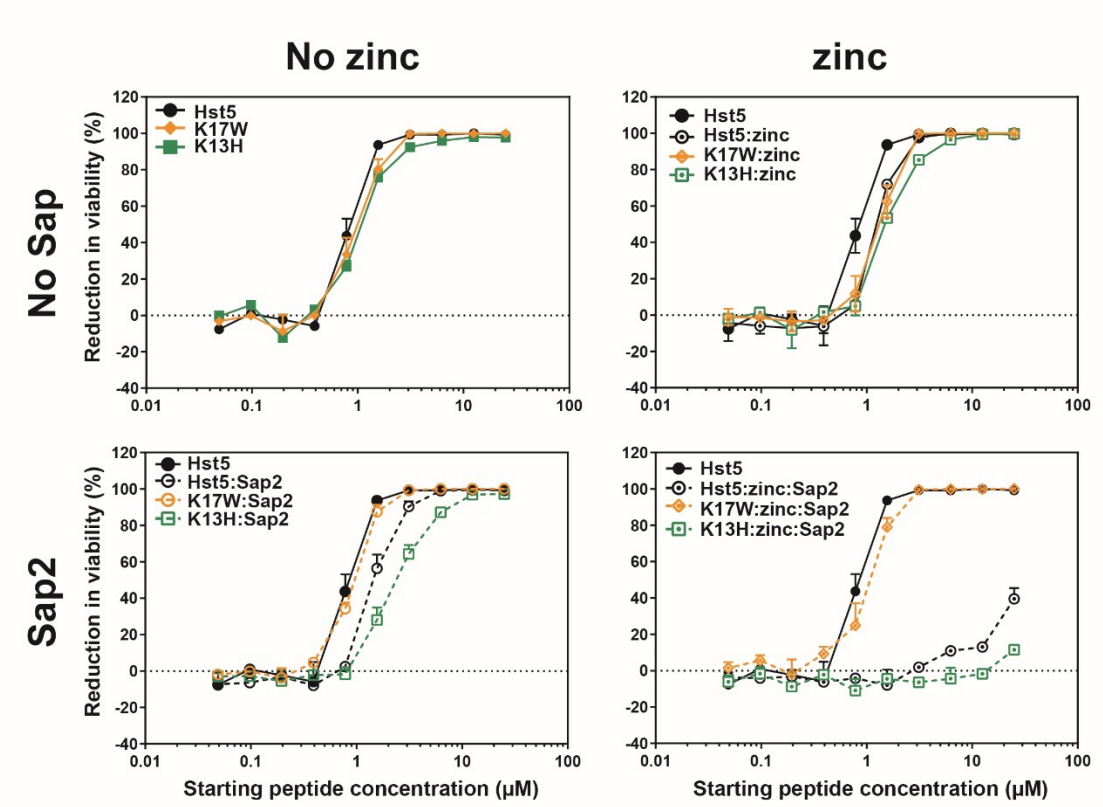

Figure 4.8. Antifungal activity of Hst5, K17W, and K13H after incubation with zinc at a 2:1 zinc-to-peptide ratio and Sap2. After incubation for 2 hrs at 37 °C, Samples were serially diluted in a 96-well plate from 75 μg/mL to .14 μg/mL. Samples were then mixed with *C. albicans* cells at 5.0×10^5 cells/mL and incubated for 30 min at 30 °C in 1 mM NaPB, after which cells were inoculated and cultured. Error bars represent the standard error of the mean ($N = 3$).

4.3.12. K17W prevents biofilm formation better than parent Hst5

The ability of *C. albicans* to form biofilms results in an 1,000-fold increase in the drug resistance of *C. albicans* [101-103]. Despite zinc's ability to modulate the activity of Hst5 variants, we have shown that the K17W variant has greater activity than Hst5 in the absence and presence of zinc and Saps. We used an 2,3-Bis-(2-

Methoxy-4-Nitro-5-Sulfophenyl)-2H-Tetrazolium-5-Carboxanilide (XTT) -based metabolic assay to determine which variants have the greatest reduction in biofilm formation (**Figure 9A**). The Hst5 variants had only a 39.1% reduction in biofilm at the highest concentration, and K17W showed an 84.1% reduction in biofilm formation (**Figure 9B**). This shows that variants designed for improved proteolytic stability can have both enhanced antifungal activity and antibiofilm activity.

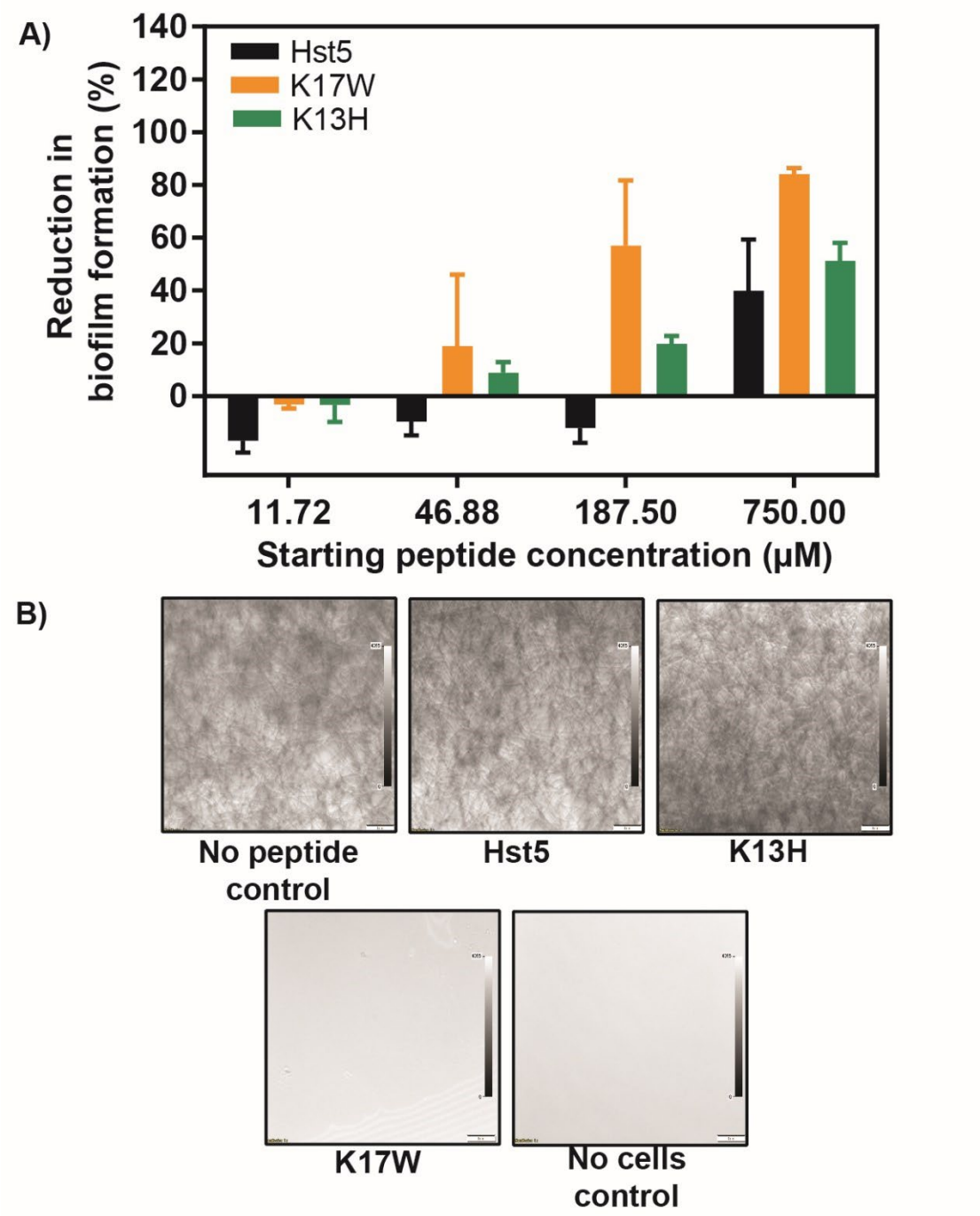

Figure 4.9. Prevention of Biofilm formation by of Hst5 variants. Peptide were is serial diluted 2:1 in water until from 1500 µM to 1.5 µM. Samples were then mixed with *C. albicans* cells at 1.0×10^6 cells/mL and incubated for 24 h at 37 °C in RPMI1640. A) 0.5 g/L of XTT with 1µM menadione was then added to wells and absorbance was measured at 621 nm. Error bars represent the standard error of the mean ($N = 4$). B) Images were taken of wells treated with 187.5 µg/mL of peptide using n inverted fluorescence microscope (20 × magnification).

4.4. *Discussion*

This chapter explored the impact of different amino acid properties at the K13 and K17 residues of Hst5, as previous work has shown that Hst5 variants with K17 substitutions have improved proteolytic stability and antifungal activity when compared to Hst5, while K13 variants have varied proteolytic stability, but reduced activity. We evaluated the proteolytic stability of the peptide in the presence of Saps as well as the antifungal activity against *C. albicans* of full-length peptide and peptide after proteolysis by Saps. We further assessed the proteolytic stability in the presence of zinc or saliva, as Hst5 is a salivary peptide, which means it is in the presence of saliva and dietary metals.

The positive charge at the K13 residue seems to provide the most protection for Hst5 regardless of Sap (**Table 4.3**). This is evident given that of the K13 variants, the K13R variants was either as stable or more stable than Hst5 after proteolysis by Sap1, Sap2, Sap3, or Sap9, suggesting the charge at K13 may help prevent proteolysis. Similar to previous work in our lab, the K13E variants were more prone to proteolysis by Sap9 than the parent Hst5 [35], which is believed to be due to the presence of negatively charged residues C-terminal to basic amino acids [42]. Notably, K13R has improved stability in the presence of Sap2, which could imply the importance of greater charged interactions introduced by the guanidino group. After proteolysis by Sap3, Hst5 and K13R have similar stability, but K13E is more stable than the parent peptide. All other K13 variants were less stable than Hst5. The contrary amino acid properties showing the most beneficial effect when it comes to proteolytic stability

against Sap3, suggests the importance of electrostatic interactions in preventing proteolysis by Sap3.

In terms of the antifungal activity, except for the K13E variant, full-length K13 variants could retain their antifungal activity. The reduction in activity by K13E is consistent with the literature [35, 74]. This Shows that K13 is important for antifungal activity. Furthermore, after proteolysis by Saps, all K13 variants had reduced antifungal activity compared to degraded Hst5. Of these variants, the K13R was the most similar to the parent Hst5, showing the importance of the positive charge group at K13.

The incubation of Hst5 with proteases leads to interesting results. Except for K17E incubated with Sap6, proteolysis by Sap5, Sap6, and Sap10, does not affect the activity of Hst5 or Hst5 variants. In the case of Sap6-treated K17E, the antifungal activity becomes similar to that of Hst5, possibly suggesting that while Sap6 does not degrade Hst5, it could protect it from other proteases that could be found on the surface of *C. albicans* by binding to the peptide [34-36]. After proteolysis by Sap1, Sap2, Sap3, and Sap9, the antifungal activity of K17E is greater than degraded Hst5, suggesting that fragments made by the proteolysis of K17E retain more activity than the fragments from degraded Hst5. After incubation with Sap3, K17L was the only K17 variant with reduced activity against *C. albicans*. Although K17L and Hst5 retain similar levels of intact peptide, the fragments formed by the degradation of K17L may be less active than those formed by Hst5. Of these variants, the K17W variants had the greatest increase in activity after proteolysis by Saps, seemingly

matching the fully intact Hst5 when both are degraded by Sap. This shows that the large aromatic and hydrophobic residue at K17 improves the antifungal activity after incubation with Saps, more than likely resulting from improved proteolytic stability.

Regarding antifungal activity, except for the K17E variant, the full-length peptides for the K17 variants were as active against *C. albicans* as the parent Hst5. Tsai et al. found that K17 was not important for the antifungal activity of Hst5 after substitution of K17 to glutamine [74]. However, we showed that introducing glutamate reduces the antifungal activity preventing a 100% reduction in the viability of *C. albicans*. While activity is not entirely removed, the reduction is more than likely due to Hst5 reduced interactions with the negatively charged *C. albicans* membrane [14].

Saliva is a complex mixture containing proteolytic enzymes such as cysteine cathepsins, the serine cathepsin A, the aspartic cathepsin D, and metalloproteases [46, 95]. As a salivary peptide, Hst5 is naturally in the presence of these enzymes, so we assessed the proteolytic activity of these variants in the presence of saliva. The variants we designed were designed for the purpose of improving proteolytic stability to Saps, so while K17W and K17L had improved proteolytic stability and K13R had reduced proteolytic stability, the difference in stability is small, showing that engineering these peptides to be stable against Saps is not sufficient to make them stable against other proteases in saliva.

Part of the complex mixture of enzymes in saliva are metals that are included in our diets, such as zinc [100]. The presence of zinc has been shown to impact the activity of Hst5, with lower zinc-to-peptide ratios enhancing its activity and higher ratios

hindering its activity[79, 81, 99]. The reduction in anti-fungal activity was theorized to be cause by zinc binding to Hst5 and preventing it from internalizing into *C. albicans[81]*. We assessed the K13H variant of Hst5 because McCaslin et al. showed the importance of histidine in the zinc-binding properties of Hst5 [82]. As expected K13H competed against Zincon greater than most of the variants tested for zinc binding. While this variant competed for zinc the most, it also showed the least effect on activity from increased titrations of zinc, indicating that enhanced the ability to bind to zinc may play a role in enhancing the activity of these variants, or a possible shift In metal binding residues. However, when Saps are included, zinc potentially catalyzes the degradation of Hst5, resulting in reduced activity. Overall, at higher concentrations of zinc, zinc binding seems to prevent reduction of antifungal activity, however, in the presence of purified protease, zinc binding reduces proteolytic stability of variants that are not resistant to cleavage by Hst5.

The ability of *C. albicans* to form biofilms results in an increased resistance to antifungal agents. Since the K17W variant was more proteolytically stable and retained significant antifungal activity after incubation with Saps—at a level similar to that of undegraded Hst5--we assessed its ability to prevent the formation of *C. albicans* biofilms. We found that K17W was more effective at preventing canidadia yeast growth and biofilm formation than the parent Hst5. Helmerhorst et al. believed that increasing the amphipathicity increased antifungal activity, and designed variants with increased activity, by enhancing the amphiphathicity [76]. As the K17 residue is in the hydrophobic portion of the Hst5, it is possible that substituting a large hydrophobic residue at K17 could increase the amphipathicity (**Figure 4.10**).

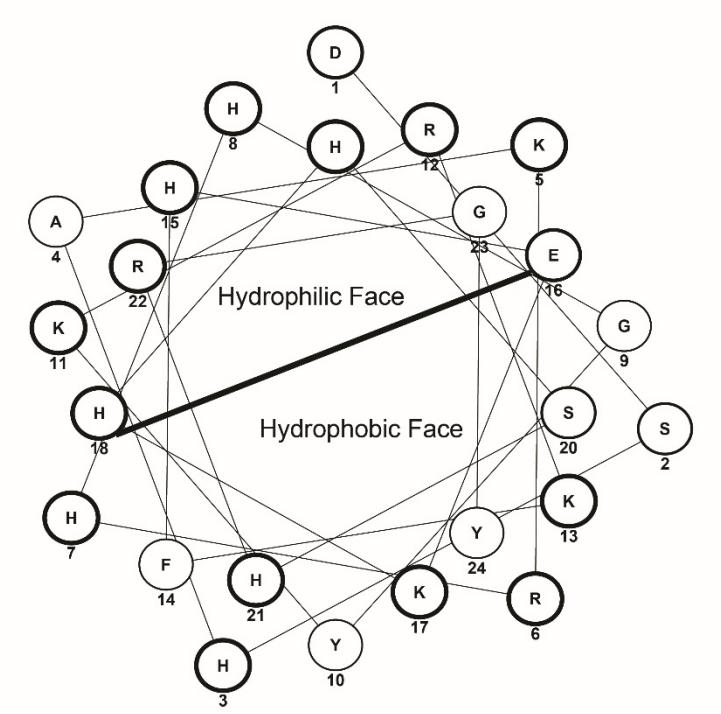

Figure 4.10. Helical wheel structure of Hst5 generated at https://clemlab.github.io/helicalwheel/

4.5. *Conclusion*

In conclusion, completed a detailed investigation into the effects of amino acid substitutions at the K13 and K17 residues of Hst5, aiming to understand its proteolytic stability and the resulting antifungal activity against *Candida albicans*. Our findings demonstrate that with the exception of K13R, modifications at the K13 residue significantly increased proteolysis by Saps. On the other hand, the K17 substitutions showed increased proteolytic stability and antifungal activity. Notably, the introduction of bulky hydrophobic residues like tryptophan at the K17 position markedly improved the overall proteolytic stability and enhanced the antifungal performance, potentially through increased amphipathicity which may prevent enzymatic access and degradation. Furthermore, the experimental insights into the interactions of these variants with saliva and zinc underscore the complexity of

peptide activity in physiological conditions, revealing that while certain variants can bind zinc effectively, this might inadvertently catalyze their degradation by Saps.

These findings provide valuable guidance for the design of more effective antifungal peptides, considering the dynamic and challenging environment of the human body. Future studies should continue to explore the balance between proteolytic stability and antifungal efficacy to develop optimized peptides that can be deployed effectively in clinical settings to combat fungal pathogens.

5. Chapter 5: Development of a screen for proteolytic stability of peptides

5.1. *Introduction*

Antifungal peptides are a means of combating fungal pathogens that may cause infections. Histatin 5 (Hst5) is an antifungal peptide with activity against *Candida albicans*. However, *C. albicans* produces a family of 10 secreted aspartyl proteases (Sap). Currently, rational design strategies have been utilized to engineer variants of Hst5 that are proteolytically stable against Saps [34, 35]. However, this strategy is limited by the number of peptides that can be screened, potentially being both time-consuming and costly. To enhance the likelihood of discovering the most advantageous substitution, it is crucial to screen larger peptide libraries. Therefore, establishing a high-throughput platform is necessary to identify proteolytically stable variants. Directed evolution refers to a protein engineering technique that mimics natural selection in that the best variant survives the selection process from a library of proteins. Yeast surface display (YSD) is a display technique that can utilize this concept for screening protein or peptide libraries. YSD was first demonstrated in 1997 by Boder & Wittrup, where they generated a library of the 4-4-20 anti-fluorescein scFv and enriched for mutants that best bound to FITC-dextran using flow cytometry [59]. YSD takes advantage of the 725 amino acid protein a-agglutinin 1 (Aga1) that is anchored onto the cell wall via β-glucan covalent linkage (**Figure 5.1**) [104]. The 69 amino acid protein Aga2 is genetically fused directly to a hemagglutinin (HA) epitope tag, which is linked to a protein/peptide of interest (POI).

The C-terminus of the POI can be linked to a c-myc epitope tag. The expression of the Aga2- POI fusion protein is generally induced through a GAL1/10 promotor, and the construct is secreted to the surface of the cell wall where Aga1 and Aga2 are bound by disulfide bonds [105, 106]. The inclusion of the HA tag confirms that the construct is anchored on the surface of the cell wall, while c-myc allows the usage of fluorescent label-based techniques, such as flow cytometry, to identify that the full construct is on the surface of the yeast.

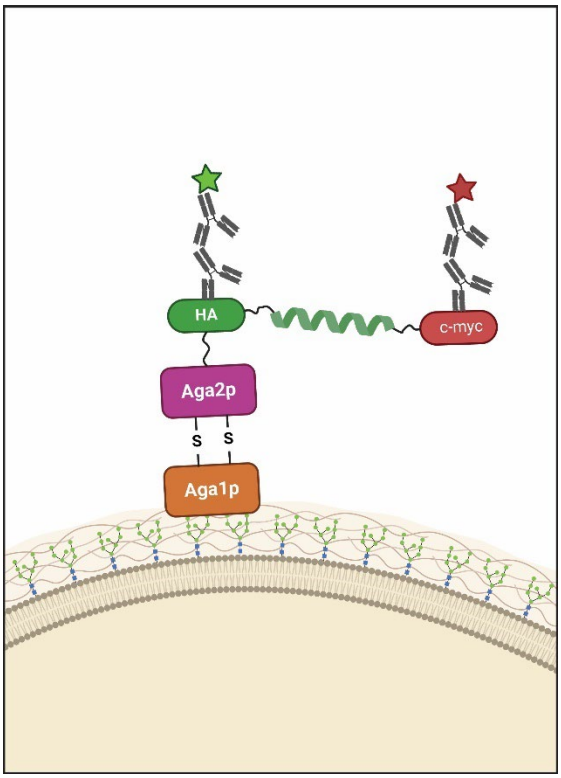

Figure 5.1. Schematic of the yeast surface display platform. The YSD construct is anchored on the cell wall of *S. cerevisiae* by disulfide bonds between Aga1p and Aga2p. Aga2p is linked to the HA epitope tag with is connected via a short liker to the peptide of interest. The C-terminus of the peptide of interest is the c-myc tag which identifies the full construct on the surface of *S. cerevisiae*. Figure made in BioRender.com

Prior work utilizing the YSD platform normally focuses on mutating the protein of interest to identify the best binders. The type of proteins that have been engineered

for these purposes include growth factors, antibody fragment, and epidermal growth factor receptors to identify the best binder [59, 60, 107-109]. Notably, peptides have been engineered on the YSD platform, as Huisman et al. reported the use of peptide display to develop a library of peptide variants. However, this was again to assess the best binder of the peptide library to the major histocompatibility complex [60]. YSD has also been used to observe proteolysis of peptides, where Knyphausen et al. engineered a library of the *Staphylococcus aureus* serin-protease-like protease SplB to cleave a bait-peptide on the alpha-2-macroglobulins(A2M) to assess the platform's ability to identify better cleavers (**Figure 5.2**) [61]. While this platform provides an opportunity to engineer proteases, it does not allow evolution of the peptide.

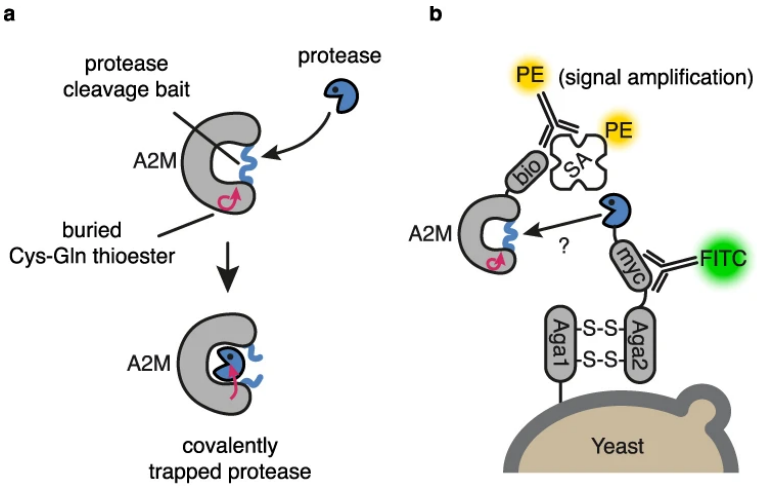

Figure 5.2. Schematic of engineered a library of the *Staphylococcus aureus* serin-protease-like protease SplB to cleave a bait-peptide on alpha-2-macroglobulins. A) The protease cleaves the bait peptide and the buried Cys-Gln thioester covalently traps the protease in A2M. B) The protease of interest is displayed on the yeast surface display construct with a fluorescein isothiocyanate (FITC)-conjugated anti-myc tag antibody, and A2M is linked to biotin, which binds to a Phycoerythrin-conjugated streptavidin (SA), which s can be recognized by a Phycoerythrin conjugated anti-streptavidin antibody containing Phycoerythrin. Figure reprinted from open access journal *[61]* licensed under a Creative Commons Attribution 4.0 International License.

Our lab previously explored the possibility of using YSD for displaying Hst5 on the surface of *S. cerevisiae* to identify proteolytically stable variants. In this work, Hst5 was successfully expressed on the surface of *S. cerevisiae*, the construct was degraded while on the yeast surface, and the conditions for display and degradation (expression pH and temperature, and degradation temperature) were optimized [110]. However, the difference between stable and unstable Hst5 variants must be improved for the platform to become a valid screening method [110]. The reason for the lack of discrimination between the more proteolytically stable and less proteolytically stable peptides was possibly due to the protease not being able to access the peptide on the construct. Lown et al. describe the YSD construct as being linked randomly within the cell wall β-glucan, with the maximum cell wall thickness being ~115 nm [111], and the pCTCon2 fusion construct having a length of ~15nm [108, 112]. In their work, they assessed how different linker lengths (40, 80, 641 amino acids) impact the ability to identify better binders. Their work shows that greater linker lengths, enabled enrichment of a μM-affinity binder and improved enrichment of nM-affinity binders. Increasing the length of the linker in the Hst5 constructed displayed on yeast cells could allow proteases better access to the peptide and improve our ability to discriminate between Hst5 variants with different levels of proteolytic stability.

In this chapter, we studied the induction media conditions to improve the surface display of the antimicrobial peptide Hst5, assessed the impact of longer linkers on the expression of the yeast surface display construct, optimized the degradation conditions for the proteases Sap2 and Sap9, Our improved system allowed us to differentiate between the proteolytically unstable variants K13L and the

proteolytically stable variant K11RK17R resulting in a YSD system that can potentially be used to screen for proteolytically stable peptide variants.

5.2. Methods

5.2.1. *Strains, proteases, and plasmids*

Purified Sap1, Sap2, Sap3, Sap5, Sap6, Sap9, and Sap10 were provided by B. Hube at Friedrich Schiller University Jena, Germany). Sap1, Sap2, and Sap3, were purified by ion exchange chromatography and desalted into 0.1 M sodium citrate buffer, while Sap9 was produced without its GPI anchor, purified by ion exchange chromatography, and desalted into 0.1 M sodium citrate buffer [42]. The *S. cerevisiae* strain EBY100 was provided by Zvi Kelman at the Institute for Bioscience & Biotechnology Research (Rockville, MD).

5.2.2. *Plasmid construction*

The pCTCon2-Hst5 (control plasmid) was previously designed in our lab for displaying Hst5 using YSD [110], and the pCT40 and pCT641 plasmids were provided by Benjamin Hackel at the University of Minnesota [108, 113]. YSD plasmids generally have an ampicillin resistance (AmpR) gene, The auxotrophic marker Trp1, and a galactose inducible (Gal1/10) promoter (**Figure 5.3**). The AmpR gene provides selective pressure during plasmid replication in *Escherichia coli*, as media containing ampicillin only allows the growth of cells that have AmpR. Similarly, the Trp1 gene provides selective pressure in *S. cerevisiae*, as only cells that can produce their own tryptophan can grow in tryptophan-deficient media. The galactose-inducible promoter enhances the expression of the yeast surface display

construct. pCT40 and pCT641 additionally encode linkers containing 40 and 641 amino acids, respectively, that are expressed between the HA tag and Hst5 (**Figure 5.3**). The linkers contain proline, alanine, and serine in a nearly random order.

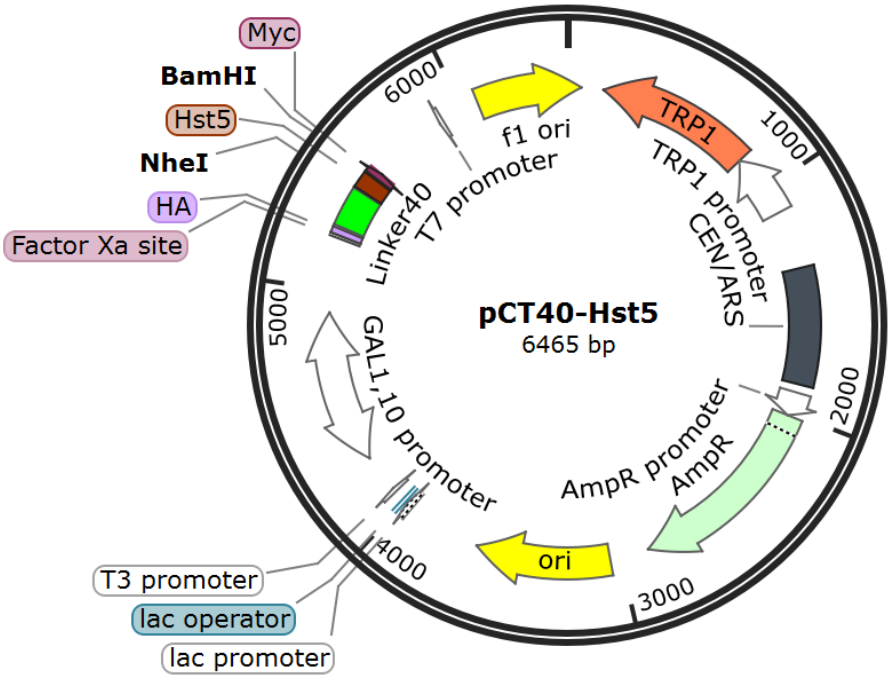

Figure 5.3. Plasmid map for the pCT40-Hst5 plasmid. This contains the Gal1/10 promoter, the yeast surface display construct containing an HA tag, 40 amino acid linker containing, Hst5, and the c-myc tag.

To prepare the backbone of pCT40 and pCT641 for inserting Hst5 variants, the restriction enzymes BamHI and NheI were used to cut the plasmid, leaving sticky ends on the plasmid backbone. The oligonucleotides coding for Hst5 consisted of the two oligonucleotide pairs NheI-Hst5-Top1 and NheI-Hst5-Bot1, and BamHI-Hst5-Top2 and BamHI-Hst5-Bot2(**Table 5.1**). Each oligonucleotide was phosphorylated individually before annealing to its respective partner. After annealing each pair separately, the sticky ends were present, allowing the pairs to ligate together and into the backbone (**Figure 5.4**). After ligating both pairs into the backbone, the plasmids

were desalted and separately transformed into *E. coli* DH5α for plasmid propagation. After replicating the plasmid DNA in *E. coli*, the DNA for each construct was isolated and purified, and the sequences of pCT40-Hst5 and pCT641-Hst5 were confirmed by Sanger sequencing (Genewiz; Frederick, MD). The plasmids were then transformed into *Saccharomyces cerevisiae* strain EBY100. This plasmid construction process was repeated to also obtain plasmids encoding for the K13L and K11RK17R peptides in place of Hst5(**Table 5.1**).

Table 5.1. Sequence of oligonucleotides used to construct pCT40 and pCT641 plasmids.

Peptide		Oligonucleotide	Sequence[a,b]
Hst5	Pair 1	NheI-Hst5-Top1	5′ - c t a g c GATTCTCATGCAAAACGCCATCACGGGTATAAGCGCAAG- 3′
		NheI-Hst5-Bot1	3′ - g CTAAGAGTACGTTTTGCGGTAGTGCCCATATTCGCGTTCAAG- 5′
	Pair 2	BamHI-Hst5-Top2	5′ - TTCCACGAAAAGCACCACAGTCATCGCGGGTACg - 3′
		BamHI-Hst5-Bot2	3 - ′ GTGCTTTTCGTGGTGTCAGTAGCGCCCATGc c t a g - 5′
K13L	Pair 1	NheI-K13L-Top1	5' - c t a g c GATTCTCACGCAAAGCGTCATCACGGGTATAAAAGATTG- 3'
		NheI-K13L-Bot1	3' - g CTAAGAGTGCGTTTCGCAGTAGTGCCCATATTTTCTAACAAG- 5'
	Pair 2	BamHI-Hst5-Top2	5' - TTCCACGAAAAGCACCACAGTCATCGCGGGTACg - 3'
		BamHI-Hst5-Bot2	3' - GTGCTTTTCGTGGTGTCAGTAGCGCCCATGc c t a g - 5 3'
K11RK17R	Pair 1	NheI-K11R-Top1	5' - c t a g c GATTCCCACGCGAAGCGTCATCATGGGTATCGTCGTAAG- 3'
		NheI-K11R-Bot1	3' - g CTAAGGGTGCGCTTCGCAGTAGTACCCATAGCAGCATTCAAG- 5'
	Pair 2	BamHI-K17R-Top2	5' - TTCCACGAGAGGCATCACAGTCATCGTGGATACg - 3'
		BamHI-K17R-Bot2	3' - GTGCTCTCCGTAGTGTCAGTAGCACCTATGc c t a g - 5'

[a]*Red letters represent overhangs where the 2 pairs will anneal.*
[b]*Lower case letter represent sticky ends for NdehI and BamHI restriction enzymes.*

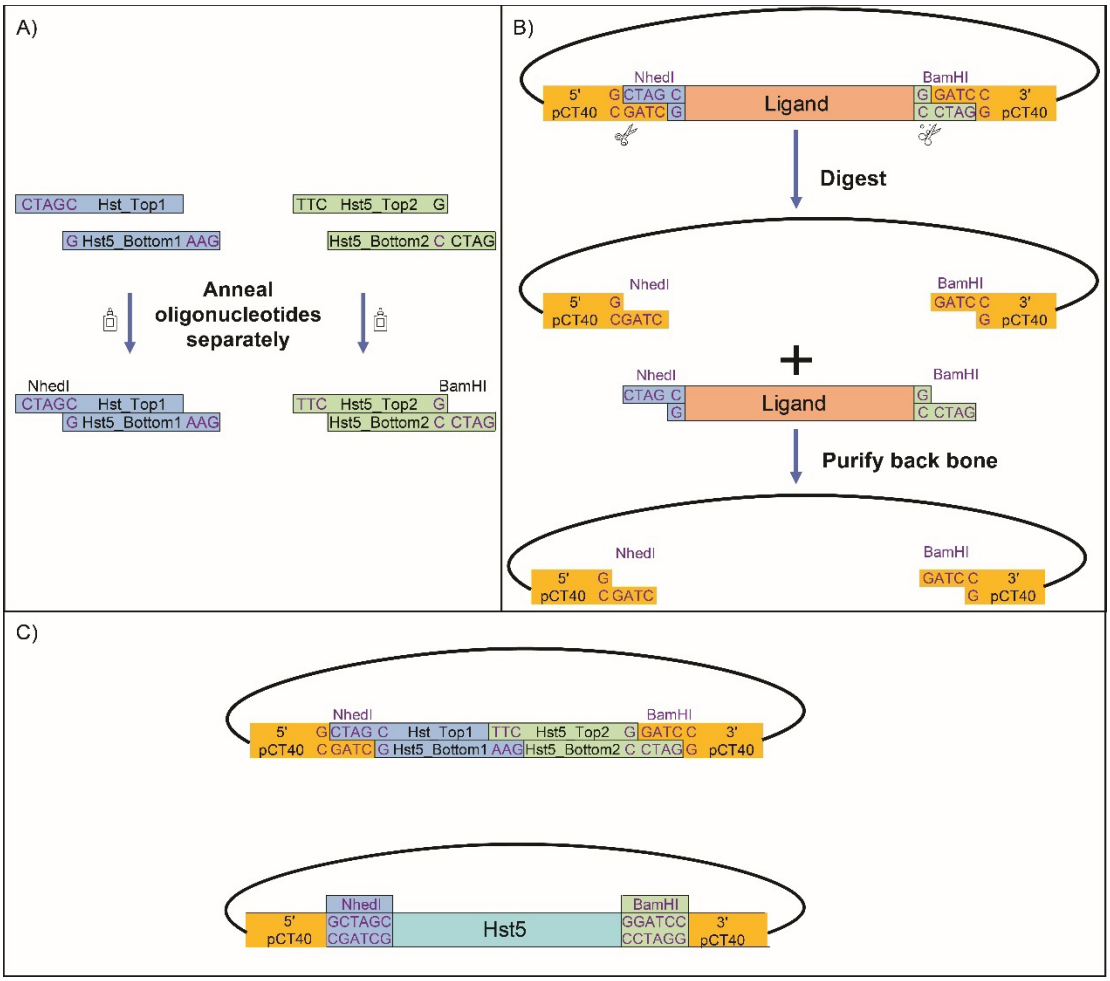

Figure 5.4. Schematic for inserting Hst5 oligonucleotides into the pCT40 plasmid. A) Hst5 two pairs of Hst5 oligonucleotides are annealed separately. B) The backbone for the pCT40 plasmid is prepared by cleaving the previous insert out using the NhedI and BamHI restriction enzymes. The pCT40 backbone is then purified. C) The two annealed oligo pairs and the backbone are ligated together.

5.2.3. Culture conditions

After transforming the plasmids into *S. cerevisiae*, cells were plated onto a synthetic dextrose casamino acids (SD-CAA) yeast minimal media agar plate (**Table 5.2**). Cells were then inoculated into 10 mL of SD-CAA growth media (**Table 5.2**) and grown overnight in a 30 °C incubator shaker for 30 – 36 h to an OD between (2 – 4). After overnight growth, the cell culture was centrifuged at 3,900 ×g for 5 minutes at 4 °C, and the supernatant was discarded. The pellet was then suspended in 1 mL of

synthetic galactose casamino acids (SG-CAA) synthetic yeast minimal expression media (**Table 5.2**), transferred to a 125 mL shake flask containing 49 mL of the SG-CAA, and incubated in a 30 °C incubator shaker for 24 h to an OD between 5 – 6, after which either 50 mL was transferred to a 50 mL centrifuged tube for Western blotting or 2.4×10^7 cells were aliquoted into 1.7 mL centrifuge tubes for flow cytometry or proteolysis. (For example, if $OD_{600} = 6$, the cell density was approximately 6.00×10^7 cells/mL, so aliquots were 400 µL per tube) [114].

Table 5.2. Components for growth media and protein induction media.

Component property	Component	SD-CAA agar	SD-CAA growth media	SG-CAA induction media
Nitrogen source	Yeast nitrogen base (w/o amino acids and ammonium sulfate)	6.7	6.7	6.7
Amino acid source	Casamino acids	5	5	5
Buffer	Sodium citrate	-	10.4	-
	Citric acid Monohydrate	-	7.4	-
	Na_2HPO_4	5.4	-	5.4
	NaH_2PO_4	8.56	-	8.56
Sugar	Galactose	-	-	20
	Dextrose	20	20	2
Agar	Sorbital	182	-	-
	Agar	25	-	-
pH		4.5	4.5	4.5

5.2.4. Western blotting

Western blots were performed by harvesting induction media containing EBY100 cells with the appropriate plasmids. Cells were transferred to a tared 50 mL centrifuged tube and centrifuged at 3,900 ×g for 5 minutes at 4 °C, and the supernatant was discarded. The mass of the cells in the tube was then determined, and

the pellet was resuspended in an appropriate volume of yeast protein extraction reagent (Y-PER, Thermo Scientific) as described by the manufacturer protocol. The mixture was placed on a tube rotator for 20 minutes at room temperature. Afterward, the mixture was centrifuged at 16,000 ×g for 10 min, and the supernatant was transferred to a separate container. The samples were aliquoted into tubes (20 µL per tube) and mixed with 5× Sodium dodecyl sulfate (SDS) page loading dye containing dithiothreitol 4:1 sample to dye. The samples were boiled at 95-100 °C for 10 minutes, after which they were quickly centrifuged and loaded on a mini-PROTEAN® TGX precast gel (Bio-Rad) for 35 min at 200 V.

The gel containing the separated proteins was then transferred onto a polyvinylidene fluoride (PVDF) transfer membrane using the Trans-Blot Turbo Transfer System (Bio-Rad) at 1 A and 25 V for 30 min. Afterward, the membrane was blocked using Tris-buffered-saline (TBS) with Tween20 (TBST) and 5% (w/v) powdered milk and incubated overnight at 4 °C. The membrane was then washed 3 times for 10 minutes with TBST on a microplate shaker at 230 RPM and stained for 1 h with 14 mL of anti-myc tag antibody conjugated to horseradish peroxidase (HRP) (Abcam: ab1326) diluted 1:3000 in TBST (applied directly on top of the membrane). The membrane was then washed 6 times for 10 minutes with TBST and once for 5 minutes with TBS. 1 mL of Clarity Western ECL substrate (Bio-Rad) was added to the membrane, and the gels were then imaged using a ChemiDoc (Bio-Rad) and the Image Lab software (Bio-Rad).

5.2.5. Proteolysis of yeast surface display construct

After inducing protein expression in SG-CAA, cells were prepared for proteolysis by washing them 3 times in 2 mM NaPB after which the supernatant was discarded and the pellet was resuspended in 100 µL of 0.75 µg/mL Sap2. The samples were then incubated at 37 °C for 30 min and then centrifuged to separate the construct that remained attached to the cell wall from the solubilized portion. The supernatant (100 µL) was then transferred to a separate tube for analysis by mass spectrometry, while the pellet was thoroughly decanted and prepared for flow cytometry.

5.2.6. Flow cytometry

Cells immediately after protein induction or proteolysis were washed 3 times in ice-cold 1× PBS, and resuspended in 100 µL of 1× PBS containing 1:100 diluted chicken anti-c-myc antibody (Exalpha: ACMYC) and anti-HA tag antibody [HA.C5] (Abcam: ab18181). The mixture was placed on a tube rotator at 4 °C for 30 minutes after which the samples was washed 3 times in ice-cold 1× PBS and in the dark, resuspended in 100 µL of 1× PBS containing 1:50 diluted Alexa Fluor 647 goat anti-chicken IgG (H+L) (Thermofisher: A21449) and Alexa Fluor 488 goat anti-mouse IgG (H+L) (Thermofisher: A11029). The mixture was placed on a tube rotator at 4 °C for 45 min, after which the sample was washed 2 times and resuspended in ice-cold 1× PBS. The samples were then transferred to 10 mL centrifuge tubes and prepared for analysis.

Samples were assessed using the FACSCanto II (BD; Franklin Lakes, NJ). Data was collected on the BD FACSDiva software and analyzed using Floreada.IO, a free

website analysis tool. For analysis, *S. cerevisiae* strain EBY100 without plasmid was used to establish the gates. Establishing the gates involved screening 30,000 cells (events) and isolating events during detection. Live cells were isolated using forward and side scatter filters, while single cells were isolated using only forward scatter. Events were plotted on a bivariate log-log plot with signals corresponding to Alexa-Flour 488 (x-axis, HA tag) and Alexa-Flour 647 (y-axis, c-myc tag). As EBY100 cells do not contain the c-myc and HA tag, gates were design to contain EBY100 in Q3.

5.2.7. Mass spectrometry

Mass spectrometry was used to determine the Saps cleaved the peptides and compare the abundance of the fragments produced. After incubating the peptides with Saps or saliva as described for the proteolytic degradation assays, 30 µL of each sample was desalted using a Glygen C-18 TopTip microspin column (Glygen), following the manufacturer's protocol. The binding solution for each peptide was 0.1% formic acid, and the release solution was 0.1% formic acid and 80% acetonitrile. Each sample (19 µL) was spiked with 1 µL of the peptide MFRA (0.01 µg/mL in 0.1% formic acid and 80% acetonitrile) to facilitate comparison between samples. Samples were analyzed on a Bruker Maxis II mass spectrometer (in the University of Maryland Mass Spectrometry Facility) with an electron spray ionization source and quadrupole-time of flight analyzer. Samples were directly injected into the Maxis II, and data were acquired between m/z 400 – 4000 with full sensitivity resolution (FSR) of > 50,000.

After acquiring the data, the mass spectra for each sample were analyzed using the Bruker Compass DataAnalysis software, using BioTools in tandem with Sequence Editor to identify each peak. In the Bruker Compass Software, each mass spectrum was individually deconvoluted to consolidate the m/z values for peptides with varying charges. The deconvoluted mass spectra were then transfer to BioTools and Sequence editor where the molecular weights of the peptides and their fragments were calculated and compared to the mass spectra peaks with a tolerance of ± m/z = 0.2.

5.3. *Results*

We incorporated Hst5 and variants into the YSD platform to assess its suitability for identifying peptide variants with enhanced proteolytic stability. The c-myc and HA tag were incorporated to confirm that the construct is on the surface of *S. cerevisiae*. If degradation occurs, only the HA tag of the protein will be detected and a majority of cells should be detected in Q3. Otherwise, both HA and c-myc tags should be detected, and most events should be in Q2 (**Figure 5.5**). We investigated the role of linker lengths (0, 40, and 641 amino acids), inoculation media (pH, temperature, time, and composition), and degradation conditions (pH, temperature, time, and protease concentration).

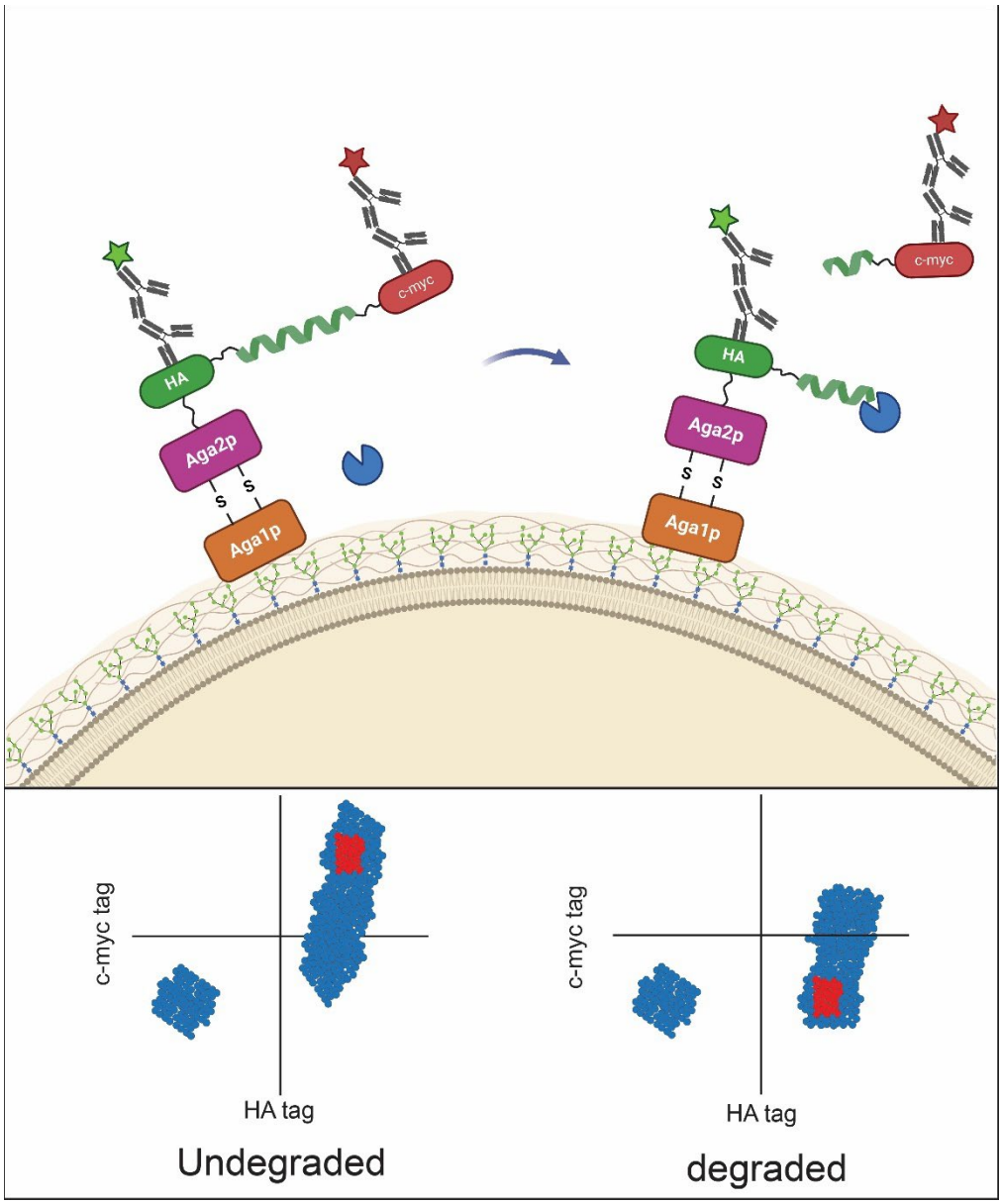

Figure 5.5. Schematic of the degradation of the Hst5 on the surface of *S. cerevisiae*. Before the protease cleaves the peptide of interest, both HA and c-myc tags are present, and a majority of the events in the bivariate plot are in Q2. After the protease cleaves the peptide of interest, a majority of cell should contain only the HA tag and remain in Q3. Figure made in BioRender.com

5.3.1. Peptide variants can be expressed on the YSD construct

To determine if all YSD constructs generated by pCTcon2-Hst5, pCT40-Hst5, pCT641-Hst5, pCT40-K11RK17R, and pCT40-K13L were fully expressed, we

utilized Western blotting. Validation was performed using c-myc epitope tags, as only fully expressed constructs would contain the c-myc tag. Cells containing the pCTcon2-Hst5 plasmid were used as our control, as this was previously found to express Hst5 on its surface. Bands were observed for the pCTcon2-Hst5, pCT40-Hst5, and pCT641-Hst5 at approximately 30, 40, and 97 kDa respectively (**Figure 5.6**). Each construct has bands below the noted molecular weight bands, which are potentially degradation products from our YSD construct. From the results, the protein's expression was enhanced after 3 days of protein induction at 20 °C, and both pCT40 and pCT641 improved the expression after 1 day in induction media compared to pCT40.

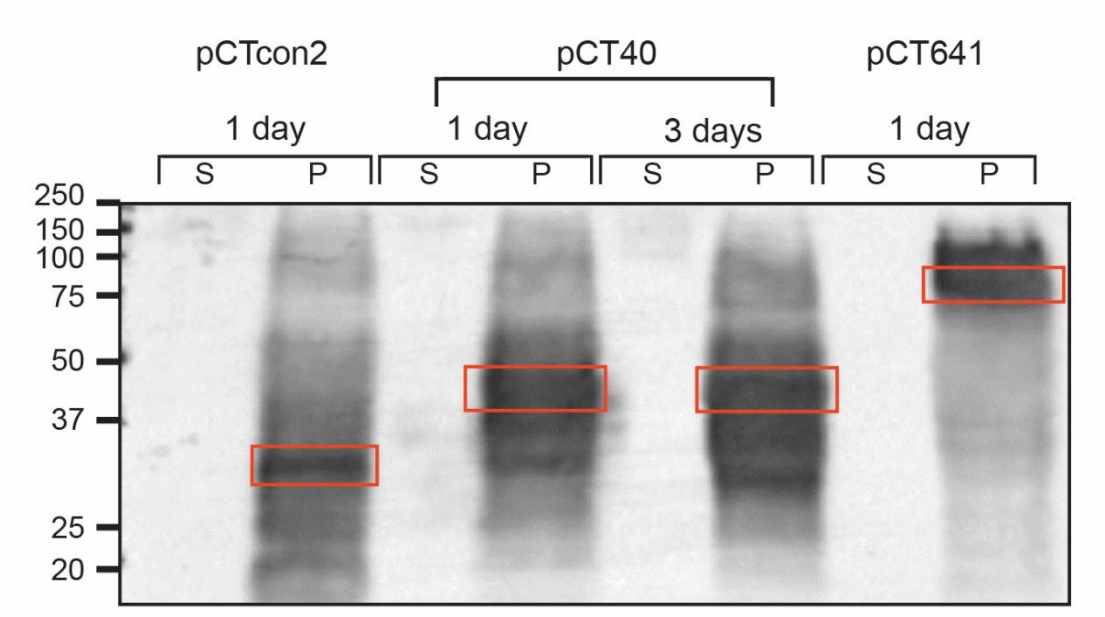

Figure 5.6. Western blot of Aga2-Hst5 in the pCTcon2, pCT40, and pCT641 plasmids. Protein expression was induced at 20 °C for 1 day for all linkers and 3 days for pCT40-Hst5 to determine if experience improves. Detection of the c-myc epitope tag. S and P represent samples collected from the supernatant and the pellet of the cells, respectively.

Bands were also observed for the pCT40-Hst5, pCT40-K11RK17R, and pCT40-K13L with molecular weights of 48 kDa (**Figure 5.7**). Similarly to the different linkers, degradation products for each construct can be found below the peptide band, with pCT40-Hst5 having less noticeable degradation products. This confirms the expression of all tested constructs.

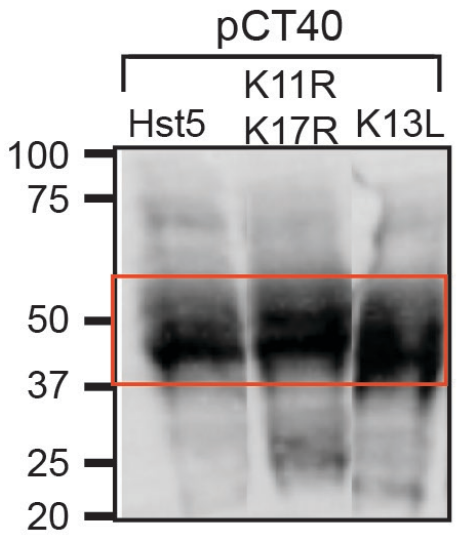

Figure 5.7. Western blot of Aga2-K13L, Aga2-K11RK17R, and Aga2-Hst5 the pCT40 plasmids. Detection of the c-myc epitope tag is shown with the Bio-Rad all-blue molecular weight ladder. Protein expression is enhanced at higher temperature and lower pH.

To identify the optimal conditions for the expression and display of YSD constructs, Western blotting and flow cytometry were used respectively. In flow cytometry, constructs were identified using both HA and c-myc epitope tags (**Figure 5.5**). EBY100 cells without the plasmids were used to calibrate the location of quadrant gates, and the percentage of cells in each gate was quantified. The conditions with the most cells having the c-myc tag and HA tag are deemed to be the best conditions.

Conditions tested include incubation duration, incubation temperature, media pH, and media composition.

Initial optimization was done on the duration of protein expression in induction media at 20 °C. After 1 day of incubation, 14.17% of cells have both the c-myc and HA Tag, while after 3 days, 44.89% of cells retain both tags (**Figure 5.8**). Therefore, 3 days were the best conditions for improving the display as most cells with both the c-myc and HA tag were observed.

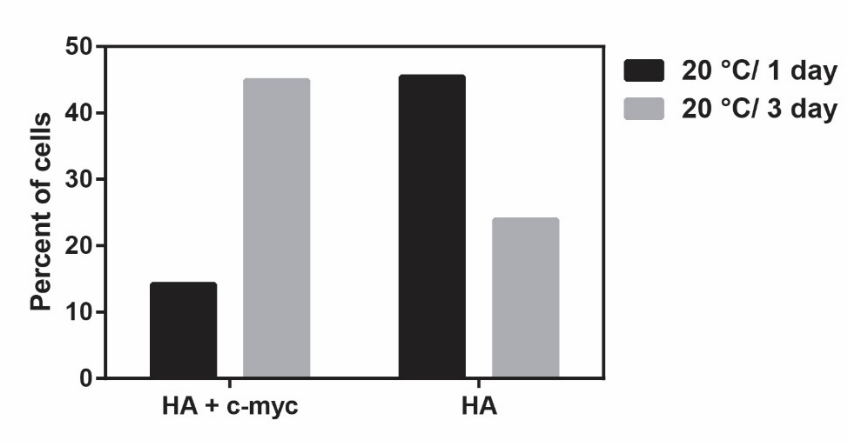

Figure 5.8. Expression time optimization for pCTCon2-Hst5 at 20 °C. The percentage of cells with both the HA and c-myc epitope tag, as well as only the HA tag is plotted from 1 day and 3 days. A bivariate plot of the intensity for both HA (Alexa-Flour 488 antibody) and c-myc (Alexa-Flour 647 antibody) used to generate this bar graph is in **Appendix Figure C.1**.

We assessed the impacts of reducing the induction time from 3 days to 1 day and increasing the induction temperature from 20 °C to 30 °C. After 3 days of incubation at 20 °C, 48.83% of cells have both the c-myc tag and HA tag, while after 1 day at

30 °C, 56.05% of cells have the c-myc and HA Tags (F**igure 5.9**). This confirmed that induction time can be reduced by increasing the incubation temperatures.

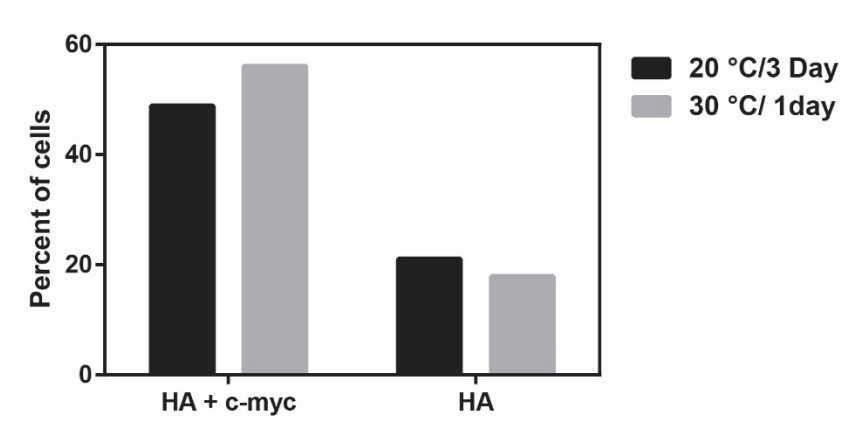

Figure 5.9. Expression temperature and time optimization for pCTCon2-Hst5. The percentage of cells with both the HA and c-myc epitope tag, as well as only the HA tag is plotted from 1 day and 3 days. A bivariate plot of the intensity for both HA (Alexa-Flour 488 antibody) and c-myc (Alexa-Flour 647 antibody) used to generate this bar graph is in **Appendix Figure C.2**.

To understand the impact of temperatures on protein expression after 1 day of incubation, we utilized a Western blot. The blot shows the band for the pCT40-Hst5 YSD construct at 42 kDa. An optimal expression is observed at 30 °C; furthermore, as temperature increases, there are more degradation products (**Figure 5.10**). Based on the results, 30 °C was determined to be the optimal temperature for protein expression and reducing the amount of degradation products.

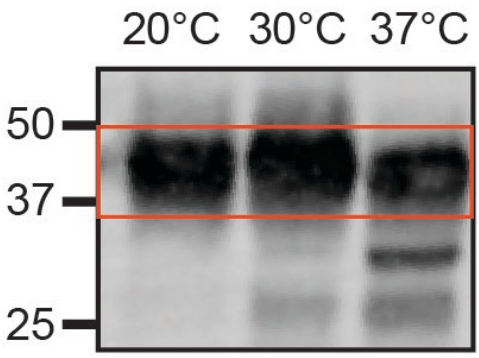

Figure 5.10. Western Blot of Aga2-Hst5 in the pCT40 plasmids. Protein expression was induced at 20 °C, 30 °C, and 37 °C. Detection of c-myc epitope tag is shown with the Bio-Rad all blue molecular weight ladder.

We studied increasing the linker length to improve the display of our construct. We evaluated the display of different linker lengths at the tested conditions using flow cytometry. Notably, the optimized temperature and time increased the number of cells with both c-myc tag and HA tag for each construct. pCTCon2-Hst5 had 62.18% of cells with both c-myc and HA tag, while pCT40-Hst5 and pCT641-Hst5 had 56.05% and 32.67%, respectively (**Figure 5.11**). pCT641-Hst5 consistently had the fewest events in Q2. The results show that the longer linker length reduces the overall display of proteins on the surface of the *S. cerevisiae*.

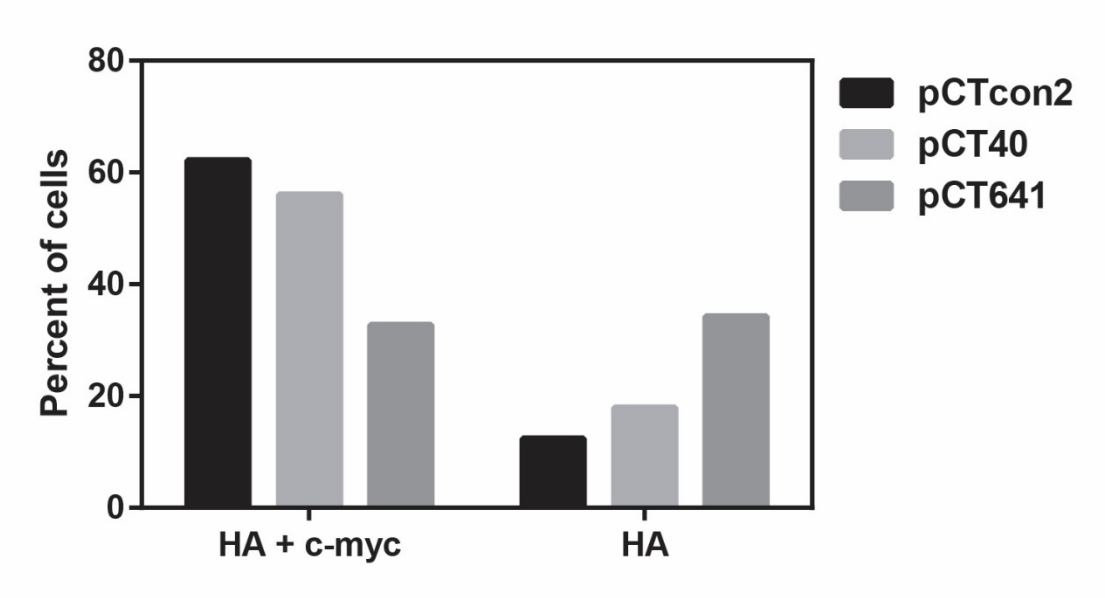

Figure 5.11. Linker length optimization profiles for pCTcon2-Hst5, pCT40-Hst5, pCT641-Hst5. Protein expression was induced at 30 °C for 24 hours. The percentage of cells with both the HA and c-myc epitope tag, as well as only the HA tag is plotted. A bivariate plot of the intensity for both HA (Alexa-Flour 488 antibody) and c-myc (Alexa-Flour 647 antibody) used to generate this bar graph is in **Appendix Figure C.3**.

To assess how protein display is impacted by a single round of freeze-thaw, we used flow cytometry. After 24 h incubation in induction media, cells were stored at -20 °C. According to the data, the display of both constructs was not affected by a single freeze-thaw process, and cells that display the protein can be stored for analysis up to 24 hours later (**Figure 5.12**). During this optimization process, we noticed that improvements in the media resulted in better display for all constructs. For this reason, we continued to use pCT40 instead of optimizing all constructs.

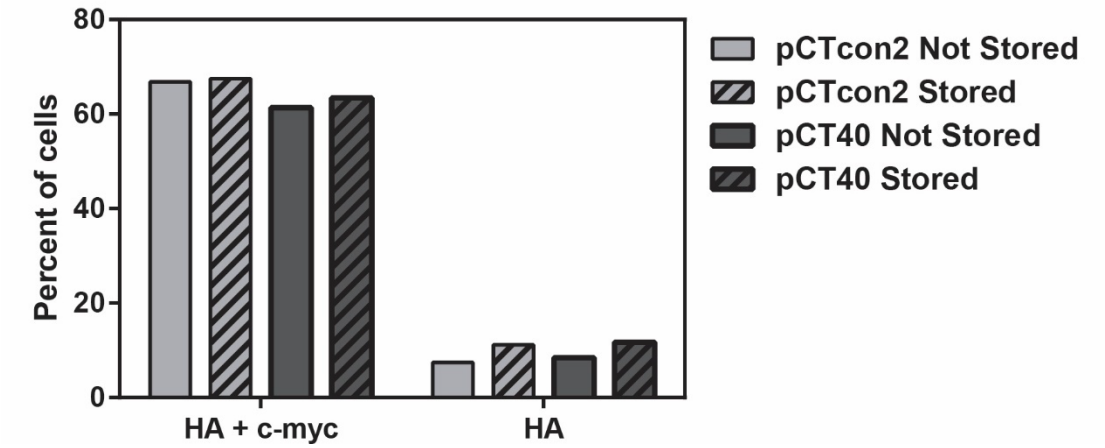

Figure 5.12. Differentiation between harvested cell and cells that were not harvested for pCTcon2-Hst5 and pCT40-Hst5. Protein expression was induced at 30 °C for 24 hours, following which cells were pelleted, decanted, and stored at -20 °C. Cells that were not stored were prepared, and the results were compared. The percentage of cells with both the HA and c-myc epitope tag, as well as only the HA tag is plotted. A bivariate plot of the intensity for both HA (Alexa-Flour 488 antibody) and c-myc (Alexa-Flour 647 antibody) used to generate this bar graph is in **Appendix Figure C.4**.

To determine the impact of media pH on protein expression, we optimized the induction media pH utilizing a Western blot. The blot shows a band for the pCT40-Hst5 construct at 40 kDa. The lowest pH tested (pH 3.5) showed the optimal expression; additionally, as pH decreased, the expression of the full construct increased; however, there was also an increase in the amount of degradation product (**Figure 5.13**). Based on the results, pH 3.5 was determined to be the optimal temperature for protein expression as the degradation products observed were minimal compared to the amount of expressed protein.

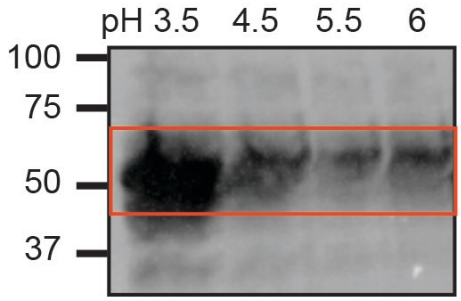

Figure 5.13. Western Blot of Aga2-Hst5 in the pCT40 plasmids. Protein expression was induced in SG-CAA media previously described at pH 3.5, pH 4.5, pH 5.5, and pH 6.0 and at 30 °C. Detection of the c-myc epitope tag is shown with the Bio-Rad all-blue molecular weight ladder.

Optimization of the induction media was concluded by assessing the impacts of different glucose levels on the expression of the protein. The induction media contained galactose, which is used to promote the induction of the construct, and glucose, which promotes cell growth. We determined how varying glucose concentrations impacted the expression of the full protein construct; we also tested rich media induction (yeast extract, peptone, and galactose; YEP-gal) vs minimal media (SG-CAA) induction. The blot shows a band a 47.1 kDa for the pCT40-Hst5 construct, with the optimal glucose levels being no glucose. As glucose levels decreased, the expression increased for the full protein construct, and a similar increase in the amount of degradation products. Interestingly, the rich media expression showed the least degradation product, but similar expression levels to 1.0× glucose levels (our baseline glucose levels of 0.2% w/v) (**Figure 5.14**). After analyzing the results, we concluded that the absence of glucose in the induction media enhanced the expression of our protein construct. Additionally, the increase in degradation products was proportional to those in other lanes, making no glucose the most suitable.

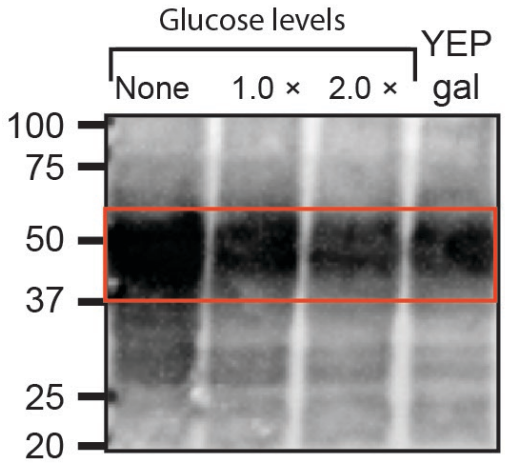

Figure 5.14. Western Blot of Aga2-Hst5 in the pCT40 plasmids. Protein expression was induced in SG-CAA media with varying dextrose levels: No glucose, 1× glucose, and 2× glucose at pH 3.5 and 30 °C. We also tested the rich media Yeast extract peptone galactose at 30 °C. Detection of the c-myc epitope tag is shown with the Bio-Rad all-blue molecular weight ladder. Optimization of degradation conditions.

5.3.2. Degradation can be observed on the surface of S. cerevisiae

Prior to screening a library of variants, it is essential to determine that the platform allows us to observe degradation and that peptides of enhanced and reduced stability can be discriminated between and selected. After expressing the full protein construct in expression media, degradation was evaluated by incubating cells with Sap9 at 220 µg/mL and 22.0 µg/mL in 2 mM NaPB for 24 hours. Samples were labeled with the appropriate HA and c-myc epitope tag antibodies and analyzed using flow cytometry (**Figure 5.15**). No degradation was observed after incubating parent construct pCT40-Hst5 with protease at 30 °C temp and pH 7.4; therefore, optimization began by adjusting the temperature to 37 °C and testing degradation at different pH.

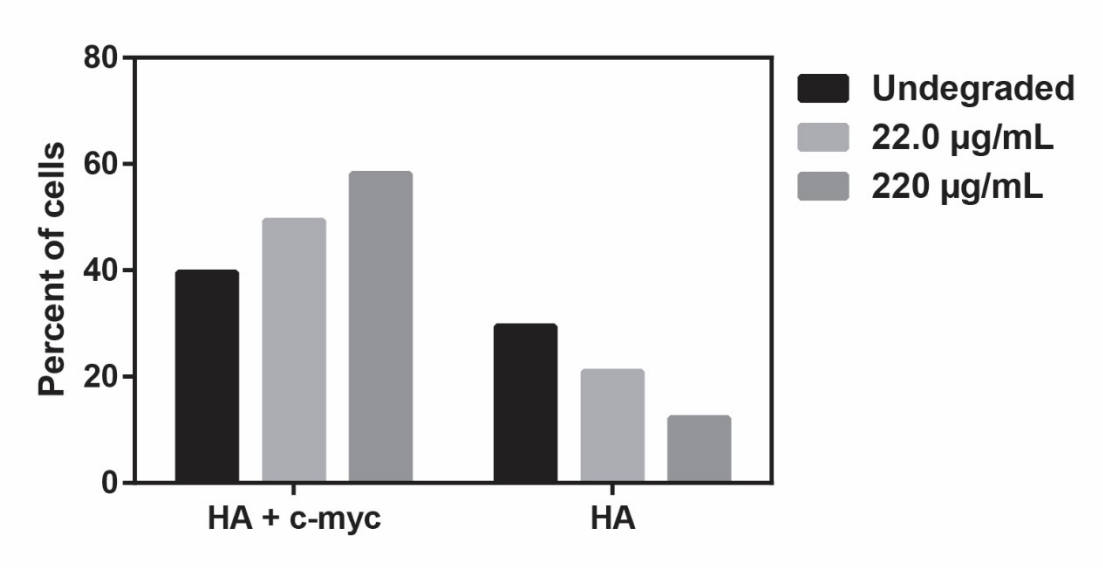

Figure 5.15. Initial degradation profile for pCT40-Hst5 at varying concentrations. Protein expression was induced at 30 °C for 24 hours. Cells were then pelleted, washed, and suspended in Sap9 at varying concentrations in 2 mM NaPB. Samples were incubated at 30 °C for 24 hours. The percentage of cells with both the HA and c-myc epitope tag, as well as only the HA tag is plotted from 1 day and 3 days. A bivariate plot of the intensity for both HA (Alexa-Flour 488 antibody) and c-myc (Alexa-Flour 647 antibody) used to generate this bar graph is in **Appendix Figure C.5**.

The pH optimization was conducted using flow cytometry to determine the ideal degradation pH. The results showed that at 37 °C, the protease exhibited activity against the YSD construct and caused degradation at all pH levels, except at pH 8.5. At pH 8.5, the construct remained undegraded (**Figure 5.16**), indicating that the protease was inactive against the peptide under these conditions. This finding helped us identify a range of pH at which protease can degrade the protein construct effectively. As the physiological condition of interest is a pH of 7.4, as is the pH of saliva, optimization is continued at this pH.

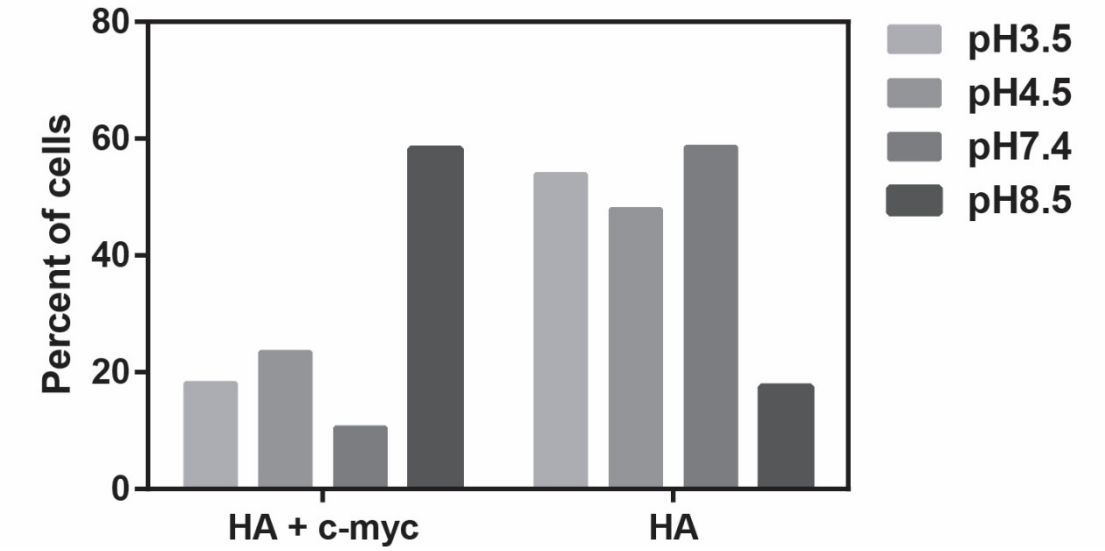

Figure 5.16. Degradation profile for pCT40-Hst5 with Sap9 at varying pH. Protein expression was induced at 30 °C for 24 hours. Cells were then pelleted, washed, and suspended in 100 µL of 100 µg/mL Sap9 in 2 mM NaPB at various pH. Samples were incubated at 37 °C for 24 hours. The percentage of cells with both the HA and c-myc epitope tag, as well as only the HA tag is plotted. A bivariate plot of the intensity for both HA (Alexa-Flour 488 antibody) and c-myc (Alexa-Flour 647 antibody) used to generate this bar graph is in **Appendix Figure C.6**.

Next, we tested degradation for previously tested proteases(Sap1, Sap2, Sap3, and Sap9). While evaluating the additional proteases, we also evaluated whether the degradation time could be reduced to 30 min. Cells were incubated with each Sap at 100 µg/mL and, as expected, at the tested conditions, proteolysis was observed for Sap1, Sap2, and Sap9; however, degradation was not observed at for Sap3, showing that for future work involving Sap3 (**Figure 5.17**), these conditions need to be further optimized.

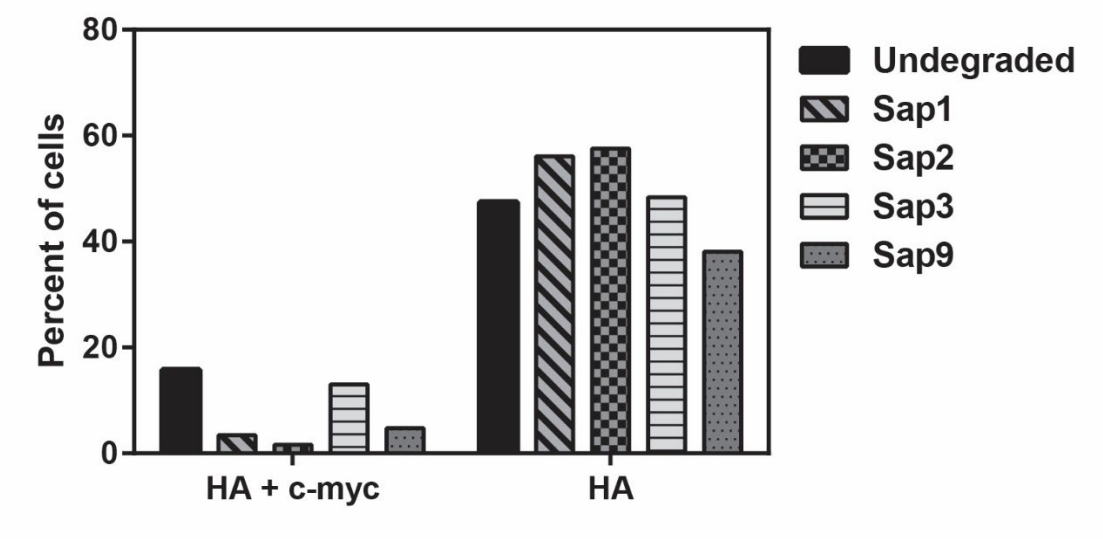

Figure 5.17. Degradation profile for pCT40-Hst5 with No Sap, Sap1, Sap2, Sap3, and Sap9. Protein expression was induced at 30 °C for 24 hours. Cells were then pelleted, washed, and suspended in 100 µL of 100 µg/mL Sap9 in 2 mM NaPB at pH 7.4. Samples were incubated at 37 °C for 24 hours. The percentage of cells with both the HA and c-myc epitope tag, as well as only the HA tag is plotted. A bivariate plot of the intensity for both HA (Alexa-Flour 488 antibody) and c-myc (Alexa-Flour 647 antibody) used to generate this bar graph is in **Appendix Figure C.7**.

Next, we assessed the incubation time with Sap2 to determine the minimal time needed to observe degradation (**Figure 5.18**). From this data, 30 min was enough to observe complete removal of the c-myc tag from most constructs. However, as time continued degradation of the entire yeast surface display construct was observed as observed by the HA tag signal decreasing (**Appendix Figure C.8**), showing that the HA tag and potentially the pCT40 linker were being degraded. This result suggested that in the presence of Sap2, Incubation times longer than 30 min can be inimical, as shown by an intense decrease in constructs with the after 30 min c-myc tag.

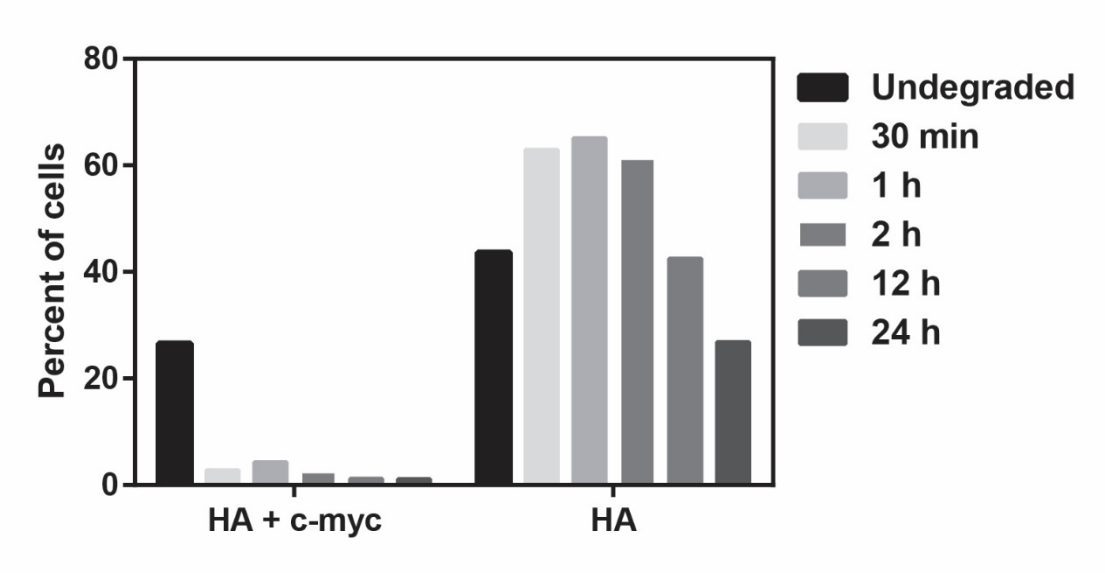

Figure 5.18. Degradation of pCT40-Hst5 after incubation with Sap2 at varying times. Protein expression was induced at 30 °C for 24 hours. Cells were then pelleted, washed, and suspended in 100 µL of 100 µg/mL Sap2 in 2 mM NaPB at pH 7.4. Samples were incubated at 37 °C for 24 hours. The percentage of cells with both the HA and c-myc epitope tag, as well as only the HA tag is plotted. A bivariate plot of the intensity for both HA (Alexa-Flour 488 antibody) and c-myc (Alexa-Flour 647 antibody) used to generate this bar graph is in **Appendix Figure C.8**.

Ikonomova et al. previously determined that Sap2 degrades Hst5 variants [34, 35]; therefore, it was essential to optimize the concentration so that we can differentiate between variants that are more or less stable than the parent Hst5. In this experiment, it was found that the peptide which was not degraded had 36.32% of cells with both the c-myc and HA tag. As expected, the lowest protease concentration of 0.78 µg/mL gave the next highest result, with 8.83% of cells displaying both the c-myc and HA tag. (**Figure 5.19**). This result indicates that proteolysis of the YSD construct can be observed at relatively low Sap2 concentrations nearly similar to those in chapter 2 and 3, in this case only 0.78 µg/mL was necessary.

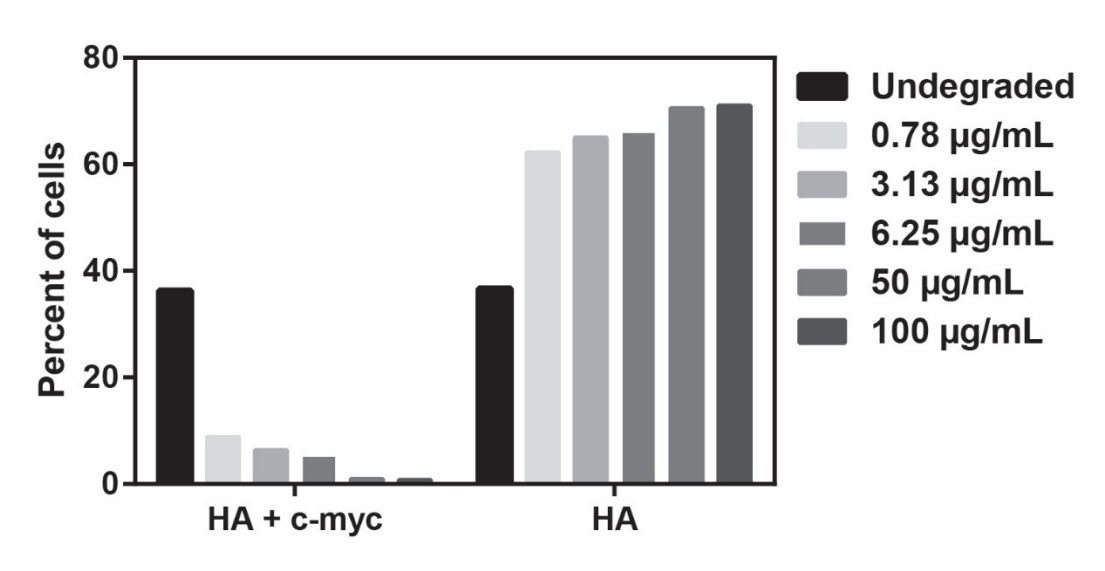

Figure 5.19. Degradation profile for pCT40-Hst5 after incubation with Sap2 at varying concentrations. Protein expression was induced at 30 °C for 24 hours. Cells were then pelleted, washed, and suspended in 100 µL of Sap2 (at concentrations listed in the figure) in 2 mM NaPB at pH 7.4. Samples were incubated at 37 °C for 30 min. The percentage of cells with both the HA and c-myc epitope tag, as well as only the HA tag is plotted. A bivariate plot of the intensity for both HA (Alexa-Flour 488 antibody) and c-myc (Alexa-Flour 647 antibody) used to generate this paragraph is in **Appendix Figure C.9**.

Degradation by Saps has been observed at hydrophobic residues; however, proline and serine are unlikely to be cleaved by Sap2, while there may be cleavage at alanine [89]. Therefore, a linker made of these residues would be likely to be stable against proteases. In this work, after degrading the protein construct and pellet and collecting the supernatant of the sample, we then analyze the degradation fragments in the supernatant with mass spectrometry. Fragments identified from the undegraded construct were considered the background signal, as these may have resulted from proteases secreted by *S. cerevisiae*. The results show cleavage at the $(G_4S)_3$ and 40 amino acid linkers; however, more cleavage was observed at the peptide of interest at lower concentrations (**Figure 5.20)**. This is probably because at higher concentrations, the construct was entirely degraded, showing fewer fragments, while

at low concentrations, the degraded fragments were less processed and could be detected in the solution.

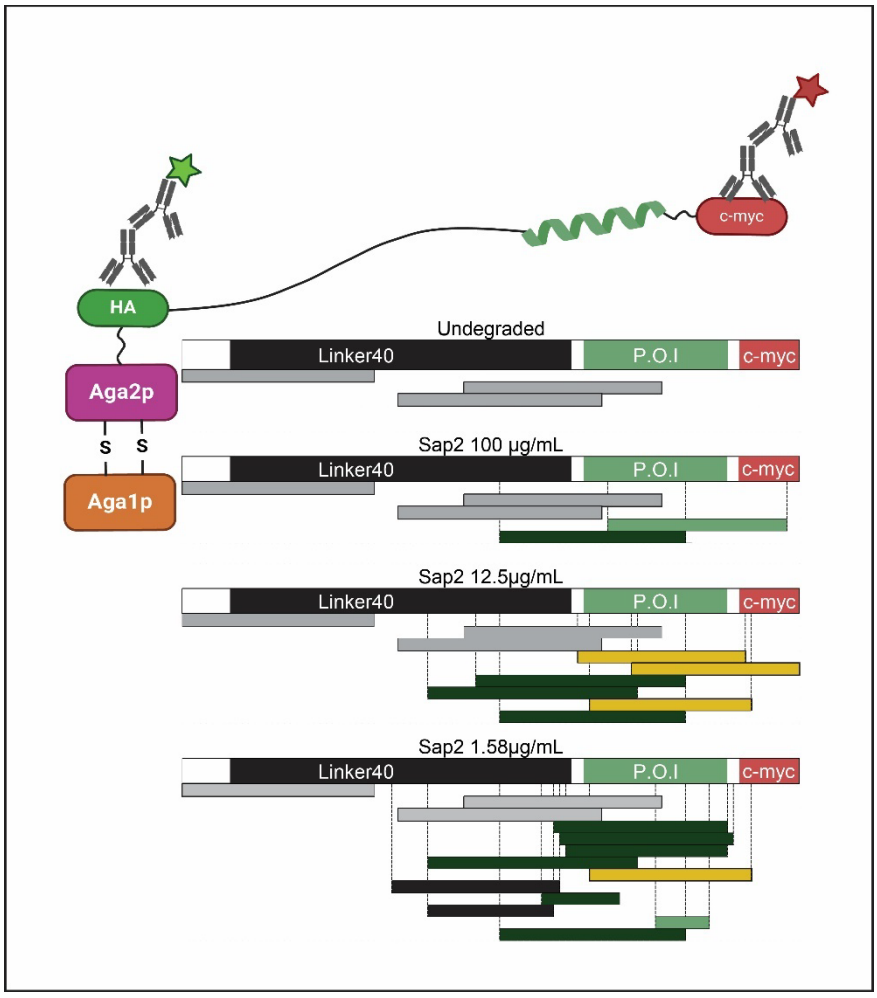

Figure 5.20. Fragments identified from degradation of YSD construct by Sap2 at varying concentrations. Protein expression was induced at 30 °C for 24 hours. Cells were then pelleted, washed, and suspended in 100 µL of Sap2 (at concentrations listed in the figure) in 2 mM NaPB at pH 7.4. Samples were incubated at 37 °C for 30 min, after which cells were pelleted and the supernatant was collected, and fragments were identified using mass spectrometry. Undegraded pCT40 was also analyzed to identify fragments formed before adding proteases, these fragments are 4-35, 51-83, and 40-72. Figure made in BioRender.com.

5.3.3. Differences in proteolytic stability can be observed

After incorporating our optimized degradation conditions, we assessed the impact of linker lengths on the degradation of Hst5. Of the constructs, pCTcon2-Hst5 had

47.65% of cells with both c-myc and HA tag, seemingly have greater display than pCT40-Hst5 (37.06%) and pCT641-Hst5(41.75%). However, after proteolysis, pCT40-Hst5 and pCT641-Hst5 have an 86.7% and 73.4% reduction of cells with a c-myc tag, respectively, while pCTcon2-Hst5 only has a 65.1% reduction (**Figure 5.21**). This could mean that the longer linkers are more accessible to Sap2 at these concentrations. In this case, the more accessible display system would increase.

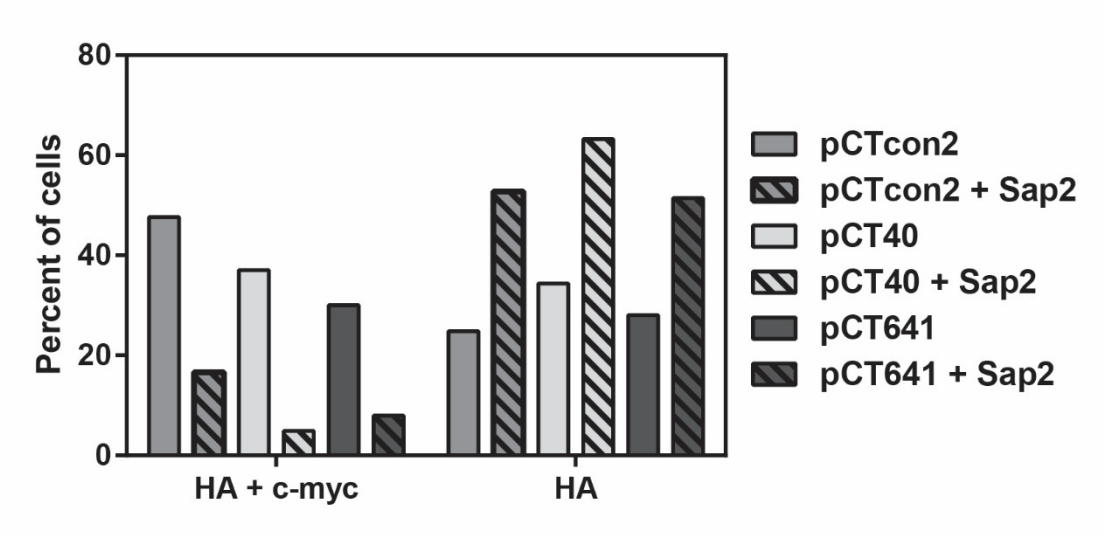

Figure 5.21. Degradation profile for pCTCon2-st5, pCT40-Hst5, and pCT641-Hst5 after incubation with Sap2. Protein expression was induced at 30 °C for 24 hours. Cells were then pelleted, washed, and suspended in 100 µL of 0.39 µg/mL Sap2 in 2 mM NaPB at pH 7.4. Samples were incubated at 37 °C for 30 min. The percentage of cells with both the HA and c-myc epitope tag, as well as only the HA tag is plotted. A bivariate plot of the intensity for both HA (Alexa-Flour 488 antibody) and c-myc (Alexa-Flour 647 antibody) used to generate this bar graph is in **Appendix Figure C.10**.

For the YSD proteolysis screen to be effective, we must differentiate between stable and unstable variants of Hst5. We made constructs containing K11RK17R (more stable than Hst5) and K13L (less stable than Hst5). As expected, pCT40-K11RK17R had a 30.4% reduction of cells with c-myc and HA tag, while Hst5 had a 86.7% reduction for K11RK17R, making K11RK17R more stable than the parent Hst5.

While K13L seems to express less of the full construct than the other two variants, which is more than likely due to proteolysis by the proteases from *S. cerevisiae*, pCT40-Hst5 and pCT40-K11RK17R express fully and show that pCT40-K11RK17R is more stable than the former two (**Figure 5.22)**. Therefore, proteolytic stability is conserved in the full-length construct. Showing that differences in proteolytic stability can be observed after proteolysis at the optimized conditions.

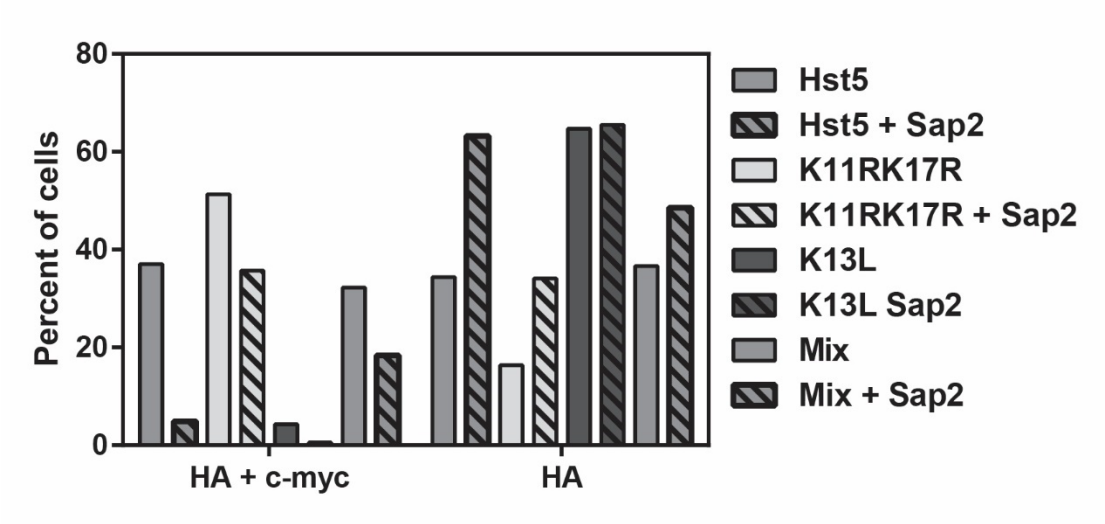

Figure 5.22. Degradation profile for pCT40-Hst5, pCT40-K11RK17R, and pCT40-K13L after incubation with Sap2. Protein expression was induced at 30 °C for 24 hours. Cells were then pelleted, washed, and suspended in 100 µL of 0.39 µg/mL Sap2 in 2 mM NaPB at pH 7.4. Samples were incubated at 37 °C for 30 min. The percentage of cells with both the HA and c-myc epitope tag, as well as only the HA tag is plotted. A bivariate plot of the intensity for both HA (Alexa-Flour 488 antibody) and c-myc (Alexa-Flour 647 antibody) used to generate this bar graph is in **Appendix Figure C.11**.

5.4. *Discussion*

In study, we optimized conditions to improve the expression and display of the Hst5 construct on the surface of *S. cerevisiae* and identified conditions that would allow degradation to occur (**Table 5.5**). From the conditions tested, the optimal expression conditions identified were incubation in SG-CAA without glucose at 30 °C and at pH

4.5 for 24 h; the best degradation conditions for Sap2 were 0.39 µg/mL of Sap2 in 2 mM NaPB, at 37 °C at pH below 7.4.

Table 5.3. Optimized conditions for protein expression and construct degradation.

Tested variables	Protein expression	Degradation
Temperature	30 °C	37 °C
pH	3.5	7.4
Glucose levels	0 ×	-
Concentration	-	0.78 (µg/mL)
Time	24 h	30 min
Linker length	40 amino acids	

Notably, while we could express all constructs, there are a few limitations. While K13L was expressed (**Figure 5.7**), there was little to no display on the cells' surface. This could be because *S. cerevisiae* has proteases that degrade the construct. This could also be why there are differences between Hst5 and K11RK17R before degradation (**Figure 5.22**). Prior work also shows that incubating Hst5 with *C. albicans* can result in degradation[34-36], so potentially during the degradation process *S. cerevisiae* cells may be interacting with the construct and degrading them. Furthermore, while increasing the linker length increased the expression of the construct (**Figure 5.6**), the display seen via flow cytometry decreases, which is the opposite trend observed by Lown et al. [108]. However, after proteolysis of the pCTCon2-Hst5 and pCT40-Hst5 constructs we notice that more of the pCT40 constructs are degraded. The longer linker allowed Lown et al. to get more reliable interactions between their ligand and binder, which could mean in our case while the longer linker does not display as well as the pCTCon2 construct, but it could help get more consistent proteolysis of our peptide. However, according to the mass

spectrometry results, cleavage is also happening at the pCT40-Hst5 linkers (**Figure 5.21**), so a longer linker that extends the peptide beyond the cell's surface may not be favorable if the linker sequence cannot be optimized to prevent proteolysis.

Through the optimization of growth, protein expression, and degradation conditions, we have shown that we are able to differentiate between stable and unstable peptide variants. To optimize this system, we must increase the proteolytic stability of the linker. Koelsch et al. found that Saps do not cleave near proline but can cleave near alanine [89]. The linkers used in this case are proline, alanine, and serine combinations. Lown et al. used a Gaussian chain model to identify an all-proline linker that would extend beyond the cell wall and more than likely not be degraded by Saps [89, 108]. Ultimately, the use of an all-proline linker is a critical step towards engineering more robust and effective peptide-based systems. This approach may not only enhance the stability of the peptides but also improve the overall efficiency of the screening process.

5.5. *Conclusion*

In this study, we optimized the conditions for expressing and displaying the Hst5 construct on the surface of *S. cerevisiae*, with optimal expression achieved at 30 °C and pH 4.5 in SG-CAA media without glucose. Despite effective expression, challenges in surface display, particularly for K13L suggest proteolysis by yeast proteases. Notably, the largest linker length, contrary to the findings of Lown et al., led to decreased surface display as observed through flow cytometry. Moreover, the degradation studies revealed that constructs with longer linkers, although providing

consistent proteolysis, also experienced significant cleavage, especially in pCT40-Hst5 constructs. This indicates that while longer linkers may facilitate more consistent interactions, they may also increase susceptibility to proteolytic cleavage. Mass spectrometry confirmed cleavage at these longer linkers, suggesting that optimization of linker sequences to enhance proteolytic resistance is crucial. Our findings underscore the importance of linker optimization to prevent degradation, aiming to improve the efficiency of screening processes and the development of stable, effective peptide therapeutics.

6. Chapter 6: Summary and recommendation for future work

In this dissertation, we demonstrated that protein engineering approaches can be implemented to understand the interactions between Hst5 and proteases. In Chapters 3 and 4, variants of Hst5 were designed using rational design to understand the impact of modifications at the lysine residues of Hst5 on the proteolytic stability of Hst5. Chapter 3 showed that after incubation with Sap1, Sap2, and Sap3 proteases, K17L had enhanced proteolytic stability and maintained its antifungal activity. We assessed the novel variant K11RK17L and expanded the repertoire of tested Saps to improve Hst5's proteolytic stability. Chapter 4 showed the impact of different amino acid properties at the K13 and K17 residues on the proteolytic stability of Hst5 variants in the presence of zinc and Saps. This resulted in identifying the K17W proteolytically stable variant, which retain the most activity of the tested variants in the presence of Saps and zinc. Both chapters also show a potential link of proteolytic stability to antifungal activity; however, further engineering is needed as improvements in proteolytic stability in the presence of saliva are marginal. Chapter 5 described initial work on a novel screening method for proteolytic stability utilizing yeast surface display. The work shown in this chapter indicates that differences in proteolytic stability between the peptide variants can be seen, showing great potential for screening larger libraries.

Building on the work in this dissertation, we recommend further experiments. These experiments strive to enhance our understanding of the interactions between Hst5, Saps, and saliva to improve the therapeutic potential of Hst5.

6.1. Screening a library of peptides using the yeast surface display system and potential further improvements

In Chapter 5, strides were made to utilize yeast surface display as a screening method for a library of peptides. Utilizing flow cytometry, we showed that K11RK17R was more proteolytically stable than the wild-type Hst5 in the presence of Sap9 and Sap2. However, further work must be done to enhance this system if it is to be used to screen a library of peptides. The yeast surface display construct containing the K11RK17R variants of Hst5 was prepared. I propose a mock screen where these variants are mixed at a varying ratio and K11RK17R to Hst5 1:1, 1:10, 1:100, and 1:1000, followed by treating the *S. cerevisiae* cells with Saps and screening the resulting cell suspension through flow cytometry and collecting cells that retain both the c-myc and HA tag. If 95% of the cells collected are the constructs for K11RK17R, peptide libraries can be generated using error-prone polymerase chain reaction (ep-PCR). In using ep-PCR, the Hst5 gene will be amplified using ep-PCR with different ratios of dNTP or increased concentration of $MgCl_2$.These methods have been shown to increase the error rate of Taq polymerase [115]. The generated library of variants can then be screened and sorted repeatedly to improve the enrichment of proteolytically stable peptides (**Figure 6.1**).

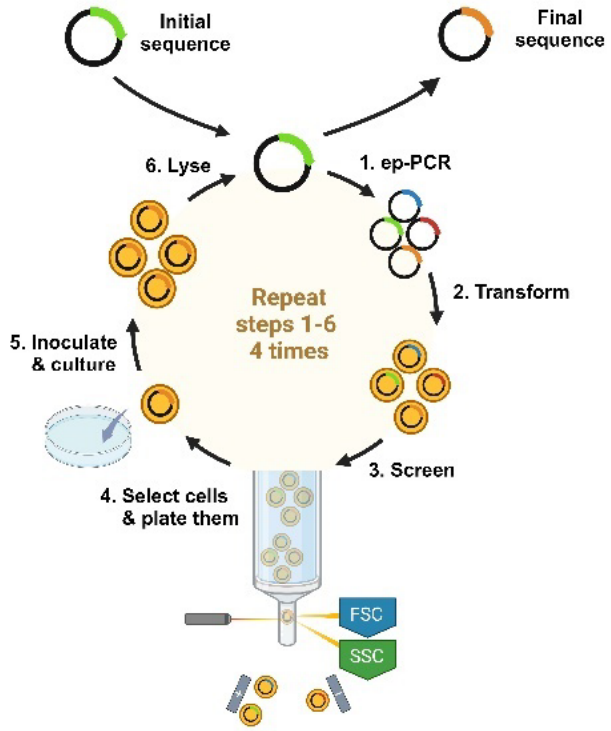

Figure 6.1. Schematic library design and screening portions. First, lyse the bacteria strain with the plasmid of interest. Next, use ep-PCR to build a diverse library. Finally, transform *S. cerevisiae* with the plasmid to finish the library design portion. Next, screen using FACS, collecting c-myc and HA positive samples and repeat the analysis on the collection for enrichment. Samples are plated and inoculated, after which steps 1-6 are repeated. After the final inoculation, plasmids from the isolated cells can be sequenced to identify the stable mutants. Figure made in BioRender.com.

One improvement that can be made to the current system is the linker. In Chapter 5, we determined the optimal linker to be the 40 amino acid linker $(PAS)_{40}$. However, we also showed that this linker is cleaved by the Sap2. This is in agreement with work by Schilds et al., which showed that Saps cleave near alanine [89], making the $(PAS)_{40}$ linker prone to proteolysis. However, in their work, Schilds et al. showed that Saps do not cleave near proline. The potential of using a linker with only proline is shown in the work by Lown et al., where they hypothesize that a linker containing only proline would improve display on the surface of yeast [108]. If these

experiments are to be continued, substituting the linker for one purely made of prolines could enhance our results.

6.2. *Yeast extracellular reticulum sequestration screening*

While YSD has been used to engineer peptides for binding and larger proteins for proteolytic stability, it has not been used for engineering peptides for proteolytic stability. Yeast endoplasmic reticulum sequestration screening (YESS) is a powerful tool that has currently been used to engineer proteases for enhanced activity (**Figure 6.2**). However, given that both the peptide and protease are encoded into the plasmid, we propose that YESS can be used to engineer both protease and peptide. In this method, a fusion construct is generated with the peptide of interest and a counter sequence coding for the protease. At the C-terminus of both sequences, there is an endoplasmic reticulum retention peptide sequence, FEHDEL. When the peptide construct and protease are expressed, FEHDEL signals both to be sent to the endoplasmic reticulum rather than the surface of the cell. The protease cleaves the peptide construct while in the ER, and, due to the linkage of the peptide to Aga2, the sequence can express on the surface of the cell and be observed using flow cytometry [116]. While this system may be complex, it introduces the potential for engineering both protease and peptide and improving our understanding of the interactions between human salivary peptide Hst5 and pathogen *C. albicans* Saps.

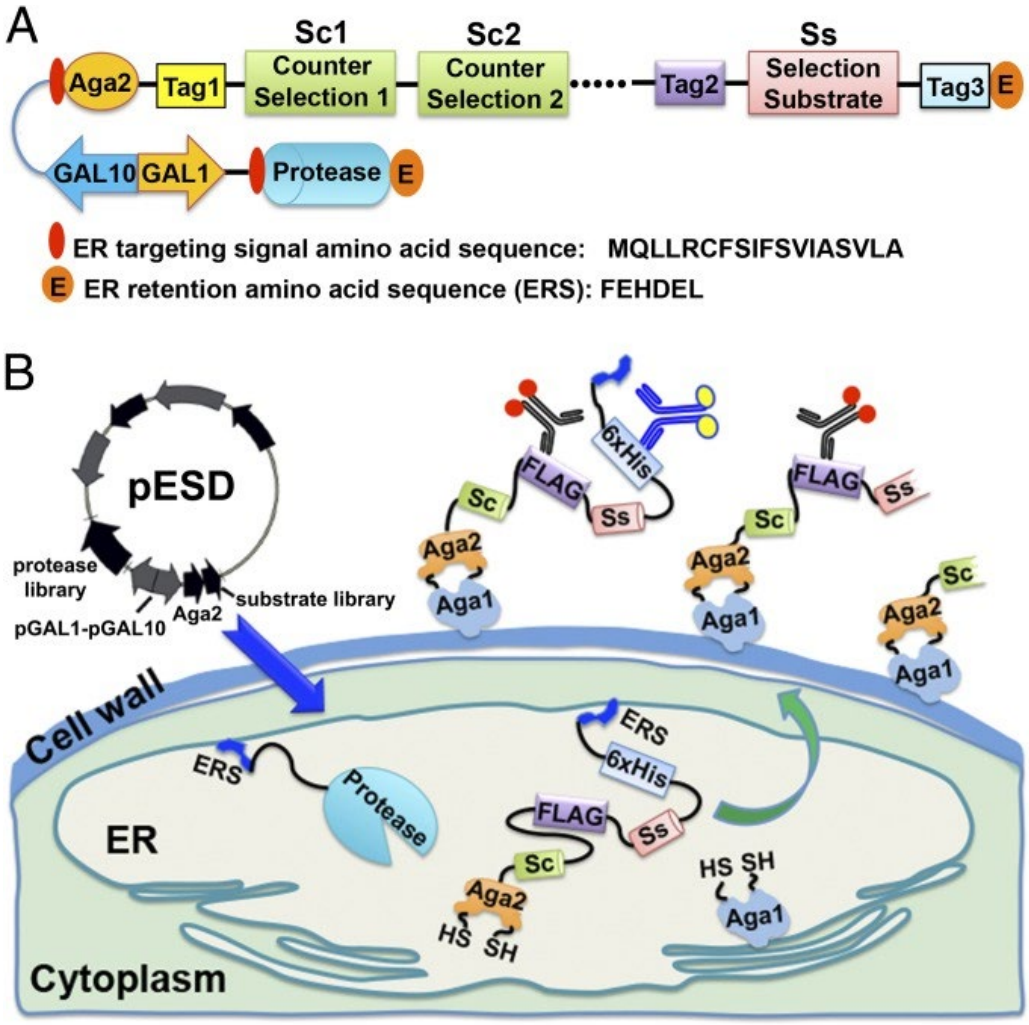

Figure 6.2. Schematic of the yeast endoplasmic reticulum sequestration screening. The peptide construct and protease are signaled for the endoplasmic reticulum, where proteolysis occurs. The peptide construct is then displayed on the surface of the yeast to be screened by flow cytometry. The figure is taken from [117].

6.3. Production and purification of Saps

In this dissertation, Saps have been graciously produced by B. Hube from Friedrich Schiller University, Germany [42], in their native sequence; however studying Sap mutations could further enhance our understanding of the interactions between Saps and Hst5. Saps are normally produced in *Pichia pastoris* and purified using either ion exchange chromatography or ultrafiltration. In order to understand what residues in

the Saps are playing an important role in the interaction between Saps and Hst5, protein engineering techniques could be utilized to screen Sap variants for enhanced proteolysis. Furthermore, Sap2 plays a role in the pathogenicity of *C. albicans*; however, its variant V273L is shown to be more pathogenic by degrading complement molecules that are essential for the human immune response. Generating variants of the Sap to assess proteolytic stability against *C. albicans* would further enhance our ability to engineer proteolytically stable variants of Hst5.

6.4. *Designing variants with improved proteolytic stability in the presence of Hst5 and proteases in saliva*

Chapters 3 and 4 showed that protein engineering techniques can successfully generate variants that are proteolytically stable against Saps. However, engineering resistance to Saps led to only marginal improvements in stability in the presence of saliva. The K5R, K17L, or K17W variants provide a great starting point for engineering proteolytic stability against saliva and must be included in future designs. Based on Chapters 3 and 4, proteolysis by saliva formed fragments near K5, E16, K17, and H18, among others. Additional variants should be assessed for improved proteolytic stability in the presence of saliva (**Table 6.1**). The K5RK17W variant was designed because these substitutions were found to be favorable in the presence of saliva. K13HK17W was designed to determine how improving zinc binding and proteolytic stability impacts antifungal activity. Glutamate was found to reduce the antifungal activity when substituted into the K13 and K17 residues of Hst5. E16LK17W and E16delK17W were designed to determine how removing the negative charge would impact proteolytic stability and antifungal activity.

R6WK13WK17W variants were designed to increase the amphiphilicity of the peptide, as strengthening secondary structure properties may increase the proteolytic stability.

Table 6.1. Recommendation for Hst5 variants with improved properties.

Peptide	Sequence [a,b]																							
	1	2	3	4	5	6	7	8	9	10	11	12	13	14	15	16	17	18	19	20	21	22	23	24
Hst5	D	S	H	A	K	R	H	H	G	Y	K	R	K	F	H	E	K	H	H	S	H	R	G	Y
K17W	-	-	-	-	-	-	-	-	-	-	-	-	-	-	-	-	W	-	-	-	-	-	-	-
K5RK17W	-	-	-	-	R	-	-	-	-	-	-	-	-	-	-	-	W	-	-	-	-	-	-	-
K13HK17W	-	-	-	-	-	-	-	-	-	-	-	-	H	-	-	-	W	-	-	-	-	-	-	-
E16LK17W	-	-	-	-	-	-	-	-	-	-	-	-	-	-	-	L	W	-	-	-	-	-	-	-
K5W	-	-	-	-	W	-	-	-	-	-	-	-	-	-	-	-	-	-	-	-	-	-	-	-
E16delK17W	-	-	-	-	-	-	-	-	-	-	-	-	-	-	-	*	-	W	-	-	-	-	-	-
R6WK13WK17W	-	-	-	-	-	W	-	-	-	-	-	-	W	-	-	-	W	-	-	-	-	-	-	-

[a] *The asterisk represents a deletion of amino acid residues.*
[b] *The hyphens represent retained amino acids.*

6.5. Assessing the activity of Hst5 variants in the presence of metals

In Chapter 4, we explored how the presence of zinc can impact the proteolytic stability of the peptide and the antifungal activity of the peptide. Human diets consist of variants of divalent metals, not just zinc. Prior work has shown that in the presence of iron, the proteolytic stability of Hst5 against trypsin is increased. However, in the same publication, zinc enhanced the proteolytic stability of Hst5 [118], contrary to the findings of this dissertation. Trypsin is a serine protease, while Saps are aspartyl proteases, and the differing results for trypsin and Saps suggest that divalent metals have different roles for the different classes of proteases. Furthering our understanding of how these metals impact the proteolytic stability of Hst5 will not only bring light to the interactions of Hst5 and saliva but will also increase the potential for the peptides as oral therapeutics.

6.6. *Creating coatings with antifungal peptides*

Hst5's K11RK17R variant was previously coated onto the surface of polyelectrolyte multilayers and reduced biofilm formation on these surfaces, showing great potential as a coating for medical devices [102]. Healthcare-associated fungal infections (HAFI) are becoming recognized as a major threat in immunocompromised patients, costing the US healthcare system >$7.2 billion annually [119]. With the advancement of medical technology, more aggressive and invasive treatments and transplantations have increased the risk of infections in patients [120]. The most commonly isolated species in these infections are *Candida* spp., *Cryptococcus* spp., *Aspergillus* spp., and *Trichosporon* spp [119, 121, 122]. Treatment of HAFI is complicated by these yeast species' ability to form biofilms and adhere to the surface of biomedical devices [123, 124]. Surface coatings that contain antifungal agents have been previously tested [125, 126]. However, there is a concern that fungal pathogens may become resistant to these drugs. To address this concern, I suggest evaluating the practical effects of using Hst5 variants as a surface coating for stents and catheters.

To utilize Hst5 variants as surface coating, a few steps need to be considered. First, a compatible polymer needs to be identified; prior work has shown that poly-L-lysine and poly-L-glutamic acid can be compatible as a coating for antimicrobial peptides and that biofilm formation has been hindered in the presence of antimicrobial peptides [127, 128]. In order to ensure the safety and effectiveness of medical devices that are intended for long-term use, it is crucial to assess the degradation profile of polymers used in these devices. One way to do this is by testing the duration of the

drug, which involves assessing the biofilm formation and degradation of the polymer over time using RPMI 1640 media and mass spectrometry. Additionally, it is important to evaluate biofilm reduction and toxicity to ensure that the antifungal properties of the device are retained and that the polymer is compatible with the body. Finally, in vivo experimentation using a mouse model could be conducted to determine the practicality of these experiments. By following these steps, we could make progress in using the Hst5 peptide as an antifungal surface coating to prevent infections.

A. Appendix A

Appendix Table A.1. P-values for proteolysis of Hst5 and variants by Saps and saliva. Two-way ANOVA tests with α = .05 and Dunnett's multiple comparison tests (degraded Hst5 as the control) were performed for statistical analysis.

P-values (Proteolysis assay)								
	Sap1	Sap2	Sap3	Sap5	Sap6	Sap9	Sap10	Saliva
K5R	< 0.0001	0.789	0.970	> 0.9999	> 0.9999	0.863	> 0.9999	> 0.9999
K11R	< 0.0001	< 0.0001	0.109	> 0.9999	> 0.9999	0.401	> 0.9999	0.000
K13R	0.954	0.107	1.000	> 0.9999	> 0.9999	0.991	> 0.9999	0.993
K17R	0.146	0.002	0.960	> 0.9999	> 0.9999	< 0.0001	> 0.9999	0.857
K11RK17R	0.001	0.179	0.055	> 0.9999	> 0.9999	< 0.0001	> 0.9999	1.000
K5L	< 0.0001	< 0.0001	< 0.0001	> 0.9999	> 0.9999	0.321	> 0.9999	0.002
K11L	< 0.0001	< 0.0001	< 0.0001	> 0.9999	> 0.9999	< 0.0001	> 0.9999	> 0.9999
K13L	< 0.0001	< 0.0001	< 0.0001	> 0.9999	> 0.9999	< 0.0001	> 0.9999	0.820
K17L	0.016	< 0.0001	0.630	> 0.9999	> 0.9999	< 0.0001	> 0.9999	0.001
K11RK17L	0.012	< 0.0001	0.000	> 0.9999	> 0.9999	< 0.0001	> 0.9999	1.000

Appendix Table A.2. P-values for proteolysis of Hst5 and variants by Saps and saliva. Two-way ANOVA tests with α = .05 and Dunnett's multiple comparison tests (degraded Hst5 as the control for Samples treated with Saps and undegraded Hst5 as the control for untreated sample) were performed for statistical analysis.

	P-values (Antifungal assay)							
	Sap1	Sap2	Sap3	Sap5	Sap6	Sap9	Sap10	No Sap
K5R	0.600	< 0.0001	0.404	0.866	0.000	0.004	< 0.0001	0.031
K11R	< 0.0001	0.966	0.390	1.000	0.559	0.250	0.395	0.000
K13R	< 0.0001	< 0.0001	0.998	0.984	0.228	0.018	0.297	< 0.0001
K17R	0.000	< 0.0001	0.028	0.992	0.024	< 0.0001	0.829	0.098
K11RK17R	0.146	< 0.0001	< 0.0001	0.781	0.069	< 0.0001	0.382	0.043
K5L	< 0.0001	< 0.0001	< 0.0001	0.320	0.755	0.029	< 0.0001	< 0.0001
K11L	< 0.0001	< 0.0001	< 0.0001	0.159	0.102	< 0.0001	1.000	0.798
K13L	< 0.0001	< 0.0001	< 0.0001	1.000	0.732	< 0.0001	0.846	0.993
K17L	0.248	0.002	0.001	0.955	0.987	< 0.0001	0.342	0.012
K11RK17L	0.049	0.005	< 0.0001	0.998	0.004	< 0.0001	0.308	0.234
Concentration (μg/mL)	4.69	9.38	18.75	4.69	2.34	9.38	4.69	4.69

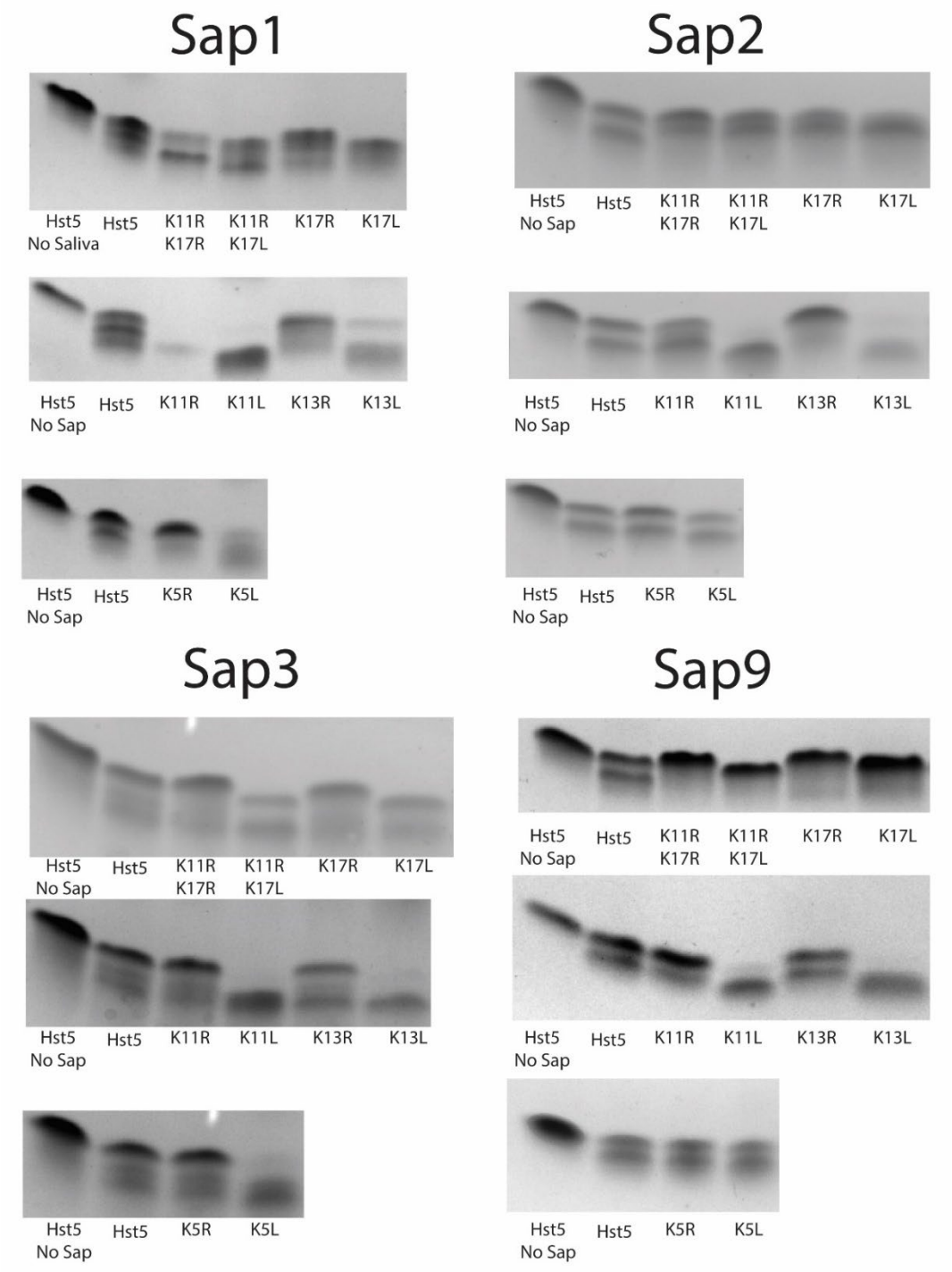

Appendix Figure A.1. Gel images for proteolysis of Hst5 variants by Sap1, Sap2, Sap3, and Sap9.

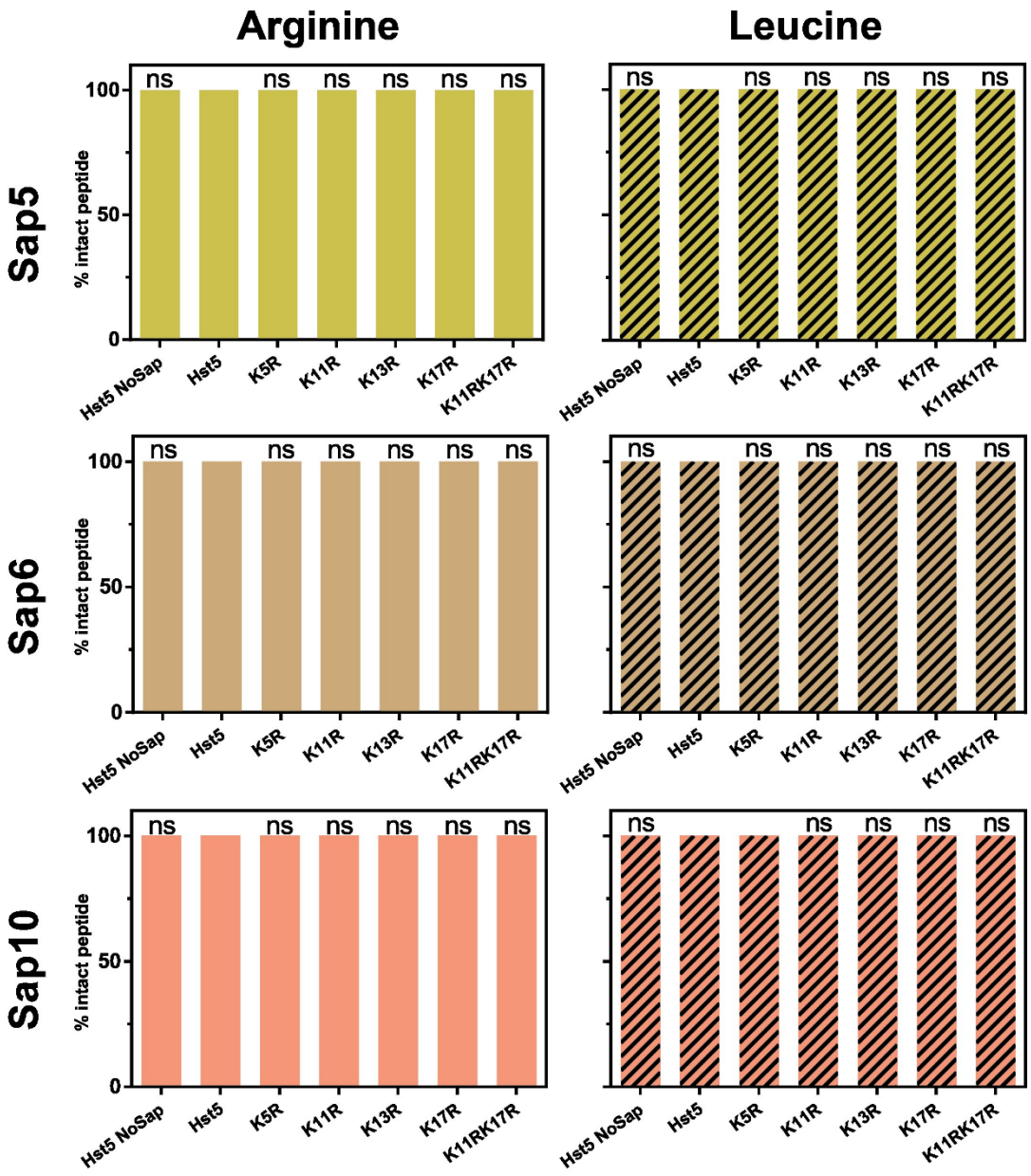

Appendix Figure A.2. Degradation of Hst5 by purified Sap5, Sap6, or Sap10. After incubation for 2 h at 37 °C, we used gel electrophoresis to separate fragments from fully intact peptides and quantified the gel images using densitometric analysis. Error bars represent the standard error of the mean (N = 9 Hst5 No Sap and Hst5 + Sap, while N = 3 for all other variants). The number of asterisks indicates the level of statistical significance against parent Hst-5 incubated with cells: NS for P > 0.05, * for $P \leq$ 0.05, ** for $P \leq 0.01$, and **** for $P \leq 0.0001$.

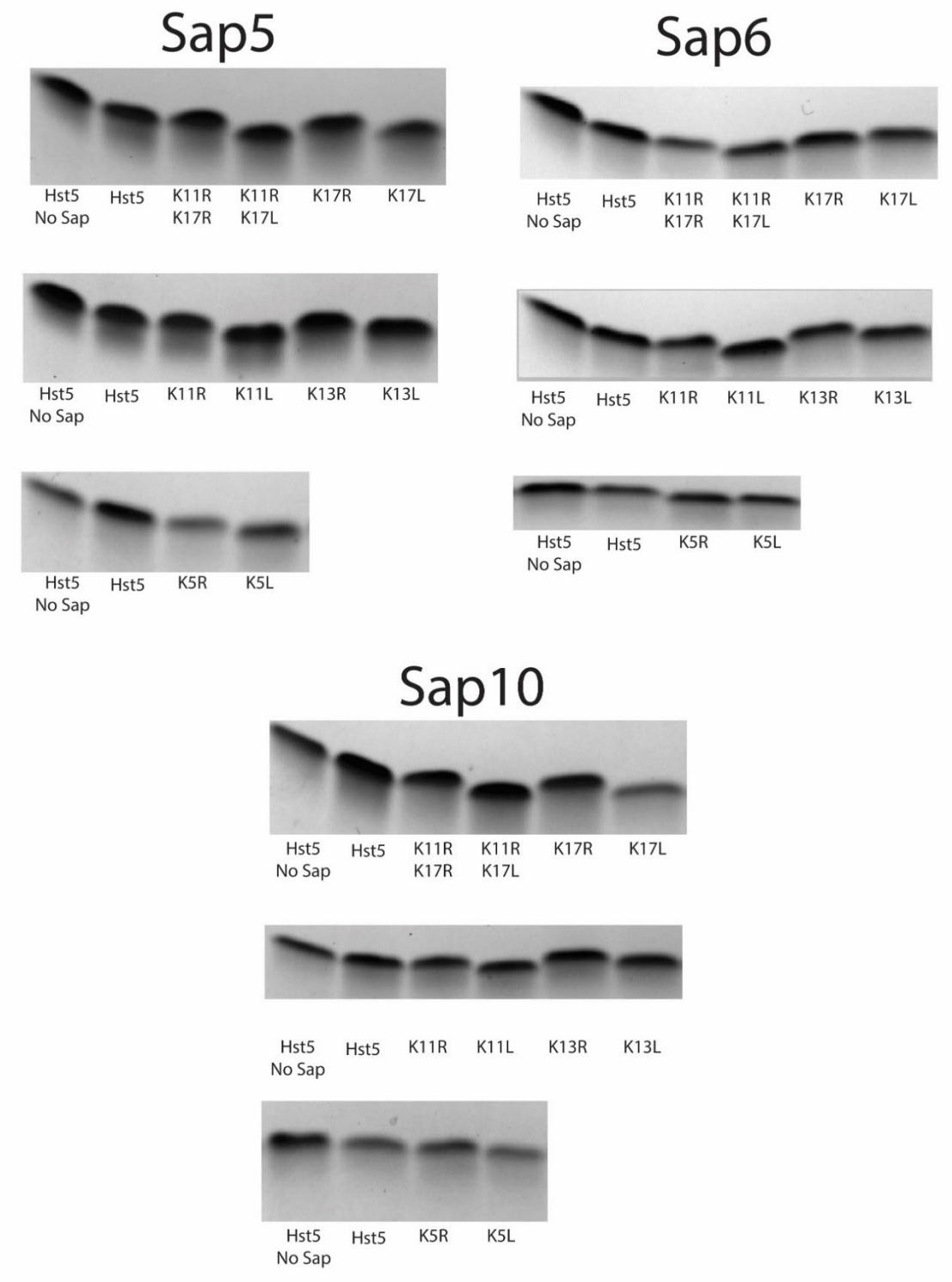

Appendix Figure A.3. Gel images for proteolysis of Hst5 variants by Sap1, Sap2, Sap3, and Sap9.

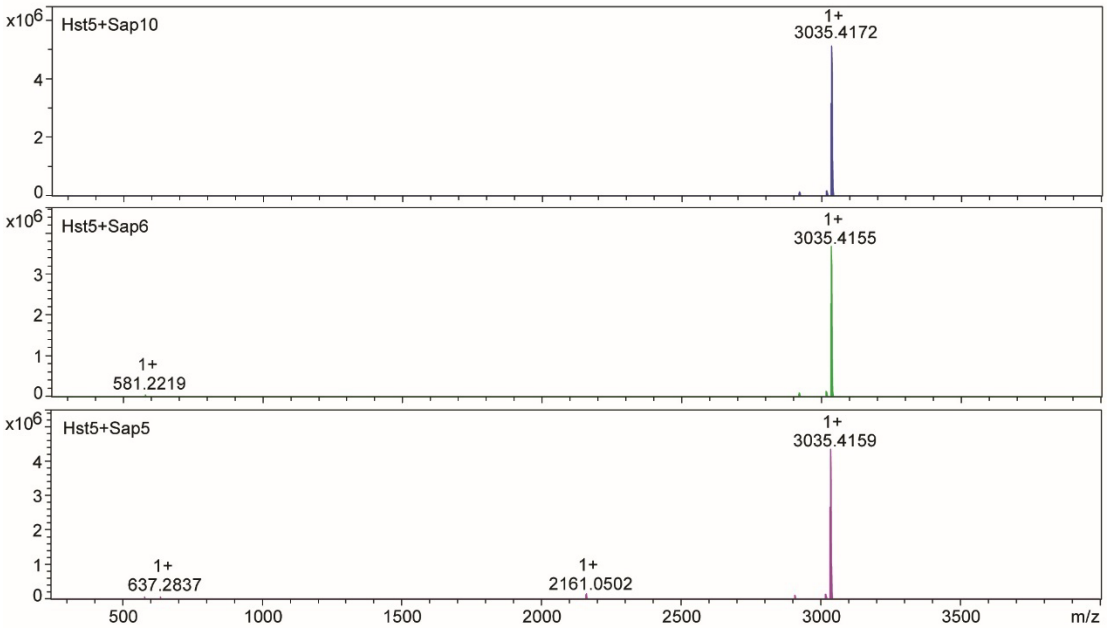

Appendix Figure A.4. Mass spectra for the degradation of Hst5, by Sap5, Sap6, and Sap10.

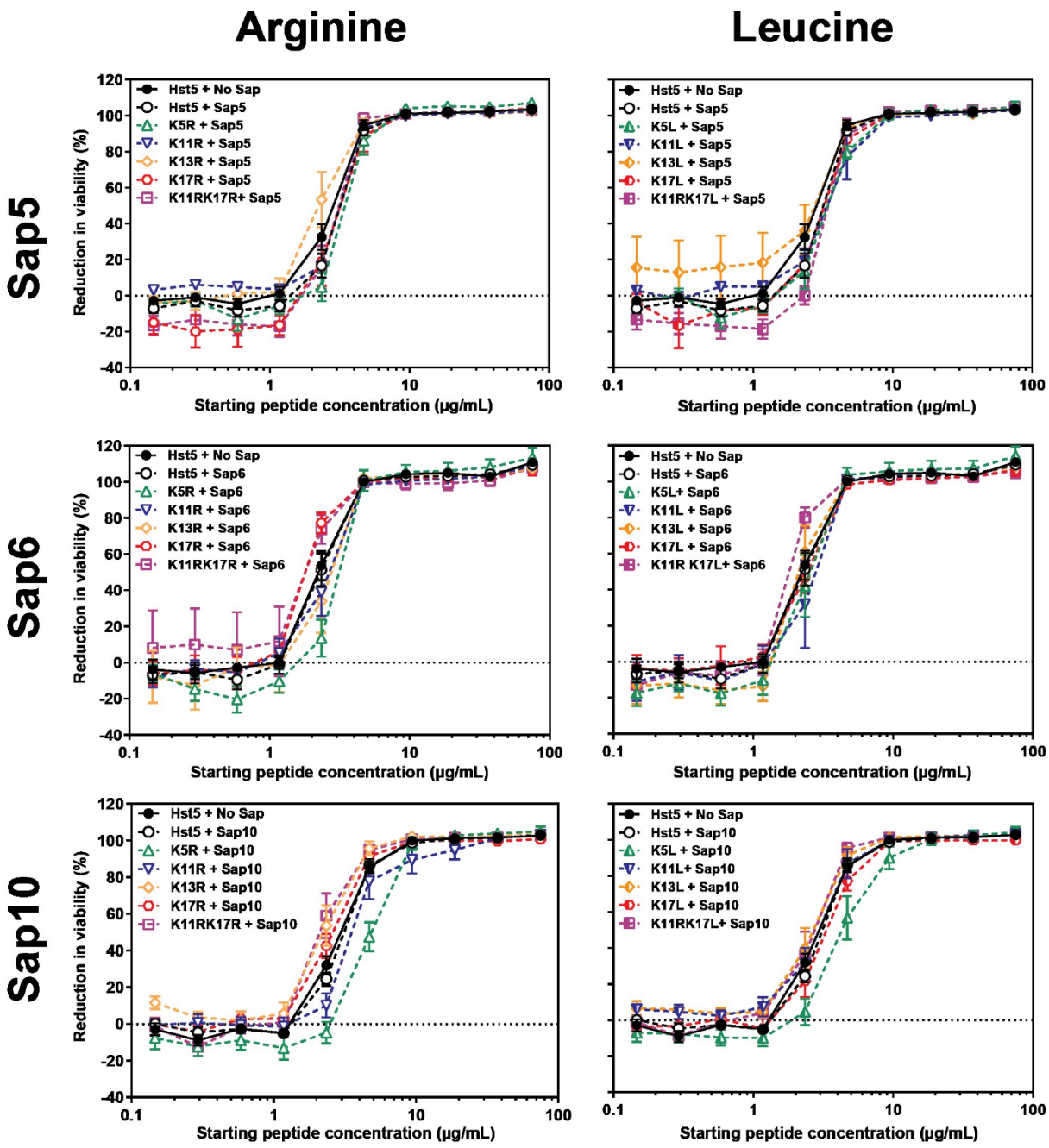

Appendix Figure A.5. Antifungal activity of Hst5 variants after incubation with Sap5, Sap6, or Sap10. After incubation for 2 hrs at 37 °C, Samples were serially diluted in a 96-well plate from 75 µg/mL to .14 µg/mL. Samples were then mixed with *C. albicans* cells at 5.0 × 105 cells/mL and incubated for 30 min at 30 °C in 1 mM NaPB, after which cells were inoculated and cultured. Error bars represent the standard error of the mean (N = 18 Hst5 No Sap and Hst5 + Sap, while N = 6 for all other variants). Two-way ANOVA tests with $\alpha = .05$ and Dunnett's multiple comparison tests (degraded Hst5 as the control) were performed for statistical analysis. $P < .05$ was deemed as significant.

Appendix Figure A.6. Gel images for proteolysis of Hst5 variants by saliva.

B. Appendix B

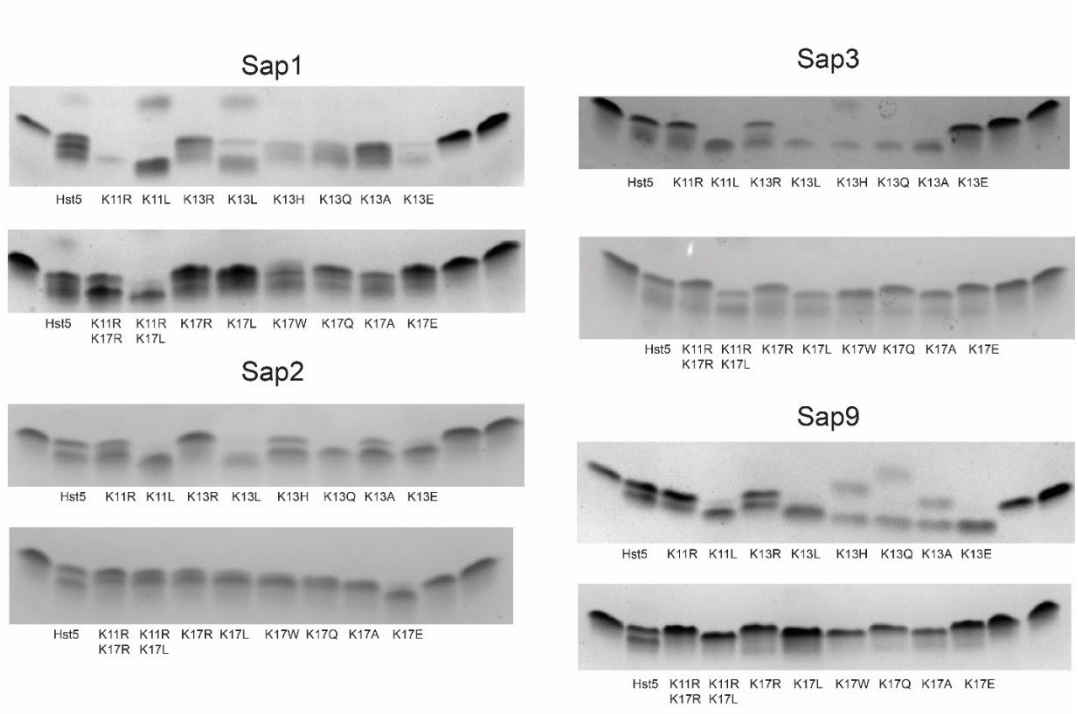

Appendix Figure B.1. Gel images for proteolysis of Hst5 variants by Sap1, Sap2, Sap3, and Sap9.

Appendix Table B.1. P-values for proteolysis of Hst5 and variants by Saps and saliva. Two-way ANOVA tests with $\alpha = .05$ and Dunnett's multiple comparison tests (degraded Hst5 as the control) were performed for statistical analysis.

	P-values (Proteolysis assay)							
	Sap1	Sap2	Sap3	Sap5	Sap6	Sap9	Sap10	Saliva
K13R	0.9145	0.0286	0.9998	> 0.9999	> 0.9999	0.9877	> 0.9999	0.0122
K13L	< 0.0001	< 0.0001	< 0.0001	> 0.9999	> 0.9999	< 0.0001	> 0.9999	0.4414
K13H	0.0016	< 0.0001	< 0.0001	> 0.9999	> 0.9999	< 0.0001	> 0.9999	0.8503
K13Q	0.0001	< 0.0001	< 0.0001	> 0.9999	> 0.9999	< 0.0001	> 0.9999	0.9854
K13A	0.0079	< 0.0001	< 0.0001	> 0.9999	> 0.9999	0.946	> 0.9999	0.0507
K13E	0.0013	< 0.0001	0.0008	> 0.9999	> 0.9999	< 0.0001	> 0.9999	0.9614
K17R	0.059	0.010	1.000	> 0.9999	> 0.9999	< 0.0001	> 0.9999	1.000
K17L	0.160	< 0.0001	0.940	> 0.9999	> 0.9999	< 0.0001	> 0.9999	0.047
K17W	0.082	< 0.0001	< 0.0001	> 0.9999	> 0.9999	< 0.0001	> 0.9999	0.049
K17Q	0.006	< 0.0001	0.003	> 0.9999	> 0.9999	< 0.0001	> 0.9999	1.000
K17A	0.267	< 0.0001	0.033	> 0.9999	> 0.9999	< 0.0001	> 0.9999	1.000
K17E	0.022	0.189	0.007	> 0.9999	> 0.9999	< 0.0001	> 0.9999	0.412

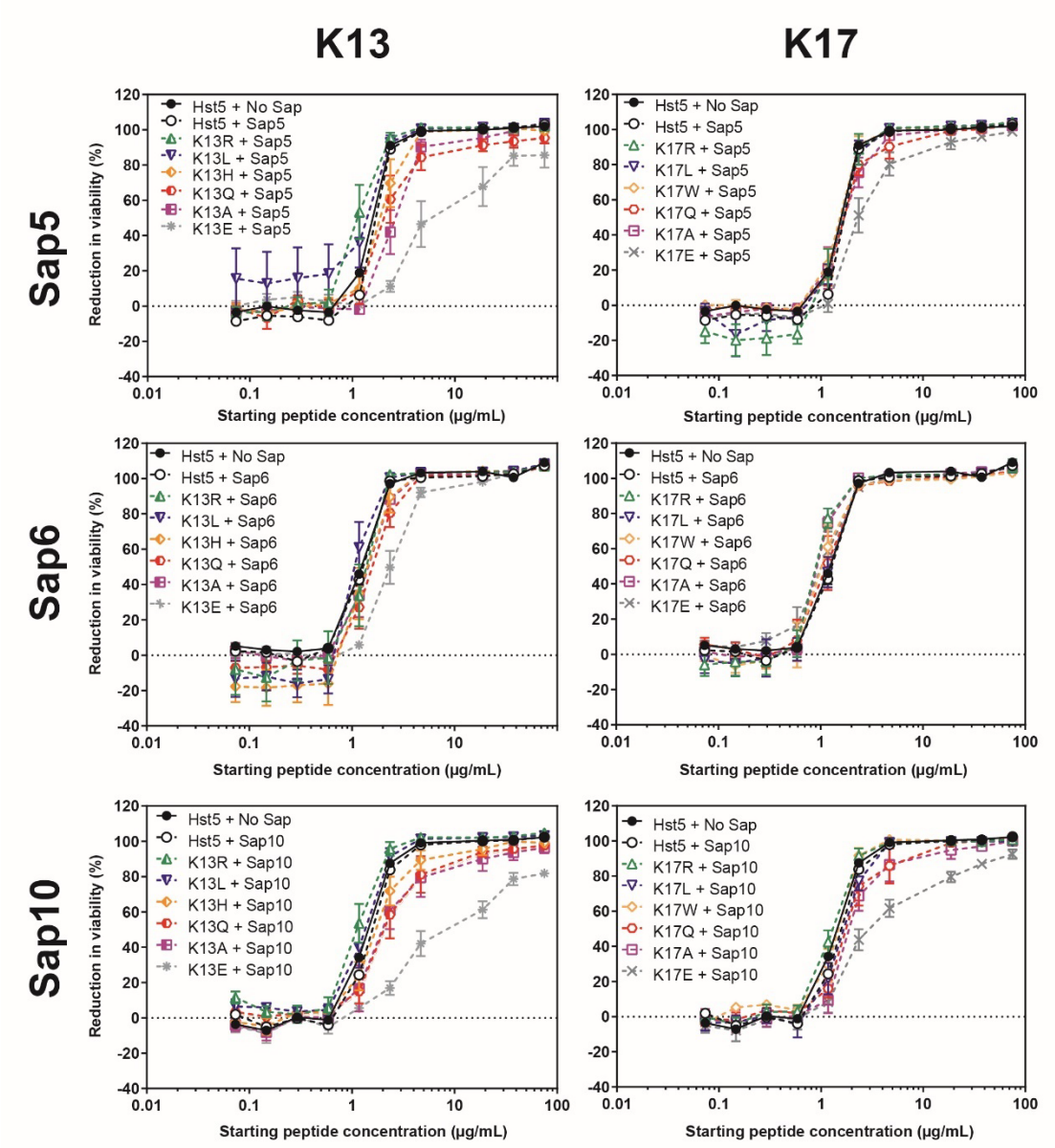

Appendix Figure B.2. Antifungal activity of Hst5 variants after incubation with Sap5, Sap6, or Sap10. After incubation for 2 hrs at 37 °C, Samples were serially diluted in a 96-well plate from 75 µg/mL to .14 µg/mL. Samples were then mixed with *C. albicans* cells at 5.0 × 105 cells/mL and incubated for 30 min at 30 °C in 1 mM NaPB, after which cells were inoculated and cultured. Error bars represent the standard error of the mean (N= 18 Hst5 No Sap and Hst5 + Sap, while N = 6 for all other variants). Two-way ANOVA tests with α = .05 and Dunnett's multiple comparison tests (degraded Hst5 as the control) were performed for statistical analysis. P < .05 was deemed as significant.

Appendix Table B.B.2. P-values for proteolysis of Hst5 and variants by Saps and saliva. Two-way ANOVA tests with α =.05 and Dunnett's multiple comparison tests (degraded Hst5 as the control for Samples treated with Saps and undegraded Hst5 as the control for untreated sample) were performed for statistical analysis.

	P-values (Antifungal assay)							
	Sap1	Sap2	Sap3	Sap5	Sap6	Sap9	Sap10	No Sap
K13R	< 0.0001	0.9921	< 0.0001	0.8816	0.9935	0.0447	0.2697	< 0.0001
K13L	< 0.0001	< 0.0001	< 0.0001	0.9919	0.9996	< 0.0001	0.7241	0.9982
K13H	< 0.0001	< 0.0001	< 0.0001	0.0265	0.6279	< 0.0001	0.2496	0.049
K13Q	< 0.0001	< 0.0001	< 0.0001	0.0002	0.0429	< 0.0001	0.0004	< 0.0001
K13A	< 0.0001	< 0.0001	< 0.0001	< 0.0001	0.4761	< 0.0001	0.0018	0.0003
K13E	< 0.0001	< 0.0001	< 0.0001	< 0.0001	< 0.0001	< 0.0001	< 0.0001	< 0.0001
K17R	< 0.0001	0.002	0.914	> 0.9999	0.994	< 0.0001	0.592	< 0.0001
K17L	0.110	0.001	< 0.0001	0.997	1.000	< 0.0001	0.721	< 0.0001
K17W	< 0.0001	0.001	0.002	0.997	0.628	< 0.0001	0.584	< 0.0001
K17Q	< 0.0001	0.000	0.887	0.285	0.043	< 0.0001	0.355	< 0.0001
K17A	< 0.0001	0.000	0.971	0.033	0.476	< 0.0001	0.037	< 0.0001
K17E	0.002	0.242	0.997	< 0.0001	< 0.0001	0.012	< 0.0001	< 0.0001
Concentration (μg/mL)	4.69	9.38	18.75	4.69	4.69	18.75	4.69	4.69

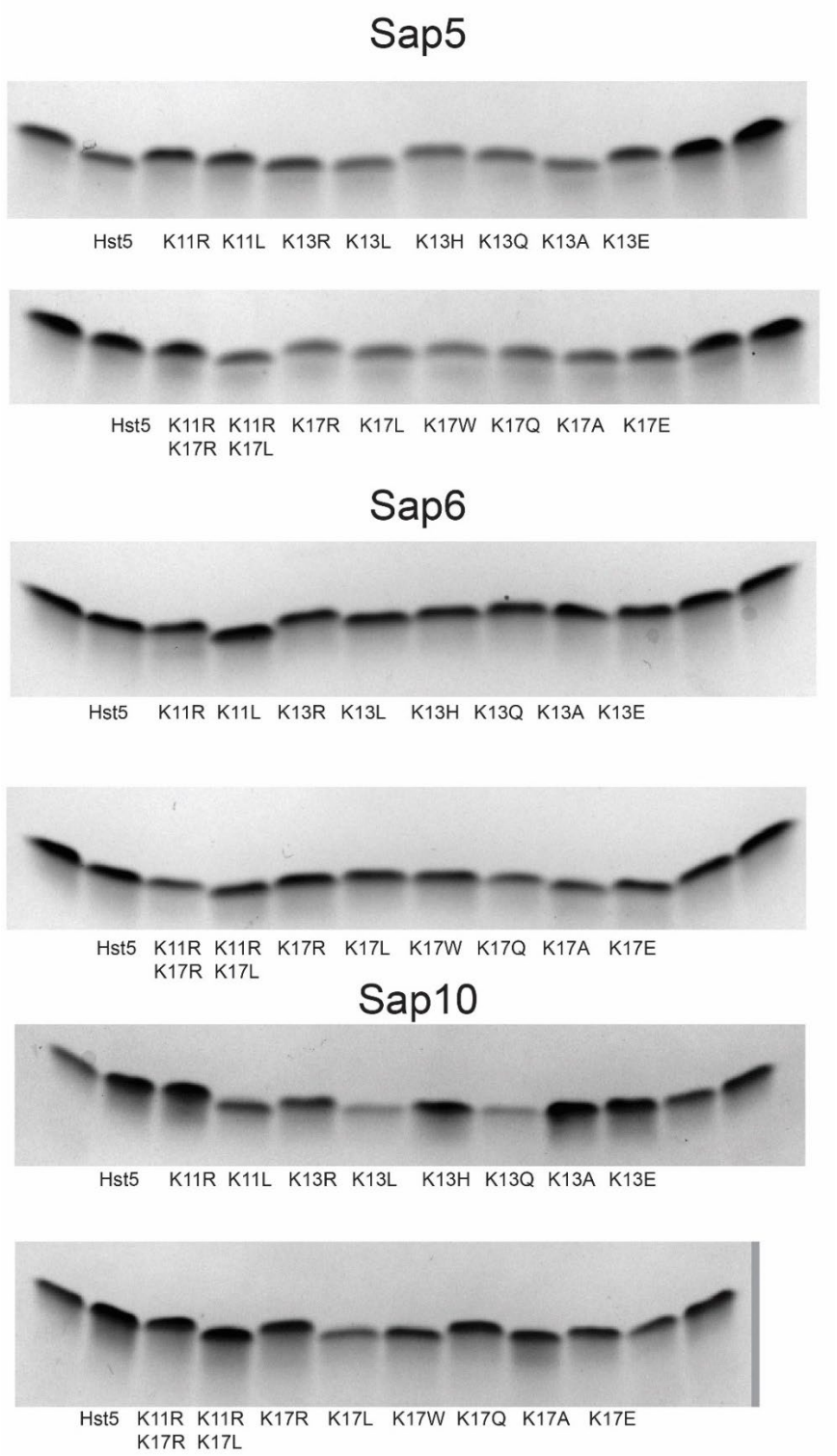

Appendix Figure B.3. Gel images for proteolysis of Hst5 variants by Sap1, Sap2, Sap3, and Sap9.

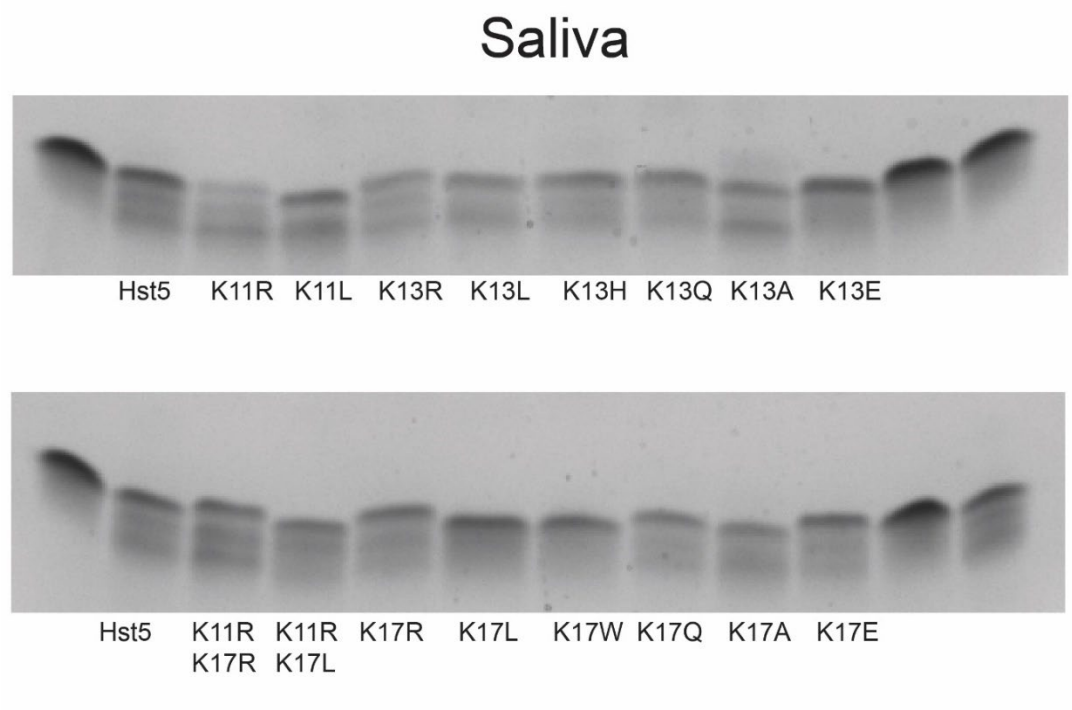

Appendix Figure B.4. Gel images for proteolysis of Hst5 variants by saliva.

Appendix Table B.3. *P*-values for zinc competition of Hst5 and variants against Zincon. Two-way ANOVA tests with α = .05 and Dunnett's multiple comparison tests (Hst5 as the control) were performed for statistical analysis.

	P-values (Zincon competition)					
K17W	> 0.9999	0.9397	0.1607	0.0264	0.1165	0.7346
K13H	0.9998	0.9998	0.9998	0.9996	0.9974	0.0828
Zinc: peptide	0:1	1:2	1:1	2:1	4:1	4:1

Appendix Table B.4. *P*-values for Hst5 and variants antifungal activity against *C. albicans* in the presence of different titrations of zinc. Two-way ANOVA tests with α = .05 and Dunnett's multiple comparison tests (Hst5 as the control) were performed for statistical analysis.

	P-values (Antifungal assay with zinc)				
K17W	> 0.9999	0.267	0.8025	0.0218	0.9964
K13H	> 0.9999	0.0051	< 0.0001	0.001	0.9954
Zinc: peptide	20:1	10:1	5:1	2.5:1	1.25:1

Appendix Table B.5. *P*-values for Hst5 biofilm formation in the presence and absence of zinc and Sap2. Two-way ANOVA tests with α = .05 and Dunnett's multiple comparison tests (Hst5 as the control) were performed for statistical analysis.

P-values (Antifungal assay Sap and zinc)												
	No Sap/No Zinc			No Sap/Zinc			Sap/No Zinc			Sap/Zinc		
Concentration (μM)	Hst5	K17W	K13H	Hst5	K17W	K13H	Hst5	K17W	K13H	Hst5	K17W	K13H
25.00	> 0.9999	0.9997	0.9996	0.9997	0.9997	0.9999	> 0.9999	0.9997	0.9994	< 0.0001	0.9997	< 0.0001
12.50	> 0.9999	> 0.9999	0.9994	0.9999	> 0.9999	0.9998	0.9999	> 0.9999	0.999	< 0.0001	> 0.9999	< 0.0001
6.25	> 0.9999	0.9998	0.996	0.9998	0.9998	0.9991	> 0.9999	0.9998	0.1101	< 0.0001	0.9998	< 0.0001
3.13	> 0.9999	0.9999	0.7331	0.9995	0.9999	0.0347	0.4058	> 0.9999	< 0.0001	< 0.0001	> 0.9999	< 0.0001
1.56	> 0.9999	0.0561	0.0023	< 0.0001	< 0.0001	< 0.0001	< 0.0001	0.8464	< 0.0001	< 0.0001	0.0223	< 0.0001
0.78	> 0.9999	0.252	0.0047	< 0.0001	< 0.0001	< 0.0001	< 0.0001	0.3252	< 0.0001	< 0.0001	0.0011	< 0.0001
0.39	> 0.9999	0.8611	0.3858	0.9999	0.999	0.6325	0.9994	0.2204	0.9952	0.9999	0.018	0.9952
0.20	> 0.9999	0.7988	0.2723	0.9577	0.9996	0.8855	0.9998	0.9996	0.999	0.9997	0.9999	0.8
0.10	> 0.9999	0.9997	0.9741	0.7248	0.9993	> 0.9999	0.6484	0.9997	0.992	0.9544	0.9772	0.9992
0.05	> 0.9999	0.9854	0.7094	0.9959	0.7966	0.896	> 0.9999	0.8942	0.9705	0.9908	0.385	0.9996

Appendix Table B.6. *P*-values for Hst5 biofilm formation prevention activity against *C. albicans*. Two-way ANOVA tests with α = .05 and Dunnett's multiple comparison tests (Hst5 as the control) were performed for statistical analysis.

P-values (Biofilm prevention assay)				
K17W	0.0292	0.0004	0.2173	0.746
K13H	0.8346	0.1504	0.5463	0.7504
Concentration (μg/mL)	750	187.5	46.9	11.7

C. Appendix C

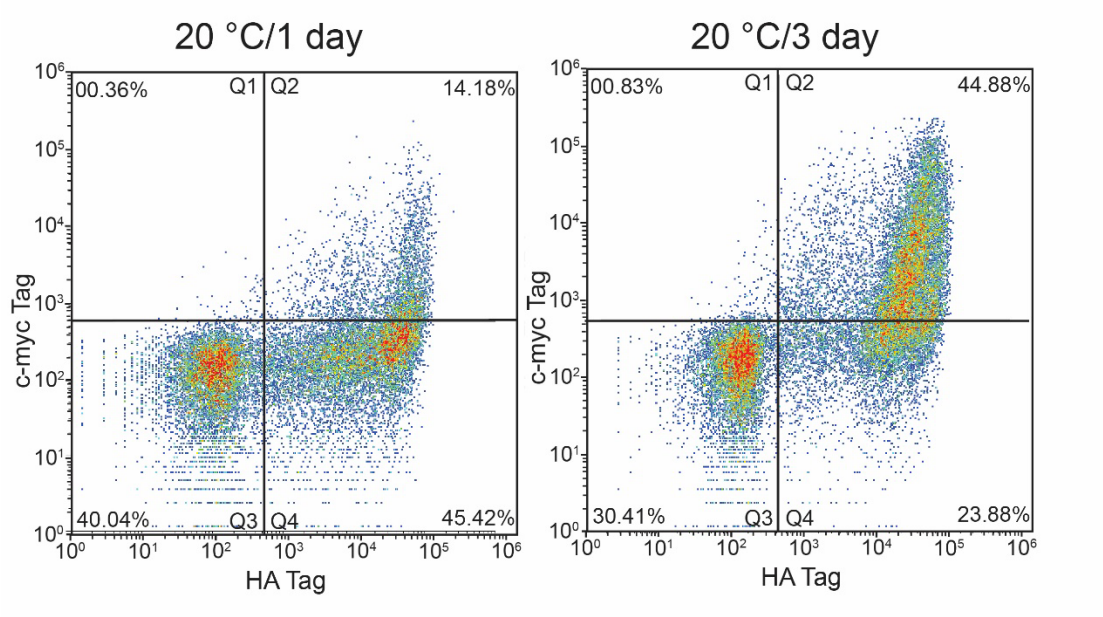

Appendix Figure C.1. Expression time optimization profiles for pCTCon2-Hst5 at 20 °C. Bivariate plots of the intensity for both HA (Alexa-Flour 488 antibody) and c-myc (Alexa-Flour 647 antibody) were plotted with quadrants based the *Saccharomyces cerevisiae* EBY100 strain without plasmids. Each dot corresponds to a single cell and heatmaps indicate the number of cells in an area. Percentages represent the percent of total events (cell count) in each quadrant. Q1 represents cells with the c-myc tag but without the HA tag (not expected as the construct starts with the HA tag, possible degradation products), Q2 represents cells with both the c-myc and HA tag (fully expressed construct), Q3 represents cells without both c-myc and HA tag (none of the construct expressed), and Q4 represent represents cells without the c-myc tag but with the HA tag (partially expressed construct).

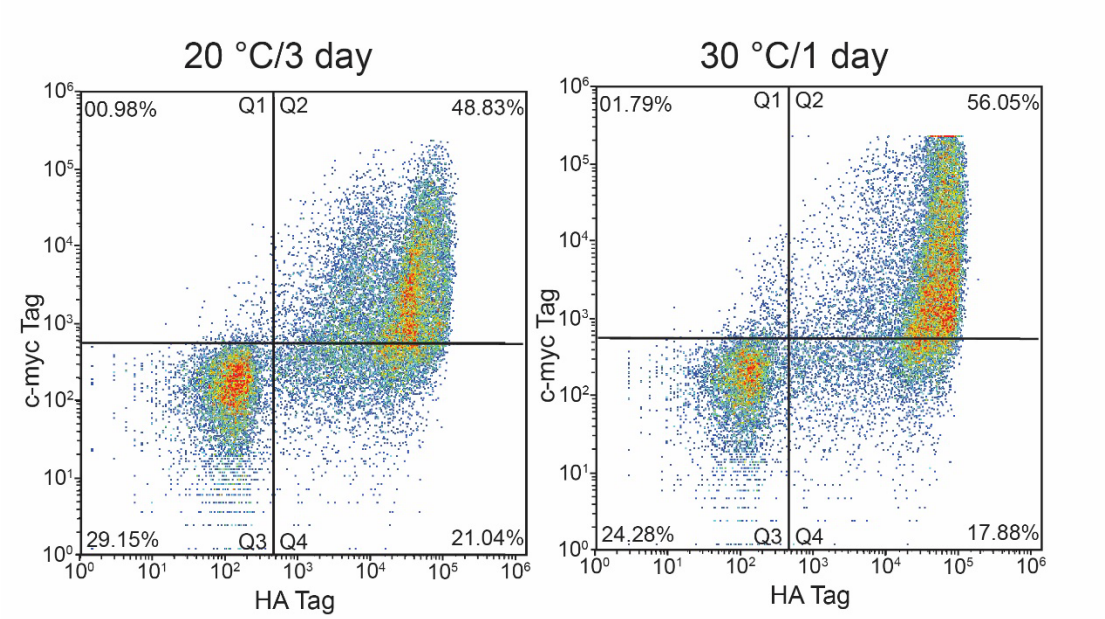

Appendix Figure C.2. Expression temperature and time optimization profiles for pCTCon2-Hst5. Bivariate plots of the intensity for both HA (Alexa-Flour 488 antibody) and c-myc (Alexa-Flour 647 antibody) were plotted with quadrants based the Saccharomyces cerevisiae EBY100 strain without plasmids. Each dot corresponds to a single cell and heatmaps indicate the number of cells in an area. Percentages represent the percent of total events (cell count) in each quadrant. Q1 represents cells with the c-myc tag but without the HA tag (not expected as the construct starts with the HA tag, possible degradation products), Q2 represents cells with both the c-myc and HA tag (fully expressed construct), Q3 represents cells without both c-myc and HA tag (none of the construct expressed), and Q4 represent represents cells without the c-myc tag but with the HA tag (partially expressed construct).

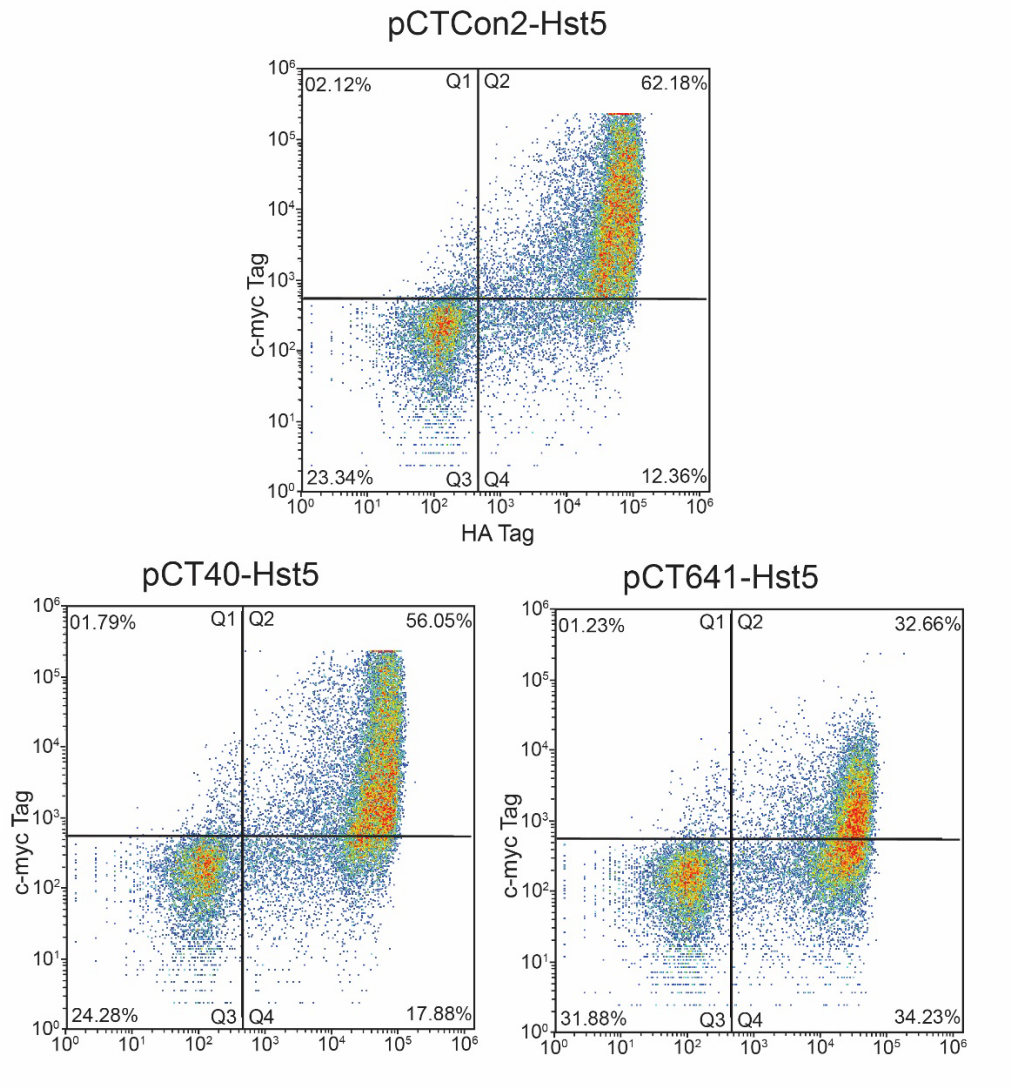

Appendix Figure C.3. Linker length optimization profiles for pCTcon2-Hst5, pCT40-Hst5, pCT641-Hst5. Protein expression was induced at 30 °C for 24 hours. Bivariate plots of the intensity for both HA (Alexa-Flour 488 antibody) and c-myc (Alexa-Flour 647 antibody) were plotted with quadrants based the *Saccharomyces cerevisiae* EBY100 strain without plasmids. Each dot corresponds to a single cell and heatmaps indicate the number of cells in an area. Percentages represent the percent of total events (cell count) in each quadrant. Q1 represents cells with the c-myc tag but without the HA tag (not expected as the construct starts with the HA tag, possible degradation products), Q2 represents cells with both the c-myc and HA tag (fully expressed construct), Q3 represents cells without both c-myc and HA tag (none of the construct expressed), and Q4 represent represents cells without the c-myc tag but with the HA tag (partially expressed construct).

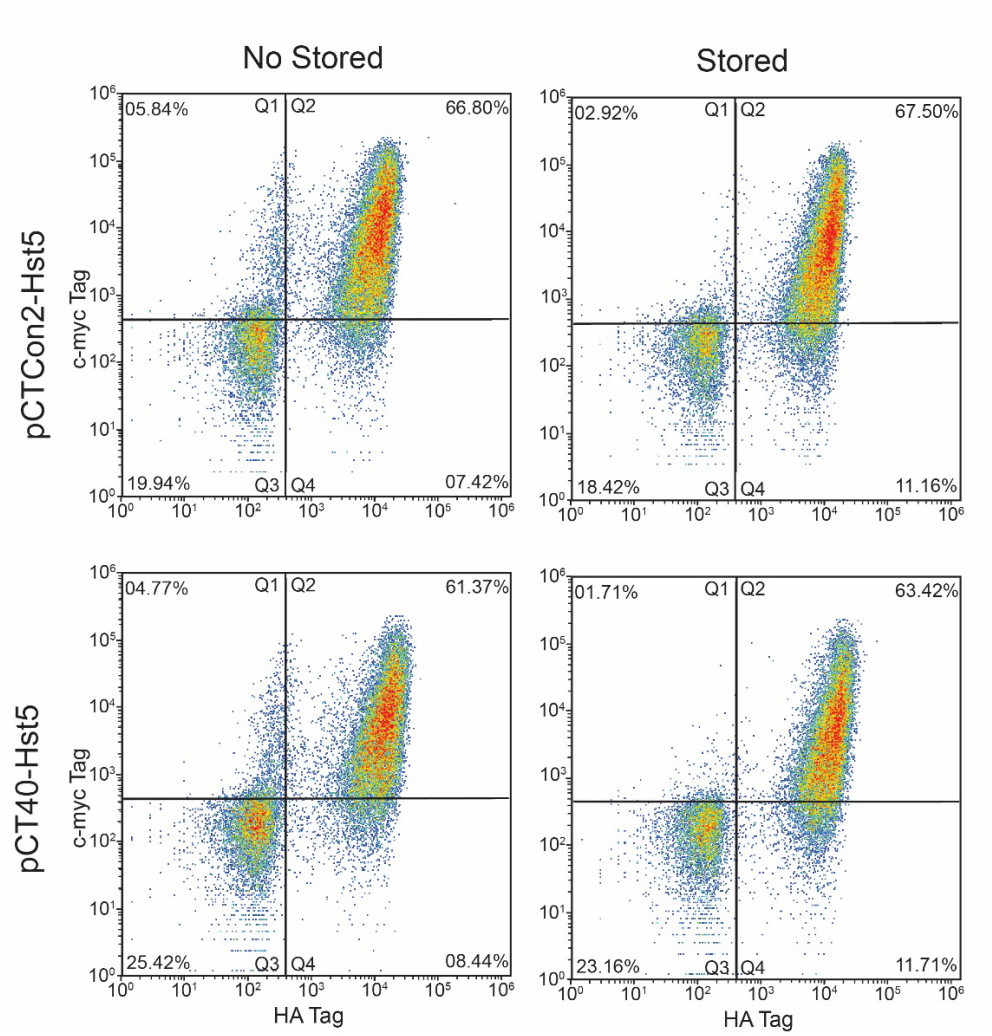

Appendix Figure C.4. Differentiation between harvested cell and cells that were not harvested for pCTcon2-Hst5 and pCT40-Hst5. Protein expression was induced at 30 °C for 24 hours, harvested cells were pelleted, decanted, and stored at 20 °C, unharvested cells were prepared and the results were compared. Bivariate plots of the intensity for both HA (Alexa-Flour 488 antibody) and c-myc (Alexa-Flour 647 antibody) were plotted with quadrants based the Saccharomyces cerevisiae EBY100 strain without plasmids. Each dot corresponds to a single cell and heatmaps indicate the number of cells in an area. Percentages represent the percent of total events (cell count) in each quadrant. Q1 represents cells with the c-myc tag but without the HA tag (not expected as the construct starts with the HA tag, possible degradation products), Q2 represents cells with both the c-myc and HA tag (fully expressed construct), Q3 represents cells without both c-myc and HA tag (none of the construct expressed), and Q4 represent represents cells without the c-myc tag but with the HA tag (partially expressed construct).

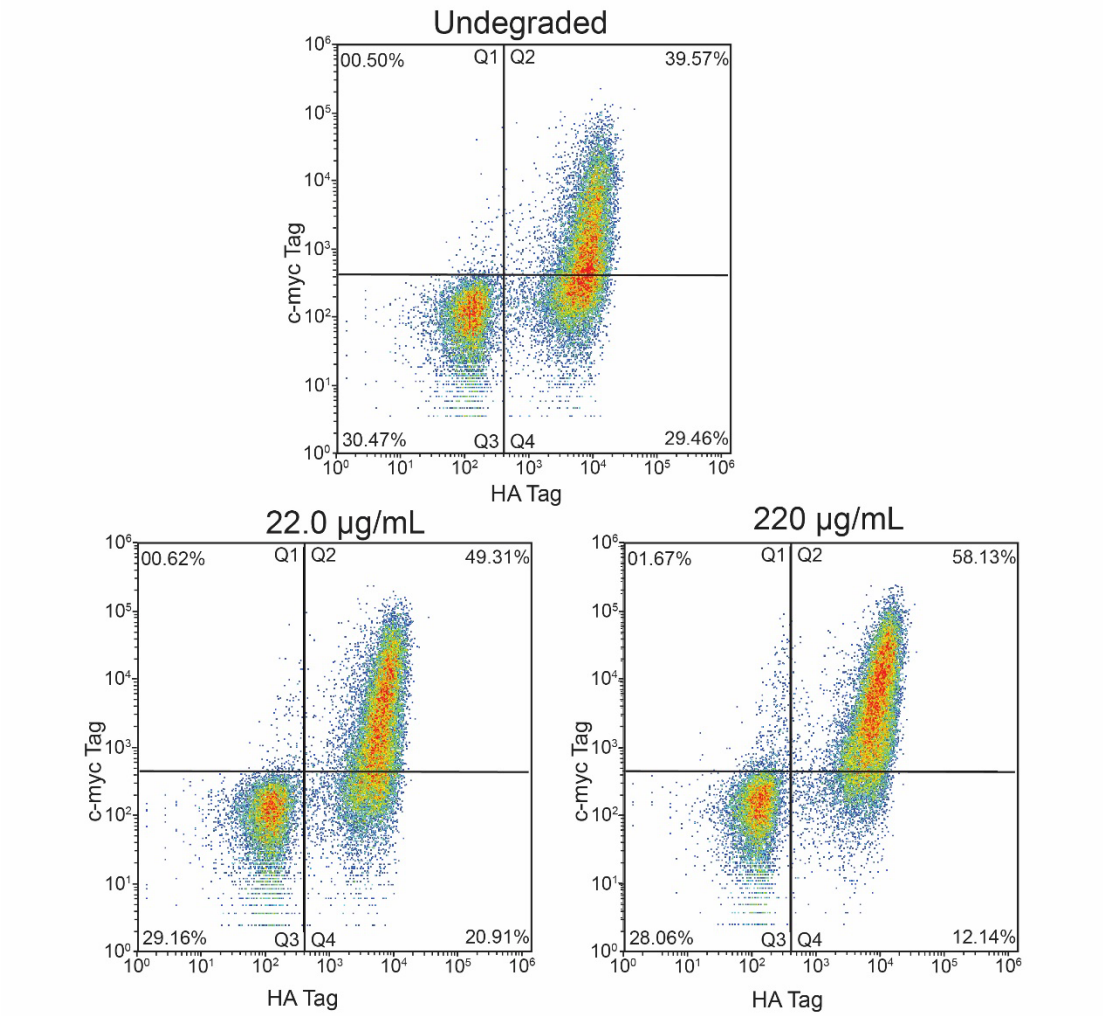

Appendix Figure C.5. Initial degradation profile for pCT40-Hst5 at varying concentrations. Protein expression was induced at 30 °C for 24 hours. Cells were then pelleted, washed, and suspended in Sap9 at varying concentrations in 2 mM NaPB. Samples were incubated at 30 °C for 24 hours. Bivariate plots of the intensity for both HA (Alexa-Flour 488 antibody) and c-myc (Alexa-Flour 647 antibody) were plotted with quadrants based the Saccharomyces cerevisiae EBY100 strain without plasmids. Each dot corresponds to a single cell and heatmaps indicate the number of cells in an area. Percentages represent the percent of total events (cell count) in each quadrant. Q1 represents cells with the c-myc tag but without the HA tag (not expected as the construct starts with the HA tag, possible degradation products), Q2 represents cells with both the c-myc and HA tag (fully expressed construct), Q3 represents cells without both c-myc and HA tag (none of the construct expressed), and Q4 represent represents cells without the c-myc tag but with the HA tag (partially expressed construct).

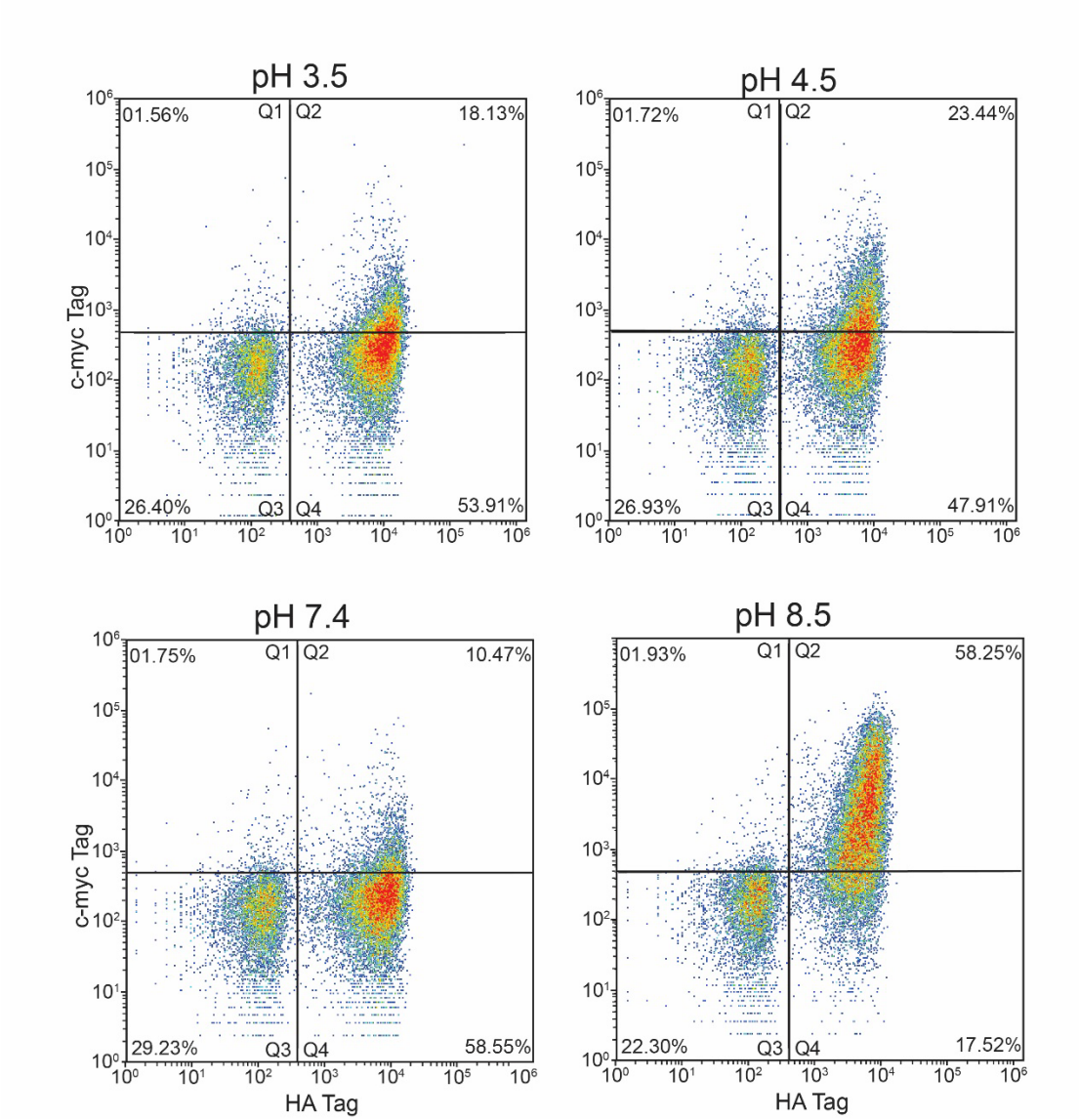

Appendix Figure C.6. Degradation profile for pCT40-Hst5 with Sap9 at varying pH. Protein expression was induced at 30 °C for 24 hours. Cells were then pelleted, washed, and suspended in 100 µL of 100 µg/mL Sap9 in 2 mM NaPB at various pH. Samples were incubated at 37 °C for 24 hours. Bivariate plots of the intensity for both HA (Alexa-Flour 488 antibody) and c-myc (Alexa-Flour 647 antibody) were plotted with quadrants based the Saccharomyces cerevisiae EBY100 strain without plasmids. Each dot corresponds to a single cell and heatmaps indicate the number of cells in an area. Percentages represent the percent of total events (cell count) in each quadrant. Q1 represents cells with the c-myc tag but without the HA tag (not expected as the construct starts with the HA tag, possible degradation products), Q2 represents cells with both the c-myc and HA tag (fully expressed construct), Q3 represents cells without both c-myc and HA tag (none of the construct expressed), and Q4 represent represents cells without the c-myc tag but with the HA tag (partially expressed construct).

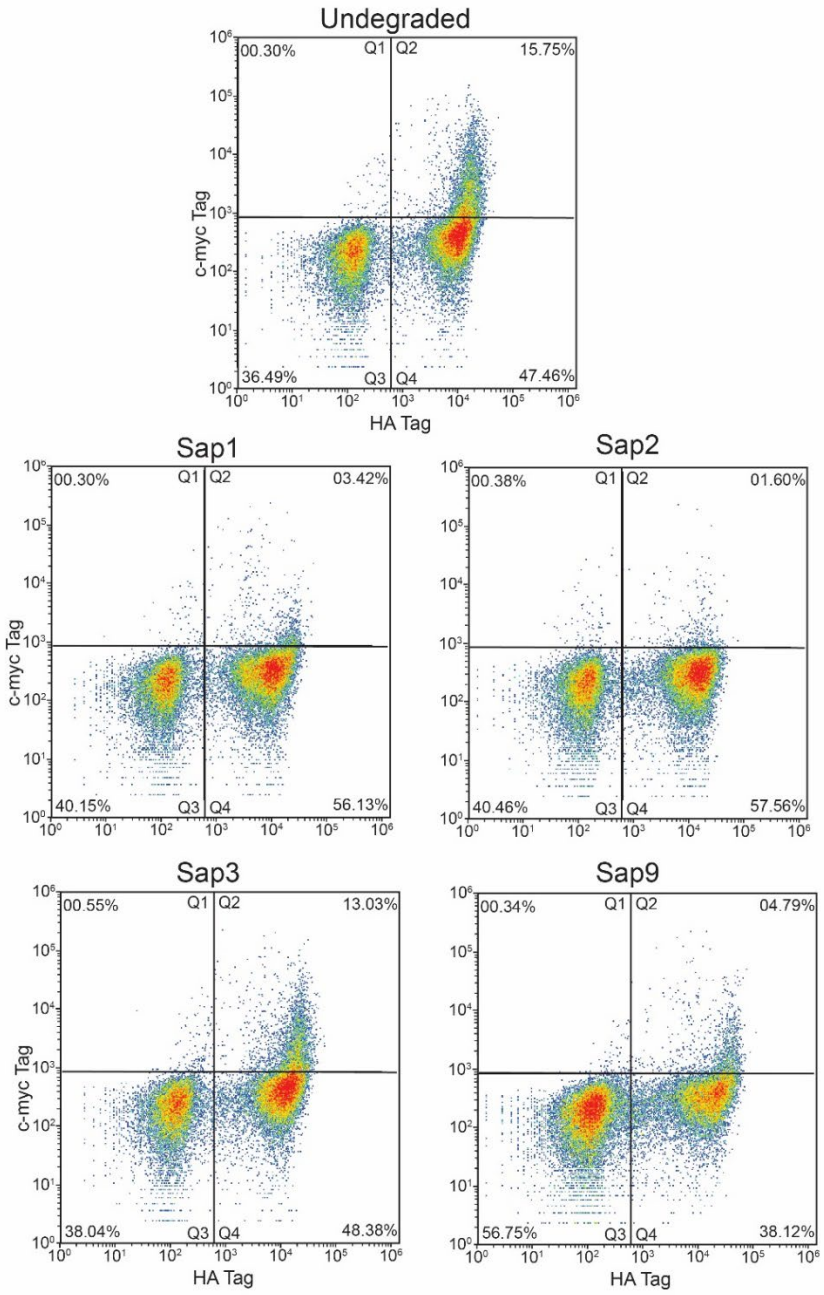

Appendix Figure C.7. Degradation profile for pCT40-Hst5 with No Sap, Sap1, Sap2, Sap3, and Sap9. Protein expression was induced at 30 °C for 24 hours. Cells were then pelleted, washed, and suspended in 100 µL of 100 µg/mL Sap9 in 2 mM NaPB at pH 7.4. Samples were incubated at 37 °C for 24 hours. Bivariate plots of the intensity for both HA (Alexa-Flour 488 antibody) and c-myc (Alexa-Flour 647 antibody) were plotted with quadrants based the *Saccharomyces cerevisiae* EBY100 strain without plasmids. Each dot corresponds to a single cell and heatmaps indicate the number of cells in an area. Percentages represent the percent of total events (cell count) in each quadrant. Q1 represents cells with the c-myc tag but without the HA tag (not expected as the construct starts with the HA tag, possible degradation products), Q2 represents cells with both the c-myc and HA tag (fully expressed construct), Q3 represents cells without both c-myc and HA tag (none of the construct expressed), and Q4 represent represents cells without the c-myc tag but with the HA tag (partially expressed construct).

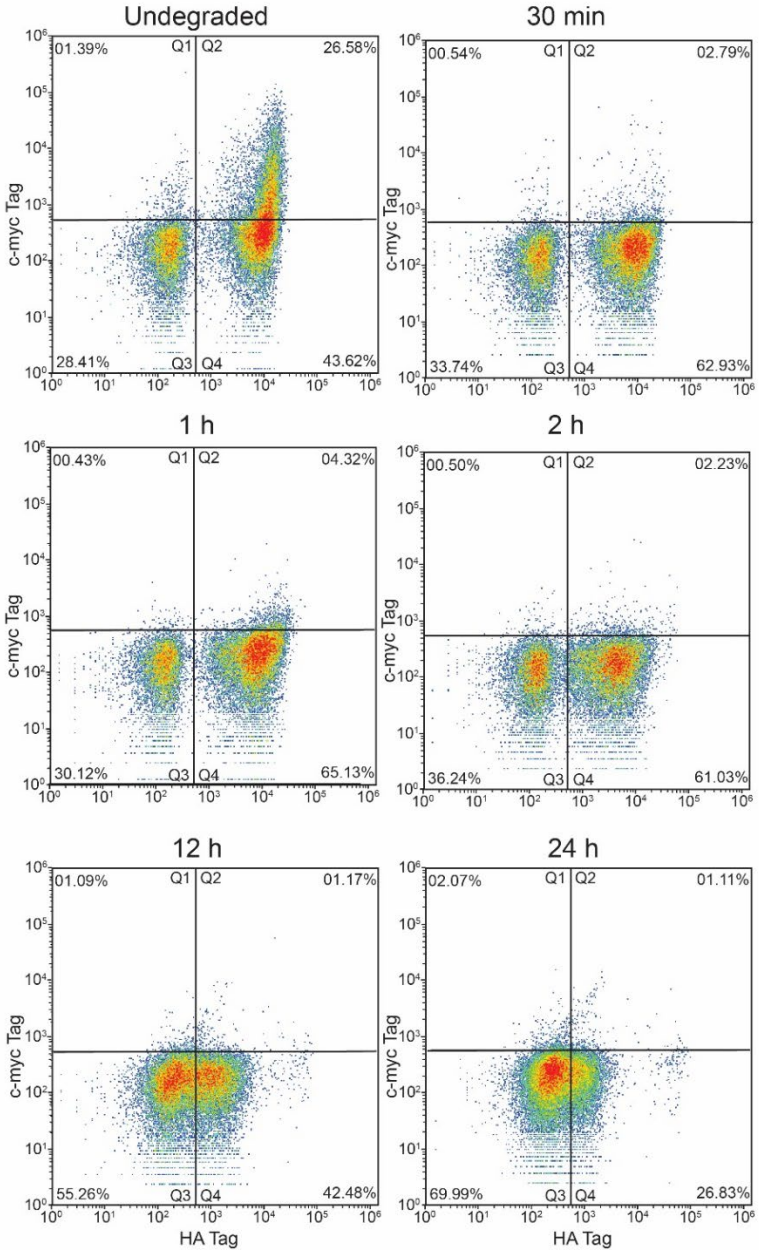

Appendix Figure C.8. Degradation profile for pCT40-Hst5 after incubation with Sap2 at varying times. Protein expression was induced at 30 °C for 24 hours. Cells were then pelleted, washed, and suspended in 100 µL of 100 µg/mL Sap2 in 2 mM NaPB at pH 7.4. Samples were incubated at 37 °C for 24 hours. Bivariate plots of the intensity for both HA (Alexa-Flour 488 antibody) and c-myc (Alexa-Flour 647 antibody) were plotted with quadrants based the *Saccharomyces cerevisiae* EBY100 strain without plasmids. Each dot corresponds to a single cell and heatmaps indicate the number of cells in an area. Percentages represent the percent of total events (cell count) in each quadrant. Q1 represents cells with the c-myc tag but without the HA tag (not expected as the construct starts with the HA tag, possible degradation products), Q2 represents cells with both the c-myc and HA tag (fully expressed construct), Q3 represents cells without both c-myc and HA tag (none of the construct expressed), and Q4 represent represents cells without the c-myc tag but with the HA tag (partially expressed construct).

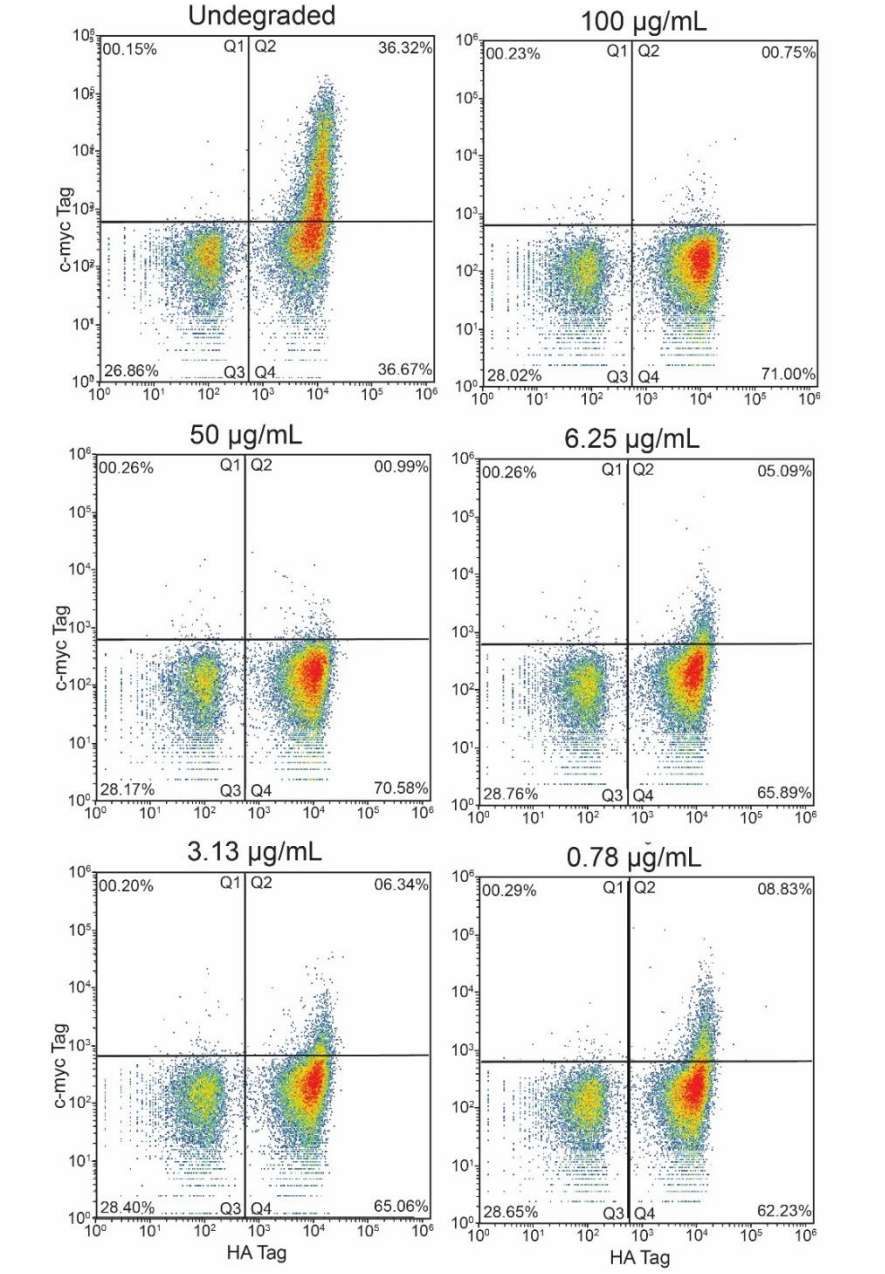

Appendix Figure C.9. Degradation profile for pCT40-Hst5 after incubation with Sap2 at varying concentrations. Protein expression was induced at 30 °C for 24 hours. Cells were then pelleted, washed, and suspended in 100 µL of Sap2 (at concentrations listed in the figure) in 2 mM NaPB at pH 7.4. Samples were incubated at 37 °C for 30 min. Bivariate plots of the intensity for both HA (Alexa-Flour 488 antibody) and c-myc (Alexa-Flour 647 antibody) were plotted with quadrants based the Saccharomyces cerevisiae EBY100 strain without plasmids. Each dot corresponds to a single cell and heatmaps indicate the number of cells in an area. Percentages represent the percent of total events (cell count) in each quadrant. Q1 represents cells with the c-myc tag but without the HA tag (not expected as the construct starts with the HA tag, possible degradation products), Q2 represents cells with both the c-myc and HA tag (fully expressed construct), Q3 represents cells without both c-myc and HA tag (none of the construct expressed), and Q4 represent represents cells without the c-myc tag but with the HA tag (partially expressed construct).

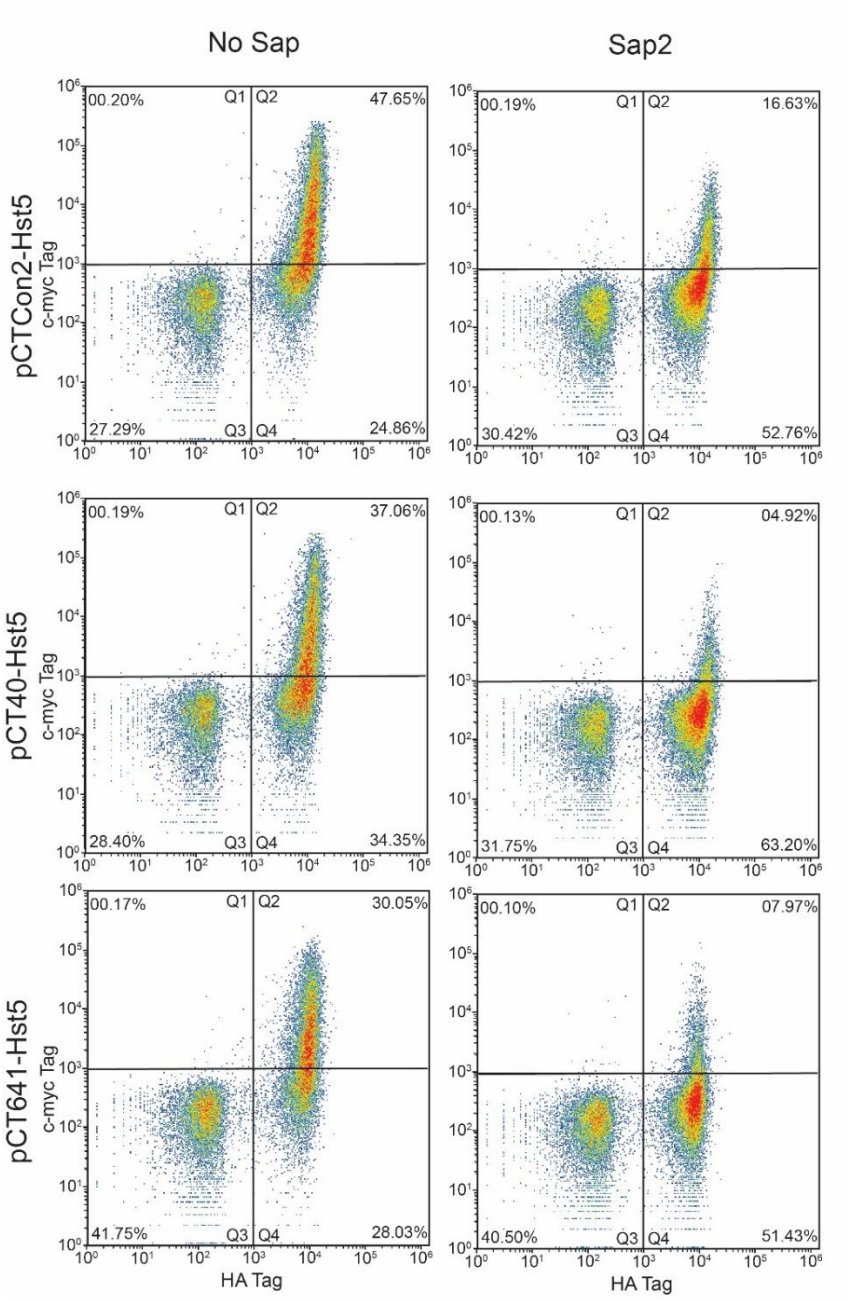

Appendix Figure C.10. Degradation profile for pCTCon2-st5, pCT40-Hst5, and pCT641-Hst5 after incubation with Sap2. Protein expression was induced at 30 °C for 24 hours. Cells were then pelleted, washed, and suspended in 100 µL of 0.39 µg/mL Sap2 in 2 mM NaPB at pH 7.4. Samples were incubated at 37 °C for 30 min. Bivariate plots of the intensity for both HA (Alexa-Flour 488 antibody) and c-myc (Alexa-Flour 647 antibody) were plotted with quadrants based the *Saccharomyces cerevisiae* EBY100 strain without plasmids. Each dot corresponds to a single cell and heatmaps indicate the number of cells in an area. Percentages represent the percent of total events (cell count) in each quadrant. Q1 represents cells with the c-myc tag but without the HA tag (not expected as the construct starts with the HA tag, possible degradation products), Q2 represents cells with both the c-myc and HA tag (fully expressed construct), Q3 represents cells without both c-myc and HA tag (none of the construct expressed), and Q4 represent represents cells without the c-myc tag but with the HA tag (partially expressed construct).

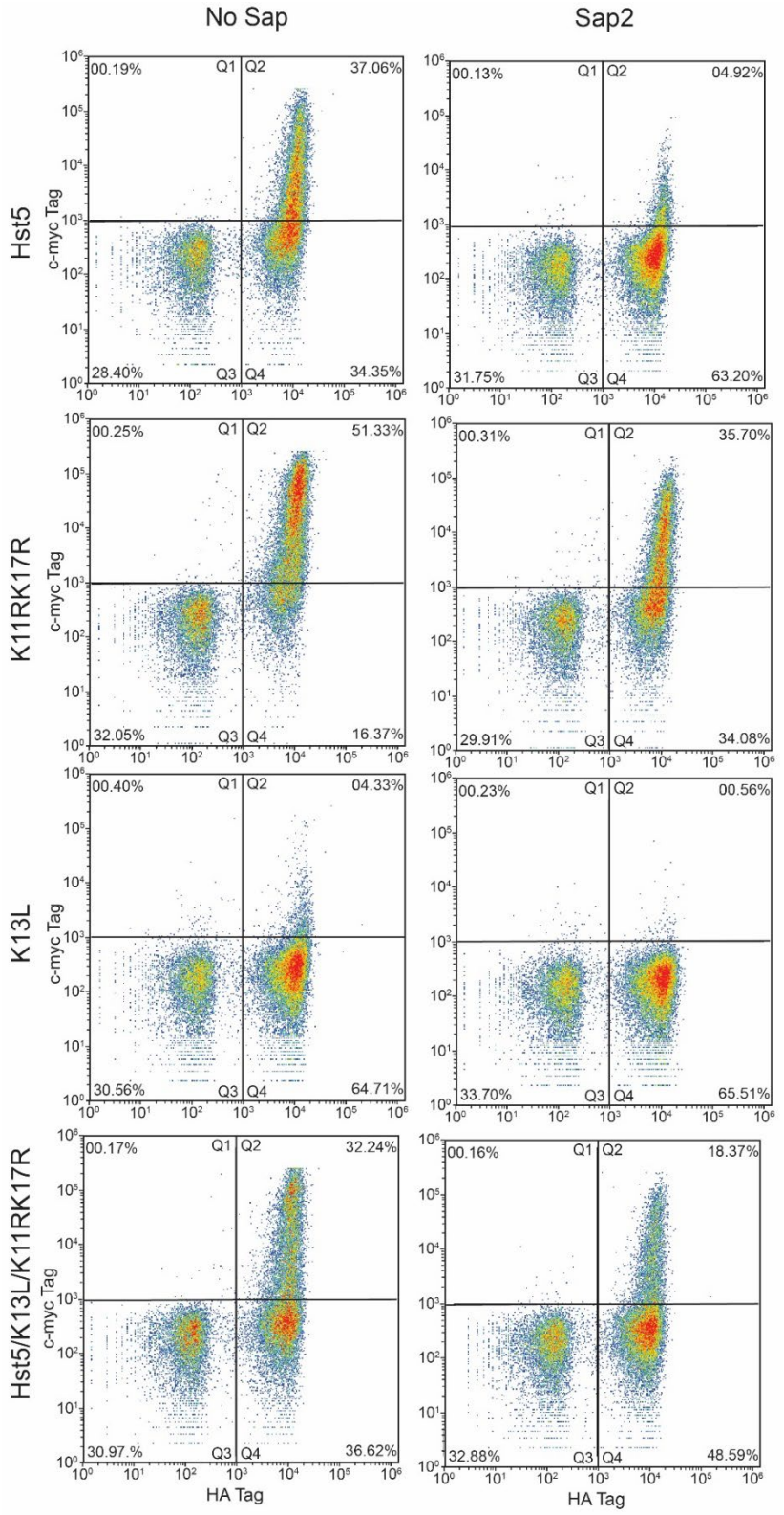

Appendix Figure C.11. Degradation profile for pCT40-Hst5, pCT40-K11RK17R, and pCT40-K13L after incubation with Sap2. Protein expression was induced at 30 °C for 24 hours. Cells were then

pelleted, washed, and suspended in 100 µL of 0.39 µg/mL Sap2 in 2 mM NaPB at pH 7.4. Samples were incubated at 37 °C for 30 min. Bivariate plots of the intensity for both HA (Alexa-Flour 488 antibody) and c-myc (Alexa-Flour 647 antibody) were plotted with quadrants based the *Saccharomyces cerevisiae* EBY100 strain without plasmids. Each dot corresponds to a single cell and heatmaps indicate the number of cells in an area. Percentages represent the percent of total events (cell count) in each quadrant. Q1 represents cells with the c-myc tag but without the HA tag (not expected as the construct starts with the HA tag, possible degradation products), Q2 represents cells with both the c-myc and HA tag (fully expressed construct), Q3 represents cells without both c-myc and HA tag (none of the construct expressed), and Q4 represent represents cells without the c-myc tag but with the HA tag (partially expressed construct).

Bibliography

[1] R AN, Rafiq NB. Candidiasis. StatPearls. Treasure Island (FL)2024.

[2] Belazi M, Velegraki A, Fleva A, Gidarakou I, Papanaum L, Baka D, et al. Candidal overgrowth in diabetic patients: potential predisposing factors. Mycoses. 2005;48:192-6.

[3] Darwazeh AM, Lamey PJ, Samaranayake LP, MacFarlane TW, Fisher BM, Macrury SM, et al. The relationship between colonisation, secretor status and in-vitro adhesion of *Candida albicans* to buccal epithelial cells from diabetics. J Med Microbiol. 1990;33:43-9.

[4] Tang HJ, Liu WL, Lin HL, Lai CC. Epidemiology and prognostic factors of candidemia in elderly patients. Geriatr Gerontol Int. 2015;15:688-93.

[5] Carlstedt K, Krekmanova L, Dahllof G, Ericsson B, Braathen G, Modeer T. Oral carriage of *Candida* species in children and adolescents with Down's syndrome. Int J Paediatr Dent. 1996;6:95-100.

[6] Komatsu T, Watanabe K, Hamada N, Helmerhorst E, Oppenheim F, Lee MC. Association between antimicrobial peptide histatin 5 levels and prevalence of *Candida* in saliva of patients with Down syndrome. Antibiotics (Basel). 2021;10.

[7] Mohiddin G, Narayanaswamy AB, Masthan KM, Nagarajan A, Panda A, Behura SS. Oral Candidal and Streptococcal carriage in Down syndrome patients. J Nat Sci Biol Med. 2015;6:300-5.

[8] Perlin DS. Resistance to echinocandin-class antifungal drugs. Drug Resist Updat. 2007;10:121-30.

[9] Garcia-Effron G, Lee S, Park S, Cleary JD, Perlin DS. Effect of *Candida glabrata* FKS1 and FKS2 mutations on echinocandin sensitivity and kinetics of 1,3-beta-D-glucan synthase: implication for the existing susceptibility breakpoint. Antimicrob Agents Chemother. 2009;53:3690-9.

[10] Sawistowska-Schroder ET, Kerridge D, Perry H. Echinocandin inhibition of 1,3-beta-D-glucan synthase from *Candida albicans*. FEBS Lett. 1984;173:134-8.

[11] Klis FM, de Groot P, Hellingwerf K. Molecular organization of the cell wall of *Candida albicans*. Med Mycol. 2001;39 Suppl 1:1-8.

[12] Munro CA, Winter K, Buchan A, Henry K, Becker JM, Brown AJ, et al. Chs1 of *Candida albicans* is an essential chitin synthase required for synthesis of the septum and for cell integrity. Mol Microbiol. 2001;39:1414-26.

[13] Hoot SJ, Smith AR, Brown RP, White TC. An A643V amino acid substitution in Upc2p contributes to azole resistance in well-characterized clinical isolates of *Candida albicans*. Antimicrob Agents Chemother. 2011;55:940-2.

[14] Lattif AA, Mukherjee PK, Chandra J, Roth MR, Welti R, Rouabhia M, et al. Lipidomics of *Candida albicans* biofilms reveals phase-dependent production of phospholipid molecular classes and role for lipid rafts in biofilm formation. Microbiology (Reading). 2011;157:3232-42.

[15] Ellis D. Amphotericin B: spectrum and resistance. J Antimicrob Chemother. 2002;49 Suppl 1:7-10.

[16] Lamb DC, Kelly DE, Schunck WH, Shyadehi AZ, Akhtar M, Lowe DJ, et al. The mutation T315A in *Candida albicans* sterol 14alpha-demethylase causes reduced enzyme activity and fluconazole resistance through reduced affinity. J Biol Chem. 1997;272:5682-8.

[17] Niimi K, Niimi M. [The mechanisms of resistance to echinocandin class of antifungal drugs]. Nihon Ishinkin Gakkai Zasshi. 2009;50:57-66.

[18] Revie NM, Iyer KR, Robbins N, Cowen LE. Antifungal drug resistance: evolution, mechanisms and impact. Curr Opin Microbiol. 2018;45:70-6.

[19] de Kruijff B, Demel RA. Polyene antibiotic-sterol interactions in membranes of *Acholeplasma laidlawii* cells and lecithin liposomes. 3. Molecular structure of the polyene antibiotic-cholesterol complexes. Biochim Biophys Acta. 1974;339:57-70.

[20] Baginski M, Resat H, McCammon JA. Molecular properties of amphotericin B membrane channel: a molecular dynamics simulation. Mol Pharmacol. 1997;52:560-70.

[21] Anderson TM, Clay MC, Cioffi AG, Diaz KA, Hisao GS, Tuttle MD, et al. Amphotericin forms an extramembranous and fungicidal sterol sponge. Nat Chem Biol. 2014;10:400-6.

[22] Kelly SL, Lamb DC, Kelly DE, Manning NJ, Loeffler J, Hebart H, et al. Resistance to fluconazole and cross-resistance to amphotericin B in *Candida albicans* from AIDS patients caused by defective sterol delta5,6-desaturation. FEBS Lett. 1997;400:80-2.

[23] Lee Y, Puumala E, Robbins N, Cowen LE. Antifungal drug resistance: molecular mechanisms in *Candida albicans* and beyond. Chem Rev. 2021;121:3390-411.

[24] Georgopapadakou NH, Walsh TJ. Antifungal agents: chemotherapeutic targets and immunologic strategies. Antimicrob Agents Chemother. 1996;40:279-91.

[25] Vanden Bossche H, Marichal P, Gorrens J, Bellens D, Moereels H, Janssen PA. Mutation in cytochrome P-450-dependent 14 alpha-demethylase results in decreased affinity for azole antifungals. Biochem Soc Trans. 1990;18:56-9.

[26] White TC. Increased mRNA levels of ERG16, CDR, and MDR1 correlate with increases in azole resistance in *Candida albicans* isolates from a patient infected with human immunodeficiency virus. Antimicrob Agents Chemother. 1997;41:1482-7.

[27] Moretta A, Scieuzo C, Petrone AM, Salvia R, Manniello MD, Franco A, et al. Antimicrobial peptides: A new hope in biomedical and pharmaceutical fields. Front Cell Infect Microbiol. 2021;11:668632.

[28] Huan Y, Kong Q, Mou H, Yi H. Antimicrobial peptides: classification, design, application and research progress in multiple fields. Front Microbiol. 2020;11:582779.

[29] Talapko J, Mestrovic T, Juzbasic M, Tomas M, Eric S, Horvat Aleksijevic L, et al. Antimicrobial Peptides-Mechanisms of Action, Antimicrobial Effects and Clinical Applications. Antibiotics (Basel). 2022;11.

[30] Oppenheim FG, Xu T, McMillian FM, Levitz SM, Diamond RD, Offner GD, et al. Histatins, a novel family of histidine-rich proteins in human parotid secretion. Isolation, characterization, primary structure, and fungistatic effects on *Candida albicans*. J Biol Chem. 1988;263:7472-7.

[31] Helmerhorst EJ, Reijnders IM, van't Hof W, Simoons-Smit I, Veerman EC, Amerongen AV. Amphotericin B- and fluconazole-resistant *Candida* spp., *Aspergillus fumigatus*, and other newly

emerging pathogenic fungi are susceptible to basic antifungal peptides. Antimicrob Agents Chemother. 1999;43:702-4.

[32] Torres SR, Garzino-Demo A, Meiller TF, Meeks V, Jabra-Rizk MA. Salivary histatin-5 and oral fungal colonisation in HIV+ individuals. Mycoses. 2009;52:11-5.

[33] Khan SA, Fidel PL, Thunayyan AA, Varlotta S, Meiller TF, Jabra-Rizk MA. Impaired histatin-5 levels and salivary antimicrobial activity against *C. albicans* in HIV infected individuals. Journal of AIDS & clinical research. 2013;4:193.

[34] Ikonomova SP, Moghaddam-Taaheri P, Jabra-Rizk MA, Wang Y, Karlsson AJ. Engineering improved variants of the antifungal peptide histatin 5 with reduced susceptibility to *Candida albicans* secreted aspartic proteases and enhanced antimicrobial potency. FEBS J. 2018;285:146-59.

[35] Ikonomova SP, Moghaddam-Taaheri P, Wang Y, Doolin MT, Stroka KM, Hube B, et al. Effects of histatin 5 modifications on antifungal activity and kinetics of proteolysis. Protein Sci. 2020;29:480-93.

[36] Meiller TF, Hube B, Schild L, Shirtliff ME, Scheper MA, Winkler R, et al. A novel immune evasion strategy of candida albicans: proteolytic cleavage of a salivary antimicrobial peptide. PLoS One. 2009;4:e5039.

[37] Puri S, Friedman J, Saraswat D, Kumar R, Li R, Ruszaj D, et al. *Candida albicans* Shed Msb2 and Host Mucins Affect the Candidacidal Activity of Salivary Hst 5. Pathogens. 2015;4:752-63.

[38] Bochenska O, Rapala-Kozik M, Wolak N, Aoki W, Ueda M, Kozik A. The action of ten secreted aspartic proteases of pathogenic yeast *Candida albicans* on major human salivary antimicrobial peptide, histatin 5. Acta Biochim Pol. 2016;63:403-10.

[39] Newport G, Agabian N. KEX2 influences *Candida albicans* proteinase secretion and hyphal formation. J Biol Chem. 1997;272:28954-61.

[40] Zawrotniak M, Bochenska O, Karkowska-Kuleta J, Seweryn-Ozog K, Aoki W, Ueda M, et al. Aspartic proteases and major cell wall components in *Candida albicans* trigger the release of neutrophil extracellular traps. Front Cell Infect Microbiol. 2017;7:414.

[41] Kulshrestha A, Gupta P. Secreted aspartyl proteases family: a perspective review on the regulation of fungal pathogenesis. Future Microbiol. 2023;18:295-309.

[42] Schild L, Heyken A, de Groot PW, Hiller E, Mock M, de Koster C, et al. Proteolytic cleavage of covalently linked cell wall proteins by *Candida albicans* Sap9 and Sap10. Eukaryot Cell. 2011;10:98-109.

[43] Gropp K, Schild L, Schindler S, Hube B, Zipfel PF, Skerka C. The yeast *Candida albicans* evades human complement attack by secretion of aspartic proteases. Mol Immunol. 2009;47:465-75.

[44] Coates L, Tuan HF, Tomanicek S, Kovalevsky A, Mustyakimov M, Erskine P, et al. The catalytic mechanism of an aspartic proteinase explored with neutron and X-ray diffraction. J Am Chem Soc. 2008;130:7235-7.

[45] Helmerhorst EJ, Alagl AS, Siqueira WL, Oppenheim FG. Oral fluid proteolytic effects on histatin 5 structure and function. Arch Oral Biol. 2006;51:1061-70.

[46] Lomate PR, Bonning BC. Distinct properties of proteases and nucleases in the gut, salivary gland and saliva of southern green stink bug, Nezara viridula. Sci Rep. 2016;6:27587.

[47] Jie Bao G, Kari K, Tervahartiala T, Sorsa T, Meurman JH. Proteolytic activities of oral bacteria on ProMMP-9 and the effect of synthetic proteinase inhibitors. Open Dent J. 2008;2:96-102.

[48] Paster BJ, Boches SK, Galvin JL, Ericson RE, Lau CN, Levanos VA, et al. Bacterial diversity in human subgingival plaque. J Bacteriol. 2001;183:3770-83.

[49] Naglik JR, Newport G, White TC, Fernandes-Naglik LL, Greenspan JS, Greenspan D, et al. In vivo analysis of secreted aspartyl proteinase expression in human oral candidiasis. Infect Immun. 1999;67:2482-90.

[50] Li W, Yu D, Gao S, Lin J, Chen Z, Zhao W. Role of *Candida albicans*-secreted aspartyl proteinases (Saps) in severe early childhood caries. Int J Mol Sci. 2014;15:10766-79.

[51] Konakbayeva D, Karlsson AJ. Strategies and opportunities for engineering antifungal peptides for therapeutic applications. Curr Opin Biotechnol. 2023;81:102926.

[52] Thennarasu S, Nagaraj R. Design of 16-residue peptides possessing antimicrobial and hemolytic activities or only antimicrobial activity from an inactive peptide. Int J Pept Protein Res. 1995;46:480-6.

[53] Markert Y, Koditz J, Mansfeld J, Arnold U, Ulbrich-Hofmann R. Increased proteolytic resistance of ribonuclease A by protein engineering. Protein Eng. 2001;14:791-6.

[54] Tobin MB, Gustafsson C, Huisman GW. Directed evolution: the 'rational' basis for 'irrational' design. Curr Opin Struct Biol. 2000;10:421-7.

[55] Rao A, Chopra S, Ram G, Gupta A, Ranganathan A. Application of the "codon-shuffling" method. Synthesis and selection of de novo proteins as antibacterials. J Biol Chem. 2005;280:23605-14.

[56] Navon SP, Kornberg G, Chen J, Schwartzman T, Tsai A, Puglisi EV, et al. Amino acid sequence repertoire of the bacterial proteome and the occurrence of untranslatable sequences. Proc Natl Acad Sci U S A. 2016;113:7166-70.

[57] Bidlingmaier S, Su Y, Liu B. Combining phage and yeast cell surface antibody display to identify novel cell type-selective internalizing human monoclonal antibodies. Methods Mol Biol. 2015;1319:51-63.

[58] Daugherty PS, Chen G, Olsen MJ, Iverson BL, Georgiou G. Antibody affinity maturation using bacterial surface display. Protein Eng. 1998;11:825-32.

[59] Boder ET, Wittrup KD. Yeast surface display for screening combinatorial polypeptide libraries. Nat Biotechnol. 1997;15:553-7.

[60] Huisman BD, Balivada PA, Birnbaum ME. Yeast display platform with expression of linear peptide epitopes for high-throughput assessment of peptide-MHC-II binding. J Biol Chem. 2023;299:102913.

[61] Knyphausen P, Rangel Pereira M, Brear P, Hyvonen M, Jermutus L, Hollfelder F. Evolution of protease activation and specificity via alpha-2-macroglobulin-mediated covalent capture. Nat Commun. 2023;14:768.

[62] Baum BJ, Bird JL, Millar DB, Longton RW. Studies on histidine-rich polypeptides from human parotid saliva. Arch Biochem Biophys. 1976;177:427-36.

[63] Balekjian AY, Longton RW. Histones isolated from human parotid fluid. Biochem Biophys Res Commun. 1973;50:676-82.

[64] Pollock JJ, Denepitiya L, MacKay BJ, Iacono VJ. Fungistatic and fungicidal activity of human parotid salivary histidine-rich polypeptides on *Candida albicans*. Infect Immun. 1984;44:702-7.

[65] Campese M, Sun X, Bosch JA, Oppenheim FG, Helmerhorst EJ. Concentration and fate of histatins and acidic proline-rich proteins in the oral environment. Arch Oral Biol. 2009;54:345-53.

[66] Raj PA, Marcus E, Sukumaran DK. Structure of human salivary histatin 5 in aqueous and nonaqueous solutions. Biopolymers. 1998;45:51-67.

[67] Li XS, Reddy MS, Baev D, Edgerton M. *Candida albicans* Ssa1/2p is the cell envelope binding protein for human salivary histatin 5. J Biol Chem. 2003;278:28553-61.

[68] Jang WS, Bajwa JS, Sun JN, Edgerton M. Salivary histatin 5 internalization by translocation, but not endocytosis, is required for fungicidal activity in *Candida albicans*. Mol Microbiol. 2010;77:354-70.

[69] Mochon AB, Liu H. The antimicrobial peptide histatin-5 causes a spatially restricted disruption on the *Candida albicans* surface, allowing rapid entry of the peptide into the cytoplasm. PLoS Pathog. 2008;4:e1000190.

[70] Kumar R, Chadha S, Saraswat D, Bajwa JS, Li RA, Conti HR, et al. Histatin 5 uptake by *Candida albicans* utilizes polyamine transporters Dur3 and Dur31 proteins. J Biol Chem. 2011;286:43748-58.

[71] Helmerhorst EJ, van't Hof W, Breeuwer P, Veerman EC, Abee T, Troxler RF, et al. Characterization of histatin 5 with respect to amphipathicity, hydrophobicity, and effects on cell and mitochondrial membrane integrity excludes a candidacidal mechanism of pore formation. J Biol Chem. 2001;276:5643-9.

[72] Rothstein DM, Spacciapoli P, Tran LT, Xu T, Roberts FD, Dalla Serra M, et al. Anticandida activity is retained in P-113, a 12-amino-acid fragment of histatin 5. Antimicrob Agents Chemother. 2001;45:1367-73.

[73] Raj PA, Edgerton M, Levine MJ. Salivary histatin 5: dependence of sequence, chain length, and helical conformation for candidacidal activity. J Biol Chem. 1990;265:3898-905.

[74] Tsai H, Raj PA, Bobek LA. Candidacidal activity of recombinant human salivary histatin-5 and variants. Infect Immun. 1996;64:5000-7.

[75] Tsai H, Bobek LA. Studies of the mechanism of human salivary histatin-5 candidacidal activity with histatin-5 variants and azole-sensitive and -resistant *Candida* species. Antimicrob Agents Chemother. 1997;41:2224-8.

[76] Helmerhorst EJ, Van't Hof W, Veerman EC, Simoons-Smit I, Nieuw Amerongen AV. Synthetic histatin analogues with broad-spectrum antimicrobial activity. Biochem J. 1997;326 (Pt 1):39-45.

[77] Ruissen AL, Groenink J, Helmerhorst EJ, Walgreen-Weterings E, Van't Hof W, Veerman EC, et al. Effects of histatin 5 and derived peptides on *Candida albicans*. Biochem J. 2001;356:361-8.

[78] Sun X, Salih E, Oppenheim FG, Helmerhorst EJ. Kinetics of histatin proteolysis in whole saliva and the effect on bioactive domains with metal-binding, antifungal, and wound-healing properties. FASEB J. 2009;23:2691-701.

[79] Norris HL, Kumar R, Ong CY, Xu D, Edgerton M. Zinc Binding by Histatin 5 Promotes Fungicidal Membrane Disruption in *C. albicans* and *C. glabrata*. J Fungi (Basel). 2020;6.

[80] Ayinampudi BK, Narsimhan M. Salivary copper and zinc levels in oral pre-malignant and malignant lesions. J Oral Maxillofac Pathol. 2012;16:178-82.

[81] Campbell JX, Gao S, Anand KS, Franz KJ. Zinc binding inhibits cellular uptake and antifungal activity of histatin-5 in *candida albicans*. ACS Infect Dis. 2022;8:1920-34.

[82] McCaslin TG, Pagba CV, Yohannan J, Barry BA. Specific metallo-protein interactions and antimicrobial activity in Histatin-5, an intrinsically disordered salivary peptide. Sci Rep. 2019;9:17303.

[83] Taylor M, Brizuela M, Raja A. Oral Candidiasis. StatPearls. Treasure Island (FL)2022.

[84] Komatsu T, Watanabe K, Hamada N, Helmerhorst E, Oppenheim F, Lee MC. Association between Antimicrobial Peptide Histatin 5 Levels and Prevalence of Candida in Saliva of Patients with Down Syndrome. Antibiotics-Basel. 2021;10.

[85] Sundstrom P. Adhesion in *Candida* spp. Cell Microbiol. 2002;4:461-9.

[86] Naglik JR, Moyes D, Makwana J, Kanzaria P, Tsichlaki E, Weindl G, et al. Quantitative expression of the *Candida albicans* secreted aspartyl proteinase gene family in human oral and vaginal candidiasis. Microbiology (Reading). 2008;154:3266-80.

[87] Keikha N, Yadegari MH, Rajabibazl M, Amani J, Hosseinzadeh S. The effect of released new synthetic peptide from nanofibrous scaffold of peptide/Poly (Vinyl Alcohol)/Poly l-Lactic Acid on expression of Secretory aspartyl proteinases 4 to 6 genes of *Candida albicans*. Infect Genet Evol. 2019;70:36-41.

[88] Sadeghi G, Mousavi SF, Ebrahimi-Rad M, Mirabzadeh-Ardekani E, Eslamifar A, Shams-Ghahfarokhi M, et al. In vivo and in vitro Pathogenesis and Virulence Factors of *Candida albicans* Strains Isolated from Cutaneous Candidiasis. Iran Biomed J. 2020;24:324-32.

[89] Koelsch G, Tang J, Loy JA, Monod M, Jackson K, Foundling SI, et al. Enzymic characteristics of secreted aspartic proteases of *Candida albicans*. Biochim Biophys Acta. 2000;1480:117-31.

[90] Helmerhorst EJ, Alagl AS, Siqueira WL, Oppenheim FG. Oral fluid proteolytic effects on histatin 5 structure and function. arch Oral Biol.51:1061-70.

[91] Xu L, Lal K, Santarpia RP, 3rd, Pollock JJ. Salivary proteolysis of histidine-rich polypeptides and the antifungal activity of peptide degradation products. Arch Oral Biol. 1993;38:277-83.

[92] Makambi WK, Ikonomova SP, Karlsson AJ. Quantifying the antifungal activity of peptides against *Candida albicans*. J Vis Exp. 2023.

[93] Mitchell LH, Soll DR. Commitment to germ tube or bud formation during release from stationary phase in *Candida albicans*. Exp Cell Res. 1979;120:167-79.

[94] Naglik JR, Challacombe SJ, Hube B. *Candida albicans* secreted aspartyl proteinases in virulence and pathogenesis. Microbiol Mol Biol Rev. 2003;67:400-28, table of contents.

[95] Koller G, Schurholz E, Ziebart T, Neff A, Frankenberger R, Bartsch JW. Clinical evaluation of pathognomonic salivary protease fingerprinting for oral disease diagnosis. J Pers Med. 2021;11.

[96] R AN, Rafiq NB. Candidiasis. StatPearls. Treasure Island (FL)2022.

[97] Tati S, Jang WS, Li R, Kumar R, Puri S, Edgerton M. Histatin 5 resistance of *Candida glabrata* can be reversed by insertion of Candida albicans polyamine transporter-encoding genes DUR3 and DUR31. PLoS One. 2013;8:e61480.

[98] Helmerhorst EJ, Troxler RF, Oppenheim FG. The human salivary peptide histatin 5 exerts its antifungal activity through the formation of reactive oxygen species. Proc Natl Acad Sci U S A. 2001;98:14637-42.

[99] Norris HL, Kumar R, Edgerton M. A novel role for histatin 5 in combination with zinc to promote commensalism in *C. albicans* Survivor Cells. Pathogens. 2021;10.

[100] Coleman JE. Zinc proteins: enzymes, storage proteins, transcription factors, and replication proteins. Annu Rev Biochem. 1992;61:897-946.

[101] Gulati M, Nobile CJ. *Candida albicans* biofilms: development, regulation, and molecular mechanisms. Microbes Infect. 2016;18:310-21.

[102] Moghaddam-Taaheri P, Leissa JA, Eppler HB, Jewell CM, Karlsson AJ. Histatin 5 variant reduces *Candida albicans* biofilm viability and inhibits biofilm formation. Fungal Genet Biol. 2021;149:103529.

[103] De Prijck K, De Smet N, Rymarczyk-Machal M, Van Driessche G, Devreese B, Coenye T, et al. *Candida albicans* biofilm formation on peptide functionalized polydimethylsiloxane. Biofouling. 2010;26:269-75.

[104] Lu CF, Montijn RC, Brown JL, Klis F, Kurjan J, Bussey H, et al. Glycosyl phosphatidylinositol-dependent cross-linking of alpha-agglutinin and beta 1,6-glucan in the Saccharomyces cerevisiae cell wall. J Cell Biol. 1995;128:333-40.

[105] Cappellaro C, Baldermann C, Rachel R, Tanner W. Mating type-specific cell-cell recognition of *Saccharomyces cerevisiae*: cell wall attachment and active sites of a- and alpha-agglutinin. EMBO J. 1994;13:4737-44.

[106] Johnston M, Davis RW. Sequences that regulate the divergent GAL1-GAL10 promoter in *Saccharomyces cerevisiae*. Mol Cell Biol. 1984;4:1440-8.

[107] Bowen J, Schneible J, Bacon K, Labar C, Menegatti S, Rao BM. Screening of yeast display libraries of enzymatically treated peptides to discover macrocyclic peptide ligands. Int J Mol Sci. 2021;22.

[108] Lown PS, Cai JJ, Ritter SC, Otolski JJ, Wong R, Hackel BJ. Extended yeast surface display linkers enhance the enrichment of ligands in direct mammalian cell selections. Protein Eng Des Sel. 2021;34.

[109] McMahon C, Baier AS, Pascolutti R, Wegrecki M, Zheng S, Ong JX, et al. Yeast surface display platform for rapid discovery of conformationally selective nanobodies. Nat Struct Mol Biol. 2018;25:289-96.

[110] Leissa JA. Protein engineering approaches to improve the therapeutic potential of histatin-5 for *Candida albicans* Infections.: University of Maryland; 2019.

[111] Dupres V, Dufrene YF, Heinisch JJ. Measuring cell wall thickness in living yeast cells using single molecular rulers. ACS Nano. 2010;4:5498-504.

[112] Wang L, Rivera EV, Benavides-Garcia MG, Nall BT. Loop entropy and cytochrome c stability. J Mol Biol. 2005;353:719-29.

[113] Stern LA, Schrack IA, Johnson SM, Deshpande A, Bennett NR, Harasymiw LA, et al. Geometry and expression enhance enrichment of functional yeast-displayed ligands via cell panning. Biotechnol Bioeng. 2016;113:2328-41.

[114] Smith SN, Harris DT, Kranz DM. T Cell Receptor Engineering and Analysis Using the Yeast Display Platform. Methods Mol Biol. 2015;1319:95-141.

[115] Wilson DS, Keefe AD. Random mutagenesis by PCR. Curr Protoc Mol Biol. 2001;Chapter 8:Unit8 3.

[116] Yi L, Taft JM, Li Q, Gebhard MC, Georgiou G, Iverson BL. Yeast Endoplasmic Reticulum Sequestration Screening for the Engineering of Proteases from Libraries Expressed in Yeast. Methods Mol Biol. 2015;1319:81-93.

[117] Yi L, Gebhard MC, Li Q, Taft JM, Georgiou G, Iverson BL. Engineering of TEV protease variants by yeast ER sequestration screening (YESS) of combinatorial libraries. Proc Natl Acad Sci U S A. 2013;110:7229-34.

[118] Puri S, Li R, Ruszaj D, Tati S, Edgerton M. Iron binding modulates candidacidal properties of salivary histatin 5. J Dent Res. 2015;94:201-8.

[119] Gold JAW, Ahmad FB, Cisewski JA, Rossen LM, Montero AJ, Benedict K, et al. Increased deaths from Fungal infections during the coronavirus disease 2019 pandemic-National Vital Statistics System, United States, January 2020-December 2021. Clin Infect Dis. 2023;76:e255-e62.

[120] Xia J, Wang Z, Li T, Lu F, Sheng D, Huang W. Immunosuppressed patients with clinically diagnosed invasive fungal infections: The fungal species distribution, antifungal sensitivity and associated risk factors in a tertiary Hospital of Anhui Province. Infect Drug Resist. 2022;15:321-33.

[121] Alangaden GJ. Nosocomial fungal infections: epidemiology, infection control, and prevention. Infect Dis Clin North Am. 2011;25:201-25.

[122] Hope W, Natarajan P, Goodwin L. Invasive fungal infections. Clin Med (Lond). 2013;13:507-10.

[123] Nobile CJ, Johnson AD. *Candida albicans* Biofilms and Human Disease. Annu Rev Microbiol. 2015;69:71-92.

[124] Costa A, Back-Brito GN, Mayer FL, Hube B, Wilson D. *Candida albicans* Mrv8, is involved in epithelial damage and biofilm formation. FEMS Yeast Res. 2020;20.

[125] Bagheri M, Beyermann M, Dathe M. Immobilization reduces the activity of surface-bound cationic antimicrobial peptides with no influence upon the activity spectrum. Antimicrob Agents Chemother. 2009;53:1132-41.

[126] Naderi J, Giles C, Saboohi S, Griesser HJ, Coad BR. Surface-grafted antimicrobial drugs: Possible misinterpretation of mechanism of action. Biointerphases. 2018;13:06E409.

[127] Karlsson AJ, Flessner RM, Gellman SH, Lynn DM, Palecek SP. Polyelectrolyte multilayers fabricated from antifungal beta-peptides: design of surfaces that exhibit antifungal activity against *Candida albicans*. Biomacromolecules. 2010;11:2321-8.

[128] Etienne O, Picart C, Taddei C, Haikel Y, Dimarcq JL, Schaaf P, et al. Multilayer polyelectrolyte films functionalized by insertion of defensin: a new approach to protection of implants from bacterial colonization. Antimicrob Agents Chemother. 2004;48:3662-9.